

Topological phase transitions driven by non-Abelian anyons

Dissertation
zur Erlangung des Grades eines Doktors der Naturwissenschaften
der Fakultät Physik der Technischen Universität Dortmund

Thèse de doctorat
pour obtenir le grade de Docteur
de l'Université Pierre & Marie Curie

Marc Daniel Schulz

Date of defense: 19.12.2013
Members of thesis committee: Dr. Kai P. SCHMIDT (thesis advisor)
Dr. Julien VIDAL (thesis advisor)
Prof. Philippe LECHEMINANT (referee)
Prof. Joachim STOLZE (referee)
Prof. Simon TREBST (referee)
Dr. Benoît DOUÇOT (examiner)
Dr. Carsten RAAS (examiner)
Prof. Bernhard SPAAN (examiner)

Abstract

We study quantum phase transitions and the critical behavior of topologically-ordered phases by considering various string-net models perturbed by local operators defined on the two-dimensional honeycomb lattice. More precisely, by means of high-order series expansions in combination with exact diagonalization, we analyze the phase transitions induced by the analogue of a magnetic field for the topologically-ordered phases described by doubled semion, Fibonacci, and Ising theories. We develop a quasi-particle picture of the elementary anyonic excitations for all these models. The effective models of interacting quasi-particles allow us to determine the respective phase diagrams and to analyze spectral properties of the low-energy physics. Our analysis of the low-energy spectrum leads to the first evidence of continuous quantum phase transitions out of topologically-ordered phases harboring non-Abelian anyons.

Wir untersuchen Phasenübergänge und das kritische Verhalten topologisch geordneter Phasen unter Einfluss von lokalen Störungen anhand verschiedener String-Net-Modelle, die auf dem zweidimensionalen Bienenwabengitter definiert sind. Mittels verschiedener Hochordnungsreihenentwicklungen und exakter Diagonalisierung werden Phasenübergänge zwischen verschiedenen topologisch geordneten und topologisch trivialen Phasen untersucht. Die hier betrachteten topologisch geordneten Phasen werden jeweils durch achirale Semion-, Fibonacci- und Ising-Feldtheorien beschrieben. Zur Betrachtung der gestörten String-Net-Modelle, entwickeln wir eine Quasiteilchenbeschreibung der jeweiligen elementaren anyonischen Anregungen. Diese effektiven Modelle wechselwirkender Quasiteilchen ermöglichen eine Analyse des Niederenergiespektrums und damit auch eine Bestimmung der kritischen Eigenschaften von auftretenden Phasenübergängen. Unsere Untersuchung liefert erste Anzeichen für kontinuierliche Phasenübergänge zwischen topologisch geordneten Phasen, deren elementare Anregungen fraktionale, nicht abelsche Statistik aufweisen, und topologisch trivialen Phasen.

Nous étudions les transitions de phases et le comportement critique de systèmes topologiquement ordonnés en considérant différents modèles de string-nets en présence d'une perturbation locale. Plus précisément, en utilisant à la fois des théories de perturbations à des ordres élevés ainsi que des diagonalisations exactes, nous analysons les transitions induites par l'équivalent d'un champ magnétique pour des théories d'anyons de type Fibonacci, Ising, et semionique et développons une image de type quasiparticules pour les excitations élémentaires. Les modèles effectifs de quasiparticules anyoniques en interaction nous permettent de déterminer les diagrammes de phase pour chacune de ces théories et d'analyser les propriétés spectrales de basses énergies. Ces études nous conduisent à mettre en évidence de transitions de phase quantiques continues dans des systèmes topologiquement ordonnés en présence d'anyons non-Abéliens.

Contents

| | | |
|----------|--|-----------|
| 1 | Introduction | 1 |
| I | Phase transitions in perturbed string-net models | 9 |
| 2 | Anyons | 11 |
| 2.1 | Quantum mechanics in two dimensions | 11 |
| 2.2 | Algebraic theory of anyons | 13 |
| 2.2.1 | Fusion | 13 |
| 2.2.2 | Braiding | 17 |
| 2.2.3 | Twists and spins | 18 |
| 2.2.4 | Modular S -matrix | 19 |
| 2.3 | Doubling of a theory | 19 |
| 2.4 | List of theories | 20 |
| 2.4.1 | Semions | 21 |
| 2.4.2 | Fibonacci | 22 |
| 2.4.3 | Ising | 22 |
| 2.4.4 | Toric Code | 23 |
| 2.5 | Chapter Summary | 23 |
| 3 | String-net models | 25 |
| 3.1 | The Levin-Wen Hamiltonian H_{LW} | 25 |
| 3.1.1 | String-net Hamiltonian H_{SN} | 26 |
| 3.1.2 | The fat-lattice visualization | 28 |
| 3.1.3 | The flux operator B_p | 30 |
| 3.1.4 | The dual basis | 34 |
| 3.1.5 | Properties of the eigenstates | 41 |
| 3.1.6 | Brief summary for the string-net Hamiltonian | 43 |
| 3.2 | The local Hamiltonian H_{loc} | 44 |
| 3.3 | The perturbed string-net Hamiltonian | 46 |
| 3.4 | Realizing different boundary conditions | 46 |
| 3.4.1 | The ladder | 47 |
| 3.4.2 | Open boundary conditions | 49 |
| 3.5 | Realizations of the different anyonic theories | 49 |
| 3.5.1 | The golden string net: Fibonacci anyons | 50 |
| 3.5.1.1 | The topological phase | 50 |
| 3.5.1.2 | Counting of states | 51 |

| | | |
|-----------|--|------------|
| 3.5.1.3 | The flux-full case | 53 |
| 3.5.1.4 | The $\mathbf{1}$ -phase | 53 |
| 3.5.1.5 | The τ -phase | 53 |
| 3.5.2 | Ising anyons | 54 |
| 3.5.2.1 | The topological phase | 55 |
| 3.5.2.2 | Counting of states | 55 |
| 3.5.2.3 | The flux-full case | 57 |
| 3.5.2.4 | The $\mathbf{1}$ -phase | 57 |
| 3.5.2.5 | The dimer limit | 57 |
| 3.5.3 | The Abelian cases: semions and $D(\mathbb{Z}_2)$ | 58 |
| 3.6 | Chapter Summary | 61 |
| 4 | Topological symmetry breaking | 63 |
| 4.1 | General framework | 64 |
| 4.1.1 | Condensation | 65 |
| 4.1.2 | Confinement | 66 |
| 4.2 | Examples of topological symmetry breaking | 67 |
| 4.2.1 | Phase transitions out of the doubled semion phase $D(\text{Semion})$. . . | 67 |
| 4.2.2 | Phase transitions out of the doubled Fibonacci phase $D(\text{Fib})$. . . | 68 |
| 4.2.3 | Phase transitions out of the doubled Ising phase $D(\text{Ising})$ | 68 |
| 4.3 | Chapter summary | 70 |
| 5 | Results for perturbed string-net models | 73 |
| 5.1 | Phase transitions in the semion model | 75 |
| 5.1.1 | Phase transition between topological and $\mathbf{1}$ -phase | 77 |
| 5.1.2 | Phase transition between topological and AFM-phase | 84 |
| 5.1.3 | Summary of the phase transitions in the semion model | 86 |
| 5.2 | Phase transitions for Fibonacci anyons | 87 |
| 5.2.1 | Phase transition between topological and $\mathbf{1}$ -phase | 87 |
| 5.2.2 | Phase transition between topological and τ -phase | 93 |
| 5.2.3 | Phase transition between $\mathbf{1}$ - and τ -phase | 96 |
| 5.2.4 | Summary of the phase transitions in the Fibonacci model | 97 |
| 5.3 | Phase transitions for Ising anyons | 98 |
| 5.3.1 | The valence-bond crystal | 100 |
| 5.3.2 | Phase transition between topological and $\mathbf{1}$ -phase | 101 |
| 5.3.3 | Phase transition between topological and the VBC | 105 |
| 5.3.4 | Summary of the phase transitions in the Ising model | 106 |
| 5.4 | Comparison between the different models | 107 |
| 5.5 | Chapter Summary | 109 |
| II | Series expansion techniques for perturbed string-net models | 111 |
| 6 | Methodology | 113 |
| 6.1 | Series expansions | 114 |
| 6.1.1 | Perturbative continuous unitary transformations | 115 |
| 6.1.1.1 | Continuous unitary transformations | 115 |
| 6.1.1.2 | Perturbative continuous unitary transformations | 117 |

| | | |
|----------|---|------------|
| 6.1.1.3 | Cluster additivity | 121 |
| 6.1.1.4 | Linked-Cluster Theorem | 122 |
| 6.1.2 | Degenerate perturbation theory | 124 |
| 6.1.3 | Partition technique | 127 |
| 6.1.4 | Efficient perturbation theory | 130 |
| 6.1.5 | Perturbation theory in the thermodynamic limit | 133 |
| 6.1.6 | Extrapolations | 134 |
| 6.2 | Exact diagonalization | 137 |
| 6.3 | Chapter summary | 140 |
| 7 | Implementation of the series expansion | 141 |
| 7.1 | General considerations | 141 |
| 7.2 | Implementation for the topological phase | 143 |
| 7.2.1 | Implementation of the scalar product | 146 |
| 7.2.2 | Removing the redundancy | 147 |
| 7.2.3 | Implementation details of the calculations | 150 |
| 7.3 | The non-topological phases | 150 |
| 7.3.1 | Implementation in the $\mathbf{1}$ -phase | 150 |
| 7.3.2 | Implementation of the τ -phase in the Fibonacci theory | 153 |
| 7.4 | Chapter Summary | 154 |
| 8 | Linked-cluster expansion | 155 |
| 8.1 | Graph decomposition in the topological phase | 157 |
| 8.2 | Graph expansions for non-topological phases | 167 |
| 8.2.1 | Graph expansions in the $\mathbf{1}$ -phase | 167 |
| 8.2.2 | Graph expansions in the τ -phase | 172 |
| 8.3 | Chapter Summary | 174 |
| 9 | Summary and Outlook | 177 |
| A | Series expansions for the semion model | 180 |
| A.1 | Series expansions for the topological phase | 180 |
| A.2 | Series expansions for the $\mathbf{1}$ -phase | 184 |
| B | Series expansions for Fibonacci anyons | 185 |
| B.1 | Series expansions for the topological phase | 185 |
| B.2 | Series expansions for the $\mathbf{1}$ -phase | 188 |
| B.3 | Series expansions for the τ -phase | 189 |
| C | Series expansions for Ising Anyons | 199 |
| C.1 | Series expansions for the topological phase | 199 |
| C.2 | Series expansions for the $\mathbf{1}$ -phase | 204 |
| | Bibliography | 207 |
| | Declaration of Authorship | 217 |
| | Acknowledgements | 218 |

Introduction

The secret of getting ahead is getting started.

- Mark Twain -

The main goal of modern physics is to describe and understand the various states of matter found in nature, ranging from large scales as the evolution of the universe in cosmology down to the subatomic scales of the constituting particles of matter and light in high-energy physics. In condensed-matter physics, the classification of the various phases emerging due to strong correlation effects is at the heart of current investigations.

One can characterize the different phases of matter by considering an order parameter. Any order parameter is linked to a symmetry, which is present for a given phase. Of particular importance are local order parameters as these can be related e.g. to (broken) spatial symmetries, which are of relevance in the study of condensed-matter systems, or to local-gauge symmetries essential for electrodynamics. A well-known example for a local order parameter is the magnetization of a ferromagnet.

A deeper understanding of the characteristics of a phase arises when transitions between different phases are studied. In the case of a continuous transition between two phases described by a local order parameter, the behavior of the system at the transition point does not depend on its local details but only on the symmetries characterizing the two phases. The quantities showing this universal scaling behavior are accessible either by experiments or by theoretical descriptions and thus allow to determine the symmetries involved for a given system. The corresponding theoretical framework of spontaneous symmetry breaking was developed by Landau in the 1930's [1, 2]. It has been successfully applied to many fields of physics since then. In our discussion, we shall restrict ourselves to quantum phase transitions, which are not governed by thermal fluctuations but purely by quantum fluctuations. Therefore, we consider only the case of zero temperature in the following.

In the 1980's, the discovery of the fractional quantum Hall effect [3, 4] in the two-dimensional electron gas yielded the first example of a system, which is not described by local order parameters, since different phases are not distinguishable by a local symmetry. Soon, possible connections to the phenomenology of high-temperature superconductors were pointed out [5, 6]. These findings triggered the emergence of a classification scheme invoking non-local properties and thus going beyond the Landau paradigm. This classification is the so-called topological order [7, 8].

One can characterize topological order in several ways. A formal description of topologically-ordered systems is given by topological quantum field theory [9–11]. However, the lack of a local order parameter can also be seen as a defining property for topological order [12–14]. According to the latter definition, we refer to a system in the thermodynamic limit with a spectral gap above the ground state(s) $\{|\text{gs}_\alpha\rangle\}$ as topologically ordered if we have for any operator O with bounded support

$$\langle \text{gs}_\alpha | O | \text{gs}_\beta \rangle = c \delta_{\alpha,\beta}, \quad (1.1)$$

where the constant c does not depend on the particular state $|\text{gs}_\alpha\rangle$. Thus, there is no local operator acting non-trivially within the ground-state manifold. However, topologically ordered phases can still be characterized by non-local order parameters. The corresponding quantities can, for example, be the expectation value of Wilson-loop operators on the scales of the system size [15] or properties of the topological field theory as the modular S -matrix [16].

Topological order manifests itself in different ways. One hallmark is that the ground-state degeneracy of a system depends on the topology, in which it is embedded [8]. Also, measures of the long-range entanglement such as the so-called topological entanglement entropy can witness topological order [17, 18]. The framework of topological symmetry breaking [19] has been developed in order to allow for a description of continuous phase transitions in analogy to spontaneous symmetry breaking. Let us note that although topological order allows to classify phases without local order parameters and topological symmetry breaking explains how some phase transitions between different topologically ordered phases may occur, this framework does not provide an answer to the question whether the universal properties emerging in spontaneous symmetry breaking carry over to topological phase transitions or not.

The interest in topologically ordered systems even further increased after it has been realized that the excitations have exotic exchange statistics in two dimensions [20, 21], i.e. they do not behave as bosons or fermions. It was Wilczek, who named excitations with exotic exchange statistics as anyons [22]. This fractional statistics was later on found to be intimately related to topological order [23]. There are two types of anyons.

When two Abelian anyons are exchanged, the wave function acquires a phase factor similar to the case of bosons and fermions, whereas the exchange of non-Abelian anyons represents a non-trivial unitary transformation in the corresponding Hilbert space. The latter implies in particular that the excited states are not uniquely specified by the position of the quasi-particles. These exotic particles are expected to exist in fractional quantum Hall states, e.g. the so-called Fibonacci anyons appear in the theoretical description of the fractional quantum Hall state for filling fraction $\nu = 12/5$ [24], and there is even recent experimental evidence for the so-called Ising anyons to be the elementary excitations of the corresponding state at filling fraction $\nu = 5/2$ [25–27].

Topological order switched from the stage of a purely academic interest to the focus of eventual application after it was realized that the absence of a local order parameter is equivalent to the fact that local perturbations cannot induce decoherence in topologically ordered systems [28, 29]. Thus topologically ordered systems are a suitable platform for decoherence-free quantum computation. The degenerate ground-state manifold can be used to store a quantum state, whereas the non-Abelian exchange statistics allows for the implementation of different operations [30–33]. The fact that non-Abelian anyons can be used to implement quantum computation underlines their more complex structure compared to Abelian anyons, which lack this feature. In the context of quantum information, the investigation of phase transitions out of a topologically ordered phase is, in some sense, equivalent to study the robustness of a topological quantum computer.

Let us mention that there are related phases of matter that attracted interest in recent years: the so-called symmetry-protected topological order shares a lot of features with the topological order we discussed above. In particular, topological invariants characterize both families of states. Prominent examples of the symmetry-protected topologically ordered states are the so-called topological insulators [34, 35]. The most important distinction between these two classes of phases is the presence of symmetries, which allow to classify and understand the various symmetry-protected topological-orders [36–40]. In contrast to topological ordered phases, symmetry protected topologically ordered states display only short-range entanglement [41]. Nevertheless, these phases harbor anyons as boundary modes (e.g. the so-called Majorana mode in one-dimensional wires [42, 43]), which yield promising candidates for the experimental implementation of topological quantum computation [44, 45].

The models available to study topological-ordered phases can be divided into two families. The first consists of models, in which the topological excitations emerge from more conventional microscopic (e.g. spin) degrees of freedom. To this family belong the Heisenberg models and extensions on frustrated lattices [46], quantum loop gases [47], and quantum dimer models [48–50]. However, the latter models do mostly support only

Abelian anyons as the emergence of non-Abelian statistics requires in most cases either non-local interactions between the microscopic degrees of freedom [51] or a modification of properties of the Hilbert space [52].¹

These possibilities are already built in for the second family of models as their microscopic degrees of freedom are already given in terms of anyons. The most prominent representants of this family are the lattice-gauge models [54, 55], including the celebrated toric code [28]. Also, the string-net picture [56–59] provides models realizing topological order, which will be the main focus of this thesis. These models are likely not realized in a condensed-matter system due to their fine-tuned multi-spin interactions, but serve as playground to investigate fundamental properties of topologically ordered phases.

Especially in one spatial dimension, the investigation of the latter type of models also for those harboring non-Abelian anyons is very successful, as one can often either identify integrable models [60–63] or one is able to perform accurate numerical studies to find the corresponding critical theory [64–68] for phase transitions driven by anyon interactions. Also the effect of local perturbations on non-Abelian anyons has been considered [69, 70].

However, when it comes to the investigation of phase transitions in two dimensions, considerably less is known. This is on the one hand due to the lack of analytical and numerical tools and on the other hand due to the existence of only a few exactly solvable models, which serve as a suitable starting point. Nevertheless, there are numerical works approaching the limit of two dimensions by considering quasi-one dimensional ladder systems [67, 71, 72].

One of the exactly solvable models is the toric code [28], the simplest example of a lattice gauge theory. Its general version is defined for any discrete group, its simplest version, the \mathbb{Z}_2 toric code, serves as standard model for topological order in two dimensions just as the Ising model for statistical physics. The excitations in this model can be described in terms of so-called semions, which have Abelian exchange statistics. Additionally to its theoretical importance, there is a proof of principle realization of this model in arrays of Josephson junctions [73]. If perturbed by a magnetic field, this model shows phase transitions, which can be either continuous [74–80] or discontinuous [81, 82], and it also displays multi-critical behavior. Furthermore, the limits of applicability in the context of quantum information have been investigated [83, 84]. The same richness of critical behavior has also been found for the extension to more general Abelian models [85, 86].

The non-Abelian versions of the toric code have also been described [28, 87] and also the phase diagram for some non-Abelian versions in the context of topological symmetry

¹A particular exception is Kitaev’s honeycomb model [53].

breaking [88] has been investigated [16]. However, a detailed study of the phase transitions themselves is still ongoing work, which is also due to the fact that the complexity of non-Abelian excitations results in a much larger effort within the analysis.

Another exactly solvable model is Kitaev's honeycomb model [53]. It consists of (anisotropic) two-spin terms and is either described by the Abelian \mathbb{Z}_2 toric code or by non-Abelian Ising anyons at low energy in the presence of a time-reversal symmetry breaking magnetic field. The effects of the magnetic field have been investigated [53, 89–92] and evidence for a continuous phase transition between the (chiral) non-Abelian and the paramagnetic phase has been found [93].

The third and most general class of models are the string-net models introduced by Levin and Wen [56]. As the toric code can be defined for any discrete group, string-net models can be defined for any tensor category [11], which includes not only the usual groups but also the so-called quantum groups [94, 95]. Thus, there are connections to lattice gauge theory models [96].²

The possibility to include also quantum groups allows to study the simplest possible topological phases with non-Abelian anyons. These are the phases, which harbor the already mentioned Fibonacci and Ising anyons. These phases are simpler than the non-Abelian lattice gauge theories in the sense that the Hilbert space of the microscopic degrees of freedom for Fibonacci (Ising) anyons is two- (three-) dimensional, whereas non-Abelian lattice gauge theories require at least a local dimension of six (the order of the smallest non-Abelian group D_3).

The string-net models have been shown to realize doubled Chern-Simon field theories [98, 99]. Thus these models realize achiral phases and are not directly related to any experimental setup, but they allow to study also non-Abelian excitations. One-dimensional versions [69, 70] show continuous phase transitions to chiral topological phases in the presence of local perturbations. Phase transitions between different topologically ordered phases realized in the string-net picture have been investigated for special cases [97, 100, 101] by means of duality mappings to statistical models. However, quantitative investigations of the critical properties for a continuous phase transition between topologically ordered phases harboring non-Abelian anyons, which are the ones enabling topological quantum computation, and topologically-trivial phases, which represent the overwhelming majority of known phases, are still missing for two-dimensional systems.

One goal of this thesis is to bridge this gap by providing and analyzing examples for such transitions. Therefore, we shall discuss the most important string-net models,

²Note that these string-net and toric code models defined for the same group coincide in their ground-state properties. However, the properties of the excitations differ. These differences may be removed by modifying the string-net model as in Ref. [97].

namely the ones for semions, Fibonacci, and Ising anyons and analyze the effect of a local perturbation in two spatial dimensions.

To this aim, we have to develop a description for the (non-Abelian) anyonic excitations in the string-net model, which is also valid in the presence of perturbations. This quasi-particle picture for non-Abelian anyons is the second main focus of this thesis.

In order to obtain quantitative results to study critical properties, we use computer-based analytical calculations. The implementation of these provides a tool to investigate general properties of topologically ordered phases (with Abelian and non-Abelian anyonic excitations).

However, there are a lot of details to be discussed about the way the above steps are achieved in order to contribute to a deeper understanding of the fast-developing field of quantum criticality in the context of topological order. Therefore, choices have to be made to maintain the present manuscript in a concise form.

Thus, before discussing the structure of the manuscript, let us mention what is not included in it. A substantial part of the preparation of this thesis was devoted to the investigation of critical properties of Abelian versions of the toric code, which, as a prelude, served as a playground to develop most of the essential ideas for models, which are not as complex as those harboring non-Abelian excitations. As the main focus is on phases with non-Abelian anyons, we redirect the interested reader to Ref. [86], where our findings are detailed.

Another important part of my PhD work was the study of the perturbed string-net model for Fibonacci and Ising anyons defined on a two-leg ladder, where we were able to obtain good agreement between our results for the phase diagram and critical exponents and the critical theories identified in Refs. [69, 70]. As we focus within this manuscript on the critical properties of two-dimensional systems, we shall not discuss these investigations in the following.

Additionally, we shall focus on the specific theories for semions, Fibonacci, and Ising anyons, although many others [54, 55, 65, 68, 102] can be discussed.

The remainder of this thesis aims to analyze the critical properties of phase transitions out of topologically ordered phases driven by the condensation of (non-) Abelian anyons as well as the necessary ingredients to yield a quantitative description for two-dimensional systems. As a consequence, this manuscript is divided into two parts.

In the first part, we discuss the microscopic model under investigation as well as our results for the critical properties. In Chapter 2, we give therefore a brief introduction to

the properties of a unitary modular tensor category in order to provide the vocabulary necessary to understand the details of the string-net models.

The string-net model investigated in this thesis is presented in Chapter 3. The main focus is the description of the two-dimensional model introduced by Levin and Wen [56], which includes the non-local properties of the excitations similar to the construction of Ref. [103]. We detail this construction for the Abelian case of semions as well as for the non-Abelian cases of Fibonacci and Ising anyons. We also introduce the local perturbation, which is the analog of a magnetic field in the case of toric code models, and discuss its effects for the different topological phases.

The theoretical framework describing continuous phase transitions out of topologically ordered phases is discussed in Chapter 4. We detail the possible, so-called condensate induced phase transitions for the models under investigation.

The actual results are presented in Chapter 5. We begin with the study of the perturbed string-net model for semions. The discussion of the Abelian model by considering the low-energy spectrum allows to re-discover the known results for the dual spin- $\frac{1}{2}$ transverse-field Ising model defined on the triangular lattice. Comparisons with its known properties allow us to estimate the accuracy of our results. Then, we discuss the phase diagram and the critical properties of the perturbed string-net model for Fibonacci anyons along the same lines as for the semions. We find first evidence of a second-order phase transitions out of a topologically ordered phase harboring non-Abelian anyons in two dimensions [104]. As a second example, we consider the perturbed string-net model for Ising anyons. As in the case of the Fibonacci anyons, we find phase transitions driven by condensation of the non-Abelian excitations towards a topologically trivial phase.

Thus, in this first part, we discuss the critical behavior for the perturbed topological phases. In the second part, we discuss in large detail how we obtained the low-energy spectrum. The general ideas of the different ways to derive effective models by perturbative means is presented in Chapter 6. We also detail how to combine these different ways, namely perturbative continuous unitary transformations [105], degenerate perturbation theory [106], and partition techniques [107], in order to obtain results directly valid in the thermodynamic limit. Additionally, our implementation to obtain non-perturbative results on finite-size systems by exact diagonalization is discussed.

The details of the implementations of the perturbative techniques for the different models are discussed in Chapter 7. The focus is put on particularities of the study of models featuring essential non-local properties as the fractional exchange statistics. Additionally, we discuss also implementation features for operators with large support as the multi-spin terms, which arise in the string-net Hamiltonian.

The second part is concluded in Chapter 8 by the discussion of the tools, which allow to perform a perturbative treatment of considered models up to high order and thus to obtain also quantitative results. The linked-cluster expansion, which we generalize here to topologically ordered phases, allows to obtain the quantities of interest in the thermodynamic limit by considering contributions from finite-size systems.

A brief summary of the obtained results is given together with some perspectives on future studies in the context of universal behavior of topologically ordered phases in Chapter 9.

Part I

Phase transitions in perturbed string-net models

Chapter 2

Anyons

We live in a rainbow of chaos.
- Paul Cezanne -

The aim of this chapter is to introduce the necessary ingredients to describe anyons. Therefore, we discuss the impact of the exotic braiding statistics and detail the essential aspects of the algebraic theory for anyons. This chapter is completed by a list of data for the anyonic theories, which are of major interest for this thesis.

2.1 Quantum mechanics in two dimensions

As mentioned in the previous chapter, the exotic exchange statistics triggers the general interest in anyons for the purpose of topological quantum computing. To illustrate this, let us consider the quantum mechanics of identical particles. Consider two identical particles in Figure 2.1. One particle is moved counter-clockwise around the other along the path γ . This process corresponds to a double-exchange of the two particles. In dimensions larger than two, the path γ can be contracted to a point and as the action of the exchange only depends on the homotopy-class of the path, the double exchange of two particles acts as the identity. This already tells us that the phase of the wave function, which is the consequence of a single exchange of the two particles, can only be ± 1 . The positive sign appears, if particles are bosons, the negative one for fermions. In two dimensions, the path γ is not contractible to a point, thus the above argumentation does not hold. In this case, it is instructive to consider a $(2 + 1)$ -dimensional world-line picture, where the third dimension represents time. Following the world lines during the encircling process, we see that these become braided. These braids cannot be removed by smooth variations of the world lines with fixed end-points and thus configurations of braided or unbraided world lines are in general not equivalent. As a consequence, if any two configurations represent linearly dependent states, the single exchange may

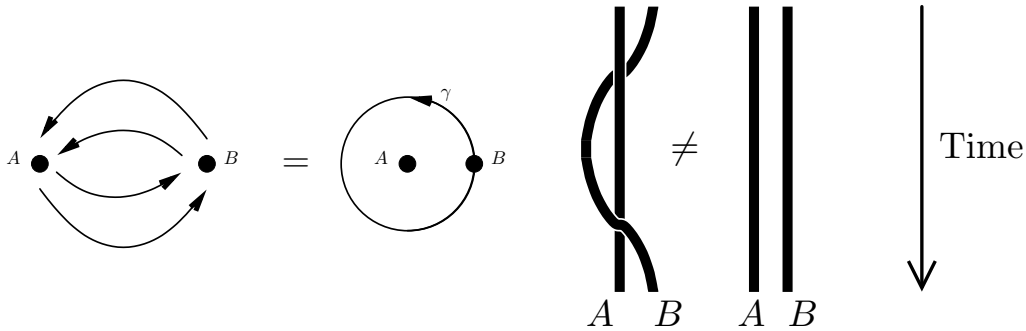


FIGURE 2.1: Braiding of two particles. The double-exchange of two particles is equivalent to move one particle around the other one. On the left-hand side, we see the encircling process from the top. On the right-hand side, we trace the world lines of the two particles during the encircling as seen from the front. The additional dimension represents the time. In two spatial dimensions, the encircling and thus the double exchange is not equivalent to the identity, as the world lines become braided during the process.

yield any phase $e^{i\theta}$ (whence the name “any-phase-on”=anyon) and not only $\theta = 0, \pi$ as in three dimensions. If both configurations represent linearly independent states, then the exchange can even yield unitary transformations in the subspace spanned by these configurations. In the former case, the anyons are called Abelian as a different order of exchanges yields the same exchange-phase in the end. In the latter, the anyons are called non-Abelian as the successive application of unitary transformations does not commute in general.

The concept of these non-trivial exchanges for N anyons is formulated by the braid group \mathcal{B}_N [108]. Defining the generators $\{\sigma_i\}_{i=1,\dots,N}$, where σ_i denotes the counter-clockwise exchange of the particles i and $i + 1$, the defining properties of the braid group, also depicted in Figure 2.2, read

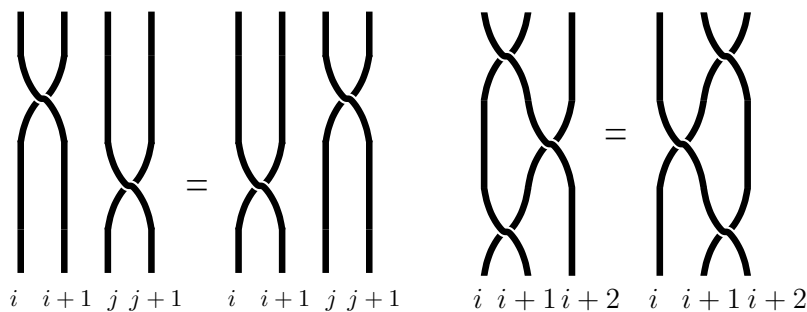


FIGURE 2.2: Pictorial presentation of the defining properties of the braid group in terms of braiding world lines. The left part represents Eq. (2.1), which states that the order of braidings of distinct world lines does not matter. The right picture represents the condition (2.2) stating that different exchanges of adjacent world lines are independent of the order as long as the world lines do not become braided with each other.

$$\sigma_i \sigma_j = \sigma_j \sigma_i \text{ for } |i - j| \geq 2 \tag{2.1}$$

$$\sigma_i \sigma_{i+1} \sigma_i = \sigma_{i+1} \sigma_i \sigma_{i+1} \quad \text{for } 1 \leq i \leq N-1. \quad (2.2)$$

States transforming according to one-dimensional representations of the braid group obey Abelian anyonic statistics, whereas non-Abelian anyons transform according to higher-dimensional irreducible representations of \mathcal{B}_N .

2.2 Algebraic theory of anyons

However, the general framework of anyons requires more theoretical input. The mathematical framework for an algebraic theory of anyons has been discussed, e.g., in different contexts such as conformal field theory [109], topological quantum field theory and modular tensor categories [11, 110], and topological quantum computation [53]. Here, we consider unitary modular tensor categories [11, 56, 110]. In the following, we list the main ingredients of an anyonic theory needed within this thesis. More details can be found e.g. references mentioned above.

Each anyonic theory requires a label set \mathcal{F} with a finite number of $(N+1)$ elements. These labels denote different quantum “numbers”, to which we refer also as particle types. The label set can be e.g. the set of group elements of a finite group [28] or irreducible representations of a (quantum) group [94]. A label set has to contain a distinguished or trivial element denoted by $\mathbf{1}$ in the following.

For completeness, let us mention that in general, one has the duality map:

$$\hat{\cdot}: \mathcal{F} \rightarrow \mathcal{F}, \quad a \mapsto \hat{a} \quad \text{with } \hat{\mathbf{1}} = \mathbf{1}. \quad (2.3)$$

Labels with $\hat{a} = a$ are called self-dual. As we are within this thesis mostly concerned with theories, which only contain self-dual labels, we assume self-duality from now on if not mentioned otherwise.

2.2.1 Fusion

The label set is endowed with an algebraic structure $\otimes: \mathcal{F} \times \mathcal{F} \rightarrow \mathcal{F}$. For $a, b \in \mathcal{F}$:

$$a \otimes b = \sum_{c \in \mathcal{F}} N_{ab}^c c, \quad (2.4)$$

with N_{ab}^c being non-negative integer. We have $\sum_c N_{ab}^c > 0 \forall a, b$, i.e. there is at least one fusion outcome for every possible fusion process. This algebraic structure is in the

context of conformal field theories also known as operator product expansion [111]. For notational convenience, we introduce

$$\delta_{a,b,c} = \begin{cases} 1 & \text{if } N_{ab}^c \neq 0 \\ 0 & \text{otherwise} \end{cases}. \quad (2.5)$$

If $N_{ab}^c = \delta_{a,b,c} \forall a, b, c$, the theory is called multiplicity-free. We will deal here only with multiplicity-free theories.

The fusion algebra represents the way, how to sum up quantum numbers. One example is the addition of angular momenta $\frac{1}{2} \otimes \frac{1}{2} = 0 \oplus 1$, i.e. two spin- $\frac{1}{2}$ representations fuse to a spin 0 and a spin 1 object.¹ In particular, fusion with the trivial particle **1** yields the same particle type, i.e.

$$N_{\mathbf{1}b}^c = N_{b\mathbf{1}}^c = \delta_{b,c}. \quad (2.6)$$

One can represent the fusion process pictorially as in the left-hand side of Figure 2.3, where the particles a and b fuse to the particle c .

If there is more than one c with $N_{aa}^c \neq 0$, the particle a has several possible fusion outcomes when fused with itself. Thus the sum of the corresponding quantum numbers is not unique and in the resulting degenerate Hilbert space spanned by these different states, exchange of these particles will be governed by non-Abelian exchange statistics.

Let us mention already here that if $N_{aa}^{\mathbf{1}} \neq 0$, the particle a is said to have the property referred to as partial trivial self-monodromy in Ref. [19].

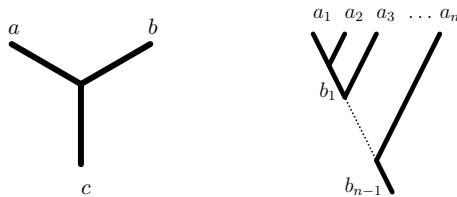


FIGURE 2.3: Diagrammatic representation of fusion processes. On the left-hand side, a single fusion process is depicted. The single vertex is invariant under the exchange of the labels a , b , and c . This implies that $N_{ab}^c = N_{bc}^a = N_{ca}^b$. The fusion diagram can also be read as splitting diagram, if the time direction is reversed [53]. On the right-hand side, concatenated fusion is depicted.

For a general fusion process, the rotation symmetry of the fusion vertex already tells us that $N_{ab}^c = N_{bc}^a = N_{ca}^b$. Together with (2.6), we see that there is a unique way to fuse two labels a to obtain the trivial label, i.e. $N_{aa}^{\mathbf{1}} = 1$.

¹Note that the group $SU(2)$, whose representations are used in this example, has infinitely many representations and thus does not yield a suitable anyonic model. However, all fusion algebras presented within this thesis can be derived as so-called quantum deformations of $SU(2)$.

By successive application of the fusion rules, we can now add up all quantum numbers as e.g. shown in Figure 2.3. Note that different fusion trees form an orthogonal basis of the Hilbert space given by the particles that fuse. The fusion trees are also known as Bratelli diagrams [110].

It is physically intuitive to require the outcome of the summation of quantum numbers to be independent of the order of the summation. This is equivalent to imposing associativity of the fusion algebra, i.e.

$$(a \otimes b) \otimes c = a \otimes (b \otimes c). \quad (2.7)$$

Equation (2.7) states that the two ways of fusing three particles to obtain a fourth one are equivalent. This means that the corresponding states are connected by a unitary transformation so that one particular fusion tree for the first way can be expressed by a linear superposition of the fusion trees of the second way. In the pictorial representation this corresponds to the so-called F -move depicted as

$$\left| \begin{array}{c} a \quad b \quad c \\ \diagdown \quad \diagup \\ e \\ \diagup \quad \diagdown \\ d \end{array} \right\rangle = \sum_f F_{cdf}^{abe} \left| \begin{array}{c} a \quad b \quad c \\ \diagdown \quad \diagup \\ f \\ \diagup \quad \diagdown \\ d \end{array} \right\rangle. \quad (2.8)$$

The coefficients F_{cdf}^{abe} are known as F -symbols, crossing-symmetries, or $6j$ -symbols. As notational convention within this thesis, we use the notation of Ref. [56] for the F -symbols. Let us note here that

$$F_{cdf}^{abe} \propto \delta_{a,b,e} \delta_{c,d,e} \delta_{a,d,f} \delta_{b,c,f}, \quad (2.9)$$

so that an F -move acting onto a state fulfilling the branching rules at the two vertices leads to a superposition of states, which also fulfill the branching rules on both vertices. Let us note that there are several symmetries relating the values of different F -symbols. For example, fusion trees, which can be obtained from the one in (2.8) by permuting the position of the different labels, yield the same numerical values in the superposition of the right-hand side of (2.8). These symmetries can be used to simplify the actual calculations performed in the following.

Let us note here that we consider within this thesis only theories, for which the F -symbols F_{cdf}^{abe} are real. This fact assures the hermiticity of the Hamiltonians discussed in Chapter 3.

In order to assure consistency of the fusion algebra, i.e. the independence of the actual order of fusion if more than three particles are involved, we consider the diagram depicted

in Figure 2.4. Consistency of the fusion algebra is equivalent to the requirement that the F -moves are defined such that this diagram commutes. This constrains the possible

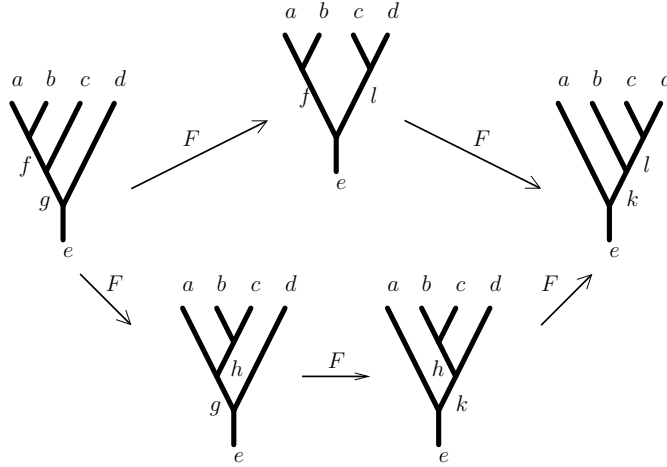


FIGURE 2.4: Successive F -moves along the upper and lower path in the diagram yield the same configuration. The F -symbols are defined such that the diagram commutes, i.e. the actual sequence of F -moves applied does not matter, as long as the same fusion diagram is obtained.

sets of F -symbols to be solutions of the so-called pentagon equations

$$\sum_h F_{cgh}^{abf} F_{dek}^{ahg} F_{dkl}^{bch} = F_{del}^{fcg} F_{lek}^{abf}. \quad (2.10)$$

The solutions of (2.10) correspond to tensor categories [94]. Note that no further condition is needed to yield consistency of the F -moves. Let us mention that for each anyon type a , the quantum dimension

$$d_a = \frac{1}{|F_{aa\mathbf{1}}^{a\mathbf{1}}|} \quad (2.11)$$

plays a distinguished role. If we have for example the labels a , b , and c with $a \otimes b = \sum_c N_{ab}^c c$, then the quantum dimensions d_a , d_b , and d_c fulfill the same equation, if the labels are replaced by them:

$$d_a d_b = \sum_c N_{ab}^c d_c. \quad (2.12)$$

In particular, anyons, which can fuse with themselves to more than one particle type and thus have non-Abelian exchange statistics, have a quantum dimension larger than one.

2.2.2 Braiding

We have seen above that non-trivial braiding is one of the defining properties of anyons. If we fix the possible particle positions, we represent the braiding of two anyons by crossing their world-lines as in Fig. 2.2, i.e.

$$R_{ab} = \begin{array}{c} \diagup \\ \diagdown \\ a \quad b \end{array} \quad (2.13)$$

The corresponding unitary transformation is called R -move and can be written in terms of the fusion trees as

$$\left| \begin{array}{c} b \quad a \\ \diagdown \quad \diagup \\ c \end{array} \right\rangle = R_c^{ab} \left| \begin{array}{c} b \quad a \\ \diagup \quad \diagdown \\ c \end{array} \right\rangle, \quad (2.14)$$

so that we can express the exchange of two particle with labels a and b as in Ref. [95] via

$$R_{ab} = \sum_c \sqrt{\frac{d_c}{d_a d_b}} R_c^{ab} \begin{array}{c} b \quad a \\ \diagup \quad \diagdown \\ c \\ \diagdown \quad \diagup \\ a \quad b \end{array}. \quad (2.15)$$

As the trivial label corresponds to the vacuum and braiding with the vacuum does not change the state, we have

$$R_c^{a1} = R_c^{1b} = 1. \quad (2.16)$$

The R -moves are representations of the braid group and thus fulfill (2.1) and (2.2). However, to be compatible with the F -moves, we can see in Figure 2.5 that the R -moves have to fulfill additionally the so-called hexagon equations

$$\sum_f F_{bdf}^{cae} R_d^{cf} F_{cdg}^{abf} = R_e^{ca} F_{bdg}^{ace} R_g^{cb} \quad (2.17)$$

$$\sum_f F_{bdf}^{cae} \left(R_d^{fc}\right)^{-1} F_{cdg}^{abf} = \left(R_e^{ac}\right)^{-1} F_{bdg}^{ace} \left(R_g^{bc}\right)^{-1} \quad (2.18)$$

The crossing symmetry and the braiding properties of an anyonic theory are thus related by the hexagon equations, so that fusion and braiding are not independent processes. Let us finally note that the pentagon and hexagon equations are homogeneous equations, so e.g. the F -symbols yielding different theories are in general defined up to multiplicative

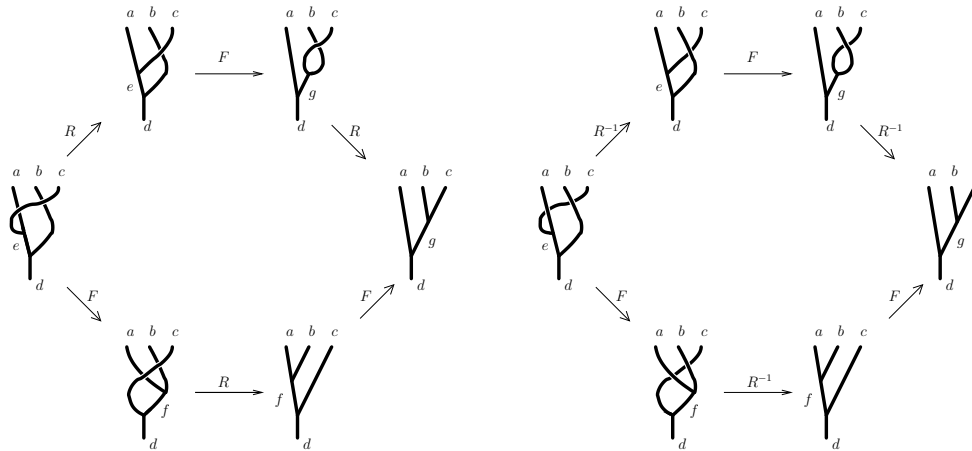


FIGURE 2.5: The sequences of R - and F -moves shown lead to the same Bratelli diagram. To be consistent, the upper and the lower paths in the diagrams have to commute. This imposes the so-called hexagon equations for the R -symbols and their inverses (2.18).

factors. To remove this ambiguity, we choose the gauge [56]

$$F_{j\mathbf{1}}^{ijk} = \delta_{i,j,k} \sqrt{\frac{d_k}{d_i d_j}} \quad (2.19)$$

without loss of generality.

2.2.3 Twists and spins

Although the exchange statistics of elementary excitations in two spatial dimensions is richer than in higher dimensions, one can introduce for each particle a the so-called twists θ_a , which are as in the higher-dimensional case linked to the particle spin s_a via the spin-statistics theorem [112]

$$\theta_a = e^{2\pi i s_a}. \quad (2.20)$$

It can be interpreted as the global phase picked up if one rotates the corresponding particle state about 2π or as the result of a double-exchange of two identical particles as in shown in Fig. 2.1. For bosons b we thus have $\theta_b = 1$, for fermions f the twist is given by $\theta_f = -1$.

The twist is also referred to as self-monodromy [19]. We will refer occasionally also to particles a with trivial self-monodromy, i.e. $\theta_a = 1$, as bosons [19], although these particles might have non-trivial braiding properties when braided around other particles.

Let us note here that the trivial particle $\mathbf{1}$ always has $\theta_{\mathbf{1}} = 1$, so that it can be interpreted as a boson.

2.2.4 Modular S -matrix

To complete our list of ingredients of anyonic models considered in this work, we discuss the topological or modular S -matrix. As already mentioned in the previous chapter, one may want to interpret an anyonic label as a flux. Fluxes through surfaces are measured by transporting an “test”-anyon along the contour of the surface. The corresponding information is encoded in the S -matrix. If an anyon of type a is transported around an anyon of type b , the resulting state is given by

$$\left| \begin{array}{c} b \\ \text{loop} \\ a \end{array} \right\rangle = \frac{S_{ab}}{S_{1b}} \left| \begin{array}{c} b \\ \text{loop} \\ 1 \end{array} \right\rangle. \quad (2.21)$$

An anyonic theory is called modular if the S -matrix is invertible. Thus, one can measure all appearing fluxes by transporting (an appropriate superposition of) anyons along the boundary of the corresponding surface. There are some particular properties of the S -matrix elements. For example, the S -matrix is symmetric. Additionally, one has $S_{0a} \sim d_a$ and the first row of the S -matrix is normalized such that $\sum_a (S_{0a})^2 = 1$. The normalization factor $\mathcal{D} = \sqrt{\sum_a d_a^2}$ is the so-called total quantum dimension [95] or total quantum order [102].

2.3 Doubling of a theory

From given anyonic theories, one can construct more complicated ones. One particular way is to consider instead of a fusion algebra \mathcal{F} its quantum double version given by $D(\mathcal{F}) = \{(a, b), a, b \in \mathcal{F}\}$. The components of the labels are referred to as left- and right-handed, respectively.

In a standard construction, the quantum double $D(\mathcal{F})$ inherits its algebraic structure from \mathcal{F} by simply taking the product of corresponding undoubled quantities, as e.g. $N_{(a_L, a_R), (b_L, b_R)}^{(c_L, c_R)} = N_{a_L, b_L}^{c_L} N_{a_R, b_R}^{c_R}$ the fusion algebra. A fusion vertex for a doubled theory is depicted in Figure 2.6.

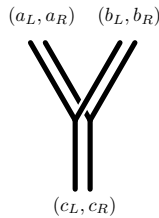


FIGURE 2.6: The fusion vertex of a doubled theory can be understood as independent fusion of the left- and right-handed components of the appearing labels.

This is equivalent to the statement that left-handed and right-handed sectors are independent of each other, i.e. the left-handed component does not have an impact on the braiding or the fusion of the right-handed component and vice versa. The different chiralities manifest themselves most prominently in the particle twist, as

$$\theta_{(a,b)} = \theta_a \theta_b^{-1} = \theta_{(b,a)}^{-1}. \quad (2.22)$$

However, there are also other ways of doubling a theory than the standard one shown above. Note that these non-trivial doubled theories arise also in the context of toric code models [28]. The most prominent example is the doubled theory $D(\mathbb{Z}_2)$. In this example modularity of the doubled theory is achieved by introducing additionally a non-trivial braiding of left- and right-handed components. The label set is given by $\mathcal{F}_{D(\mathbb{Z}_2)} = \{\mathbf{1}, \mathbf{e}, \mathbf{m}, \boldsymbol{\varepsilon}\}$ and its connection to the corresponding \mathbb{Z}_2 -theory with $\mathcal{F}_{\mathbb{Z}_2} = \{\mathbf{1}, -\mathbf{1}\}$ can be inferred from

$$\begin{aligned} \mathbf{1}_{D(\mathbb{Z}_2)} &= (\mathbf{1}_{\mathbb{Z}_2}, \mathbf{1}_{\mathbb{Z}_2}), & \mathbf{e} &= (-\mathbf{1}_{\mathbb{Z}_2}, \mathbf{1}_{\mathbb{Z}_2}), \\ \mathbf{m} &= (\mathbf{1}_{\mathbb{Z}_2}, -\mathbf{1}_{\mathbb{Z}_2}), & \boldsymbol{\varepsilon} &= (-\mathbf{1}_{\mathbb{Z}_2}, -\mathbf{1}_{\mathbb{Z}_2}). \end{aligned} \quad (2.23)$$

The braidings of the undoubled theory are all trivial, i.e. $S_{ab} = 1$ for $a, b \in \{\mathbf{1}, -\mathbf{1}\}$, so that this theory is not modular. By introducing the so-called mutual semionic statistics, i.e. $S_{-\mathbf{1}_L, -\mathbf{1}_R} = -1$, we obtain a modular doubled theory (cf. Section 2.4). This way of doubling a theory can usually be found in the context of lattice gauge theories [28].

Let us finally mention some special labels of a doubled theory: the labels, whose left- and right-handed sectors are identical, i.e.

$$\tilde{a} = (a, a) \quad (2.24)$$

are called achiral particles, as these do not have a particular chirality. In particular, their twist is always trivial, i.e. $\theta_{\tilde{a}} = 1$ [19]. We drop the $\tilde{}$ whenever it is clear from the context whether we are referring to the doubled or undoubled theory.

2.4 List of theories

To conclude, the necessary ingredients of an anyonic theory required for this thesis are given by the fusion algebra \mathcal{F} , the F -symbols, the braiding properties encoded in the twists, the R -symbols, and the S -matrix. We did not discuss above all relations between these objects as e.g. the Verlinde-formula [53]. For a more complete discussion, we refer to e.g. Refs. [11, 30, 53, 94, 95, 102].

In the following we list the data of theories, i.e. the fusion algebras, F - and R -symbols, and the S -matrix, which are of interest within the thesis. This data can be found e.g. in Refs. [95, 102]. Note that the considered fusion algebras can all be related in some fashion to quantum deformations of $SU(2)$. However, although the fusion algebras are identical, there exist several solutions for the F - and R -symbols. Thus the F -symbols used within this work do not necessarily coincide with the ones for $SU(2)_k$ given e.g. in Ref. [113].

We will concentrate within this thesis on the theory of semions as well as the $D(\mathbb{Z}_2)$ theory as examples for Abelian anyons and on Fibonacci- and Ising-anyons as the simplest examples for non-Abelian anyons. Let us mention for completeness that there are other modular theories with three labels, which harbor fusion algebras distinct from those of the previously mentioned theories: the theories denoted in Ref. [102] by \mathbb{Z}_3 and $(A_1, 5)_2$. Their study, although completely analogous to the study of the other models, is beyond the scope of this thesis, as we aim here to illustrate the physics in the simplest possible models.

The following list is organized as follows: For each theory, we give first the label set, the quantum dimensions and the twists. Then the fusion algebra is shown in tabular form. Allowed fusion vertices are depicted up to rotations. We remind that $\delta_{a,b,c} = 1$ if the fusion vertex on left-hand side of Figure 2.3 is allowed and $\delta_{a,b,c} = 0$ otherwise. We give the F -symbols, for which $F_{cd}^{abc} \neq \delta_{a,b,e} \delta_{c,d,e} \delta_{a,d,f} \delta_{b,c,f}$, as well as the R -symbols, for which $R_a^{bc} \neq \delta_{a,b,c}$. For the topological S -matrix, we denote the matrix elements for labels ordered in the same way as given in the label set.

2.4.1 Semions

Label set: $\{\mathbf{1}, \mathbf{s}\}$

Quantum dimensions: $d_{\mathbf{1}} = 1, d_{\mathbf{s}} = 1$

Twists: $\theta_{\mathbf{1}} = 1, \theta_{\mathbf{s}} = i$

Fusion algebra:

| | | |
|--------------|--------------|--------------|
| \otimes | $\mathbf{1}$ | \mathbf{s} |
| $\mathbf{1}$ | $\mathbf{1}$ | \mathbf{s} |
| \mathbf{s} | \mathbf{s} | $\mathbf{1}$ |

Fusion vertices:

$$\left\{ \begin{array}{c} \mathbf{1} \quad \mathbf{1} \\ \diagdown \quad \diagup \\ \mathbf{1} \end{array}, \begin{array}{c} \mathbf{s} \quad \mathbf{s} \\ \diagdown \quad \diagup \\ \mathbf{1} \end{array} \right\} \quad (2.25)$$

Non-trivial F -symbols:

$$F_{\mathbf{s}\mathbf{s}\mathbf{1}}^{\mathbf{s}\mathbf{s}\mathbf{1}} = -1$$

Modular S -matrix:

$$S = \frac{1}{\sqrt{2}} \begin{pmatrix} 1 & 1 \\ 1 & -1 \end{pmatrix}$$

Non-trivial R -symbols:

$$R_{\mathbf{1}}^{\mathbf{s}\mathbf{s}} = i$$

Let us note that the fusion algebra is the same as the multiplication table of the group \mathbb{Z}_2 . However, the corresponding theory is non-modular and for all F -symbols we have $F_{cdf}^{abe} = \delta_{a,b,e}\delta_{c,d,e}\delta_{a,d,f}\delta_{b,c,f}$.

2.4.2 Fibonacci

Label set: $\{\mathbf{1}, \tau\}$

Quantum dimensions: $d_{\mathbf{1}} = 1$, $d_{\tau} = \varphi$, where $\varphi = \frac{1+\sqrt{5}}{2}$ is the golden ratio.

Twists: $\theta_{\mathbf{1}} = 1$, $\theta_{\tau} = e^{\frac{4\pi i}{5}}$

Fusion algebra:

| | | |
|--------------|--------------|--------------------------|
| \otimes | $\mathbf{1}$ | τ |
| $\mathbf{1}$ | $\mathbf{1}$ | τ |
| τ | τ | $\mathbf{1} \oplus \tau$ |

Fusion vertices:

$$\left\{ \begin{array}{c} \mathbf{1} \quad \mathbf{1} \\ \diagdown \quad \diagup \\ \mathbf{1} \end{array}, \begin{array}{c} \tau \quad \tau \\ \diagdown \quad \diagup \\ \mathbf{1} \end{array}, \begin{array}{c} \tau \quad \tau \\ \diagdown \quad \diagup \\ \tau \end{array} \right\} \quad (2.26)$$

Non-trivial F -symbols:

Modular S -matrix:

Non-trivial R -symbols:

$$F_{\tau\tau\mathbf{1}}^{\tau\tau\mathbf{1}} = \varphi^{-1}, F_{\tau\tau\tau}^{\tau\tau\mathbf{1}} = \varphi^{-1/2}, \quad S = \frac{1}{\sqrt{1+\varphi^2}} \begin{pmatrix} 1 & \varphi \\ \varphi & -1 \end{pmatrix} \quad R_{\mathbf{1}}^{\tau\tau} = e^{-\frac{4\pi i}{5}}, R_{\tau}^{\tau\tau} = e^{\frac{3\pi i}{5}}.$$

$$F_{\tau\tau\mathbf{1}}^{\tau\tau\tau} = \varphi^{-1/2}, F_{\tau\tau\tau}^{\tau\tau\tau} = -\varphi^{-1}.$$

Let us mention that the theory of Yang-Lee anyons (the Galois-conjugate of the theory of Fibonacci anyons [66]) can be obtained by $\varphi \mapsto -\frac{1}{\varphi}$. However, this theory is not unitary, so we do not consider it here.

Note that the Fibonacci theory can be obtained by only considering the subalgebra of $SU(2)_3$ formed by the integer labels [57].

2.4.3 Ising

Label set: $\{\mathbf{1}, \sigma, \psi\}$

Quantum dimensions: $d_{\mathbf{1}} = 1$, $d_{\sigma} = \sqrt{2}$, $d_{\psi} = 1$

Twists: $\theta_{\mathbf{1}} = 1$, $\theta_{\sigma} = e^{\frac{\pi i}{8}}$, $\theta_{\psi} = -1$

Fusion algebra:

| | | | |
|--------------|--------------|--------------------------|--------------|
| \otimes | $\mathbf{1}$ | σ | ψ |
| $\mathbf{1}$ | $\mathbf{1}$ | σ | ψ |
| σ | σ | $\mathbf{1} \oplus \psi$ | σ |
| ψ | ψ | σ | $\mathbf{1}$ |

Fusion vertices:

$$\left\{ \begin{array}{c} \mathbf{1} \quad \mathbf{1} \\ \diagdown \quad \diagup \\ \mathbf{1} \end{array}, \begin{array}{c} \sigma \quad \sigma \\ \diagdown \quad \diagup \\ \mathbf{1} \end{array}, \begin{array}{c} \sigma \quad \sigma \\ \diagdown \quad \diagup \\ \psi \end{array}, \begin{array}{c} \psi \quad \psi \\ \diagdown \quad \diagup \\ \mathbf{1} \end{array} \right\} \quad (2.27)$$

Non-trivial F -symbols:Modular S -matrix:Non-trivial R -symbols:

$$\begin{aligned}
F_{\sigma\sigma\mathbf{1}}^{\sigma\sigma\mathbf{1}} &= \frac{1}{\sqrt{2}}, F_{\sigma\sigma\psi}^{\sigma\sigma\mathbf{1}} = \frac{1}{\sqrt{2}}, \\
F_{\sigma\sigma\mathbf{1}}^{\sigma\sigma\psi} &= \frac{1}{\sqrt{2}}, F_{\sigma\sigma\psi}^{\sigma\sigma\psi} = -\frac{1}{\sqrt{2}}, \\
F_{\psi\sigma\sigma}^{\psi\sigma\sigma} &= -1, F_{\sigma\psi\sigma}^{\sigma\psi\sigma} = -1.
\end{aligned}
\quad S = \frac{1}{2} \begin{pmatrix} 1 & \sqrt{2} & 1 \\ \sqrt{2} & 0 & -\sqrt{2} \\ 1 & -\sqrt{2} & 1 \end{pmatrix}
\quad \begin{aligned}
R_{\mathbf{1}}^{\sigma\sigma} &= e^{-\frac{\pi i}{8}}, R_{\mathbf{1}}^{\psi\psi} = -1, \\
R_{\sigma}^{\sigma\psi} &= R_{\sigma}^{\psi\sigma} = e^{-\frac{\pi i}{8}}, \\
R_{\psi}^{\sigma\sigma} &= e^{\frac{3\pi i}{8}}.
\end{aligned}$$

Let us remark here, that the fusion algebra of Ising anyons coincide with the one of $SU(2)_2$. The major difference between these two theories is given by the different spins of the σ -particle as well different braidings elements involving this particle [102].

2.4.4 Toric Code

Label set: $\{\mathbf{1}, e, m, \varepsilon\}$ Quantum dimensions: $d_{\mathbf{1}} = 1, d_e = 1, d_m = 1, d_{\varepsilon} = 1$ Twists: $\theta_{\mathbf{1}} = 1, \theta_e = 1, \theta_m = 1, \theta_{\varepsilon} = -1$

Fusion algebra:

Fusion vertices:

| | | | | |
|---------------|---------------|---------------|---------------|---------------|
| \otimes | $\mathbf{1}$ | e | m | ε |
| $\mathbf{1}$ | $\mathbf{1}$ | e | m | ε |
| e | e | $\mathbf{1}$ | ε | m |
| m | m | ε | $\mathbf{1}$ | e |
| ε | ε | m | e | $\mathbf{1}$ |

$$\left\{ \begin{array}{c} \mathbf{1} \quad \mathbf{1} \\ \diagdown \quad \diagup \\ \mathbf{1} \end{array} \right\}, \quad \left\{ \begin{array}{c} e \quad m \\ \diagdown \quad \diagup \\ \varepsilon \end{array} \right\}, \quad \left\{ \begin{array}{c} a \quad a \\ \diagdown \quad \diagup \\ \mathbf{1} \end{array} \right\} \quad (2.28)$$

$a \in \{e, m, \varepsilon\}$.

Non-trivial F -symbols:Modular S -matrix:Non-trivial R -symbols:

$$\begin{aligned}
\text{none} \quad S &= \frac{1}{2} \begin{pmatrix} 1 & 1 & 1 & 1 \\ 1 & 1 & -1 & -1 \\ 1 & -1 & 1 & -1 \\ 1 & -1 & -1 & 1 \end{pmatrix} \quad \begin{aligned}
R_{\mathbf{1}}^{ee} &= R_{\mathbf{1}}^{mm} = -R_{\mathbf{1}}^{\varepsilon\varepsilon} = 1, \\
R_{\varepsilon}^{em} &= -R_{\varepsilon}^{me} = 1, \\
R_e^{\varepsilon m} &= -R_e^{m\varepsilon} = 1, \\
R_m^{e\varepsilon} &= -R_m^{\varepsilon e} = 1.
\end{aligned}
\end{aligned}$$

This theory is the most simple doubled theory presented in Section 2.3, which can be obtained by doubling either the semion theory or the \mathbb{Z}_2 with additional non-trivial braiding relations. It also appears in the context of \mathbb{Z}_2 lattice gauge theories [28].

2.5 Chapter Summary

Within this chapter, we introduced the notion of anyons as particles with non-trivial braiding statistics in two-dimensional quantum systems.

Additionally, we presented very briefly the different ingredients for an algebraic theory of anyons, which is given here as a unitary, modular tensor category. These ingredients comprise the fusion of anyons, their self-statistical properties expressed in terms of their spin, as well their mutual statistical properties expressed by the braid-operators R . We additionally discussed the modular S -matrix, which allows to treat not only planar graphs like the fusion trees but also more involved structures.

We emphasize that this discussion is not complete at all, as we did not mention e.g. the various interplays between these different properties such as the Verlinde formula [53]. So we direct the interested reader to other works [11, 30, 53, 94, 95, 102].

The doubled theories represent a particularly simple way to construct more complex anyonic theories from simpler ones. Let us emphasize here the fact that within doubled theories, we have always labels with trivial spin, i.e. their twists equal 1. These particles, which are the generalizations of bosons in the anyonic context, play a key role in the topological symmetry breaking discussed in Chapter 5.

In the following, we shall use the ingredients introduced in this chapter to construct models harboring topologically ordered ground states as well as anyonic excitations.

String-net models

*Whatever one man is capable of conceiving,
other men will be able to achieve.*
- Jules Verne -

In this chapter, we present the microscopic models that are at the heart of this study. As we are interested in phase transitions out of topologically ordered phases, we investigate the phase diagram of a perturbed lattice model, which is known to harbor topological order.

As a starting point, we consider the string-net Hamiltonian presented by Levin and Wen [56]. The unperturbed model is exactly solvable and thus one is able to describe its ground state(s) and its excitations. These turn out to be Abelian or non-Abelian anyons depending on the particular anyonic theory used to construct the model.

The first part of this chapter is dedicated to practical insights of how to describe the eigenstates of the Levin-Wen model in terms of fluxes, which emerge from the microscopic degrees of freedom due to the particular choice of the underlying anyonic theory.

In the second part, we add a local term to the Hamiltonian in the same fashion as in Refs. [69, 70, 74, 78, 86]. We focus on the case of two-dimensional systems to investigate phase transitions driven by the interplay of the topological order and a local perturbation. We detail how to describe this type of models on different topologies and also for the different anyonic theories, namely the semions, Fibonacci and Ising anyons.

3.1 The Levin-Wen Hamiltonian H_{LW}

To discuss the Hamiltonian H_{LW} introduced by Levin and Wen [56], let us start with a general string-net Hamiltonian H_{SN} , which can also be seen as an analogue of the Hamiltonian of a lattice-gauge theory [28]. We will obtain finally the topological Hamiltonian

H_{LW} as an appropriate limit of H_{SN} .

3.1.1 String-net Hamiltonian H_{SN}

The string-net Hamiltonian can be defined on any trivalent graph. Here, we consider particular trivalent lattices on the surface of a sphere or a torus, i.e. on two-dimensional manifolds. We discuss these two cases considered in Section 3.1.4. However, as the main focus of this work is the two-dimensional hexagonal lattice depicted in Figure 3.1, we will illustrate the construction of the model for this example.

As in lattice-gauge models, the microscopic degrees of freedom reside on the links $\{e\}$ of the lattice.¹ These degrees of freedom can take the $(N + 1)$ values in the label set of a fusion algebra \mathcal{F} as introduced in Chapter 2. We refer to the basis of orthonormal product states given by

$$|\{\ell_e\}\rangle = \prod_e |\ell_e\rangle_e \quad (3.1)$$

as bond basis in the following. In pictorial representations, we color the link e according to its label ℓ_e as introduced in Section 2.4.

Within this basis, we construct the string-net model making in the following use of the different properties of the fusion algebra discussed in Section 2.2. Therefore, we define the general string-net Hamiltonian H_{SN} as

$$H_{\text{SN}} = -J_v \sum_v Q_v - J_p \sum_p B_p, \quad (3.2)$$

where the index v denotes the vertices of the considered lattice, the index p its plaquettes. We refer to Q_v as charge operator and to B_p as flux operator in analogy to lattice-gauge theories as in Ref. [28]. The action of the charge operator is defined as

$$Q_v \left| \begin{array}{c} \ell_1 \quad \ell_2 \\ \diagdown \quad / \\ \ell_3 \end{array} \right\rangle = \delta_{\ell_1, \ell_2, \ell_3} \left| \begin{array}{c} \ell_1 \quad \ell_2 \\ \diagdown \quad / \\ \ell_3 \end{array} \right\rangle, \quad (3.3)$$

where the $\delta_{\ell_1, \ell_2, \ell_3}$ is defined in (2.5). We see that the charge operator Q_v is diagonal in the bond basis. As its eigenvalues are 0 or 1, this operator is a projector. Thus it projects onto states $|\ell_1\rangle |\ell_2\rangle |\ell_3\rangle$, where ℓ_3 appears in the fusion product of the labels ℓ_1 and ℓ_2 . For $J_v > 0$ the excited states correspond to eigenvalue 0 of a Q_v and are referred to as a charge, whereas charge-free states are those, for which each vertex configuration in the lattice correspond to a fusion vertex of the theory.

¹In the following, we will use the terms bond, link, and edge homologically.

Thus for charge-free states, the fusion rules for the labels of \mathcal{F} translate to the so-called branching rules for the microscopic degrees of freedom. The name branching rules stems from the picture that for charge-free states the microscopic degrees of freedom constitute extended objects as strings of the same non-trivial label unless at some vertex this string branches into two strings, each carrying in general a different label. An example for this kind of state is depicted in Figure 3.1.

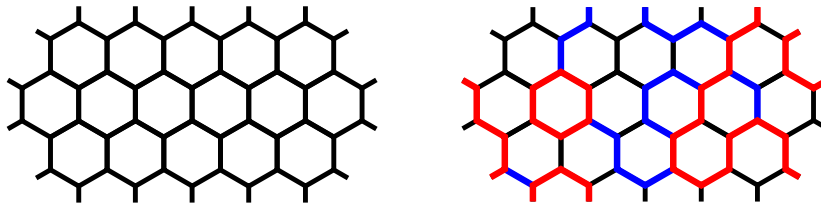


FIGURE 3.1: The string-net model is defined on the hexagonal lattice depicted on the left-hand side. The microscopic degrees of freedom are located on the edges of the lattice. In order to represent the different possible values, the microscopic degrees of freedom can take, we color the edges in the colors corresponding to the labels of the anyonic theory defined in Section 2.4. Due to the constraints induced by the charge operators, the different local degrees of freedom organize in the so-called string nets, for which one example is depicted on the right-hand side.

Let us remark here that in particular end points of strings, i.e. vertices in the lattice, where one string carrying a non-trivial label ends without branching, correspond for any anyonic theory to a charge.

This fact allows to draw analogies of this model with lattice-gauge theories, for which the strings of a given label corresponds to electric flux lines. In particular, strings carrying the trivial $\mathbf{1}$ label correspond to “neutral” flux lines, which represent the absence of non-trivial fluxes.

Let us state here that we have for the charge operators and flux operators

$$[Q_v, B_p] = 0 \quad \forall v, p. \quad (3.4)$$

We will discuss this property in more detail after having discussed the flux operators B_p . However, anticipating this result, we can already define the Levin-Wen Hamiltonian H_{LW} by

$$H_{\text{LW}} = \lim_{J_v \rightarrow \infty} H_{\text{SN}}. \quad (3.5)$$

In this limit, violations of the branching rules correspond to an infinite energy cost. As we are interested in the low-energy physics, we will discuss from now on only the charge-free sector. As the flux and charge operator commute, the action of the B_p preserves

the number of charges and can thus be without further restrictions discussed in the charge-free subspace.

3.1.2 The fat-lattice visualization

In order to discuss the flux operators, it is very useful to consider another representation of the involved degrees of freedom. This representation is the so-called fat-lattice [56]. It can be motivated by the seminal works of Turaev [110], which state that the Hilbert space of the Levin-Wen model for a given graph, i.e. the charge-free Hilbert space of the string-net model, can be linked to a topological field theory defined on the surface of a three-dimensional thickening of this graph. However, here we only use this visualization of a thickened graph, but consider a flux-line picture, where the flux lines run through the interior of the thickened links of the graph.

Let us remark here that this visualization as presented in Ref. [56] and within this chapter is close to the flux-line picture of a lattice-gauge theory. However, in the absence of charges, the picture of electric flux-lines of the lattice-gauge theory yields actually a Wilson-line representation [88, 98, 99].

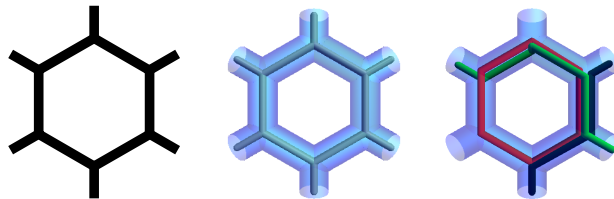


FIGURE 3.2: In the fat-lattice representation, the two-dimensional hexagonal lattice shown on the left is thickened to yield the tube network shown in the middle picture. Note that the third dimension is used as an auxiliary tool to represent the flux degrees of freedom introduced in (3.17). The original lattice is represented by the retraction skeleton located in the center of the tubes. The advantage of this representation is that it allows for a more flexible visualization of the action of the operators, which are introduced in the following. These operators can then be seen as injecting Wilson-loops into the fat lattice, which then leads to a network of string running through the fat lattice as depicted in the right-hand side.

Therefore, we consider, instead of the two-dimensional lattice, the three-dimensional tube-like network depicted in Figure 3.2. The original lattice can be recovered by considering the retraction skeleton of the three-dimensional structure. We represent now the degrees of freedom of the bonds by strings running through the tubes as illustrated in Figure 3.2. The strings are labeled (or colored) by labels of the fusion algebra \mathcal{F} .

It is obvious that this representation contains much more flexibility to represent a given state in the bond basis. Let us formalize a little bit more the rules we work with within the fat-lattice representation.

1. Consider strings only within the tubes.
2. Strings carry labels of \mathcal{F} .
3. Only closed loops are allowed (open strings correspond to charges at the end points).
4. Additional links carrying the label $\mathbf{1}$ can be introduced or removed within the tube without changing the state (neutral flux lines are invisible).
5. Strings can be smoothly deformed within the tubes.
6. F - and R -moves can be applied to transform the flux lines within the tubes.

The rules 5 and 6 can be motivated by the fact that smooth deformations of the flux lines shall not cause a difference in the resulting state if it is topologically ordered. Before discussing the relation between the fat-lattice representation and the bond basis, let us consider one example of how the above rules can be used to simplify the string configurations in the fat-lattice representation: therefore we recall the definition of the modular S-matrix (2.21), which can be also written as

$$\left| \begin{array}{c} b \\ \bigcirc \\ a \end{array} \right\rangle = \frac{S_{ab}}{S_{\mathbf{1}b}} \left| \begin{array}{c} b \\ \bigcirc \\ \mathbf{1} \end{array} \right\rangle. \quad (3.6)$$

So we can use the rules 4, 5, and 6 from above to transform string-net configurations within the tube network. For example, we can remove small loops within a tube via

$$\begin{aligned} & \begin{array}{c} k \\ | \\ i \quad j \\ | \\ l \end{array} \xrightarrow{F\text{-move}} \sum_m F_{ljm}^{jki} \begin{array}{c} k \\ | \\ m \quad j \\ | \\ l \end{array} \xrightarrow{\text{insert } \mathbf{1}\text{-loop}} \sum_m F_{ljm}^{jki} \begin{array}{c} k \\ | \\ m \quad j \\ | \\ l \\ \mathbf{1} \end{array} \\ & \stackrel{3.6}{=} \sum_m F_{ljm}^{jki} \underbrace{\frac{S_{j\mathbf{1}}}{S_{\mathbf{1}\mathbf{1}}}}_{d_j} \delta_{m,\mathbf{1}} \begin{array}{c} k \\ | \\ \mathbf{1} \quad j \\ | \\ l \end{array} \xrightarrow{\text{remove } \mathbf{1}\text{-labels}} F_{lj\mathbf{1}}^{jki} d_j \delta_{k,l} \begin{array}{c} k \\ | \\ | \\ | \\ l \end{array}. \quad (3.7) \end{aligned}$$

The term $\delta_{m,\mathbf{1}}$ appears after applying (3.6) as the label m shares a vertex with two $\mathbf{1}$ labels and thus we have necessarily $m = \mathbf{1}$ to yield a non-zero contribution since $\delta_{m,\mathbf{1},\mathbf{1}} = \delta_{m,\mathbf{1}}$. The term $\delta_{k,l}$ arises because we have $\delta_{k,\mathbf{1},l} = \delta_{k,l}$ for self-dual anyonic theories.

Due to the appearance of the $\delta_{k,l}$ in (3.7), we see that the branching and reunion of a string cannot change its label and thus the label is necessarily conserved along the string in the absence of a branching to distinct strings.

This fact allows us to relate the string network in the fat lattice to the bond basis. Therefore, one has to reduce several strings located in one tube to one string by inserting 1-strings and performing appropriate F -moves, e.g.

$$\begin{array}{c} \text{Y-junction with labels } a, b \end{array} = \begin{array}{c} \text{Y-junction with labels } a, b \text{ and a 1-string} \end{array} = \sum_c F_{bbc}^{a a 1} \begin{array}{c} \text{Y-junction with labels } a, b, c \end{array}. \quad (3.8)$$

In this example, this state will be represented in the bond basis by a superposition of the labels c for this bond.

To obtain in the end the retraction skeleton, the additional vertices introduced by contracting flux lines within a tube as in (3.8) now having the incident labels $\{a, b, c\}$ have to be removed. For this task one can proceed similar as in (3.7). In the end, we arrive from the fat lattice, through which the different strings run, to a superposition of different states represented only by the retraction skeleton, where the label ℓ_e of the unique string within a tube e corresponds one-to-one to the label ℓ_e located on the bond e in the bond basis.

Thus we see that the fat-lattice representation enables us to perform manipulations on the states in a graphical fashion.

3.1.3 The flux operator B_p

Before starting to discuss the action of the flux operator B_p in detail, let us here already give its action in the bond basis and then develop a more intuitive picture. We have [56]

$$B_p \left| \begin{array}{c} b \quad g \quad a \quad l \quad f \\ \text{hexagon } p \\ c \quad i \quad j \quad e \quad d \end{array} \right\rangle = \sum_{g', h', i', j', k', l'} \frac{d_{\mathbf{s}}}{\mathcal{D}^2} F_{sl'g'}^{a gl} F_{sg'h'}^{bhg} F_{sh'i'}^{c ih} F_{si'j'}^{d ji} F_{sj'k'}^{ekj} F_{sk'l'}^{flk} \left| \begin{array}{c} b \quad g' \quad a \quad l' \quad f \\ \text{hexagon } p \\ c \quad i' \quad j' \quad e \quad d \end{array} \right\rangle. \quad (3.9)$$

To understand this result, let us consider instead of the operator B_p the operator $B_p^{\mathbf{s}}$, which in the fat-lattice representation is given by

$$B_p^{\mathbf{s}} \left| \begin{array}{c} \text{hexagon } p \end{array} \right\rangle = \left| \begin{array}{c} \text{hexagon } p^{\mathbf{s}} \end{array} \right\rangle, \quad (3.10)$$

i.e. the operator $B_p^{\mathbf{s}}$ injects loops, which are labeled by \mathbf{s} , around the plaquette p .

The matrix elements of this operator can then be determined by the following counter-clockwise sequence of F -moves:

$$\begin{aligned}
\left\langle \begin{array}{c} b \quad g \quad a \quad l \quad f \\ \diagdown \quad \diagup \\ h \quad s \quad k \\ \diagup \quad \diagdown \\ c \quad i \quad j \quad e \\ d \end{array} \right\rangle &= \sum_{l'} F_{ssl'}^{ll1} \left\langle \begin{array}{c} b \quad g \quad a \quad l' \quad f \\ \diagdown \quad \diagup \\ h \quad s \quad k \\ \diagup \quad \diagdown \\ c \quad i \quad j \quad e \\ d \end{array} \right\rangle = \sum_{l',g'} F_{ssl'}^{ll1} F_{sl'g'}^{agl} \left\langle \begin{array}{c} b \quad g' \quad a \quad l' \quad f \\ \diagdown \quad \diagup \\ h \quad s \quad k \\ \diagup \quad \diagdown \\ c \quad i \quad j \quad e \\ d \end{array} \right\rangle \\
&= \sum_{l',g',h'} F_{ssl'}^{ll1} F_{sl'g'}^{agl} F_{sg'h'}^{bhg} \left\langle \begin{array}{c} b \quad g' \quad a \quad l' \quad f \\ \diagdown \quad \diagup \\ h' \quad s \quad k \\ \diagup \quad \diagdown \\ c \quad i \quad j \quad e \\ d \end{array} \right\rangle = \sum_{l',g',h',i'} F_{ssl'}^{ll1} F_{sl'g'}^{agl} F_{sg'h'}^{bhg} F_{sh'i'}^{cjh} \left\langle \begin{array}{c} b \quad g' \quad a \quad l' \quad f \\ \diagdown \quad \diagup \\ h' \quad s \quad k \\ \diagup \quad \diagdown \\ c \quad i' \quad j \quad e \\ d \end{array} \right\rangle \\
&= \sum_{l',g',h',i',j'} F_{ssl'}^{ll1} F_{sl'g'}^{agl} F_{sg'h'}^{bhg} F_{sh'i'}^{cjh} F_{si'j'}^{dji} \left\langle \begin{array}{c} b \quad g' \quad a \quad l' \quad f \\ \diagdown \quad \diagup \\ h' \quad s \quad k \\ \diagup \quad \diagdown \\ c \quad i' \quad j' \quad e \\ d \end{array} \right\rangle \\
&= \sum_{l',g',h',i',j',k'} F_{ssl'}^{ll1} F_{sl'g'}^{agl} F_{sg'h'}^{bhg} F_{sh'i'}^{cjh} F_{si'j'}^{dji} F_{sj'k'}^{ekj} \left\langle \begin{array}{c} b \quad g' \quad a \quad l' \quad f \\ \diagdown \quad \diagup \\ h' \quad s \quad k' \\ \diagup \quad \diagdown \\ c \quad i' \quad j' \quad e \\ d \end{array} \right\rangle \\
&= \sum_{l',g',h',i',j',k',l''} F_{ssl'}^{ll1} F_{sl'g'}^{agl} F_{sg'h'}^{bhg} F_{sh'i'}^{cjh} F_{si'j'}^{dji} F_{sj'k'}^{ekj} F_{sk'l''}^{flk} \left\langle \begin{array}{c} b \quad g' \quad a \quad l' \quad f \\ \diagdown \quad \diagup \\ h' \quad s \quad k' \\ \diagup \quad \diagdown \\ c \quad i' \quad j' \quad e \\ d \end{array} \right\rangle \\
&\stackrel{3.7}{=} \sum_{l',g',h',i',j',k',l''} F_{ssl'}^{ll1} F_{sl'g'}^{agl} F_{sg'h'}^{bhg} F_{sh'i'}^{cjh} F_{si'j'}^{dji} F_{sj'k'}^{ekj} F_{sk'l''}^{flk} F_{l'sg'}^{s'l''} d_{\mathbf{s}} \left\langle \begin{array}{c} b \quad g' \quad a \quad l' \quad f \\ \diagdown \quad \diagup \\ h' \quad s \quad k' \\ \diagup \quad \diagdown \\ c \quad i' \quad j' \quad e \\ d \end{array} \right\rangle. \tag{3.11}
\end{aligned}$$

Due to the normalization (2.19), we have

$$F_{ssl'}^{ll1} F_{l'sg'}^{s'l''} d_{\mathbf{s}} = \delta_{l',l''} \tag{3.12}$$

and thus the matrix elements of $B_p^{\mathbf{s}}$ simplifies to

$$\left\langle \begin{array}{c} b \quad g' \quad a \quad l' \quad f \\ \diagdown \quad \diagup \\ h \quad p \quad k' \\ \diagup \quad \diagdown \\ c \quad i' \quad j' \quad e \\ d \end{array} \right\rangle \left| B_p^{\mathbf{s}} \right| \left\langle \begin{array}{c} b \quad g \quad a \quad l \quad f \\ \diagdown \quad \diagup \\ h \quad p \quad k \\ \diagup \quad \diagdown \\ c \quad i \quad j \quad e \\ d \end{array} \right\rangle = \sum_{g',h',i',j',k',l'} F_{sl'g'}^{agl} F_{sg'h'}^{bhg} F_{sh'i'}^{cjh} F_{si'j'}^{dji} F_{sj'k'}^{ekj} F_{sk'l'}^{flk}. \tag{3.13}$$

Thus the operators $B_p^{\mathbf{s}}$ are twelve-link terms, which preserve the labels of the out-going links of plaquette p . Before constructing the flux-operator B_p from the $B_p^{\mathbf{s}}$, let us first discuss the commutation relation of the $B_p^{\mathbf{s}}$ and the charge operator:

$$[B_p^{\mathbf{s}}, Q_v] = 0 \quad \forall \mathbf{s}, p, v. \tag{3.14}$$

From (3.13), it is obvious that the matrix elements of B_p^s are proportional to F -symbols involving labels from the vertex neighboring the plaquette p . It results from (2.9) that the B_p^s act only non-trivially on plaquettes without neighboring charges, as otherwise the corresponding F -moves yield 0 as matrix element. Thus the B_p^s act only non-trivially within the charge-free eigenspace of the involved charge operators. Consequently, the operators B_p^s and Q_v commute with each other.

From the representation (3.10), it is also obvious that $[B_p^s, B_{p'}^{s'}] = 0 \forall s, s', p, p'$, as one can interchange, using (2.10), the order of the insertion of the different loops without changing the final result.

Let us mention here the fact that $B_p^1 = \mathbb{1}$ within the charge-free sector, as inserting a neutral flux line does not change the state of the system.

Finally, we can define the flux operator B_p by

$$B_p = \sum_s \frac{d_s}{\mathcal{D}^2} B_p^s. \quad (3.15)$$

Together with (3.13), this yields the expression for the matrix elements of B_p in (3.9). As the different B_p^s commute, the B_p also commute with each other.

The operators defined in (3.15) are projectors, as can be seen from their action on a reference state $|\text{ref}\rangle$:

$$\begin{aligned} B_p^2 |\text{ref}\rangle &= \sum_{s,s'} \frac{d_s}{\mathcal{D}^2} \frac{d_{s'}}{\mathcal{D}^2} \left| \text{hexagon}(s',s) \right\rangle = \sum_{s,s'} \sum_{s''} \frac{d_s}{\mathcal{D}^2} \frac{d_{s'}}{\mathcal{D}^2} F_{s' s' s''}^{s s s 1} \left| \text{hexagon}(s',s'') \right\rangle \\ &\stackrel{3.7}{=} \sum_{s,s'} \sum_{s''} \frac{d_s}{\mathcal{D}^2} \frac{d_{s'}}{\mathcal{D}^2} F_{s' s' s''}^{s s s 1} d_{s'} F_{s s' s''}^{s' s s' 1} \left| \text{hexagon}(s) \right\rangle \\ &= \sum_s \frac{d_s}{\mathcal{D}^2} \underbrace{\left(\sum_{s'} \frac{d_{s'}^2}{\mathcal{D}^2} \right)}_{=1} \underbrace{\sum_{s''} F_{s' s' s''}^{s s s 1} F_{s s' s''}^{s' s s' 1}}_{=1} \left| \text{hexagon}(s) \right\rangle \\ &= B_p |\text{ref}\rangle, \end{aligned} \quad (3.16)$$

where we used the fact that performing and undoing an F -move yields the initial state. Thus the possible eigenvalues of B_p are 0 and 1. Let us now discuss the corresponding eigenstates. Therefore we will make use of the modular S -matrix (3.6).

If we assume a flux f threading through the plaquette p , as represented by a flux line,² we have

$$\begin{aligned}
B_p \left| \begin{array}{c} f \\ \text{plaquette } p \end{array} \right\rangle &= \sum_s \frac{d_s}{\mathcal{D}^2} B_p^s \left| \begin{array}{c} f \\ \text{plaquette } p \end{array} \right\rangle = \sum_s \frac{d_s}{\mathcal{D}^2} \left| \begin{array}{c} f \\ s \\ \text{plaquette } p \end{array} \right\rangle \\
&= \sum_s \frac{d_s}{\mathcal{D}^2} \frac{S_{sf}}{S_{1f}} \left| \begin{array}{c} f \\ \mathbf{1} \\ \text{plaquette } p \end{array} \right\rangle = \frac{1}{\mathcal{D} S_{1f}} \sum_s S_{1s} S_{sf} \left| \begin{array}{c} f \\ \text{plaquette } p \end{array} \right\rangle \\
&= \delta_{\mathbf{1}f} \left| \begin{array}{c} f \\ \text{plaquette } p \end{array} \right\rangle, \tag{3.17}
\end{aligned}$$

where in the last step, we used the unitarity of the S -matrix and $\mathcal{D} S_{11} = 1$.

So, the operator B_p projects onto states with trivial flux $\mathbf{1}$ threading through the plaquette p and consequently a state

$$|\{\mathbf{1}_p\}_p, \text{ref}\rangle = \mathcal{N} \prod_p B_p |\text{ref}\rangle, \tag{3.18}$$

where \mathcal{N} is a normalization constant dependent of $|\text{ref}\rangle$, is a state with no flux threading through the surface, iff its norm is non-zero.

For $J_p > 0$, all ground states of H_{LW} can be represented as in (3.18) with suitable choices of states $|\text{ref}\rangle$. However, the possibly different ground states will in general not be orthogonal for different choices of $|\text{ref}\rangle$. Additionally, we observe that due the action of the operators B_p , these states will be generically a weighted superposition of nearly all states represented in the bond basis (3.1).

Let us note here that we can construct other projectors than B_p by choosing other weights of the B_p^s , i.e for $a \in \mathcal{F}$ we have

$$\mathcal{P}_p^a = S_{1a} \sum_s S_{as} B_p^s. \tag{3.19}$$

One can show analogously as in (3.17) that \mathcal{P}_p^a project onto a state with flux label a through the plaquette p . Note that $\mathcal{P}_p^{\mathbf{1}} = B_p$. Due to the unitarity of the S -matrix, we have $\mathcal{P}_p^a \mathcal{P}_p^b = \delta_{ab} \mathcal{P}_p^a$, i.e. the projectors \mathcal{P}_p^a project on orthogonal subspaces.

²Note that in the underlying field theory, the flux labels correspond to achiral labels of the doubled theory $\text{D}(\mathcal{F})$, so that one shall in principle write (f, f) instead of f here. However, for our picture, the undoubled labels are sufficient at this stage and thus we shift the discussion of the connection to the doubled theory $\text{D}(\mathcal{F})$ to the end of Section 3.1.4, where we have a better suited state representation at hand.

As we have

$$\sum_a \mathcal{P}_p^a = \sum_a S_{1a} \sum_s S_{as} B_p^s = \sum_s \left(\sum_a S_{1a} S_{as} \right) B_p^s = \sum_s \delta_{1s} B_p^s = B_p^1 = \mathbb{1}, \quad (3.20)$$

we see that we can achieve a complete description of the local excitations by including the flux labels through each plaquette. We can thus define eigenstates of H_{LW} as

$$|\{b_p\}, \{\ell_e\}\rangle = \mathcal{N} \prod_p \mathcal{P}_p^{b_p} \prod_e |\ell_e\rangle_e, \quad (3.21)$$

where $\prod_e |\ell_e\rangle_e$ corresponds to the reference state $|\text{ref}\rangle$ in (3.18). These eigenstates can be used to represent all states in the Hilbert space. We refer to the representation of states in (3.21) as flux basis. However, from the fact that it involves additionally to the bond labels (which characterize already completely a basis set of states) also the quantum numbers of the fluxes, it is clear that the states in the flux basis form an overcomplete and in particular non-orthogonal set of states. Nevertheless, it is a useful representation of the eigenstates of H_{LW} as it allows to characterize an eigenstate only by local quantities such as local fluxes and link labels.

3.1.4 The dual basis

Despite the fact that the flux basis (3.21) enables us to construct eigenstates of H_{LW} , it does not allow us to understand features like the non-trivial degeneracies arising from the non-Abelian statistics, as this information is still hidden in the bond variables of the reference state(s) $|\text{ref}\rangle$.

Therefore let us continue to construct an eigenbasis of H_{LW} , which is completely independent of the bond labels and additionally consists of orthonormal states. To achieve this, we consider operators, which are the analogue to the B_p^s , and from which we construct projectors as in (3.19). These so-called simple operators $W_{\{p_0, \dots, p_n\}}^{\pm, s}$ are defined as in the following example

$$W_{\{p_0, p_1\}}^{+, s} \left| \begin{array}{c} \text{Diagram 1} \\ p_0 \quad p_1 \end{array} \right\rangle = \left| \begin{array}{c} \text{Diagram 2} \\ p_0 \quad s \quad p_1 \end{array} \right\rangle, \quad (3.22)$$

$$W_{\{p_0, p_1\}}^{-, s} \left| \begin{array}{c} \text{Diagram 3} \\ p_0 \quad p_1 \end{array} \right\rangle = \left| \begin{array}{c} \text{Diagram 4} \\ p_0 \quad s \quad p_1 \end{array} \right\rangle, \quad (3.23)$$

i.e. these operators insert loops with label s along the boundary of the joint plaquettes $\partial\{p_0, \dots, p_n\}$.

Let us note that there are in principle two distinct ways of inserting a loop: the one labeled with '+' refers to inserting a loop from above the lattice, the one labeled with '-' from below. We will refer to the different signs as different chiralities in the following.

The matrix elements of the $W_{\{p_0, \dots, p_n\}}^{\pm, s}$ can be determined as in (3.11), but there is one additional ingredient for the calculations: if the inserted loop crosses an edge pointing inwards the surface surrounded by the loop, there are additionally to the F -moves also R -moves necessary to move the linking string labeled with s along the path of the inserted loop. This can be depicted for positive chirality as

$$\begin{aligned} \left| \begin{array}{c} i \\ s \\ k' \quad k \quad l \end{array} \right\rangle &= (R^{-1})_k^{il} \left| \begin{array}{c} i \\ s \\ k' \quad k' \quad l \end{array} \right\rangle = (R^{-1})_k^{il} \sum_{l'} F_{sk'l'}^{ilk} \left| \begin{array}{c} i \\ s \\ k' \quad l \quad l' \end{array} \right\rangle \\ &= (R^{-1})_k^{il} \sum_{l'} F_{sk'l'}^{ilk} R_{k'}^{il'} \left| \begin{array}{c} i \\ s \\ k' \quad l \quad l' \end{array} \right\rangle, \end{aligned} \quad (3.24)$$

and negative chirality respectively as

$$\begin{aligned} \left| \begin{array}{c} i \\ s \\ k' \quad k \quad l \end{array} \right\rangle &= R_k^{il} \left| \begin{array}{c} i \\ s \\ k' \quad k' \quad l \end{array} \right\rangle = R_k^{il} \sum_{l'} F_{sk'l'}^{ilk} \left| \begin{array}{c} i \\ s \\ k' \quad l \quad l' \end{array} \right\rangle \\ &= R_k^{il} \sum_{l'} F_{sk'l'}^{ilk} (R^{-1})_{k'}^{il'} \left| \begin{array}{c} i \\ s \\ k' \quad l \quad l' \end{array} \right\rangle. \end{aligned} \quad (3.25)$$

Note that we encounter an R -move involving the matrix-element $(R^{-1})_k^{il} R_{k'}^{il'}$ for the $W_{\{p_0, \dots, p_n\}}^{+, s}$ -operator, but we have $R_k^{il} (R^{-1})_{k'}^{il'}$ for $W_{\{p_0, \dots, p_n\}}^{-, s}$. Thus if these matrix elements are not identical, $W_{\{p_0, \dots, p_n\}}^{+, s}$ and $W_{\{p_0, \dots, p_n\}}^{-, s}$ are distinct operators.

However, as this is the only difference between the operators, it shall be clear that they commute with each other. Moreover, one can also conclude by the same argument that two operators of different chirality always commute, even if they do not insert a loop along the same path in the lattice.

Let us mention here that there is one important exception to the fact that two operators acting along the same path but which have opposite chiralities are distinct from each other:

$$W_{\{p\}}^{+, s} = W_{\{p\}}^{-, s} = B_p^s, \quad (3.26)$$

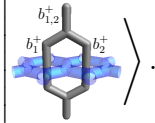
i.e. when acting only on one plaquette, the operators $W_{\{p\}}^{\pm, s}$ reduce to the same operator B_p^s , which tells us already that the eigenstates of the operator B_p are achiral.

To simplify the following discussion, we restrict ourselves, in a first step, to the operators of positive chirality, as the ones of negative chirality are completely equivalent but independent.

In analogy to the local projectors \mathcal{P}_p^a (3.19), we construct non-local projectors as

$$\mathcal{P}_{\{p\}}^{+,a} = S_{1a} \sum_s S_{as} W_{\{p\}}^{+,s}. \quad (3.27)$$

The projectors $\mathcal{P}_{\{p\}}^{+,a}$ measure the flux through the total surface $\{p\}$. This flux corresponds to the fusion product of the local flux labels b_p within the surface. We thus represent these non-local flux quantum numbers as in the following example of two plaquettes

$$\mathcal{P}_{\{p_1,p_2\}}^{+,b_{1,2}^+} \mathcal{P}_{\{p_1\}}^{+,b_1^+} \mathcal{P}_{\{p_2\}}^{+,b_2^+} |\text{ref}\rangle = \left| \begin{array}{c} b_{1,2}^+ \\ b_1^+ \quad b_2^+ \end{array} \right\rangle. \quad (3.28)$$


Note that this state only has a non-zero norm if $N_{b_1^+, b_2^+}^{b_{1,2}^+} \neq 0$, thus we also link the different flux lines representing local and non-local fluxes, which yields the corresponding fusion vertex. Let us note that this construction is similar to the one performed in Ref. [103]. In the following, we will omit the fat-lattice in pictorial representations, if the reference state $|\text{ref}\rangle$ is uniquely specified.

The aim is now to represent the states as

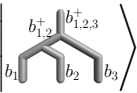
$$\left| \{b_p\}, \{b_{p_1, \dots, p_n}^\pm\} \right\rangle = \mathcal{N} \prod_p \mathcal{P}_p^{b_p} \prod_{\{p_1, \dots, p_n\}, \pm} \mathcal{P}_{\{p_1, \dots, p_n\}}^{\pm, b_{p_1, \dots, p_n}^\pm} |\text{ref}\rangle, \quad (3.29)$$

where $|\text{ref}\rangle$ is a unique reference state. A suitable choice is the state

$$|\text{ref}\rangle = \prod_e |1\rangle_e. \quad (3.30)$$

This particularly simple choice is sufficient, as it turns out that, like in Ref. [52], all eigenstates of H_{LW} have a non-vanishing overlap with this state.

In order to obtain an orthogonal basis, one has to choose the $\{p_1, \dots, p_n\}$ in a suitable way, as different projectors do in general not commute if non-Abelian anyons are involved. This can be seen for example from

$$\mathcal{P}_{1,2,3}^{+,b_{1,2,3}^+} \mathcal{P}_{1,2}^{+,b_{1,2}^+} \prod_{p=1,2,3} \mathcal{P}_p^{b_p} |\text{ref}\rangle = \left| \begin{array}{c} b_{1,2,3}^+ \\ b_1 \quad b_2 \quad b_3 \end{array} \right\rangle$$


$$= \sum_{b_{2,3}^+} F_{b_3 b_1 b_2 b_{1,2}^+ b_{2,3}^+}^{b_1 b_2 b_{1,2}^+} \left| \begin{array}{c} b_{1,2,3}^+ \\ b_1 \quad b_2 \quad b_3 \end{array} \right\rangle = \sum_{b_{2,3}^+} F_{b_3 b_1 b_2 b_{1,2}^+ b_{2,3}^+}^{b_1 b_2 b_{1,2}^+} \mathcal{P}_{1,2,3}^{+,b_{1,2,3}^+} \mathcal{P}_{2,3}^{+,b_{2,3}^+} \prod_{p=1,2,3} \mathcal{P}_p^{b_p} |\text{ref}\rangle. \quad (3.31)$$

Thus it is clear that two projectors $\mathcal{P}_{\{p_1,p_2\}}^{+,b_{1,2}^+}$ and $\mathcal{P}_{\{p_2,p_3\}}^{+,b_{2,3}^+}$ do not commute if there is more than one value for $b_{2,3}^+$, which yields a non-zero F -symbol. Thus the projectors commute, if the plaquette sets they act on are either completely disjoint or nested into each other, as the example (3.31) does not apply to this situation. The two projectors also commute if only one non-zero F -symbol appears on the right-hand side of (3.31), which is the case for Abelian theories.

If one surface is completely included (nested) in the other, the projectors commute for a general anyonic theory. We use this fact to construct a set of commuting projectors by choosing the operators $\mathcal{P}_{S_n}^{\pm,b_{S_n}^\pm}$, where

$$S_n = \{p_1, \dots, p_n\}, \quad n = 2, \dots, N_p. \quad (3.32)$$

We will refer to this basis as dual basis in the remainder of this thesis, as it is completely described by the local fluxes and their non-local fusion channels and thus by degrees of freedom originating from the (dual) lattice formed by elementary plaquettes.

However, in order to construct a complete set of states, it is necessary to incorporate the details of the surface, the lattice is embedded in.

Let us consider as first example a lattice with N_p plaquettes embedded on the surface of a sphere. As we can see in Figure 3.3, we have the two constraints

$$\mathcal{P}_{S_{N_p-1}}^{\pm,b_{S_{N_p-1}}} = \mathcal{P}_{p_{N_p}}^{b_{p_{N_p}}}, \quad (3.33)$$

$$\mathcal{P}_{S_{N_p}}^{\pm,b_{S_{N_p}}} = \mathbb{1}_{\delta_{b_{S_{N_p}}, \mathbf{1}}}, \quad (3.34)$$

as on the sphere, a loop around all but one plaquette is the same as the loop around this plaquette, which leads to (3.33). Additionally, there is no non-trivial loop around the sphere and consequently there is no boundary of S_{N_p} surrounding a plaquette, which results in the charge-free sector to (3.34).

Thus, we can represent the eigenstates for a lattice with N_p plaquettes on the sphere by the fusion diagram

$$|\{b_p\}_{p=1,\dots,N_p}, \{b_{S_n}^\pm\}_{n=2,\dots,N_p-1}\rangle = \left| \begin{array}{c} b_{1,2,3}^+ \\ b_1 \quad b_2 \quad b_3 \\ b_{1,2}^- \quad b_{1,2,3}^- \end{array} \right\rangle \dots \left| \begin{array}{c} b_{N_p} \end{array} \right\rangle, \quad (3.35)$$

where we omitted the flux lines carrying the label $b_{S_{N_p}}^\pm$ as these equal always $\mathbf{1}$.

Let us remark here that the number of states represented in the fusion diagram (3.35) equals the one for the trivalent lattice embedded on the surface of the sphere, as both graphs have the same number of vertices N_v (where $N_v = 2(N_p - 2)$ by Euler's theorem) and can thus be deformed into each other by applying suitable F -moves (c.f. Ref. [114]), which yields a unitary transformation from the lattice to the fusion diagram. Consequently, the dual basis on a sphere given by

$$|\{b_p\}_{p=1,\dots,N_p}, \{b_{S_n}^\pm\}_{n=2,\dots,N_p-1}\rangle = \mathcal{N} \prod_{\pm, n=2,\dots,N_p-1} \mathcal{P}_{S_n}^{\pm, b_{S_n}^\pm} \prod_p \mathcal{P}_p^{b_p} |\text{ref}\rangle \quad (3.36)$$

is indeed a complete basis.

Before discussing the properties of the eigenstates of H_{LW} in detail, let us first complete our discussion about the dual basis for the torus. On the torus, the constraints (3.33) and (3.34) do not hold. As can be seen in Figure 3.3, due to the non-trivial topology of the torus, not only the projectors $\mathcal{P}_{S_{N_p-1}}^{\pm, b_{S_{N_p-1}}^\pm}$ and $\mathcal{P}_{S_{N_p}}^{\pm, b_{S_{N_p}}^\pm}$ are independent, but there are additionally two non contractible loops $\mathcal{C}_{1,2}$. Along these loops, one can define in analogy to (3.23) and (3.27) the projectors

$$\mathcal{P}_{\mathcal{C}_{1,2}}^{\pm, c_{1,2}^\pm} = S_{\mathbf{1}_{c_{1,2}^\pm}} \sum_s S_{c_{1,2}^\pm s} W_{\mathcal{C}_{1,2}}^{\pm, s}. \quad (3.37)$$

However, these loops intersect and we have thus as for the non-local projectors in (3.31)

$$[\mathcal{P}_{\mathcal{C}_1}^{\pm, c_1}, \mathcal{P}_{\mathcal{C}_2}^{\pm, c_2}] \neq 0, \quad [\mathcal{P}_{\mathcal{C}_1}^{\pm, c_1}, \mathcal{P}_{\mathcal{C}_2}^{\mp, c_2}] = 0, \quad (3.38)$$

i.e. we can choose projectors (3.37) of each chirality independently, but projectors of the same chirality do not commute.

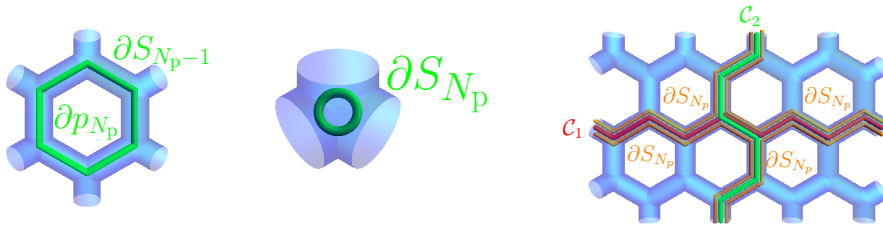


FIGURE 3.3: For the sphere, two constraints for the projectors (3.28) arise. The first one is that a loop surrounding all but one plaquette is the same as the loop encircling this plaquette. Thus the corresponding projectors coincide. Additionally, the boundary of S_{N_p} encircles no plaquette, as illustrated in the middle. Therefore the corresponding projector does not measure any flux and is thus the identity.

For the torus with its periodic boundary conditions, there are additionally to the projectors $\mathcal{P}_{S_n}^{\pm, b_{S_n}^\pm}$, $n = 2, \dots, N_p$, also the operators $\mathcal{P}_{\mathcal{C}_{1,2}}^{\pm, c_{1,2}^\pm}$, which arise due to the non-contractible cycles $\mathcal{C}_{1,2}$ forming the boundary ∂S_{N_p} of S_{N_p} .

These projectors measure the flux through the torus itself. The corresponding flux lines can be represented as in (3.39), since they do not interfere with the local fluxes and their fusion channels.

We can thus represent the dual basis for the torus as

$$\begin{aligned}
 |\{b_p\}_{p=1,\dots,N_p}, \{b_{S_n}^\pm\}_{n=2,\dots,N_p}, c^+, c^-\rangle &= \mathcal{N} \prod_{\pm} \left(\mathcal{P}_c^{\pm, c^\pm} \prod_{n=2,\dots,N_p} \mathcal{P}_{S_n}^{\pm, b_{S_n}^\pm} \right) \prod_p \mathcal{P}_p^{b_p} |\text{ref}\rangle \\
 &= \left| \begin{array}{c} \text{Diagram of a torus with flux lines } c^+ \text{ and } c^- \text{ and plaquettes } b_p \text{ and } b_{S_n}^\pm \end{array} \right\rangle. \tag{3.39}
 \end{aligned}$$

We see that the number of vertices in this representation is the same as for the hexagonal lattice on the torus ($N_v = 2N_p$), so that the dual basis is complete also for this topology.

Let us note here that one can in principle also manipulate the fusion diagrams in (3.39) by performing F - and R -moves. However these moves only commute with the Hamiltonian H_{LW} , if they let the labels b_p invariant. We omit a color-coding as in the fat lattice for notational simplicity.

So, we achieved our aim to construct with the dual basis (3.36) and (3.39) an orthogonal basis, in which the Hamiltonian H_{LW} takes the simple diagonal form

$$\begin{aligned}
 &H_{\text{LW}} |\{b_p\}_{p=1,\dots,N_p}, \{b_{S_n}^\pm\}_{n=2,\dots,N_p}, c^+, c^-\rangle \\
 &= -J_p \sum_p \delta_{b_p, \mathbf{1}} |\{b_p\}_{p=1,\dots,N_p}, \{b_{S_n}^\pm\}_{n=2,\dots,N_p}, c^+, c^-\rangle. \tag{3.40}
 \end{aligned}$$

This basis allows us for example to make the connection to the interpretation of the topological phases in terms of the surface topology fluctuations put forward in Ref. [69]. Let us note that if there is no flux through a plaquette p , we have $b_p = \mathbf{1}$. All other labels in the fusion diagram (3.39) are not effected if one removes the link corresponding to the plaquette p . However, removing this link from the fusion diagram is equivalent to remove the plaquette in the fat-lattice representation (3.17) by closing its surface as depicted in Figure 3.4.

By this visualization, one can then interpret the flux-free state(s) as a closed double surface. Excited states can then be visualized as holes pinched through the surface.

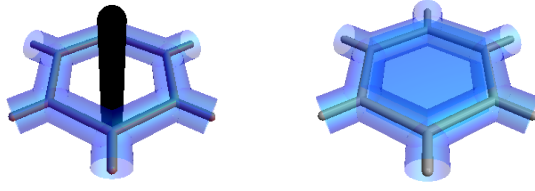


FIGURE 3.4: From the dual basis (3.36), we see that removing trivial local flux lines is equivalent to closing the corresponding plaquette p . The ground state of H_{LW} thus corresponds to a closed, double-sheeted surface [58, 110]. For non-trivial fluxes, this closing is not possible and thus excitations correspond to holes in the closed surface representing the ground state. This connection of the dual basis to the surface geometry [69] allows e.g. to obtain the axioms for a topologically ordered ground state by applying the rules for the fat-lattice representation.

Within the closed double surface, we can again use the rules for the fat-lattice representation for manipulating strings within tubes as discussed in Section 3.1.2. This allows us to recover the properties of a topologically ordered ground state discussed in Ref. [56]: As strings may be deformed arbitrarily without changing the actual state, we see that the ground-state wave function is topologically invariant. The weight of closed loops labeled with s is given by the coefficient of B_p^s in (3.15). As closed string network can be removed in a similar fashion as in (3.7), the ground-state wave function is scale invariant.

Given this properties, one can show that the weight of a given configuration in the bond basis in the ground state only depends on the number of branchings, but not on the length scale, which manifests the topological order.

Let us note also that from the dual basis representation of states, one can easily obtain the doubled representation, which allows to characterize all of the excitations of the string-net model in terms of labels of the doubled algebra $D(\mathcal{F})$ [98, 99]. This can be achieved by reflecting the lower part of the fusion diagram (3.36) or (3.39) about the surface. This is equivalent to defining the dual basis for the torus via

$$\begin{aligned}
 & \left| \{b_p\}_{p=1,\dots,N_p}, \{b_{S_n}^\pm\}_{n=2,\dots,N_p}, c^+, c^- \right\rangle = \mathcal{N} \mathcal{P}_{C_1}^{(c^+, c^-)} \prod_{n=2,\dots,N_p} \mathcal{P}_{S_n}^{(b_{S_n}^+, b_{S_n}^-)} \prod_p \mathcal{P}_p^{(b_p, b_p)} |\text{ref}\rangle \\
 & = \left| \begin{array}{c} \text{---} (c^+, c^-) \text{---} \\ \text{---} (b_{1,\dots,N_p}^+, b_{1,\dots,N_p}^-) \text{---} \\ \text{---} (b_{1,2}^+, b_{1,2}^-) \text{---} \dots \\ \text{---} (b_{1,2,3}^+, b_{1,2,3}^-) \text{---} \dots \\ \text{---} (b_1, b_1) (b_2, b_2) (b_3, b_3) \dots (b_{N_p}, b_{N_p}) \text{---} \end{array} \right\rangle. \quad (3.41)
 \end{aligned}$$

By actually performing this reflection, we also see that local excitations on the plaquettes are always achiral, as they correspond to labels (a, a) of the string rooting from the respective plaquette. In particular these excitations have twists $\theta_{(a,a)} = 1$ and can thus

be seen as bosons for any anyonic theory. By our construction, we observe that one can attribute the achirality of the local excitations to the fact that an orientable surface has an inner and an outer part [58, 110].

Let us remark that to obtain the representation of the doubled theory, one has in principle to choose the same non-contractible loop for each chirality. However, as these two sectors are independent of each other, one can also choose without loss of generality different loops for each respective chirality. Thus, one can e.g. obtain the topological degeneracy via undoubled labels encircling each non-contractible loop, as it was done to detect the topological degeneracy e.g. in Refs. [28, 86] instead of considering doubled labels encircling only one loop, as done e.g. in Ref. [88]. Note that in the latter case, the doubledness of the theory manifests itself in the fact that there are also chiral labels (a, b) with $a \neq b$ for the non-local fluxes, although the local fluxes can only be labeled by achiral labels (a, a) .

3.1.5 Properties of the eigenstates

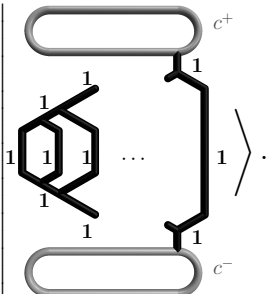
Let us now discuss the general structure of the eigenstates, in particular ground states and low-energy excitations. The special properties of each different theory are detailed in the end of this section.

We first focus on the case $J_p > 0$. In this case, we have already seen in (3.18) that the ground states of H_{LW} are given by all states, for which $b_p = \mathbf{1}$ for all plaquettes p . From the representation (3.35), it is obvious that there is a unique ground state on the sphere, namely

$$|\text{gS}_{\text{sphere}}\rangle = \left| \{\mathbf{1}\}_p, \{\mathbf{1}_{S_n^\pm}\}_{n=2, \dots, N_p-1} \right\rangle, \quad (3.42)$$

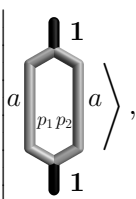
as all vertices in the fusion diagram are constrained to have only $\mathbf{1}$ as incident labels.

In contrast to this, we can see from Eq. (3.39) that this constraint does not apply to the labels c^\pm and thus these can take all $N + 1$ possible label values. Consequently, there are $(N + 1)^2$ ground states on the torus, which read

$$|\text{gS}_{\text{torus}}, c^+, c^-\rangle = \left| \{\mathbf{1}\}_p, \{\mathbf{1}_{S_n^\pm}\}_{n=2, \dots, N_p}, c^+, c^- \right\rangle = \left| \begin{array}{c} \text{Diagram} \end{array} \right\rangle. \quad (3.43)$$


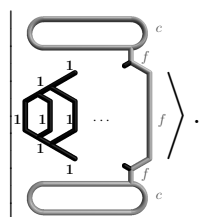
So, we observe that the ground-state degeneracy is dependent on the topology of the surface, into which the lattice is embedded. This represents a hallmark of topological order. Let us note here that our way of representing the states in the dual basis allows to reproduce easily the results obtained in Ref. [115] for the ground state degeneracy.

Additionally, we can observe that not only the ground-state degeneracy, but also the full spectrum depends on the topology of the surface. For example, on the sphere, the only closed loops in the fusion diagram are those, which involve links representing local fluxes. Thus, there is no state with only one local flux on the sphere. The lowest-energy excitation is a two-flux state (also present on the torus for e.g. $c^\pm = \mathbf{1}$), which can be represented locally in the fusion diagram as

$$|a_{p_1}, a_{p_2}\rangle = \left| \begin{array}{c} \mathbf{1} \\ \text{---} \\ a \text{---} \text{---} a \\ \text{---} \\ \mathbf{1} \end{array} \right\rangle, \quad (3.44)$$


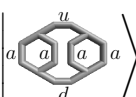
where the two local fluxes carry the same label $a \neq \mathbf{1}$. All two-flux states represented in the dual basis (3.36) can be brought into the local form shown in (3.44) by a suitable sequence of F -moves, which commutes with the Hamiltonian. So, we see that the energy of a two-flux state does not depend on the actual distance of the fluxes. Thus the flux excitations are indeed deconfined, as can already be seen from the fact that the Hamiltonian H_{LW} consists of the sum of equally weighted frustration-free projectors.

Contrary to the sphere, there are closed loops in the fusion diagram for the torus (3.39), which do not involve local fluxes. A single flux line may terminate at these loops, if the theory is non-Abelian. In particular, for each non-zero fusion matrix element N_{cc}^f with $f \neq \mathbf{1}$, we have a one-flux state

$$|b_p = f, c, c\rangle = \left| \begin{array}{c} \text{---} \\ \text{---} \\ \text{---} \\ \text{---} \\ \text{---} \\ \text{---} \end{array} \right\rangle. \quad (3.45)$$


As these matrix elements do exist only for non-Abelian theories, already the low-energy spectrum on a torus can tell us, whether a theory is Abelian or non-Abelian.

Let us now investigate the exchange statistics of the excitations. Therefore, we consider a state

$$|a_1, a_2, a_3, a_4, u, d\rangle = \left| \begin{array}{c} u \\ \text{---} \\ a \text{---} a \\ \text{---} \\ d \end{array} \right\rangle \quad (3.46)$$


with four identical fluxes located at some positions 1, 2, 3, 4 on the lattice. We assume the overall fusion channel to be labeled by the $\mathbf{1}$ -label. Note that this state exists on the sphere and on the torus. If we exchange now the position of the particles a_2 and a_3 by some sequence of local processes, we obtain the state

$$\left| \begin{array}{c} u \\ \text{---} \\ a \text{---} a \text{---} a \\ \text{---} \\ d \end{array} \right\rangle = \sum_{u', d'} F_{a a u'}^{a a u} F_{a a d'}^{a a d} \left| \begin{array}{c} u' \\ \text{---} \\ a \text{---} a \text{---} a \\ \text{---} \\ d' \end{array} \right\rangle = \sum_{u', d'} F_{a a u'}^{a a u} F_{a a d'}^{a a d} |a_1, a_3, a_2, a_4, u', d'\rangle. \quad (3.47)$$

Thus we observe that the exchange of identical particles yields in principle a unitary transformation on the degenerate states denoted by the labels of the fusion channels u, d . In the special case of an Abelian theory, we have $N_{aa}^u = N_{aa}^d = 0$ for $u, d \neq \mathbf{1}$, the exchange yields a phase factor $(F_{aa\mathbf{1}}^{aa})^2$. Let us remark here that in the case of non-Abelian anyons, the non-local fusion channels u, d represent the topologically protected qubits, on which one can act by braiding the particles as in the example above.

For the case $J_p < 0$, let us just mention here that the ground states are characterized by the fact that most of the local fluxes are non-trivial. The actual ground-state degeneracy then depends on the details of the anyonic theory, so that we shift this discussion to Section 3.5, where we discuss the different models in detail for each theory.

3.1.6 Brief summary for the string-net Hamiltonian

Before we turn to the local perturbation, let us summarize what we have achieved so far for the description of the topological Hamiltonian H_{LW} . We introduced a general string-net Hamiltonian H_{SN} (3.2) consisting of commuting charge and flux operators. The charge-free sector is obtained by imposing the branching rules as local constraints at each vertex of the underlying lattice. The appropriate basis for this prescription is the bond basis (3.1), in which the charge operators are diagonal.

In order to understand the flux operators in terms of injecting Wilson loops, we extended the bond picture to the fat-lattice representation that allows to interpret a state as a superposition of string networks. In this representation, we identify the local flux operator B_p as a projector, which project onto the flux-free states at plaquette p using the modular S -matrix as a key ingredient. We defined the flux basis (3.21) by the quantum numbers of the local fluxes and the bond label configuration. This basis has the advantage of being local, however it is overcomplete and non-orthogonal.

By extending the projector description also to larger parts of the surface and to non-local fluxes, we have been able to construct the dual basis (3.39). This basis is completely

defined in terms of orthogonal projectors and has no particular reference to the bond labels. Thus it yields an orthogonal eigenbasis of H_{LW} . Within this basis representation, we were able to discuss without a reference to a particular anyonic theory already features like the topological ground-state degeneracy and the exchange statistics of the excitations. We also discussed the fact that the underlying anyonic theory for the flux excitations residing on the plaquettes of the lattice is the doubled theory $D(\mathcal{F})$, although the microscopic degrees of freedom residing on the edges take labels in the label set \mathcal{F} .

3.2 The local Hamiltonian H_{loc}

In this section, we will discuss the simplest possible local Hamiltonian that can be used to perturb the topologically ordered phase, given by the ground states of the Hamiltonian H_{LW} (3.5). Let us mention that the perturbation presented below has already been discussed for non-Abelian theories in the Refs. [69, 70].

We define the local Hamiltonian H_{loc} by

$$H_{\text{loc}} = -J_e \sum_e \mathcal{P}_e^{\mathbf{1}}, \quad (3.48)$$

where projectors $\mathcal{P}_e^{\mathbf{1}}$ acting on the bond labels ℓ_e are defined by

$$\mathcal{P}_e^{\mathbf{1}} |\ell_e\rangle_e = \delta_{\ell_e, \mathbf{1}} |\ell_e\rangle_e. \quad (3.49)$$

This Hamiltonian is obviously diagonal in the bond basis and thus commutes with the charge operators Q_v that are also diagonal in this basis. Thus, we can discuss the eigenstates of H_{loc} within the charge-free sector. We discuss in the following the limit $J_e > 0$, as this does not depend on specific details of the underlying anyonic theory. The case $J_e < 0$ will be considered for each theory individually.

For $J_e > 0$, the ground state $|\text{gs}_{\mathbf{1}}\rangle$ is given by

$$|\text{gs}_{\text{loc}, \mathbf{1}}\rangle = \prod_e |\mathbf{1}\rangle_e. \quad (3.50)$$

In particular, the ground state is unique for any topology of the surface. Consequently, there is no topological order.

Excitations of this Hamiltonian are states with link labels $\ell_e \neq \mathbf{1}$. Due to the branching rules, there is no single-link excitation, since $\delta_{\mathbf{1}, \mathbf{1}, a} = 0$ for $a \neq \mathbf{1}$ in any anyonic theory.

Consequently, the low-energy excitations in this limit are given for $s \neq \mathbf{1}$ by

$$|6s\rangle_p = B_p^s |g_{\text{loc},\mathbf{1}}\rangle = \left| \begin{array}{c} \text{---} \\ \diagup \quad \diagdown \\ \text{---} \end{array} \right\rangle_p, \quad (3.51)$$

i.e. by the shortest possible loop around plaquette p , where the links are labeled by s . As there are N labels distinct from $\mathbf{1}$, there are N excitations per plaquette with excitation energy $6J_e$.

Despite the fact that these excitations are extended objects involving several links, they are created by the action of the local operator. Thus, it is clear that their exchange statistics is bosonic [10].

To complete our discussion of the local Hamiltonian, let us consider the action of $\mathcal{P}_e^{\mathbf{1}}$ in the dual basis. Therefore, we consider two adjacent plaquettes p_1 and p_2 , which share the inner bond e . We assume the corresponding fusion diagram ordered such that the two plaquettes are adjacently located. If we now interpret the retraction skeleton within the thickened bond as a flux line, we can use the S -matrix (3.6) to obtain a representation of $\mathcal{P}_e^{\mathbf{1}}$, which is the analogue of the definition of the projector $\mathcal{P}_p^{\mathbf{1}}$ in (3.17). More concretely, we define operators L_e^s in analogy to the B_p^s (3.10) to inject loops labeled by s around the link e such that we have

$$\mathcal{P}_e^{\mathbf{1}} \left| \begin{array}{c} b_{p_1,p_2}^+ \\ \text{---} \\ \text{---} \\ b_{p_1,p_2}^- \end{array} \right\rangle = \sum_s \frac{d_s}{\mathcal{D}^2} L_e^s \left| \begin{array}{c} b_{p_1,p_2}^+ \\ \text{---} \\ \text{---} \\ b_{p_1,p_2}^- \end{array} \right\rangle = \sum_s \frac{d_s}{\mathcal{D}^2} \left| \begin{array}{c} b_{p_1,p_2}^+ \\ \text{---} \\ \text{---} \\ b_{p_1,p_2}^- \end{array} \right\rangle. \quad (3.52)$$

The additional loop around the thickened edge can then be removed in the same manner as in (3.11) to yield finally

$$\mathcal{P}_e^{\mathbf{1}} \left| \begin{array}{c} b_{p_1,p_2}^+ \\ \text{---} \\ \text{---} \\ b_{p_1,p_2}^- \end{array} \right\rangle = \sum_s \frac{d_s}{\mathcal{D}^2} F_s^{b_{p_1,p_2}^+, b_{p_2}, b_{p_1}} F_s^{b_{p_1,p_2}^-, b_{p_2}, b_{p_1}} \left| \begin{array}{c} b_{p_1,p_2}^+ \\ \text{---} \\ \text{---} \\ b_{p_1,p_2}^- \end{array} \right\rangle. \quad (3.53)$$

Thus we can describe also the action of the local operators $\mathcal{P}_e^{\mathbf{1}}$ onto the eigenstates of H_{LW} . In general, one has to transform the fusion diagram to reorder the local fluxes such that the flux labels for the two plaquettes sharing the bond e are adjacent in the fusion diagram. This involves in general F - and R -moves and thus the matrix elements of the local perturbation depend in general not only on the local flux labels on the two adjacent plaquettes, but also on the other flux labels (local and non-local).

A more physical picture for the action of the local perturbation (3.48) onto eigenstates of H_{LW} can be given in the bond basis. Eigenstates of H_{LW} are represented in the bond basis as a superposition of roughly all basis states, where the weight of each basis state only depends, on the string-net configuration, i.e. the number of loops and branchings but not their size. In particular, there is no notion of a string tension. The local perturbation H_{loc} (3.48) weights the length of non-trivial strings and thus introduces a string tension for the string-net states.

3.3 The perturbed string-net Hamiltonian

In the last section, we presented the two Hamiltonians H_{LW} and H_{loc} , where the first realizes a topologically ordered ground state for $J_p > 0$ and the second a topologically trivial ground state. In the following, we study the Hamiltonian

$$H = H_{\text{LW}} + H_{\text{loc}} = -\cos\theta \sum_p \mathcal{P}_p^1 - \sin\theta \sum_e \mathcal{P}_e^1, \quad (3.54)$$

where we set $J_p = \cos\theta$ and $J_e = \sin\theta$ for notational convenience.

Let us remark that for the values $\theta = 0, \pi$, we obtain the exactly solvable Hamiltonian H_{LW} and H_{loc} for $\theta = \frac{\pi}{2}, \frac{3\pi}{2}$. Note that the sign of the coupling constants changes depending on the value of θ . We refer to the phases, which are realized for $\theta = 0$ as topological, to the ones for $\theta = \frac{\pi}{2}$ as “polarized” or **1**-phase. The other phases are labeled according to their specific properties, which depend on the details of the considered anyonic theory.

For different values of θ , the models are not exactly solvable in two dimensions and the excitations within the respective phases become mobile and interacting. Additionally, the Hamiltonians H_{LW} and H_{loc} yield different ground-state degeneracies (e.g. $(N+1)^2$ and one, respectively). Thus between the distinct phases, in particular between the topological and the **1**-phase, we expect a phase transition. The location and the order of the phase transitions are the focus of the analysis of the different models, which are obtained for the respective anyonic theories detailed in the following.

3.4 Realizing different boundary conditions

Up to now, we only discussed the dual basis for lattices embedded on closed surfaces as the sphere or the torus. However, in the thermodynamic limit, the actual topology of the surface only impacts the number of topological sectors given by the non-local

quantum numbers of H_{LW} that distinguish the different ground states. These sectors are decoupled in the thermodynamic limit, as the local perturbation in (3.54) cannot couple them at any finite order in perturbation theory.

Therefore it is possible to investigate the same phase diagram not only for systems with periodic boundary conditions, but also for different, and perhaps easier to handle, underlying topologies. Possible examples are an open plane or a cylinder geometry, for which the above model (3.54) has already been studied [69, 70]. In the latter cases, one has to include boundary modes in the description, whereas for the torus, a full description of the model has already been discussed in the previous chapters. Thus, we give in the following the recipe to obtain a description for systems with open boundaries from the dual basis description discussed in Section 3.1.4.

3.4.1 The ladder

Let us start with a cylinder geometry, which is used in the study of the anyonic theories on the ladder e.g. in Refs.[69, 70, 72]. We consider here a two-leg ladder as depicted in Figure 3.5 with periodic boundary conditions along the ladder direction and open boundaries perpendicular to it. Note that this ladder forms a trivalent graph, for which the Hamiltonian (3.54) can be defined consistently as for the hexagonal lattice. This ladder can be embedded into the surface of the cylinder. By adding the two caps as shown in Figure 3.5, we obtain a surface, which is topologically equivalent to the surface of a sphere.

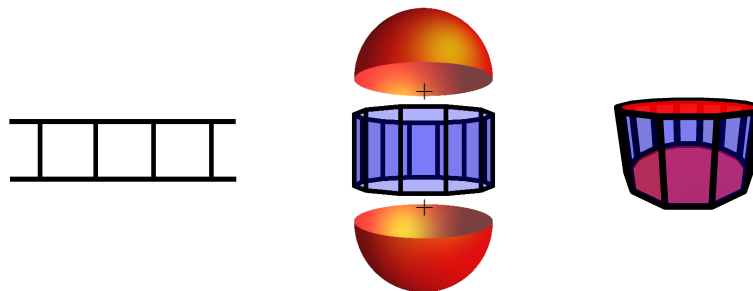


FIGURE 3.5: On the left-hand side, the two-leg ladder is depicted. With periodic boundary conditions along the legs, the ladder can be embedded in the surface of the cylinder depicted in the middle. The plaquettes, on which H_{LW} acts, are shaded in blue. The eigenbasis of H_{LW} (3.5) can be obtained by closing the holes by appropriate caps, which yield the surface depicted on the right-hand side. Its topology is equivalent to the sphere and consequently, one can use the states (3.36) to describe the eigenstates of H_{LW} also on this surface with boundaries.

To construct the dual basis for this sphere, we observe that by closing the surface, we introduced two additional plaquettes, for which one can define the projection operators in analogy to (3.19). So we obtain for the states on the closed surface the representation

(3.35), which reads here

$$\left| \left\langle \begin{array}{c} \text{---} \square \text{---} \\ p_1 \quad p_2 \end{array} \cdots \begin{array}{c} \text{---} \square \text{---} \\ p_2 \quad p_{N_p} \end{array} c_2 \right\rangle \xrightarrow{F\text{-moves}} \left| \left\langle \begin{array}{c} c_1 \\ \text{---} \square \text{---} \\ c_2 \quad p_1 \quad p_2 \end{array} \cdots \begin{array}{c} \text{---} \square \text{---} \\ p_{N_p-1} \quad p_{N_p} \\ c_1 \quad c_2 \end{array} \right\rangle \right., \quad (3.55)$$

where we have colored the flux lines corresponding to the artificial plaquettes in orange. The corresponding quantum numbers can be interpreted as the quantum numbers of the boundary modes, localized at the boundary of each artificial plaquette. As the corresponding projectors do not appear in the Hamiltonian (3.54), we perform a sequence of F -moves to obtain the right-hand side of (3.55), where only local flux projectors act on the rungs of the now periodically coupled ladder forming the fusion diagram.³

From the left-hand side of (3.55), one can read off that there are $(N + 1)$ different ground states of H_{LW} on the cylinder, which correspond to the different loops containing the two artificial flux lines, but no local flux line. We can also read off (3.55) that the number of one-flux states at plaquette p of the original ladder is at least two, which corresponds to the number of closed loops containing the local flux line at plaquette p and one of the artificial flux lines.

The action of H_{loc} is local⁴ in this fusion diagram, if it acts only on bonds, which do not form the boundary of the original ladder shown in Figure 3.5. As the boundary is formed by the legs of the ladder, this means that the local perturbation is defined to act only on the rungs of the original ladder.

From the right-hand side of (3.55), we can also see that an action of the local perturbation on all rungs of the ladder can change the value of the non-local flux.

We can read off the fusion diagram in (3.55) that the action of the operators L_p^s (3.52) in the dual basis for the cylinder (3.55) is the same as the action of the B_p^s (3.9) in the bond basis (3.1). This yields a duality mapping as presented in Refs. [69, 70] for the Hamiltonian, i.e. a transformation which maps the Hamiltonian (3.54) onto itself, but exchanges the coupling constants J_p and J_e . It turns out that for the theories considered within this thesis, the Hamiltonian is exactly solvable at the self-dual points $\theta = \frac{\pi}{4}$ and $\theta = \frac{3\pi}{4}$ [69, 70, 116], where it is critical. Due to the exact solutions, the critical exponents for the corresponding phase transitions are known [69, 70].

³The boundaries are now twisted since F -moves, which move the vertices attached to the artificial fluxes across the surface of the sphere, do not commute with the Hamiltonian H_{LW} [69]. However, in the case of non-Abelian anyons, different boundary conditions result only in a change of the degeneracies of the respective levels. So, spectral properties like the excitation gap or the ground-state energy are not affected by the choice of untwisted periodic boundary conditions in the thermodynamic limit.

⁴I.e. it can be represented as in (3.53) in terms of local fluxes and their fusion channels.

3.4.2 Open boundary conditions

In order to obtain a similar description for the case of open systems, i.e. systems defined on finite parts of an open plane, we proceed similarly to the case of the cylinder. However, as the open plane is topologically equivalent to the punctured sphere, we just need to add one additional plaquette contouring the given open system as depicted in Figure 3.6.

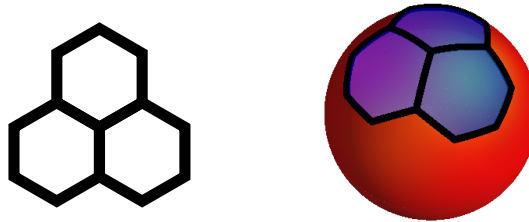


FIGURE 3.6: The states for systems with open boundary conditions, e.g. the one shown on the left, can also be described in terms of the dual basis (3.35). In order to also take into account boundary modes, one has to introduce an additional plaquette, surrounding the open finite cluster depicted on the left-hand side. This arrangement is then equivalent to the system on a sphere as shown on the right-hand side, where the additional plaquette is colored in red and the plaquettes, the Hamiltonian H_{LW} acts on, in blue. Thus, we can use the dual basis for the sphere to obtain the eigenstates of H_{LW} including the description of the non-local boundary modes (3.56).

Thus the boundary modes of the considered topological phase can be represented by one additional flux line in the dual basis

$$|\{b_p\}_{p=1,\dots,N_p}, \{b_{S_n}^\pm\}_{n=2,\dots,N_p-1}, c\rangle = \left| c \begin{array}{c} \text{---} \\ \text{---} \\ \text{---} \\ \text{---} \\ \text{---} \\ \text{---} \end{array} \begin{array}{c} \text{---} \\ \text{---} \\ \text{---} \\ \text{---} \\ \text{---} \\ \text{---} \end{array} \dots \begin{array}{c} \text{---} \\ \text{---} \\ \text{---} \\ \text{---} \\ \text{---} \\ \text{---} \end{array} \right\rangle. \quad (3.56)$$

We see that there are $(N + 1)$ different non-local boundary modes for an open system. However, we can directly read off (3.56) that there is one unique ground state of H_{LW} , which is realized for $c = \mathbf{1}$ and a unique one-flux state per plaquette and label a , realized for $c = a$.

As in the case of the ladder, the local perturbation does not change the quantum number of the boundary mode, unless it acts on the boundary itself.

3.5 Realizations of the different anyonic theories

After having discussed up to now the general framework of perturbed string-net Hamiltonians, we turn to the details of the particular models, we investigate in the following. These are the string-net model for semions, Fibonacci and Ising anyons. Our main focus is the study of the phase diagram of H (3.54) defined for a two-dimensional system as

well as the phase transitions between the different phases. Therefore we focus on the case of the two-dimensional honeycomb lattice in the thermodynamic limit.

We also analyze the Abelian semion model. As string-net models for Abelian theories with $(N + 1)$ labels are dual to $(N + 1)$ -state Potts-models [96], known results for the latter provide the possibility to cross check our results. We shall therefore also discuss the duality relation in more detail in Section 3.5.3.

3.5.1 The golden string net: Fibonacci anyons

The perturbed string-net Hamiltonian (3.54) is exactly solvable for four values of θ . For $\theta = 0, \pi$ we obtain the string-net Hamiltonian (3.5) and for $\theta = \frac{\pi}{2}, \frac{3\pi}{2}$ the local perturbation H_{loc} . Let us discuss the details of the different phases corresponding to these points.

3.5.1.1 The topological phase

As already discussed in Section 3.1.5, the system shows topological order for $\theta = 0$. The degeneracy of the ground state can be described according to (3.41) by the number of elements of the fusion algebra of the doubled Fibonacci theory $D(\text{Fib})$, which has the label set $\{(\mathbf{1}, \mathbf{1}), (\mathbf{1}, \boldsymbol{\tau}), (\boldsymbol{\tau}, \mathbf{1}), (\boldsymbol{\tau}, \boldsymbol{\tau})\}$. Thus, the ground state on the torus is four-fold degenerate.

The excitations are gapped and are given by local fluxes, which correspond to the achiral label $(\boldsymbol{\tau}, \boldsymbol{\tau})$. The chiral labels only appear in the nonlocal fusion channels. Let us note that the elementary excitation is a one-flux state (3.45) with energy gap J_p . As discussed in Section 3.1.5, these excitations are non-interacting and static non-Abelian anyons.

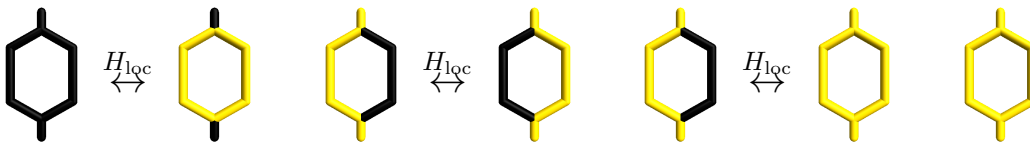


FIGURE 3.7: The processes induced by the local perturbation H_{loc} on eigenstates of H_{LW} include pair creation/annihilation, hopping terms, correlated creation/annihilation terms as well as two-flux interactions, represented by the single diagram on the right.

The action of the perturbation H_{loc} on the eigenstates of H_{LW} is given in (3.53). Processes induced by the perturbation are depicted in Figure 3.7. There are pair creation and annihilation, hopping, correlated creation and annihilation as well as pure interaction processes. Thus the local fluxes become mobile, interacting quasi-particles. Let us

remark here that the local perturbation does not change the overall fusion label, i.e. the total flux through a surface is conserved, unless the perturbation acts on its boundary.

3.5.1.2 Counting of states

Let us mention here one point, which we neglected in the general discussion: in the representation of the dual basis (3.39), we can actually compute the degeneracy of a k -flux state on a system with N_p plaquettes and thus the total dimension of the charge-free Hilbert space.

Therefore, one considers the parts of the fusion diagram corresponding to the positive and negative chirality separately. Given k local fluxes, which are now at the “leaves” of the Bratteli diagram shown in Figure 2.3 for each chirality, the other local fluxes carry label $\mathbf{1}$ and can therefore be omitted in the following consideration.

Now, one has to determine the number of all possible fusion channels $b_{S_n}^\pm$ for $n = 2, \dots, N_p$ of the local fluxes. Let us proceed iteratively to illustrate how this can be achieved.

When fusing the fluxes $b_{S_n}^\pm$ with $b_{p_{n+1}}$, there are the two possible values for $b_{S_n}^\pm = \mathbf{1}$ and $b_{S_n}^\pm = \tau$. Let $N_n^{\mathbf{1}}$ (N_n^τ) be the number of possibilities of having $b_{S_n}^\pm = \mathbf{1}$ ($b_{S_n}^\pm = \tau$). There are three possible fusion vertices for fusing $b_{S_n}^\pm$ with $b_{p_{n+1}}$ to yield $b_{S_{n+1}}^\pm$, which are depicted in Figure 3.8.

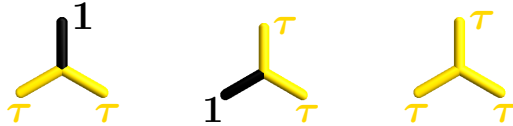


FIGURE 3.8: The three fusion vertices arising in the counting of the fusion channels. When read from left to right, the upper label describes the possible fusion outcomes $(b_{S_n}^\pm \otimes \tau) \ni b_{S_{n+1}}^\pm$, as $b_{p_n} = \tau$. When read from up to down, the upper label represents $b_{S_{N_p}}^\pm$, whereas the two lower represent c^\pm , if both are identical. Additionally, there is the trivial vertex (all labels equal $\mathbf{1}$), which contributes to the three possible ways of fusing $b_{S_{N_p}}^\pm$ with c^\pm .

We see that the number of possible configurations to have $b_{S_{n+1}}^\pm = \mathbf{1}$ is $N_{n+1}^{\mathbf{1}} = N_n^\tau$ and that for $b_{S_{n+1}}^\pm = \tau$ we have $N_{n+1}^\tau = N_n^{\mathbf{1}} + N_n^\tau$ configurations. As we have $N_1^{\mathbf{1}} = 0$ and $N_1^\tau = 1$ due to $b_{S_1}^\pm = b_{p_1}^\pm = \tau$, we obtain finally that the $N_n^{\mathbf{1},\tau}$ follow the Fibonacci sequence $(F_l)_{l \geq -1}$, which is given by

$$F_{l+1} = F_l + F_{l-1}, \text{ for } l \geq 1, \quad F_0 = 0, \quad F_{-1} = 1, \quad (3.57)$$

so that we have

$$N_n^{\mathbf{1}} = F_{n-1}, \quad N_n^{\tau} = F_n. \quad (3.58)$$

Additionally to the fusion channels of the local fluxes, the non-local fluxes c^\pm of the same chirality have to be taken into account. As the label c^\pm can take either the value $\mathbf{1}$ or τ we can again read from Figure 3.8 that for a given chirality the number of possible label configurations is

$$2N_k^{\mathbf{1}} + N_k^{\tau} = 2F_{k-1} + F_k. \quad (3.59)$$

As the fusion diagrams for the two chiralities are independent of each other, we obtain the total degeneracy D_k^{torus} of a k -flux state on a torus with N_p plaquettes

$$D_k^{\text{torus}} = \binom{N_p}{k} (F_k + 2F_{k-1})^2 = \binom{N_p}{k} (F_k^2 + 4F_{k-1}F_k + 4F_{k-1}^2), \quad (3.60)$$

where the binomial coefficient accounts for the number of possibilities to distribute k fluxes on N_p plaquettes.

Let us remark that the above way of counting the possible degenerate states represents a concrete implementation of the more general result obtained in Ref. [117]. Nevertheless, it allows us to obtain the total dimension $D_{\text{tot}}^{\text{torus}}$ of the Hilbert space for a charge-free system with N_p plaquettes by

$$D_{\text{tot}}^{\text{torus}} = \sum_{k=0}^{N_p} D_k^{\text{torus}}. \quad (3.61)$$

By replacing now $F_n = \frac{1}{2\varphi-1} \left(\varphi^n - \left(-\frac{1}{\varphi}\right)^n \right)$ (Moivre-Binet theorem), we obtain for the total dimension of the Hilbert space

$$D_{\text{tot}}^{\text{torus}} = (1 + \varphi^{-2})^{N_p} + (1 + \varphi^2)^{N_p}, \quad (3.62)$$

which agrees with the formula obtained in Ref. [114] via transfer matrix methods. Let us finally note that the counting of states is possible in the dual basis, as here the hierarchic structure of the fusion diagram allows to order the different fusion channels, which e.g. not possible in the bond basis of the hexagonal lattice.

3.5.1.3 The flux-full case

For $\theta = \pi$, we can describe the eigenstates of H (3.54) again in the dual basis. However, the overall sign of the projectors in H_{LW} is different compared to the topological phase. Consequently, the degenerate ground state is now given by the states, for which $b_p = \tau$ for every plaquette p . As we can read from (3.60), the ground-state degeneracy yields $D_{N_p}^{\text{torus}} = (F_{N_p} + 2F_{N_p-1})^2$ and thus diverges in the thermodynamic limit $N_p \rightarrow \infty$. Excitations above this set of ground states contain local $\mathbf{1}$ fluxes and are thus gapped.

However, within the infinitely degenerate ground-state manifold, a local perturbation such as H_{loc} couples different states with each other. Thus, one cannot expect the degeneracy to persist completely for some deviations from $\theta = \pi$. Consequently, the point $\theta = \pi$ is not expected to belong to an extended topological phase, but to represent rather a particular point in the phase diagram. This observation agrees with the definition of topological order given in (1.1).

3.5.1.4 The $\mathbf{1}$ -phase

Let us now turn to the case $\theta = \frac{\pi}{2}$. The ground state of the $\mathbf{1}$ -phase is unique and given by (3.50) as discussed in Section 3.2. The elementary excitations are the states $|\mathbf{6}\tau\rangle_p$ (3.51).

The action of the Hamiltonian H_{LW} onto these states can be read from (3.9). Note that there is no direct hopping term for this perturbation, i.e.

$$\langle \mathbf{6}\tau |_{p'} H_{\text{LW}} | \mathbf{6}\tau \rangle_p = 0, \quad (3.63)$$

where p and p' are neighboring plaquettes on the hexagonal lattice. Consequently, the elementary excitations become mobile only via virtual fluctuations.

3.5.1.5 The τ -phase

For $\theta = \frac{3\pi}{2}$, i.e. the negative sign of the coupling J_e , we see that the ground state is given by

$$|\text{gs}_{\text{loc},\tau}\rangle = \prod_e |\tau\rangle_e, \quad (3.64)$$

which is the state with the least number of $\mathbf{1}$ -labels on the edges. Note that $|\text{gs}_{\text{loc},\tau}\rangle$ also fulfills the branching rules, as for the Fibonacci theory, we have $\delta_{\tau,\tau,\tau} = 1$. This

state is not degenerate for any surface. Thus the corresponding phase is topologically trivial. In analogy to the $\mathbf{1}$ -phase, we refer to this phase as τ -phase.

Contrary to the $\mathbf{1}$ -phase, the elementary excitations are given here by

$$|\tau\rangle_e = |\mathbf{1}\rangle_e \prod_{e' \neq e} |\tau\rangle_{e'}, \quad (3.65)$$

which have an energy gap of $-J_e > 0$. As these states can be obtained by flipping a local link label from τ to $\mathbf{1}$, we can conclude that these excitations are bosonic [10].

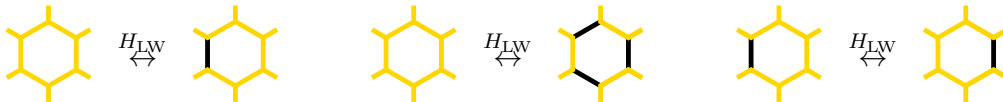


FIGURE 3.9: Some of the matrix elements of H_{LW} in the low-energy configurations of the τ -phase. We see that the action of H_{LW} creates single and multiple excitations, as well as long-range hoppings.

In Figure 3.9, we show the action of H_{LW} on some of the low-energy configurations. We observe that there are much more actions of H_{LW} on the ground state than in the $\mathbf{1}$ -phase, which generate states with one, two or three excitation. This already indicates that H_{LW} induces strong fluctuations on the ground state.

Additionally the action of H_{LW} provides hopping terms for the elementary excitations. These hopping terms are long ranged, as an excitation may hop to any bond of the plaquette, the topological Hamiltonian acts on. Thus, we see that the two “polarized” phases for the Fibonacci theory show different excitations and consequently a different action of the Hamiltonian H_{LW} on the low-energy states.

3.5.2 Ising anyons

In the following, we discuss the perturbed string-net model for Ising anyons. This theory has three labels, so that we have two distinct types of excitations. One consequence is e.g. that the phase corresponding to the value $\theta = \frac{3\pi}{2}$, is not a polarized phase as the τ -phase for the Fibonacci model. Due to the similarities with a quantum dimer model, we refer to this as dimer limit.

3.5.2.1 The topological phase

The labels describing the effective degrees of freedom for topological phase at $\theta = 0$ are given by the doubled Ising theory $D(\text{Ising})$, which has the label set

$$\{(\mathbf{1}, \mathbf{1}), (\mathbf{1}, \boldsymbol{\psi}), (\boldsymbol{\psi}, \mathbf{1}), (\boldsymbol{\psi}, \boldsymbol{\psi}), (\boldsymbol{\sigma}, \boldsymbol{\sigma}), (\boldsymbol{\sigma}, \mathbf{1}), (\mathbf{1}, \boldsymbol{\sigma}), (\boldsymbol{\sigma}, \boldsymbol{\psi}), (\boldsymbol{\psi}, \boldsymbol{\sigma})\}. \quad (3.66)$$

The number of ground states is therefore 9. The achiral labels corresponding to possible labels for the fluxes are given by $(\mathbf{1}, \mathbf{1})$, $(\boldsymbol{\sigma}, \boldsymbol{\sigma})$, and $(\boldsymbol{\psi}, \boldsymbol{\psi})$, the chiral labels only appear in the non-local fusion channels.

Note that the $(\boldsymbol{\psi}, \boldsymbol{\psi})$ -anyon is Abelian, i.e. it only has a unique fusion channel, when fused with itself. The $(\boldsymbol{\sigma}, \boldsymbol{\sigma})$ -anyon is non-Abelian. We observe that the branching rules restrict the number of local $(\boldsymbol{\sigma}, \boldsymbol{\sigma})$ -fluxes to be even.

The action of the local perturbation H_{loc} is given by (3.53) and results in similar processes as depicted in Figure 3.7. However, let us note here that only pairs of the same label are created or annihilated, but the correlated creation may involve distinct local flux-labels. Otherwise, the perturbation has the same flux-conserving property as for the Fibonacci theory, as it does not change a flux through a surface unless it acts on its boundary. Through the action of the perturbation the local fluxes become mobile and interacting quasi-particles.

3.5.2.2 Counting of states

Let us note here that we can determine the dimension of the Hilbert space analogously to Section 3.5.1.2. However, we have two labels for non-trivial fluxes and thus we have to sum over the number of states with $k_{\boldsymbol{\psi}}$ $(\boldsymbol{\psi}, \boldsymbol{\psi})$ -fluxes and $k_{\boldsymbol{\sigma}}$ $(\boldsymbol{\sigma}, \boldsymbol{\sigma})$ -fluxes

$$D_{\text{tot}}^{\text{torus}} = \sum_{k_{\boldsymbol{\psi}}, k_{\boldsymbol{\sigma}}} D_{k_{\boldsymbol{\psi}}, k_{\boldsymbol{\sigma}}}^{\text{torus}}. \quad (3.67)$$

The degeneracies $D_{k_{\boldsymbol{\psi}}, k_{\boldsymbol{\sigma}}}^{\text{torus}}$ can e.g. be obtained by first fusing the $k_{\boldsymbol{\psi}}$ Abelian $\boldsymbol{\psi}$ -labels, for which we have in analogous notations as in Section 3.5.1.2

$$N_{k_{\boldsymbol{\psi}}}^{\mathbf{1}} = \begin{cases} 1 & k_{\boldsymbol{\psi}} \text{ even} \\ 0 & k_{\boldsymbol{\psi}} \text{ odd} \end{cases}, \quad N_{k_{\boldsymbol{\psi}}}^{\boldsymbol{\psi}} = \begin{cases} 0 & k_{\boldsymbol{\psi}} \text{ even} \\ 1 & k_{\boldsymbol{\psi}} \text{ odd} \end{cases}, \quad (3.68)$$

as for Abelian fluxes, the overall fusion channels are already uniquely determined by the local fluxes. For the non-Abelian $\boldsymbol{\sigma}$ -labels, we have for $k_{\boldsymbol{\sigma}} > 1$, due to the fusion vertices of the Ising theory (2.27), the following non-zero multiplicities $N_{k_{\boldsymbol{\sigma}}\boldsymbol{\sigma}}^a$ of fusing

k_σ σ -labels to label a

$$N_{2n\sigma}^{\mathbf{1}} = N_{2n\sigma}^\psi = N_{(2n-1)\sigma}^\sigma, \quad N_{(2n+1)\sigma}^\sigma = N_{2n\sigma}^{\mathbf{1}} + N_{2n\sigma}^\psi. \quad (3.69)$$

As we have $N_{\mathbf{1}}^\sigma = 1$, we see that

$$N_{2n\sigma}^{\mathbf{1}} = N_{2n\sigma}^\psi = N_{(2n+1)\sigma}^\sigma = 2^n. \quad (3.70)$$

To obtain the total degeneracy on the torus, one has to take into account the flux labels c^\pm . As we have $\mathbf{1} \otimes \sigma = \psi \otimes \sigma = \sigma$, the number of ψ -labels does not impact the result, if $k_\sigma > 0$. Note that there is no fusion vertex with an odd number of σ -labels, so that the overall fusion channel of the local fluxes has to be either $\mathbf{1}$ or ψ . We can read off the fusion vertices (2.27), that there are three ways to fuse an overall fusion channel $\mathbf{1}$ with the possible labels of c^\pm , whereas there is only one possibility of fusing an overall fusion channel ψ , as $\delta_{\psi, c^\pm, c^\pm} = \delta_{c^\pm, \sigma}$.

Thus, we get in total

$$D_{k_\psi, k_\sigma}^{\text{torus}} = \begin{cases} \binom{N_p}{k_\psi} \binom{N_p - k_\psi}{k_\sigma} (3N_{k_\sigma\sigma}^{\mathbf{1}} + 1N_{k_\sigma\sigma}^\psi)^2 & k_\sigma > 0 \\ \binom{N_p}{k_\psi} (3N_{k_\psi\psi}^{\mathbf{1}} + 1N_{k_\psi\psi}^\psi)^2 & k_\sigma = 0 \end{cases}, \quad (3.71)$$

where the binomial coefficients account for the number of possibilities to distribute the fluxes on N_p plaquettes.

Let us note that one can transform the lengthy expression (3.71) with some algebra to obtain the degeneracy of a k -flux state

$$D_{k_\psi+k_\sigma}^{\text{torus}} = \binom{N_p}{k_\psi+k_\sigma} \left(1 + 6(-1)^{k_\psi+k_\sigma} + 2 \cdot 3^{k_\psi+k_\sigma} \right) \quad (3.72)$$

The latter form can be easily summed over to obtain the total dimension of the Hilbert space, which reads

$$D_{\text{tot}}^{\text{torus}} = 2 \cdot 4^{N_p} + 2^{N_p}. \quad (3.73)$$

Let us note here that if one sums only the degeneracies of the levels with $k_\sigma = 0$ and omits the values σ for c^\pm , one obtains the total dimension for the semionic theory to be

$$D_{\text{sem, tot}}^{\text{torus}} = \sum_{k=0}^{N_p/2} \binom{N_p}{2k} = 2 \cdot 2^{N_p}, \quad (3.74)$$

as it shares the fusion rules with the restricted set $\{(a, b), a, b \in \{\mathbf{1}, \psi\}\}$.

3.5.2.3 The flux-full case

For $\theta = \pi$, we are in the same situation as for the Fibonacci theory: the ground states are states, where a non-trivial flux is located on every plaquette. Additionally to the fact that there are two types of non-trivial fluxes, also the non-unique fusion channels of the σ -labels lead to an infinite ground-state degeneracy in the thermodynamic limit. Also in the present case, the local perturbation couples the different states, and thus this degeneracy is expected to split at least partially.

3.5.2.4 The 1-phase

As described for the general string-net model, the unique ground state $|\text{gs}_{\text{loc},\mathbf{1}}\rangle$ is given by (3.50). The gapped elementary excitations are

$$|6\sigma\rangle_p = B_p^\sigma |\text{gs}_{\text{loc},\mathbf{1}}\rangle = \left| \begin{array}{c} \text{---} \\ \text{---} \\ \text{---} \\ \text{---} \\ \text{---} \\ \text{---} \end{array} \right\rangle, \quad (3.75)$$

$$|6\psi\rangle_p = B_p^\psi |\text{gs}_{\text{loc},\mathbf{1}}\rangle = \left| \begin{array}{c} \text{---} \\ \text{---} \\ \text{---} \\ \text{---} \\ \text{---} \\ \text{---} \end{array} \right\rangle, \quad (3.76)$$

on which the Hamiltonian H_{LW} acts as described in (3.9) and thus introduces similar processes as for the Fibonacci theory. In particular, there is no direct hopping term, so that also here the elementary excitations become mobile only via virtual fluctuations. Nevertheless, the topological Hamiltonian couples the two excitations on the same plaquette p , i.e.

$$\langle 6\psi|_p H_{\text{LW}} |6\sigma\rangle_p = \frac{d_\sigma}{\mathcal{D}^2} \neq 0, \quad (3.77)$$

so that the elementary excitations mix under the action of H_{LW} .

3.5.2.5 The dimer limit

Contrary to the Fibonacci theory, the ground state for $\theta = \frac{3\pi}{2}$ is not unique, but degenerate. This is because the only fusion vertex without label $\mathbf{1}$ is given by the one related

to $\delta_{\sigma,\sigma,\psi} = \delta_{\sigma,\psi,\sigma} = \delta_{\psi,\sigma,\sigma} = 1$. Consequently, there are the three ways

$$\begin{array}{ccc}
 \begin{array}{c} \sigma \quad \sigma \\ \diagdown \quad / \\ \psi \end{array} &
 \begin{array}{c} \sigma \quad \psi \\ \diagdown \quad / \\ \sigma \end{array} &
 \begin{array}{c} \psi \quad \sigma \\ \diagdown \quad / \\ \sigma \end{array}
 \end{array}
 \tag{3.78}$$

of assigning this fusion vertex to a vertex of the actual lattice. One observation is that

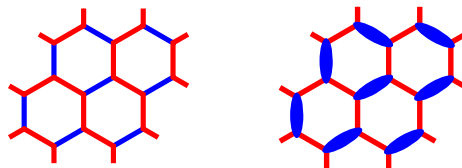


FIGURE 3.10: For $\theta = \frac{3\pi}{2}$, we see that the ground states correspond to the states with one ψ and two σ as incident labels. The corresponding states can be seen as dimer coverings of the hexagonal lattice, by assigning a dimer to each bond labeled by the label ψ .

there is one link labeled by ψ per vertex. By considering now these links as dimers as in Figure 3.10, we see that the ground states correspond to complete dimer coverings of the hexagonal lattice. Defects of these dimer coverings correspond to excitations $-J_e > 0$.

Let us note already here that the action of H_{LW} induces terms within the ground-state manifold, and thus the dimer limit is not expected to belong to an extended phase for small deviations from $\theta = \frac{3\pi}{2}$. We observe, that these terms go beyond the ones usually considered for quantum dimer models (cf. e.g. to Refs. [49, 118]). Consequently, the analysis of the phases arising in the vicinity of this point in the phase diagram is not as straightforward as e.g. for the **1**-phase.

3.5.3 The Abelian cases: semions and $D(\mathbb{Z}_2)$

For the Abelian case of the semions and the $D(\mathbb{Z}_2)$ theory, we can actually describe the Hamiltonian H (3.54) in terms of the transverse-field Ising model defined on the dual, i.e. the triangular lattice. In order to understand this result, let us proceed in two steps. The first consists in realizing that the degrees of freedom, which are relevant for the matrix elements of the local Hamiltonian, are given by achiral labels. Within this achiral sector, one can show in a second step that the Hamiltonian (3.54) for doubled semions coincides with the one of the $D(\mathbb{Z}_2)$ theory (2.23). As discussed in Ref. [56], this theory is equivalent to a \mathbb{Z}_2 -gauge theory [119]. The latter is dual to the transverse-field Ising model for an open plane (as detailed e.g. in Ref. [120]) and thus we can finally understand the different phases of the perturbed anyonic model in terms of the known phases of the transverse-field Ising model.

For the first step, let us remind that for Abelian anyons, there is also a unique fusion outcome, so we have always $b_{S_n}^+ = b_{S_n}^-$. Thus the fusion channels of local fluxes are in the doubled representation (3.41) always achiral. Let us note that the label for the non-local flux (c^+, c^-) may be chiral, but as we have necessarily $b_{S_{N_p}}^+ = b_{S_{N_p}}^- = \mathbf{1}$ for Abelian theories, the non-local fluxes are decoupled from the local fusion channels.

Consequently, the matrix elements of the local perturbation for appropriately ordered local fluxes in the dual basis (3.53) are given by

$$\mathcal{P}_e^{\mathbf{1}} \left| \begin{array}{c} c \\ \text{---} \\ a \text{---} \text{---} b \\ \text{---} \\ c \end{array} \right\rangle = \sum_{t, a', b'} \frac{d_t}{\mathcal{D}^2} \left(F_{t a' b'}^{c b a} \right)^2 \left| \begin{array}{c} c \\ \text{---} \\ a' \text{---} \text{---} b' \\ \text{---} \\ c \end{array} \right\rangle. \quad (3.79)$$

We can see by comparing the possible values of the matrix elements of the semionic (cf. Section 2.4.1) and the $D(\mathbb{Z}_2)$ theory (cf. Section 2.4.4), that the matrix elements in (3.79) coincide if we replace \mathbf{s} by $-\mathbf{1}$.

As we have additionally in the achiral sector for these theories

$$\left| \begin{array}{c} c \\ \text{---} \\ a \text{---} \text{---} b \\ \text{---} \\ c \end{array} \right\rangle = \left| \begin{array}{c} c \\ \text{---} \\ b \text{---} \text{---} a \\ \text{---} \\ c \end{array} \right\rangle = R_c^{a b} \left(R_c^{b a} \right)^{-1} \left| \begin{array}{c} c \\ \text{---} \\ b \text{---} \text{---} a \\ \text{---} \\ c \end{array} \right\rangle = \left| \begin{array}{c} c \\ \text{---} \\ b \text{---} \text{---} a \\ \text{---} \\ c \end{array} \right\rangle, \quad (3.80)$$

i.e. the R -moves necessary to transform the fusion diagram into the local form (3.79), do not change the matrix elements of the local perturbation for Abelian theories. In particular (3.80) shows that particles labeled by (\mathbf{s}, \mathbf{s}) and $\boldsymbol{\varepsilon} = (-\mathbf{1}, -\mathbf{1})$ have bosonic exchange statistics.

Consequently, the Hamiltonian (3.54) for the semionic theory and the $D(\mathbb{Z}_2)$ theory coincide. As already detailed in Ref. [56], we can express (3.54) for the $D(\mathbb{Z}_2)$ theory

$$H = -\frac{J_p}{2} \sum_p \left(\mathbf{1} + \prod_{e \in p} \sigma_e^x \right) - \frac{J_e}{2} \sum_e \left(\mathbf{1} + \sigma_e^z \right), \quad (3.81)$$

where the $\sigma_e^{x,z}$ are the Pauli matrices, and we use the representation $\sigma_e^z |\pm \mathbf{1}\rangle_e = \pm |\pm \mathbf{1}\rangle_e$. As e.g. detailed in Ref. [120], we can obtain the transverse-field Ising model from (3.81) by introducing the mapping

$$\prod_{e \in p} \sigma_e^x \rightarrow \tilde{\sigma}_e^x, \quad \sigma_e^z \rightarrow \tilde{\sigma}_p^z \tilde{\sigma}_{p'}^z, \quad (3.82)$$

where p, p' denote the plaquettes neighboring the link e . Finally, we obtain up to a constant energy shift the Hamiltonian H_{TFIM}

$$H_{\text{TFIM}} = -\frac{J_p}{2} \sum_p \tilde{\sigma}_e^x - \frac{J_e}{2} \sum_{\langle p, p' \rangle} \tilde{\sigma}_p^z \tilde{\sigma}_{p'}^z. \quad (3.83)$$

Thus we have mapped the perturbed topological Hamiltonian onto the transverse-field Ising model on an open system. Note that we have not discussed the effect of the boundary conditions yet.

As the topological Hamiltonian H_{LW} is mapped onto the field term in (3.83), we see that for $\theta = 0$ and for $\theta = \pi$, there is a topologically ordered phase of $D(\mathbb{Z}_2)$ type. The ground state is unique for (3.83) as described in (3.42). Note that the number of flipped spins with respect to the ground state is constrained to be even.

The limit $\theta = \frac{\pi}{2}$ corresponds to the ferromagnetic Ising model on the triangular lattice. However, the ground state of the string-net model is unique, as due to the conserved boundary mode (3.56) one ferromagnetic ground state is fixed. Excitations are anti-ferromagnetic bonds at the boundary of domains with plaquettes labeled by $\mathbf{1}_p$ and $-\mathbf{1}_p$ respectively.

The limit $\theta = \frac{3\pi}{2}$ corresponds to the anti-ferromagnetic (AFM) Ising model on the triangular lattice. Due to the frustrating geometry of the triangular lattice, the ground state is infinitely degenerate. Note that also here, the \mathbb{Z}_2 -symmetry of the spin- $\frac{1}{2}$ Ising model is broken by the conserved non-local boundary mode in the original model.

Let us finally note here that this mapping can be seen as a special case of the duality mapping for unperturbed (Abelian) string-net models onto $(N + 1)$ -state Potts models presented in Ref. [96], which is extended to handle also the perturbation H_{loc} . This mapping introduces a domain-wall picture for the labels defined on the bonds of the hexagonal lattice. As we start from a description dual to the bond basis, we employ additionally the duality of the resulting gauge model to the Ising model to obtain the same result. The advantage of the ways presented above is that it allows to make the connection of the semionic model and the lattice-gauge model to show that these two coincide for the given perturbation.

Additionally, from the above construction it is clear that one cannot construct, by similar means, an analog mapping for the non-Abelian case, where the involved R -moves do not cancel. So, for Fibonacci and Ising anyons, we do not expect e.g. a phase transition out of the topological phase described in a one-to-one correspondence of the topological excitations to the ones of a statistical spin model.

3.6 Chapter Summary

In this chapter we introduced the microscopic models investigated in Chapter 5.

Therefore, we presented the Hamiltonian H_{LW} introduced by Levin and Wen [56]. This exactly solvable Hamiltonian is defined in terms of the properties of a general anyonic model as presented in Chapter 2. We discussed its properties making use of the bond basis (3.1), defined completely in terms of the microscopic degrees of freedom, as well as the flux basis (3.20), which characterizes the eigenstates of H_{LW} the most local way possible. Finally we constructed the dual basis, which allows to determine properties such as (ground-state) degeneracies in a straightforward fashion. Let us emphasize here that the construction of the dual basis, which is an orthonormal and complete eigenbasis, has not been reported in the literature to the best of our knowledge.⁵ It turns out that the eigenbasis of the topological Hamiltonian is described in terms of an anyonic theory, which is the doubled version of the theory from which the microscopic model is constructed.

We discussed also the effects of different surface topologies including boundaries on the spectrum of the string-net model. This allows to treat the string-net Hamiltonian not only for periodic boundary conditions, but also open boundaries.

To perturb the topological phase with a local operator, we introduced the Hamiltonian H_{loc} . This term represents the simplest local perturbation and is the analogon of a single parallel field in the study of the Abelian toric code models [71, 75, 77–79].

We discussed on general grounds the different phases to be expected in the phase diagram of a perturbed string-net model. This discussion was then detailed for the three different types of anyons, for which we investigated the perturbed topological Hamiltonian: the non-Abelian Fibonacci and Ising anyons as well as the Abelian semions. For the latter, it turns out that the model is equivalent to the transverse-field Ising model. For the non-Abelian anyons, there is no such an equivalence.

By investigating the limiting cases of the topological and the local Hamiltonian, we identify for the Fibonacci theory the doubled topological phase and two topologically trivial phases. The latter phases, called $\mathbf{1}$ - and $\boldsymbol{\tau}$ -phase, are the analog of the paramagnetic phase in the study of the perturbed toric code but they are different due to the differences between the $\mathbf{1}$ and $\boldsymbol{\tau}$ of the Fibonacci theory.

⁵However, the low-energy Hilbert space as been described for the ladder geometry e.g. in Ref. [69] and a similar picture for anyonic states has been developed in Ref. [103].

For the Ising anyons, we find a richer variety of limiting cases. Additionally to the topological and the $\mathbf{1}$ -phase, we find for $\theta = \frac{3\pi}{2}$ that the effective model is described in this limit by a model build from quantum dimers.

In the following chapters we shall investigate the possible phase transitions of these three different models.

Topological symmetry breaking

*In all chaos there is a cosmos,
in all disorder a secret order.
- Carl Gustav Jung -*

In the previous section, we discussed the perturbed string-net model (3.54), which harbors topological ordered and topological trivial phases. When tuning the relative couplings or respectively the control parameter θ in (3.54) (not to be confused the twist θ_a of a particle a), phase transitions occur.

In principle, there are two types of phase transitions: those, where the system's ground state changes because another state becomes lower in energy, and those, where the ground state remains the same, but changes its characteristics. The latter case is referred to as a continuous phase transition.

If a continuous phase transition takes place between two non-topologically ordered phases, the change of the ground-state wave function can be captured by a local order parameter [1, 2]. This local order parameter transforms according to the representations of the symmetry groups, which describe the symmetries of the two phases between which the transition occurs. A continuous phase transition is then possible if one symmetry group can be reduced or broken to the other one, i.e. if one symmetry group is a subgroup of the other [121, 122]. The properties of the ground-state wave function and the local order parameter at the transition point are then only dependent on the involved symmetries and not on microscopic details of the underlying model.

This yields the characterization of phase transitions in terms of universality classes. The critical properties, as e.g. critical exponents, coincide for phase transitions of the same universality class and can be used to identify a phase transition investigated for a given microscopic Hamiltonian. However, topologically ordered phases cannot be characterized by any local order parameter. Consequently, the approach to phase transitions

via the Landau paradigm of symmetry breaking does not apply in general to phase transitions out of topological phases.

In some cases, there is an effective dual description of the topological phase, in which a local order parameter in the dual theory can capture a phase transition. This is for example the case if the low-energy spectrum only contains particles with trivial mutual braiding statistics, as e.g. for the semions discussed in Section 3.5.3 or for \mathbb{Z}_N -anyons [86, 96].

However, these local dual descriptions do not exist for non-Abelian anyons, as there e.g. the non-trivial degeneracies of excited states cannot be captured locally.

Therefore, a formalism analogous to Landau's symmetry breaking paradigm has been developed [19, 100] based on the algebraic structure of the anyonic theories presented in Chapter 2, i.e. the fusion algebra \mathcal{F} plays in this framework the role of the symmetry group in the Landau-Ginzburg theory. This framework, to which one also refers as Hopf-symmetry breaking [123] is the focus of the present chapter.

4.1 General framework

Let us note here that e.g. topologically ordered phases also arise in the context of gauge symmetries [19, 28, 86]. These gauge symmetries cannot be broken by a local order parameter [124]. However, it is possible to describe condensates with order parameters. So, we consider here continuous phase transitions, which are driven by the condensation of one or more particles to form, together with the ground state of the original phase, the ground state of the broken one.

In order to discuss these phase transitions, we will proceed along the lines of Ref. [19] in two steps. In the first step, we shall reduce the fusion algebra \mathcal{F} describing the original phase by condensation of an excitation into the vacuum of an intermediate algebra \mathcal{F}' . This intermediate algebra contains all possible excitations in the other phase, but is not required to only describe deconfined particles. Thus it may also contain representations, which either do not correspond to point-like particles or correspond to particles having non-trivial braiding statistics with the condensate. Both types lead in the absence of boundaries to the confinement of the corresponding representations in the resulting phase, which will be described by a fusion algebra $\bar{\mathcal{F}}$. The confined representations can eventually be used to describe boundary modes of the broken phase [19].

4.1.1 Condensation

For the condensation picture of the phase transition, it is useful to think about the labels of the fusion algebra \mathcal{F} as irreducible representations of a (quantum) group.

Irreducible representations $\{a\}$ of \mathcal{F} , which are reducible representations of the subalgebra \mathcal{F}' , can be decomposed in terms of irreducible representations $\{\bar{a}\}$ of \mathcal{F}' . This splitting can be described by

$$a \rightarrow \sum_{\bar{a} \in \mathcal{F}'} n_{\bar{a}}^a \bar{a}, \quad (4.1)$$

where a is an irreducible representation of \mathcal{F} , the \bar{a} are the irreducible representations of \mathcal{F}' and $n_{\bar{a}}^a$ are the integer multiplicities appearing in the decomposition. Note that this is the exact analogue of the decomposition of representations in the case of the reduction of the symmetry group within Landau's paradigm. We refer to the labels a as lifts of \bar{a} if $n_{\bar{a}}^a \neq 0$.

Additionally, it is possible that distinct representations of \mathcal{F} correspond to the same representation of \mathcal{F}' , so that different particles become identified via the transition.

The possible fusion algebras \mathcal{F}' are required to be well-behaved, i.e. the fusion algebra of the labels is an associative, well-defined algebra with a unique trivial label. Additionally, we require also for the labels in \mathcal{F}' that $N_{\bar{a}\bar{a}}^{\bar{1}} \leq 1$, i.e. there is a unique way to couple to the vacuum.

In order for the fusion algebras \mathcal{F} and \mathcal{F}' to be compatible with each other, we require that the transition to the reduced algebra and the fusion rules commute, i.e. if $a \otimes b = \sum_c N_{ab}^c c$, we have

$$a \otimes b \rightarrow \left(\sum_{\bar{a} \in \mathcal{F}'} n_{\bar{a}}^a \bar{a} \right) \otimes \left(\sum_{\bar{b} \in \mathcal{F}'} n_{\bar{b}}^b \bar{b} \right) = \sum_{\bar{a}, \bar{b} \in \mathcal{F}'} n_{\bar{a}}^a n_{\bar{b}}^b \bar{a} \otimes \bar{b} = \sum_{c \in \mathcal{F}} N_{ab}^c \left(\sum_{\bar{c} \in \mathcal{F}'} n_{\bar{c}}^c \bar{c} \right). \quad (4.2)$$

This constraint leads e.g. to the necessary condition

$$a \rightarrow \sum_{\bar{a} \in \mathcal{F}'} n_{\bar{a}}^a \bar{a} \Rightarrow d_a = \sum_{\bar{a} \in \mathcal{F}'} n_{\bar{a}}^a d_{\bar{a}}, \quad (4.3)$$

which is helpful to identify possible candidates of \mathcal{F}' .

In order to have a non-trivial condensation, there has to be at least one label $b \neq \mathbf{1}$ such that $n_{\mathbf{1}}^b \neq 0$, i.e.

$$b \rightarrow \bar{\mathbf{1}} + \sum_{\bar{b} \neq \bar{\mathbf{1}}} n_{\bar{b}}^b \bar{b}. \quad (4.4)$$

However, not only properties like the fusion rules of the algebra \mathcal{F} carry over to the intermediate algebra \mathcal{F}' , but also other properties like spins and mutual braiding statistics. We discuss how this point impacts the excitations of the symmetry-reduced phase in the following section.

4.1.2 Confinement

Not all excitations of the symmetry-reduced phase described the fusion algebra \mathcal{F}' will be point-like, deconfined particles. The latter are then described by the resulting fusion algebra $\bar{\mathcal{F}}$.

To see this, one has to consider the fact that properties of representations $\bar{a} \in \mathcal{F}'$ like the spin are inherited from the lifts $a \in \mathcal{F}$.

As point-like particles have a well-defined spin, we see directly that representations \bar{a} with lifts having distinct spins cannot be point-like. As extended excitations correspond to regions, where the original phase is restored, these will have an extensive energy cost with respect to the vacuum of the resulting phase, which contains the condensate. Consequently these excitations will be confined, i.e. not present in the low-energy spectrum.

This tells us directly that the condensing particle b has to fulfill $\theta_b = 1$, in order to yield a meaningful, i.e. deconfined, vacuum.

Additionally, we require the excitations in the resulting phase to have trivial braiding statistics with the condensate in order to obtain a well-defined fusion algebra, which in particular fulfills (2.16). Excitations not fulfilling this condition interact with the condensate and consequently become confined. Note that this is the analog of the Higgs mechanism discussed in high-energy physics [125–127].

So we obtain the final fusion algebra $\bar{\mathcal{F}}$ by eliminating all representations in \mathcal{F}' not fulfilling the above conditions. For notational brevity, we label the representations in $\bar{\mathcal{F}}$ the same as in \mathcal{F}' . Note that the fusion algebra $\bar{\mathcal{F}}$ turns out to be a closed algebra [19] and thus yields a meaningful description of a topological phase.

However, the confined particles may also be present in the physical system if there is a boundary between a region with and without condensate. In the same sense, the

confined labels of \mathcal{F}' may appear as boundary modes in the resulting phase. This occurs e.g. in case of the two-leg ladder geometry investigated in Ref. [69, 70]. Here the system consists mostly of the boundary (the legs), where is no condensate present. Thus, extended excitations coupling to the boundary have only a finite energy cost and consequently no confinement takes place.

Let us discuss now the examples, which are relevant for the anyonic theories considered in this thesis.

4.2 Examples of topological symmetry breaking

In this section, we consider the possible condensate-induced phase transitions for the models of interest within this thesis. Therefore we will give the intermediate algebra. In the case of topological non-trivial resulting phases, we give the fusion algebra of it, too.

4.2.1 Phase transitions out of the doubled semion phase D(Semion)

We discuss here the case of the fusion algebra of the doubled semion model $D(\text{semion}) = \{(\mathbf{1}, \mathbf{1}), (\mathbf{1}, \mathbf{s}), (\mathbf{s}, \mathbf{1}), (\mathbf{s}, \mathbf{s})\}$. The only achiral label except $(\mathbf{1}, \mathbf{1})$ is (\mathbf{s}, \mathbf{s}) . The quantum dimensions of all labels equal 1, so that no splitting of the corresponding representations can occur. Therefore we have as the only possibility of a symmetry reduction:

$$\begin{aligned} (\mathbf{1}, \mathbf{1}) &\rightarrow \bar{\mathbf{1}}, & (\mathbf{s}, \mathbf{s}) &\rightarrow \bar{\mathbf{1}}, \\ (\mathbf{1}, \mathbf{s}) &\rightarrow \bar{\mathbf{s}}, & (\mathbf{s}, \mathbf{1}) &\rightarrow \bar{\mathbf{s}}. \end{aligned} \tag{4.5}$$

So, the intermediate algebra is the fusion algebra of the semionic theory.

As the particles $(\mathbf{1}, \mathbf{s})$ and $(\mathbf{s}, \mathbf{1})$ do not have the same spin, the resulting particle $\bar{\mathbf{s}}$ has to be confined. Thus the phase arising via topological symmetry breaking from the doubled semion theory does not have deconfined topological excitations and is thus topologically trivial.

This result also holds for the $D(\mathbb{Z}_2)$ model, as here the fusion algebra is identical to the one for $D(\text{Semion})$. However, the spin of the only possible excitation $-\bar{\mathbf{1}}$ is well-defined, but its non-trivial braiding relation with $(-\mathbf{1}, -\mathbf{1})$ leads to the confinement.

4.2.2 Phase transitions out of the doubled Fibonacci phase D(Fib)

The label set of the doubled Fibonacci theory is given by

$$\mathcal{F}_{\text{D(Fib)}} = \{(\mathbf{1}, \mathbf{1}), (\mathbf{1}, \boldsymbol{\tau}), (\boldsymbol{\tau}, \mathbf{1}), (\boldsymbol{\tau}, \boldsymbol{\tau})\}. \quad (4.6)$$

We have the quantum dimensions $d_{(\mathbf{1}, \mathbf{1})} = 1, d_{(\mathbf{1}, \boldsymbol{\tau})} = \varphi, d_{(\boldsymbol{\tau}, \mathbf{1})} = \varphi, d_{(\boldsymbol{\tau}, \boldsymbol{\tau})} = \varphi^2$. In particular, the quantum dimension of the only non-trivial achiral representation $(\boldsymbol{\tau}, \boldsymbol{\tau})$ is larger than two. Thus, it splits within the symmetry breaking. The other quantum dimensions are smaller than two and thus, the corresponding representations do not split. Thus we have

$$\begin{aligned} (\mathbf{1}, \mathbf{1}) &\rightarrow \bar{\mathbf{1}}, & (\boldsymbol{\tau}, \boldsymbol{\tau}) &\rightarrow \bar{\mathbf{1}} + \bar{\boldsymbol{\tau}}, \\ (\mathbf{1}, \boldsymbol{\tau}) &\rightarrow \bar{\boldsymbol{\tau}}, & (\boldsymbol{\tau}, \mathbf{1}) &\rightarrow \bar{\boldsymbol{\tau}}, \end{aligned} \quad (4.7)$$

i.e. the undoubled theory for Fibonacci anyons as the only possible result of the symmetry breaking.

As in the case of the semions, the spin of the remaining excitation $\bar{\boldsymbol{\tau}}$ is not well-defined, as the spins of the three different lifts $(\boldsymbol{\tau}, \boldsymbol{\tau})$, $(\mathbf{1}, \boldsymbol{\tau})$ and $(\boldsymbol{\tau}, \mathbf{1})$ do not coincide. Thus, there are no deconfined particles in the resulting phase and consequently, this phase is topologically trivial.

4.2.3 Phase transitions out of the doubled Ising phase D(Ising)

The label set of the doubled Ising theory is given by (3.66). There are two types of achiral excitations, namely $(\boldsymbol{\sigma}, \boldsymbol{\sigma})$ and $(\boldsymbol{\psi}, \boldsymbol{\psi})$. Whereas $d_{(\boldsymbol{\psi}, \boldsymbol{\psi})} = 1$, so that the particle $(\boldsymbol{\psi}, \boldsymbol{\psi})$ cannot split, we have $d_{(\boldsymbol{\sigma}, \boldsymbol{\sigma})} = 2$ and thus this particle may split in the symmetry reduction process. Let us note here that the other particles have quantum dimension lower than two and thus do not split.

We have two achiral particles and thus in principle (at least) two ways of symmetry breaking. Let us begin with the condensation of $(\boldsymbol{\sigma}, \boldsymbol{\sigma})$:

For this condensation, we have the only possible intermediate algebra

$$\begin{aligned} (\mathbf{1}, \mathbf{1}) &\rightarrow \bar{\mathbf{1}}, & (\boldsymbol{\sigma}, \boldsymbol{\sigma}) &\rightarrow \bar{\mathbf{1}} + \bar{\boldsymbol{\psi}}, \\ (\mathbf{1}, \boldsymbol{\psi}) &\rightarrow \bar{\boldsymbol{\psi}}, & (\boldsymbol{\psi}, \mathbf{1}) &\rightarrow \bar{\boldsymbol{\psi}}, & (\boldsymbol{\psi}, \boldsymbol{\psi}) &\rightarrow \bar{\mathbf{1}}, \\ (\mathbf{1}, \boldsymbol{\sigma}) &\rightarrow \bar{\boldsymbol{\sigma}}, & (\boldsymbol{\psi}, \boldsymbol{\sigma}) &\rightarrow \bar{\boldsymbol{\sigma}}, & (\boldsymbol{\sigma}, \mathbf{1}) &\rightarrow \bar{\boldsymbol{\sigma}}, & (\boldsymbol{\sigma}, \boldsymbol{\psi}) &\rightarrow \bar{\boldsymbol{\sigma}}. \end{aligned} \quad (4.8)$$

So, the algebra after condensation coincides with the one of the Ising theory. However, as (σ, σ) braids non-trivially with all other particles except (ψ, ψ) , all excitations in the resulting phase are confined and thus this phase is topologically trivial.

Let us note here that all symmetry reductions obtained so far are of the form

$$(a, b) \rightarrow \sum_{\bar{c}} N_{ab\bar{c}}^c, \quad (4.9)$$

i.e. the doubled algebra is reduced to the undoubled one. This type of symmetry reduction is actually possible for every doubled theory. However, due to the confinement of excitations, the resulting phase is in general trivial.

However, for the condensation of the (ψ, ψ) -particle, we have additionally to the condensation discussed above the possibility that the (σ, σ) -particle splits, but not in the trivial particle. Then we have

$$\begin{aligned} (\mathbf{1}, \mathbf{1}) &\rightarrow \bar{\mathbf{1}}, & (\psi, \psi) &\rightarrow \bar{\mathbf{1}}, \\ (\mathbf{1}, \psi) &\rightarrow \bar{\psi}, & (\psi, \mathbf{1}) &\rightarrow \bar{\psi}, \\ (\sigma, \sigma) &\rightarrow \bar{\lambda}_1 + \bar{\lambda}_2, \\ (\mathbf{1}, \sigma) &\rightarrow \bar{\sigma}, & (\psi, \sigma) &\rightarrow \bar{\sigma}, & (\sigma, \mathbf{1}) &\rightarrow \bar{\sigma}, & (\sigma, \psi) &\rightarrow \bar{\sigma}. \end{aligned} \quad (4.10)$$

Note that the lifts of $\bar{\sigma}$ have different spins and thus $\bar{\sigma}$ is confined in the resulting phase. The $\bar{\psi}$ is not confined for $\bar{\lambda}_1, \bar{\lambda}_2 \neq \bar{\mathbf{1}}$ as $\theta_{(\mathbf{1}, \psi)} = \theta_{(\psi, \mathbf{1})} = -1$ and its trivial braiding with (ψ, ψ) .

There are two possible choices for the fusion algebra to be consistent:

$$\begin{array}{c|cccc} \otimes & \bar{\mathbf{1}} & \bar{\lambda}_1 & \bar{\lambda}_2 & \bar{\psi} \\ \hline \bar{\mathbf{1}} & \bar{\mathbf{1}} & \bar{\lambda}_1 & \bar{\lambda}_2 & \bar{\psi} \\ \bar{\lambda}_1 & \bar{\lambda}_1 & \bar{\mathbf{1}} & \bar{\psi} & \bar{\lambda}_2 \\ \bar{\lambda}_2 & \bar{\lambda}_2 & \bar{\psi} & \bar{\mathbf{1}} & \bar{\lambda}_1 \\ \bar{\psi} & \bar{\psi} & \bar{\lambda}_2 & \bar{\lambda}_1 & \bar{\mathbf{1}} \end{array} \quad \begin{array}{c|cccc} \otimes & \bar{\mathbf{1}} & \bar{\lambda}_1 & \bar{\lambda}_2 & \bar{\psi} \\ \hline \bar{\mathbf{1}} & \bar{\mathbf{1}} & \bar{\lambda}_1 & \bar{\lambda}_2 & \bar{\psi} \\ \bar{\lambda}_1 & \bar{\lambda}_1 & \bar{\psi} & \bar{\mathbf{1}} & \bar{\lambda}_2 \\ \bar{\lambda}_2 & \bar{\lambda}_2 & \bar{\mathbf{1}} & \bar{\psi} & \bar{\lambda}_1 \\ \bar{\psi} & \bar{\psi} & \bar{\lambda}_2 & \bar{\lambda}_1 & \bar{\mathbf{1}} \end{array}. \quad (4.11)$$

The left fusion-rule table coincides with the one described in Section 2.4.4 for the $D(\mathbb{Z}_2)$ theory. In addition to the fusion rules, also the spins coincide as

$$\theta_{\bar{\lambda}_1} = \theta_{\bar{\lambda}_2} = \theta_{(\sigma, \sigma)} = 1, \quad \theta_{\bar{\psi}} = \theta_{(\mathbf{1}, \psi)} = -1. \quad (4.12)$$

So, we see that there is a possible continuous phase transition between the $D(\text{Ising})$ and the $D(\mathbb{Z}_2)$ phases. This phase transition is described in large detail e.g. in Ref. [101] for the transition from the $D(SU(2)_2)$ to $D(\mathbb{Z}_2)$ theory. As $D(SU(2)_2)$ and $D(\text{Ising})$ have

the same fusion algebra [102], we expect a phase transition of the same type. Let us note that this transition has also been investigated for $D(SU(2)_k)$ for general values of k [100].

The right fusion-rule table is the multiplication table of the group \mathbb{Z}_4 . It has e.g. been discussed in Ref. [128] in the context of one-dimensional quantum chains. However, with these fusion rules and the spin values (4.12), there is no unitary modular anyonic theory [19, 102]. Thus for this choice, we do not have a phase transition in two dimensions between two anyonic theories as defined in Chapter 2.

So for the case of the doubled Ising theory, we find two possible phase transitions out of the topological phase. One is driven by the simultaneous condensation of both achiral particles and results in a topologically trivial phase. In contrast to this, the second phase transition is driven by condensation of the Abelian achiral particle, leading to a topologically ordered phase, which corresponds to the $D(\mathbb{Z}_2)$ theory. Let us note here that for the models discussed in Chapter 3, the perturbation H_{loc} (3.48) provides dynamics to both particles and thus drives, as we shall discuss in Chapter 5, a condensation of both anyons, resulting in the topologically trivial phase. If one chooses a perturbation which provides only dynamics to the $(\psi, \bar{\psi})$ -particle, e.g. by a perturbation term L_e^ψ (3.52), one expects the second phase transition as discussed in Ref. [101] to take place.

4.3 Chapter summary

In this chapter, we have presented the framework of topological symmetry breaking. It generalizes the spontaneous symmetry breaking for non-topologically ordered phases and yields criteria, under which conditions a continuous phase transition may occur. This concept is based on the breaking of the fusion algebra \mathcal{F} by condensation of a particle into the ground state to a subalgebra \mathcal{F}' . This subalgebra may still describe e.g. extended excitations. The subalgebra $\bar{\mathcal{F}}$, which describes the deconfined, point-like excitations of the resulting phase is obtained by eliminating all representations of \mathcal{F}' , which are extended particles or possess non-trivial braiding statistics with the formed condensate.

We have discussed the possible condensation scenarios for the theories of interest within this thesis. The respective condensation of all achiral (quasi-) particles is driven by the local perturbation H_{loc} (3.48), and thus it is very likely that all achiral excitations of H_{LW} condense to yield a continuous phase transition to a topological trivial phase.

As we are considering here doubled anyonic phases, we find that there is always the possibility of a continuous phase transition to a topologically trivial phase by the simultaneous condensation of all achiral excitations. In the case of the Ising anyons, we find a possible continuous transition to another topologically ordered phase described by the $D(\mathbb{Z}_2)$ fusion algebra as described in Refs. [100, 101].

Therefore we have for the three distinct theories presented in Chapter 3 always the possibility of a continuous phase transition between topologically ordered and trivial phases. We shall investigate the different phase transitions in this model for each case. Let us note here that although the framework of condensate-induced symmetry breaking allows to understand continuous phase transitions, it does not enable us to identify the analog of universality classes for models described by different fusion algebras. Therefore we expect the phase transitions for the different anyonic theories to be different.

Results for perturbed string-net models

The shortest answer is doing the thing.
- Ernest Hemingway -

In this chapter, we shall investigate the phase diagram and phase transitions for the three different microscopic models presented in the previous chapters, namely the perturbed string-net model (3.54) for semions, Fibonacci anyons, and Ising anyons. We study these systems in the thermodynamic limit on a hexagonal lattice as depicted in Figure 3.1.

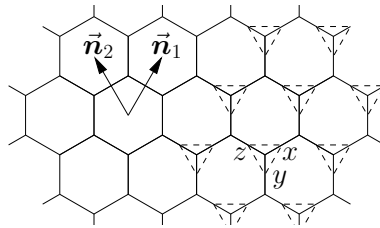


FIGURE 5.1: To describe the elementary excitations of the topological and the **1**-phase, which are defined on the plaquettes of the triangular lattice, the lattice vectors \vec{n}_1 and \vec{n}_2 are chosen. For the elementary excitations residing on the links of the lattice, i.e. the excitations of the τ -phase, we give additionally the unit cell indicated by the dashed triangle, where the three different links are denoted by x , y , and z , respectively.

For our description of the low-energy physics, we choose the unit cells depicted in Figure 5.1. Note that the low-energy degrees of freedom are located either on the plaquettes $\{p\}$ for the topological and the **1**-phase for all three considered models or on the links $\{e\}$ for the τ -phase of the Fibonacci model. Therefore we employ for the first case the unit cells for the triangular lattice formed by the plaquettes and for the second the triangular lattice formed by the three-link unit cells.

To determine the phase diagram and the phase transitions of the respective models, we investigate their low-energy physics. Therefore we determine the ground-state energy per plaquette e_0 and the gap of the lowest-energy excitation Δ using the methods discussed in large detail in Chapter II.

Let us mention here only that we derive the effective Hamiltonians $H_{0\text{qp}}^{\text{eff}}$ for the ground state(s) and $H_{1\text{qp}}^{\text{eff}}$ for the elementary excitations, which decouple the respective sectors from the rest of the Hilbert space.

In the case of a unique ground state, $H_{0\text{qp}}^{\text{eff}}$ is a 1×1 matrix, and so the ground-state energy per plaquette reads

$$e_0 = \frac{1}{N_p} \langle \text{gs} | H_{0\text{qp}}^{\text{eff}} | \text{gs} \rangle = \frac{1}{N_p} \mathcal{E}_0, \quad (5.1)$$

where $|\text{gs}\rangle$ is the reference state for the series expansion, N_p is the number of plaquettes in the lattice, and \mathcal{E}_0 is the extensive ground-state energy.

The effective Hamiltonian $H_{1\text{qp}}^{\text{eff}}$ is of the general form

$$H_{1\text{qp}}^{\text{eff}} = \sum_{\vec{l}} \sum_{\vec{r}, \alpha, \beta} t_{\vec{r}}^{\alpha, \beta} |\vec{l} + \vec{r}, \alpha\rangle \langle \vec{l}, \beta|, \quad (5.2)$$

where \vec{l} denotes the position of the unit cell, $\vec{r} = n_1 \vec{n}_1 + n_2 \vec{n}_2$ with $n_1, n_2 \in \mathbb{Z}$ is a lattice vector, and the indices α and β summarize possibly appearing additional quantum numbers as e.g. flux labels.

The hopping elements $t_{\vec{r}}^{\alpha, \beta}$ are given by

$$t_{\vec{r}}^{\alpha, \beta} = \langle \vec{l} + \vec{r}, \alpha | H^{\text{eff}} - \delta_{\alpha, \beta} \delta_{\vec{r}, \vec{0}} \mathcal{E}_0 | \vec{l}, \beta \rangle, \quad (5.3)$$

where H^{eff} is a method-dependent effective Hamiltonian as discussed in Chapter 6.

For translationally invariant systems, the effective Hamiltonian (5.2) is (block-) diagonalized by the unitary Fourier transform defined as

$$|\vec{k}, \alpha\rangle = \frac{1}{\sqrt{N_c}} \sum_{\vec{l}} e^{-i\vec{k}\vec{l}} |\vec{l}, \alpha\rangle, \quad (5.4)$$

where N_c is the number of unit cells in the lattice. Note that in the thermodynamic limit, the infinitely extended lattice is invariant under translations. So, we can always apply this transformation.

The matrix elements of the effective Hamiltonian $H_{\vec{k}}^{\text{eff}}$ take in this basis the simple form

$$\left(H_{\vec{k}}^{\text{eff}} \right)_{\beta, \alpha} = \langle \vec{k}, \beta | H_{1\text{qp}}^{\text{eff}} | \vec{k}, \alpha \rangle = \sum_{n_1, n_2} e^{i\vec{k}\vec{l}} t_{n_1 \vec{n}_1 + n_2 \vec{n}_2}^{\alpha, \beta}. \quad (5.5)$$

The dispersion $\omega(\vec{k})$ is then obtained by diagonalizing the finite-dimensional matrix $H_{\vec{k}}^{\text{eff}}$. Note that in the case of the absence of additional quantum numbers, $\omega(\vec{k})$ is directly given by the right-hand side of Eq. (5.5).

The global minimum of the dispersion in \vec{k} at the value \vec{k}_c gives the elementary excitation gap $\Delta = \omega(\vec{k}_c)$. This quantity is of particular interest in the context of condensate-induced phase transitions as detailed in Chapter 4. Within this framework, the condensate is formed by the condensation of an elementary excitation, thus the elementary particle-gap necessarily closes at the transition point.

In what follows, our main focus is the study of the phase transition between the topological and the **1**-phase, as it is present for the three investigated models.

5.1 Phase transitions in the semion model

In this section, we analyze the perturbed string-net model (3.54) for semions. The different series expansions discussed can be found in Appendix A.

As detailed in Section 3.5.3, this model is dual to the spin- $\frac{1}{2}$ transverse-field Ising model on the triangular lattice. Consequently the spectra of these two models coincide up to degeneracies. For the transverse-field Ising model, the phase diagram and the phase transitions are well known [129–133].

In particular, the phase transition from the paramagnetic to the ferromagnetic phase (corresponding to the phase transition from the topological to the **1**-phase in the language of Chapter 3) is a standard example for a continuous quantum phase transition [134], being in the universality class of the classical Ising model in three dimensions (c.f. Refs. [129, 130] and references therein).

Additionally, the phase transition from the paramagnetic to the anti-ferromagnetic phase is known to be in the same universality class as the three-dimensional classical XY-model [131, 133]. Thus, we shall use the analysis of this data as a verification of our procedure to obtain the low-energy spectrum and to validate the analysis applied also in the non-Abelian cases.

The global picture for the semion model is given in Figure 5.2, where we show the ground-state energy per plaquette e_0 and the low-energy gap Δ as a function of the control parameter θ (3.54). For the ground-state energy, we show the series expansions around the exactly solvable limits $\theta = 0$, $\theta = \pi$ (red) and $\theta = \frac{\pi}{2}$ (blue). Additionally, we show exact-diagonalization data for two different system sizes (gray and black).

Note that on the periodic systems considered in the exact diagonalization, the number of excitations is constrained to be even. In order to achieve a matching of the obtained spectra from exact diagonalization and the series expansion, we show for the semion

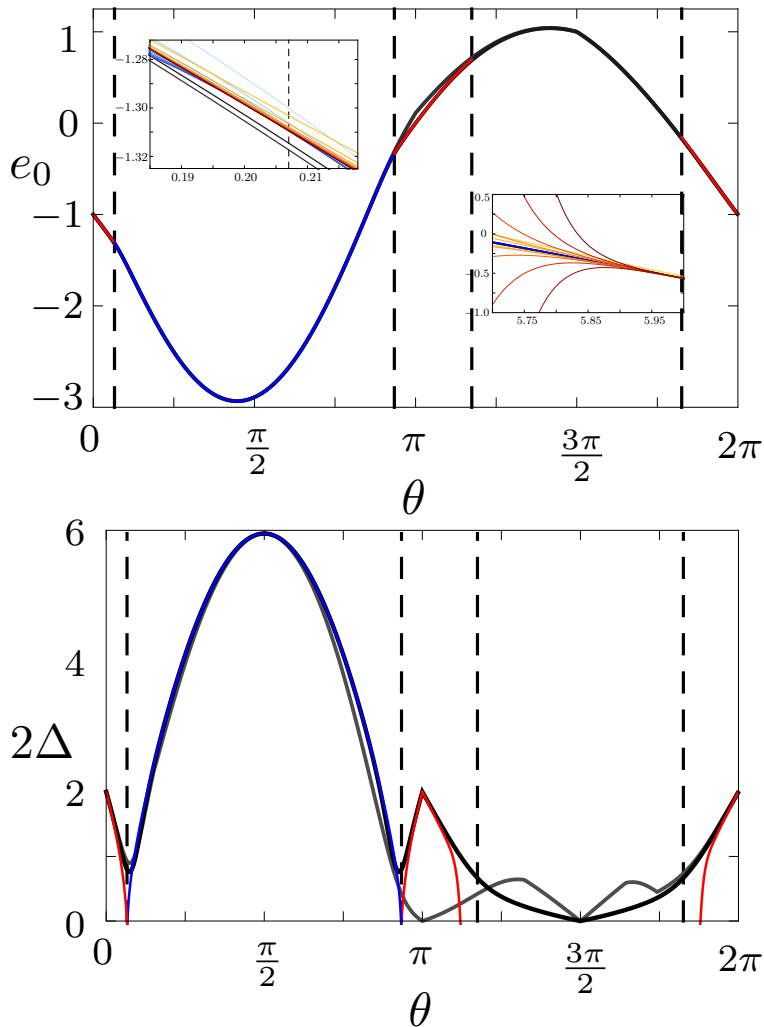


FIGURE 5.2: The ground-state energy e_0 (top) and the low-energy gap 2Δ (bottom) in dependence of the control parameter θ . We show data from series expansions for the different limits (red for the limit $\theta = 0, \pi$, blue for the limit $\theta = \frac{\pi}{2}$). Additionally, data from exact diagonalization is given (gray for the $N_p = 9$ and black for the $N_p = 12$ system). The left inset shows the crossing of the different curves for the ground state energy around $\theta \approx 0.207$ for different orders of the series expansion. In the right inset, we show the series expansion for e_0 from order one (orange) to order eleven (dark red) around $\theta = 5.73$.

model not the elementary-particle gap Δ obtained by the series expansion, but the lower band edge of the two-particle continuum 2Δ .¹

The two topological phases found for $\theta = 0$ and $\theta = \pi$ are identical due to the $\mathbf{1} \leftrightarrow \mathbf{s}$ symmetry of the fusion algebra. Thus, we only consider the phase transitions out of the topologically ordered phase to which the point $\theta = 0$ belongs, as the analogue case exists also in the case of the non-Abelian theories.

¹For the very special case of this model, the lower-band edge of the two-particle continuum coincides with twice the single-particle gap Δ , as the dispersion is minimal at the momenta \vec{k} , for which $2\vec{k}$ is equivalent to $\pm\vec{k}$. We shall discuss this in more detail when discussing the results in Section 5.1.1.

5.1.1 Phase transition between topological and 1-phase

As can already be seen from Figure 5.2, there are two different situations encountered in the study of the phase transitions with series-expansion techniques: either series expansions for both phases are known and can be analyzed in a joint fashion, or series expansions are only available for one phase, in which case one is restricted to use only information from one side of the phase transition. We find the former scenario for the transition from the topological to the 1-phase and the latter for the transition from the topological to the dual of the anti-ferromagnetic phase.

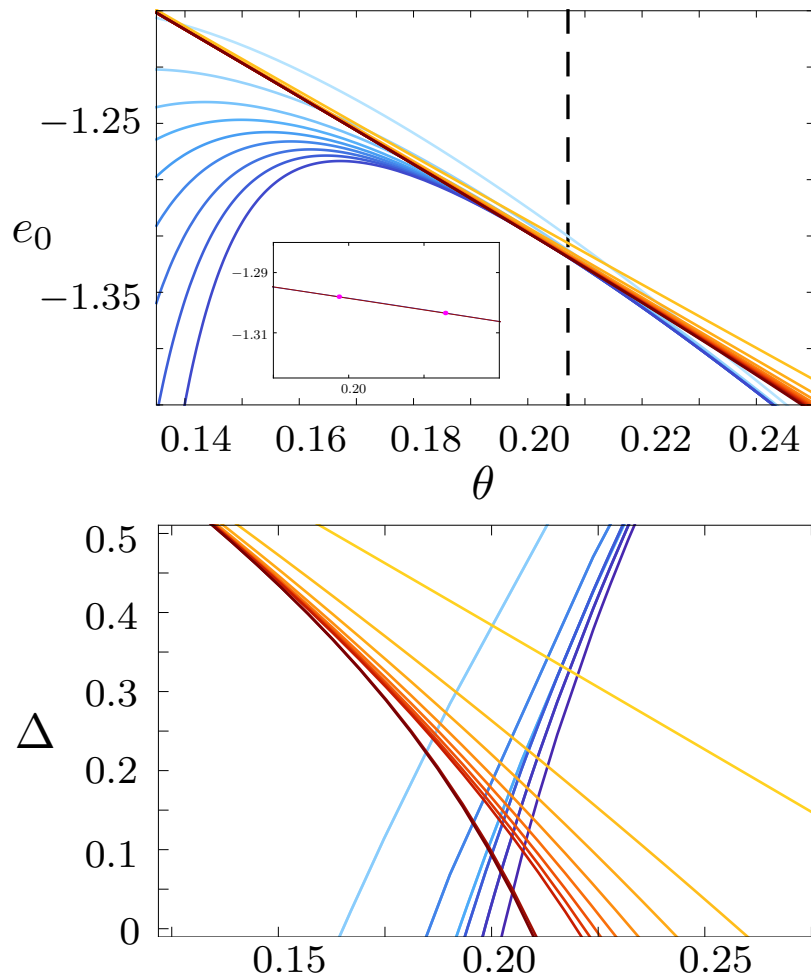


FIGURE 5.3: The ground-state energy e_0 (top) and the one-particle gap Δ (bottom) around $\theta \approx 0.2$. The series for e_0^{top} is depicted from order one (orange) to eleven (red), the series for e_0^1 from order one (light blue) to 18 (dark blue). The series for Δ_{top}^+ is shown from the order one (orange) to order eleven (dark red), the series for Δ_1 from order one (light blue) to twelve (dark blue). All series behave monotonously, i.e. for higher orders the respective values decrease. The insets shows the behavior of the series in a large zoom to depict the two crossing points of the series for order nine (e_0^{top}) and 18 (e_0^1) by magenta dots.

In the following, we detail our findings for the transition between the topological and the 1-phase. The analysis of the other phase transition is performed by a simpler analysis

similar as e.g. in Ref. [133].

In Figure 5.3, we show the series for the ground-state energy e_0 and the gap Δ around $\theta \approx 0.2$. We depict the series order by order, with orders ranging e_0 in the topological phase from one to eleven and for the **1**-phase up to 18 in $t = \tan \theta$. We give here the series up to order four

$$e_0^{\text{top}} = \cos \theta \left(-1 - \frac{3}{2} \cdot t - \frac{3}{8} \cdot t^2 - \frac{3}{8} \cdot t^3 - \frac{87}{128} \cdot t^4 + \mathcal{O}(t^5) \right), \quad (5.6)$$

$$e_0^{\mathbf{1}} = \sin \theta \left(-3 - \frac{1}{2} \cdot t^{-1} - \frac{1}{24} \cdot t^{-2} - \frac{1}{17280} \cdot t^{-4} + \mathcal{O}(t^{-6}) \right). \quad (5.7)$$

Note that for the series valid in the **1**-phase, odd orders vanish. This is due to the \mathbb{Z}_2 symmetry of the phase, which, together with the “acting-twice” property of the topological Hamiltonian discussed in Section 7.3.1, leads to the vanishing of odd orders for the topologically-trivial phase.

One can see that both series for the ground-state energy seem to match very well in the interval $\theta \in [0.19, 0.21]$, however it is not obvious how to state precisely, where the phase transition between the two phases is located. Additionally, if one identifies the location of the phase transition via a crossing point of two finite-order series, both series have generically a different slope at the crossing point. Thus one is naively led to conclude that the phase transition is of first order, as the ground-state energy given by the minimum of the two series shows a kink at the crossing point. In order to be able to detect reliably a continuous or second-order phase transition, one has to extrapolate the information contained in the series expansions to the infinite-order limit and verify that the kink vanishes in this limit.

In the case considered here, the ground-state energies converge monotonously with order, i.e. all coefficients of the series have the same sign (cf. Eqs. (A.1) and (A.53)). We can use this to extrapolate the crossing points of the series for the ground-state energy e_0^{top} at order n with the series for $e_0^{\mathbf{1}}$ at order $2n$. Note that this choice of different orders is arbitrary, however it can be motivated by the fact that the perturbation operators appearing in the effective Hamiltonian have the same extension of n plaquettes for an order n calculation in the topological phase and for an order $2n$ calculation in the **1**-phase due to the “acting-twice” property. Thus, the involved operators act on the same length scale, leading to this choice of comparison. Note that in the limit of infinite order, every possible choice should lead to the same result.

We find here two crossing points for the ground-state energy series per n . We depict their position for a given n in Figure 5.5 as function of the inverse order $\frac{1}{n}$. Note that, if the positions of the two crossing points meet in the limit of infinite order, the first

derivative of the ground-state energy has to be continuous. In this case, our results are consistent with a continuous phase transition.²

However, before discussing the results of this finite-order scaling in more detail, let us turn to the data provided by considering the elementary-excitation gap. The gap of the topological phase Δ_{top}^+ is determined up to order eleven, the gap $\Delta_{\mathbf{1}}$ is taken from Ref. [130] up to order 11 to consider the same orders as obtained for the non-Abelian cases. They read up to order four

$$\Delta_{\text{top}}^+ = \cos \theta \left(1 - 3 \cdot t - 3 \cdot t^2 - \frac{21}{4} \cdot t^3 - \frac{63}{4} \cdot t^4 + \mathcal{O}(t^5) \right), \quad (5.8)$$

$$\Delta_{\mathbf{1}} = \sin \theta \left(6 - \frac{1}{6} \cdot t^{-2} - \frac{1}{432} \cdot t^{-4} + \mathcal{O}(t^{-6}) \right). \quad (5.9)$$

Note that both gaps are the minimum of the respective dispersions $\omega(\vec{\mathbf{k}})$ at $\vec{\mathbf{k}}_c = \vec{0}$. This allows us to obtain the lower-band edge $\omega_{2\text{qp}}^-$ of the two-particle continuum depicted in Figure 5.2 via

$$\omega_{2\text{qp}}^- = \min_{\vec{\mathbf{k}}, \vec{\mathbf{q}}} \left(\omega(\vec{\mathbf{k}} + \vec{\mathbf{q}}) + \omega(-\vec{\mathbf{q}}) \right) = 2 \min_{\vec{\mathbf{k}}} \omega(\vec{\mathbf{k}}) = 2\Delta, \quad (5.10)$$

where we used the fact that the $\vec{\mathbf{k}}$ -point minimizing the dispersion is also the minimum of the two-particle continuum.

In the case of a continuous phase transition, we expect the elementary-excitation gap to go to zero simultaneously from both sides of the transition point. As we can see in Figure 5.3, this is not the case for a finite-order series. So, we shall proceed as in the case of the ground-state energy and extrapolate to the limit of infinite order.

Therefore, we consider the zeros of both gaps as well as the location of the crossing points of the two curves. In contrast to the ground-state energy, we consider for the crossing points both gap series at the same order n . This is due to the fact that for the non-Abelian cases, we reach about the same orders in the series expansion for the topological and the $\mathbf{1}$ -phase.

Let us already note here that in principle, one can perform an extrapolation by a dlog-Padé approximant for each gap separately. However, due to differences in the convergence of both series, we find that the results of these separately performed extrapolations do in general not coincide for the orders considered here. Consequently, these will not yield a consistent picture and we do not discuss them here.

²Note that one can never rigorously exclude a (weak) first-order transition within this approach, as a distinction between a small but finite or a vanishing kink in the ground-state energy is not obvious.

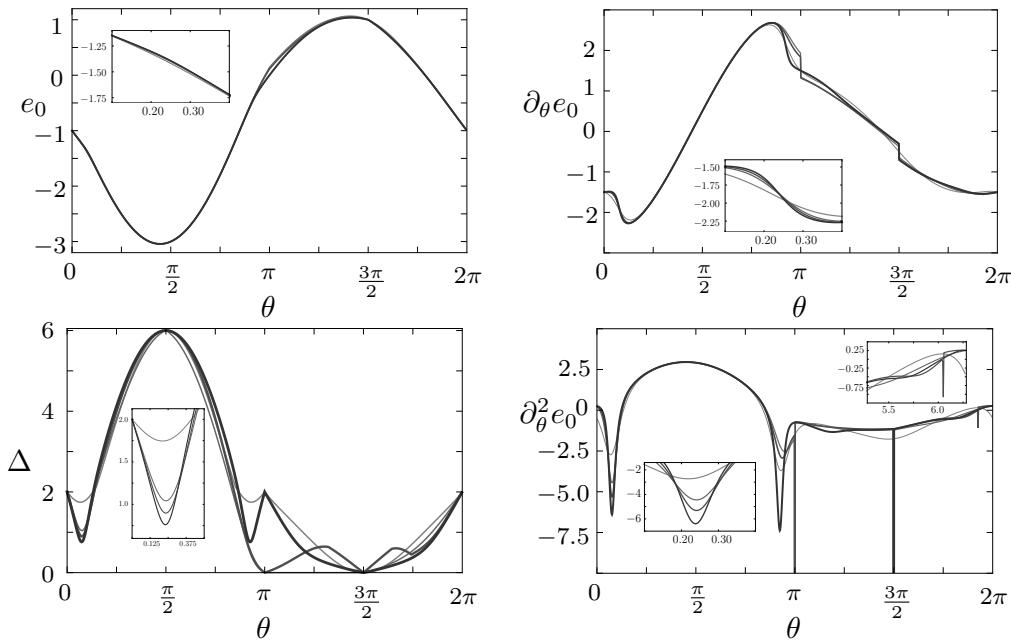


FIGURE 5.4: The exact diagonalization data for the system with $N_p = 4, 7, 9,$ and 12 (colored in light gray to black). We show the ground-state energy per plaquette, its first and second derivative, as well as the low-energy gap Δ . Note that for the region $\theta \in [\pi, 2\pi]$, one can observe strong finite-size effects due to frustration.

Additionally to the data obtained by series expansions, we also diagonalized the perturbed string-net model (3.54) on finite, periodic systems as detailed in Section 6.2. We shall now consider the results depicted in Figure 5.4, where the ground-state energy per plaquette e_0 , its first and second derivative as well as the low-energy gap Δ are given.

For the region $\theta \in [0.1, 0.3]$ (c.f. the insets in Figure 5.4), we observe a well converged ground-state energy. In the same region, the first derivative $\partial_\theta e_0$ steepens with system size, but converges on the scales considered here. The second derivative $\partial_\theta^2 e_0$ shows no tendency to converge, as far as one can tell from the system sizes considered. In order to obtain quantities valid for the thermodynamic limit, we shall perform a finite-size scaling. We are interested here in the location of the phase transition, which, if of second order, should be signaled by a closing gap and a diverging second derivative of the ground-state energy. Therefore, we consider the gap minimum and the minimum of $\partial_\theta^2 e_0$. This data is given together with the data of the series expansion in Figure 5.5. Additionally, we shall discuss the value of the gap Δ at its minimum for the different system sizes. We plot the different quantities against either inverse order or inverse system size $\frac{1}{N_p}$.

We observe that the data obtained by series expansions and by exact diagonalization differ significantly. This is due to the fact that the low-energy excitations for the periodic systems, on which exact diagonalizations are performed, are not single but pairs of

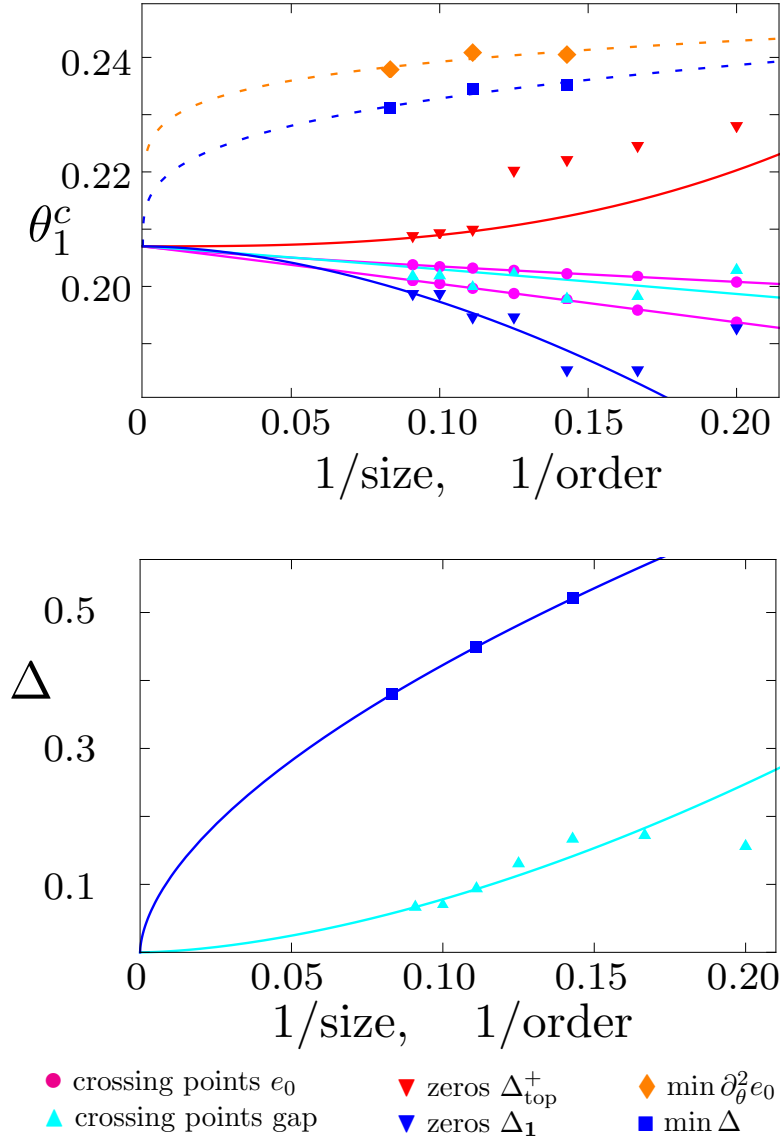


FIGURE 5.5: The finite-order and finite-size scaling is performed for the location of the phase transition (top) or the elementary-excitation gap at the transition point (bottom). The lines are power-law fits to the data points (c.f. text). The estimate for the location of the critical point $\theta_1^c \approx 0.207$ is obtained by a least-square fit of the crossing points of the series expansions of the ground-state energy e_0 . We observe good compatibility of all data points with a continuous phase transition at θ_1^c , except for the data from exact diagonalization. The data obtained for the elementary-excitation gap is consistent with a convergence to zero in the limit of infinite order/size. Note that the ED results for the gap are divided by a factor of two to be comparable to the series expansion results.

excitations. Thus the length scales necessary for a converging finite-size scaling are significantly larger.

The estimate of the location of the phase transition $\theta_1^c = 0.207$ is obtained by a least-square fit of the data points with a power-law behavior

$$a_n \approx (\theta_n - \theta_1^c)^{\gamma_a}, \quad (5.11)$$

where the quantities (θ_n, a_n) are the location and the value of the different crossing points or minima for different orders or system sizes n .

Let us note that this way of extrapolating the perturbative data to the infinite-order limit is heuristic. This can already be seen in the data for the zeros of the gap Δ_{top}^+ , which shows a large jump between order eight and nine, indicating that the impact of higher-order terms cannot always be predicted from the lower orders. Nevertheless, for a converging expansion this scaling is supposed to work, once one has reached suitably high orders in the expansion.

This scaling allows to obtain a quantitatively similar result³ as an analysis involving even higher orders and considering directly the order parameter as performed e.g. in Ref. [129]. We observe in the lower plot in Figure 5.5 that also the values for the gap at the crossing point (minimum) are compatible with the convergence to zero if one increases the order the (size) of the system. The fits to the points are again power-law functions.

Having obtained the location of the phase transition by this scaling, we turn now to the determination of the universality class. Therefore one considers the critical exponents. The most important one for our analysis is the exponent associated with the gap. It is defined by

$$\Delta \propto |\theta - \theta^c|^{z\nu} \quad (5.12)$$

and can be obtained by dlog-Padé extrapolation of the series expansion for the gap as detailed in Section 6.1.6. Note that this exponent is a product of the dynamical exponent z and the exponent ν associated with the divergence of the correlation length at the phase transition point.

| $z\nu$ obtained for Δ_{top}^+ | | | | $z\nu$ obtained for $\Delta_{\mathbf{1}}$ | | | |
|---|---------|---------|-----------|---|---------|---------|-----------|
| N | [N/N-1] | [N / N] | [N / N+1] | N | [N/N-1] | [N / N] | [N / N+1] |
| 2 | - | 0.645 | 0.646 | 2 | - | - | 0.758 |
| 3 | 0.646 | 0.646 | 0.646 | 3 | 0.734 | 0.684 | 0.645 |
| 4 | 0.646 | 0.646 | 0.646 | 4 | 0.632 | - | 0.617 |
| 5 | 0.646 | 0.645 | 0.648 | 5 | 0.606 | 0.624 | - |

TABLE 5.1: The critical exponent $z\nu$ for the phase transition between topological and $\mathbf{1}$ -phase obtained by biased dlog-Padé extrapolations. Unphysical results for the exponent, i.e. those with $z\nu < 10^{-3}$, are discarded.

³We note that in the units of Ref. [129], the location of the phase transition $\tan \theta_1^c = 0.210$ agrees with the $x_c = 0.20974$ given there. The estimate is obtained there by considering the series expansion of the susceptibility up to order 14.

We perform dlog-Padé extrapolations of the gap series for the topological and the **1**-phase, which we bias on the location θ_1^c determined previously. The results are listed in Table 5.1.

As the series for the topological phase is the same as in Ref. [129], we obtain the same result, i.e. a critical exponent $z\nu = 0.65$. However, for the **1**-phase, we use less orders than in Ref. [130] (eleven instead of 18). We find that our results are not at all converged and thus we consider the values obtained via Δ_{top}^+ . Let us note that the most precise value is given by $\nu = 0.6301$ in Ref. [135]

| z obtained for Δ_{top}^+ | | | |
|--|---------|---------|-----------|
| N | [N/N-1] | [N / N] | [N / N+1] |
| 2 | - | 1.3 | 1.1 |
| 3 | 1.3 | 1.3 | 1.3 |
| 4 | 1.1 | 1.3 | 1.3 |
| 5 | 1.3 | 1.3 | - |

TABLE 5.2: The critical exponent z for the phase transition between topological and **1**-phase obtained by the variation of biased dlog-Padé extrapolations around $\vec{k}_c = \vec{0}$.

The dynamical critical exponent z is also associated with the dispersion in the vicinity of the closing point, i.e.

$$\omega(\vec{k})\Big|_{\theta=\theta^c} \sim \left| \vec{k} - \vec{k}_c \right|^z. \quad (5.13)$$

We can determine this exponent by varying the value of \vec{k} in the biased dlog-Padé extrapolants used to determine $z\nu$. This yields the values shown in Table 5.2. By comparing the value with the known value $z = 1$, we see that there is a deviation of about roughly 30%, which is larger than for the exponent $z\nu$. This is due to the fact that we use a variation of an approximant to determine the exponent and not the approximant itself. Let us remark that these large deviations for the dynamical exponent z have also been found in other studies of the Ising model [136].

Having determined these two exponents, one can obtain further ones by hyper-scaling relations [137]. For example, the relation

$$2 - \alpha = \nu(d + z), \quad (5.14)$$

where $d = 2$ is the spatial dimension of the system, yields the critical exponent α that is associated to the specific heat, or in our case of a zero-temperature phase transition to the second derivative of the ground-state energy i.e.

$$\partial_\theta^2 e_0 \sim |\theta - \theta^c|^{-\alpha}. \quad (5.15)$$

Note however that in case of a second-order phase transition, we have $\alpha < 1$ as $\partial_\theta e_0$ diverges otherwise. If one can obtain values for α by other means, one can check, whether relation (5.15) holds. Let us remark here that the exponent α is not easily obtained by the means of series expansions [129], so we use the relation (5.14) to infer that $\alpha \approx 0.10$. This value is consistent with the relatively small slope of $\partial_\theta e_0 \sim (\theta - \theta_1^c)^{-\alpha+1}$, which can be observed in the exact-diagonalization data shown in Figure 5.4.

Even though this type of analysis seems artificial as there are more straightforward ways to extract the location of the phase transition as well as the associated exponents for the transverse-field Ising model by a direct analysis of the model itself as in Refs. [129, 130]. Note however that also in these studies, the critical exponents differ from the ones obtained by the investigation of the classical, three-dimensional Ising model as e.g. in Ref. [135, 138, 139] by about 5%.

We shall use these differences to estimate the order of magnitude of the uncertainty of our results for $z\nu$, as differences up to roughly 10% for this critical exponent may arise also in some examples for analogous studies, as e.g. the ones performed in Refs. [86, 133]. Note that these uncertainties cannot be estimated in a more systematic fashion as they depend on the details of the particular model.

Before analyzing the finite-order and finite-size behavior of the data for the second phase transition out of the topologically ordered phase, let us discuss the obvious finite-size effects in Figure 5.4 for the region $\theta \in [\pi, 2\pi]$.

For $\theta \approx \pi$ the flux-full state is the ground state in thermodynamic limit due to the exchange symmetry $\mathbf{1} \leftrightarrow \mathbf{s}$. However, on finite systems with an odd number of plaquettes, the flux-full state is not part of the Hilbert space. Thus for systems with an odd number of plaquettes at $\theta = \pi$, the extensive number of ground states is given by the states with only one flux-free plaquette.

Around $\theta = \frac{3\pi}{2}$, the Hamiltonian (3.54) is equivalent to the anti-ferromagnetic (AFM) Ising model in a transverse field, which is frustrated on the triangular lattice. Due to this frustration, the spectrum depends strongly on the system size. Therefore, we do not expect the exact diagonalization in the region $\theta \approx \frac{3\pi}{2}$ to be as converged as for the unfrustrated case $\theta \approx \frac{\pi}{2}$, especially for the excited states. Consequently, we focus on the perturbative results, as these do not suffer from finite-size effects.

5.1.2 Phase transition between topological and AFM-phase

For this phase transition, we cannot proceed in the analysis as for the previously discussed phase transition, as here we only have perturbative expansions valid for one phase

and additionally strongly system-size dependent exact-diagonalization data. Therefore, we analyze the data of the gap of the topological phase to pinpoint the location of the phase transition.

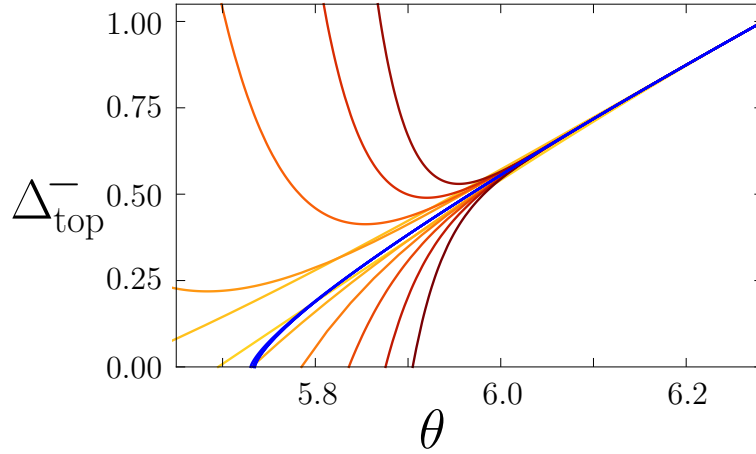


FIGURE 5.6: The series of the gap Δ_{top}^- in the topological phase is depicted from order one (yellow) to order eleven (dark red). Additionally to the alternating series, we give the dlog-Padé extrapolations (blue), which determine the location of the phase transition at $\theta_2^c = 5.73$.

In Figure 5.6, we show the one-particle gap Δ_{top}^- , determined up to order eleven, which minimizes the dispersion $\omega(\vec{k})$ for $\vec{k} = \pm(\frac{2\pi}{3}, -\frac{2\pi}{3})$ for $\theta < 0$ in the topological phase. Note that $2\vec{k}$ is equivalent to $-\vec{k}$ and thus, as for the other phases, the lower band edge is given by twice the gap.

The gap reads up to order four

$$\Delta_{\text{top}}^- = \cos \theta \left(1 + \frac{3}{2} \cdot t + \frac{3}{8} \cdot t^2 + \frac{15}{16} \cdot t^3 + \frac{243}{128} \cdot t^4 \right). \quad (5.16)$$

Note that the agreement of our series expansions with the one obtained in Refs. [129, 130, 133] already allows us to check the validity of our procedure to obtain the series expansions.

We show in Figure 5.6 also the dlog-Padé extrapolants of the gap. We see that the alternating series is extrapolated to yield a closing gap at $\theta_2^c = 5.73$ in accordance with Refs. [132, 133].

In Table 5.3, we give the zeros of the approximants as well as the estimated exponents $z\nu$ and z . The corresponding values for the classical three-dimensional XY model are given by $\nu = 0.67$ [140] and $z = 1$ [131] respectively, so we observe a deviation of our results slightly larger than the error estimates discussed above.

| θ_2^c obtained from Δ_{top}^- | | | |
|--|---------|---------|-----------|
| N | [N/N-1] | [N / N] | [N / N+1] |
| 2 | - | 5.749 | 5.730 |
| 3 | 5.721 | 5.735 | 5.733 |
| 4 | 5.733 | 5.734 | 5.735 |
| 5 | 5.735 | 5.733 | - |

| $z\nu$ obtained from Δ_{top}^- | | | z obtained from Δ_{top}^- | | | | |
|--|---------|---------|---|---|---------|---------|-----------|
| N | [N/N-1] | [N / N] | [N / N+1] | N | [N/N-1] | [N / N] | [N / N+1] |
| 2 | - | 0.65 | 0.75 | 2 | - | 1.3 | 1.4 |
| 3 | 0.81 | 0.72 | 0.73 | 3 | 1.5 | 1.4 | 1.4 |
| 4 | 0.73 | 0.72 | 0.72 | 4 | 1.4 | 1.4 | 1.4 |
| 5 | 0.72 | 0.72 | - | 5 | 1.4 | 1.4 | - |

TABLE 5.3: The location of the phase transition $\theta_2^c = 5.73$ and the values of the critical exponents $z\nu = 0.72$ and $z = 1.4$ are obtained by dlog-Padé extrapolation of the gap Δ_{top}^- .

5.1.3 Summary of the phase transitions in the semion model

In the above section, we presented our results for the perturbed string-net model for semions. We determined the phase diagram and analyzed the phase transitions between the different phases. The comparison with the results for the transverse-field Ising model allows for an estimate of the accuracy of our results.

We find in total four continuous phase transitions between a topologically ordered and a topologically-trivial phase, two of them related to each other by the $\mathbf{1} \leftrightarrow \mathbf{s}$ symmetry of the semion fusion algebra.

We performed series expansions for the topological and the $\mathbf{1}$ -phase. The location of the phase transition between these phases is determined via a finite-order and finite-size scaling. Using the so obtained position of the phase transition $\theta_1^c = 0.207$ as bias, we obtain the critical exponent associated with the gap, i.e. $z\nu = 0.65$, by a dlog-Padé extrapolation. Comparison with the values available in the literature leads to an estimate of the error of about 10% for this exponent. Additionally, we obtain an estimate for the dynamical exponent $z = 1.3$ by investigation of the gap closing behavior in dependence of the wave vector \vec{k} . Additionally, we discussed also the exponent α related to the divergence of the second derivative of the ground-state energy.

The phase transition between the topological and the frustrated phase is investigated only by means of series expansions for the topological phase. We perform unbiased dlog-Padé extrapolations to obtain the position of the phase transition $\theta_2^c = 5.73$ and the critical exponent $z\nu = 0.72$. Additionally, we obtain the estimate $z \approx 1.4$.

The comparison of the obtained values with the ones for the three-dimensional Ising model (three-dimensional XY model) reveals that we obtain the critical exponent $z\nu$ with an error of about 10% and z with an error of about 40%.

5.2 Phase transitions for Fibonacci anyons

The results discussed in this chapter can also be found in Ref. [104]. The exact-diagonalization results for the non-Abelian models have been provided by Dr. S. Dusuel and Dr. J. Vidal.

For the perturbed string-net model with Fibonacci anyons, we discussed in Section 3.5.1 the three exactly solvable points with finite ground-state degeneracy at $\theta = 0$, $\theta = \frac{\pi}{2}$, and $\theta = \frac{3\pi}{2}$. We show the overall picture for the phase diagram in Figure 5.7.

It shows a good coincidence of the exact-diagonalization and the (extrapolated) perturbative results for the ground-state energy. Thus, we conclude that the three different phases discussed in Section 3.5.1, the topological, the $\mathbf{1}$ -, and the $\boldsymbol{\tau}$ -phase, are the three phases constituting the phase diagram.

In the vicinity of the transitions between the topological and the $\mathbf{1}$ -phase at θ_1^c and between the topological and the $\boldsymbol{\tau}$ -phase at θ_2^c , also the elementary-excitation gap is well described by the perturbative results and the exact diagonalization. At the phase transition between the two non-topological phases at $\theta = \pi$, the description of the gap does not match well between the two approaches, which is due to finite-size effects as well as low-order expansions, as we shall discuss in Section 5.2.3.

The series expansion results for this section are given in Appendix B.

5.2.1 Phase transition between topological and $\mathbf{1}$ -phase

Let us first analyze the phase transition between the topological and the $\mathbf{1}$ -phase. Therefore we proceed as in Section 5.1.1 and consider the ground-state energy per plaquette e_0 around $\theta \approx 0.24$ as depicted in Figure 5.8.

Its perturbative expression in the topological phase reads up to order four

$$e_0^{\text{top}} = \cos \theta \left(-1. - 0.829180 \cdot t - 0.300000 \cdot t^2 - 0.232918 \cdot t^3 - 0.375836 \cdot t^4 \right). \quad (5.17)$$

On the scale of Figure 5.8, the series depicted up to order eleven (yellow to red) is well converged.

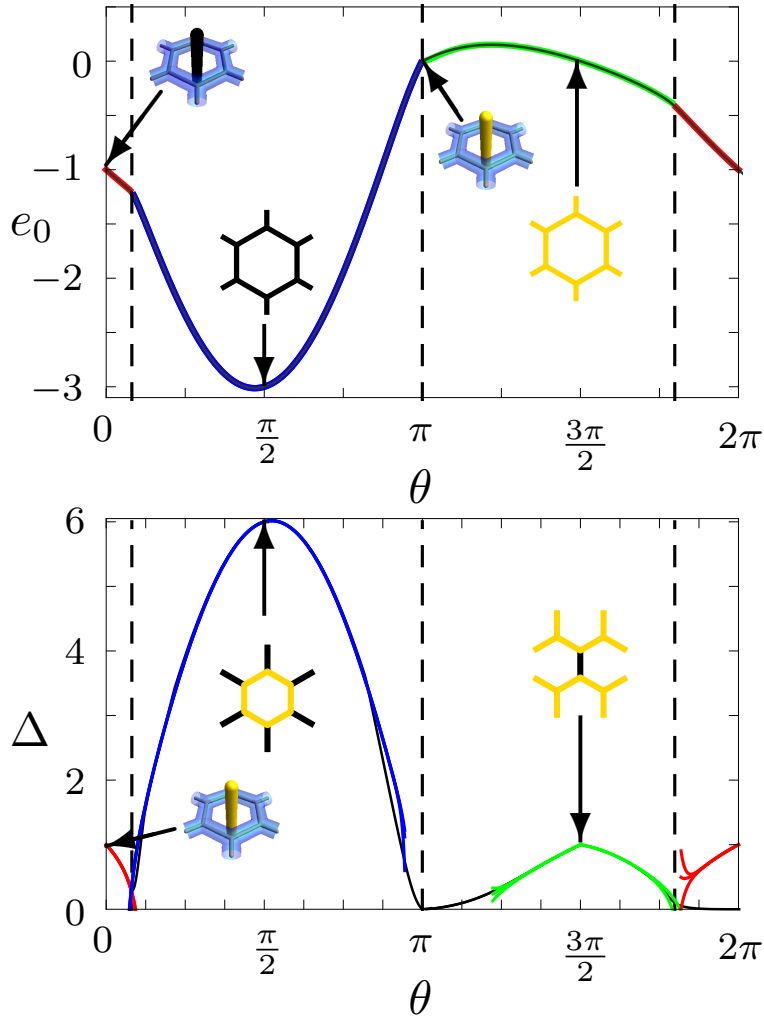


FIGURE 5.7: The combined data of the ground-state energy per plaquette e_0 and the elementary-excitation gap Δ obtained by series expansion techniques for the topological phase (red), the **1**-phase (blue), and the τ -phase (green). The insets depict the states corresponding to the shown energy level. The exact-diagonalization data for the $N_p = 12$ system (black) shows a rather good coincidence with the perturbative results on the overall scale. The details are discussed in the text for the three phase transitions indicated by the dashed lines.

The series valid in the **1**-phase is determined up to order 20 and given in Eq. (B.40). It reads up to order four

$$e_0^1 = \sin \theta \left(-3. - 0.276393 \cdot t^{-1} - 0.333333 \cdot 10^{-1} \cdot t^{-2} - 0.248452 \cdot 10^{-2} \cdot t^{-3} - 0.147309 \cdot 10^{-3} \cdot t^{-4} \right). \quad (5.18)$$

As we can see in Figure 5.8, this series still is not converged for the orders considered here.

We note that both perturbative expansions (5.17) and (5.18) have the same property as for the semion-case: the coefficients of the series have all the same sign. Thus we shall

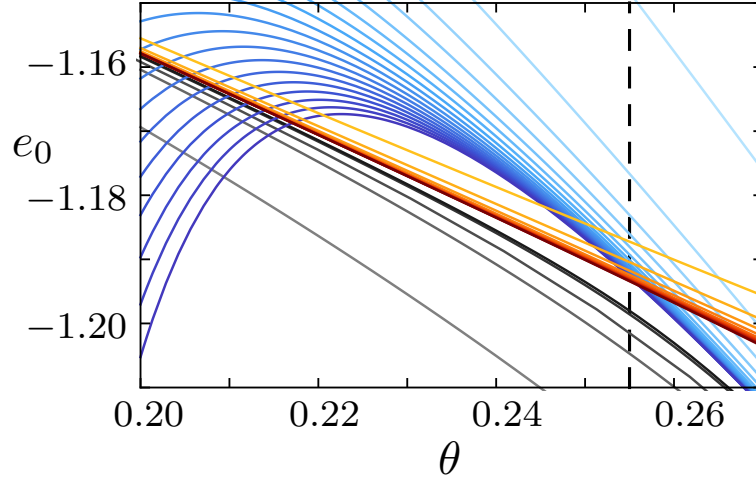


FIGURE 5.8: The perturbative results for the ground-state energy e_0 are shown order by order from order two (light blue) to order 20 (dark blue) for e_0^1 and from order two (orange) to order eleven (dark red) for e_0^{top} . There are two intersections of the series for e_0^1 and e_0^{top} , respectively. Additionally we show the results of the exact diagonalization (light gray to dark gray with increasing system size from $N_p = 4$ to $N_p = 13$). All data shows a convergent behavior, from which we estimate the location of the critical point indicated by the dashed line by a finite-order/size scaling.

analyze the location of the phase transition as in Section 5.1.1 to obtain the position of the transition at $\theta_1^c = 0.255$ indicated by the dashed line.

Additionally, we show here the ground-state energy determined by exact diagonalization for increasing system sizes (light gray to dark gray). The curves converge well for the considered system sizes.

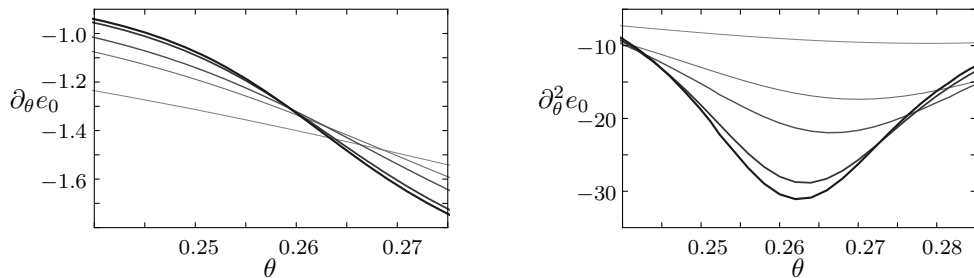


FIGURE 5.9: Behavior of the first (left) and second derivative (right) of the ground-state energy per plaquette obtained by exact diagonalization for the system sizes $N_p = 4, 7, 9, 12,$ and 13 . As for the semion model discussed in Section 5.1.1, $\partial_\theta e_0$ shows a convergent behavior, whereas $\partial_\theta^2 e_0$ does not. This indicates that the phase transition at θ_1^c is of second order.

The derivatives of the ground-state energy are given in Figure 5.9. As for the semions, we observe that the first derivative converges to a finite slope, whereas the second derivative shows no convergence.

As in Section 5.1.1, we also consider the low-energy gap Δ as depicted in Figure 5.10. The series for the gap in the topological phase Δ_{top}^+ is determined up to order ten (B.38)

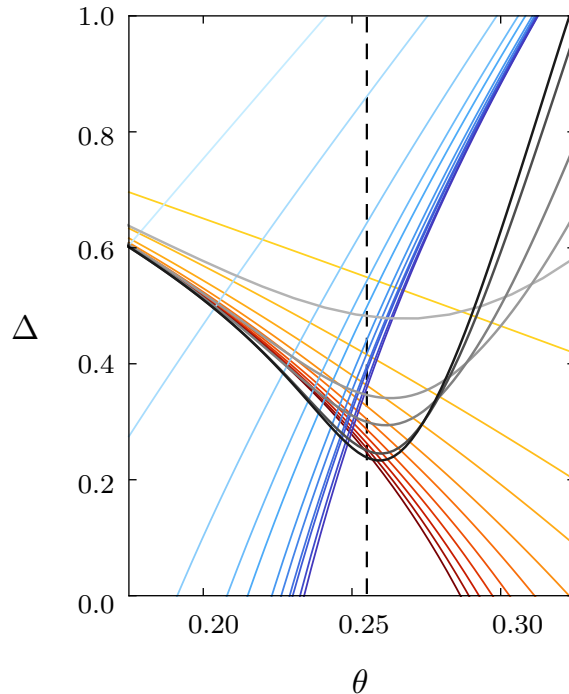


FIGURE 5.10: With the same notations as in Figure 5.8, we show the perturbative and exact-diagonalization results for the elementary-excitation gap in the region, where the phase transition between the topological and the **1**-phase occurs. The picture is qualitatively the same as for the semion model shown in Figure 5.3.

and reads up to order four

$$\Delta_{\text{top}}^+ = \cos \theta (1. - 1.658359 \cdot t - 2.029180 \cdot t^2 - 3.107113 \cdot t^3 - 8.042597 \cdot t^4). \quad (5.19)$$

We also determine the gap in the **1**-phase up to order eleven (B.53). It reads up to order four

$$\Delta^{\mathbf{1}} = \sin \theta (6. - 0.447214 \cdot t^{-1} - 0.591693 \cdot 10^{-1} \cdot t^{-2} - 0.015323 \cdot t^{-3} - 0.001826 \cdot t^{-4}). \quad (5.20)$$

We observe that the exact-diagonalization results in Figure 5.10 show a good coincidence with the series expansion for the topological phase, whereas there are deviations for the **1**-phase. This is due to the fact that in the **1**-phase, there are additional low-energy excitations on the finite-size system, corresponding to closed loops of τ -links wrapping around the torus. These cause the deviations of the exact-diagonalization data, especially in the vicinity of the phase transition, where the fluctuations induced by the topological Hamiltonian are very large.

Additionally, we observe that different values for the gap in the vicinity of the phase transition are larger than for the case of the semions, but the qualitative picture is the same.

We therefore show in Figure 5.12 the various quantities, which allow for the finite-size/order scaling as discussed in Section 5.1.1. We observe that all data is consistent

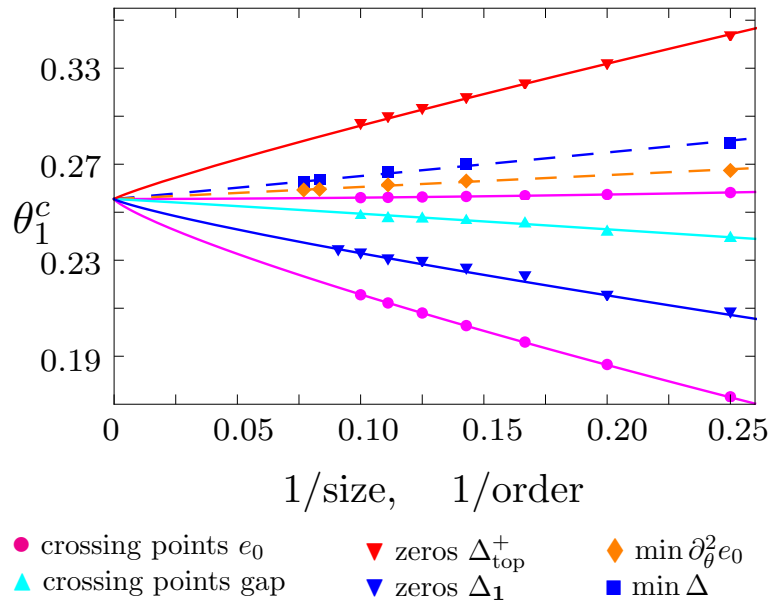


FIGURE 5.11: The finite-order and finite-size scaling is performed for the location of the phase transition. The lines are power-law fits to the data points (c.f. text). The estimate for the location of the critical point $\theta_1^c = 0.255$ is obtained by a least-square fit of the crossing points of the series expansions of the ground-state energy e_0 . We observe good compatibility of all data points with a continuous phase transition at θ_1^c .

with a second-order phase transition at $\theta_1^c = 0.255$. In contrast to the case for the semions, also the exact-diagonalization data agrees well with the series-expansion results. This is due to the fact that here the single-particle excitations are also present on the systems considered with ED.

We now performed biased dlog-Padé extrapolation for the gap in the topological phase Δ_{top}^+ , we obtain the critical exponents shown in Table 5.4. We find $z\nu = 0.33$ and a value of $z = 1$. for the dynamical exponent.

Let us remark that the low values of $z\nu$ have to be considered with caution. If one performs unbiased extrapolations for Δ_{top}^+ , one finds a critical point for $\theta \approx 0.26$, as shown in Table 5.5. This value differs from the θ_1^c given above only by a few percent, but the resulting estimate for $z\nu$ yields rather 0.42.

Thus, we encounter here the situation that a small variation in the bias causes large variations in the resulting exponent. Therefore, we shall consider values of $z\nu$ in the range of the 0.33 to 0.45 as possible. Let us note here that this consideration does not invalidate the finite-order scaling and the estimate of θ_1^c , but is the statement that the obtained orders are not sufficient for an accurate computation of the critical exponents.

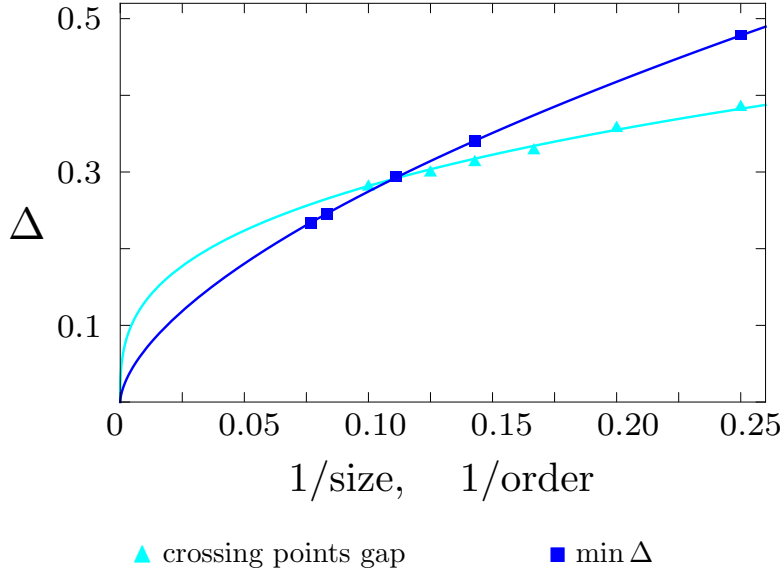


FIGURE 5.12: The finite-order and finite-size scaling for the elementary-excitation gap value is performed for the crossing point of the perturbative results and for the minimum value of the gap. The data is compatible with a power-law behavior assuming a gap closing at infinite order/size.

| $z\nu$ obtained from Δ_{top}^+ | | | | z obtained from Δ_{top}^+ | | | |
|--|---------|---------|-----------|---|---------|---------|-----------|
| N | [N/N-1] | [N / N] | [N / N+1] | N | [N/N-1] | [N / N] | [N / N+1] |
| 2 | - | 0.64 | 0.34 | 2 | - | 1.05 | 1.04 |
| 3 | 0.33 | 0.33 | 0.31 | 3 | 1.04 | 0.89 | 0.91 |
| 4 | 0.35 | 0.33 | 0.36 | 4 | 0.91 | - | 0.98 |
| 5 | 0.34 | 0.33 | - | 5 | 0.98 | - | - |

TABLE 5.4: The values of the critical exponents $z\nu = 0.33$ and $z = 1$. are obtained by biased dlog-Padé extrapolation of the gap Δ_{top}^+ for $\theta_1^c = 0.255$.

| θ_1^c obtained from Δ_{top}^+ | | | | $z\nu$ obtained from Δ_{top}^+ | | | |
|--|---------|---------|-----------|--|---------|---------|-----------|
| N | [N/N-1] | [N / N] | [N / N+1] | N | [N/N-1] | [N / N] | [N / N+1] |
| 2 | - | 0.265 | 0.264 | 2 | - | 0.48 | 0.48 |
| 3 | 0.264 | 0.259 | 0.259 | 3 | 0.48 | 0.39 | 0.41 |
| 4 | 0.2593 | 0.259* | 0.261 | 4 | 0.41 | 0.39* | 0.45 |
| 5 | 0.261 | - | - | 5 | 0.45 | - | - |

TABLE 5.5: The values for the location of the phase transition $\theta_1^c = 0.26$ obtained by unbiased dlog-Padé extrapolation differs from the one obtained by the finite-size/order scaling by a few percent. The unbiased estimate for $z\nu \approx 0.45$ differs significantly from the biased one.

However, as we have exact-diagonalization data at hand, we can perform additionally to the above analysis a data-collapse study. This analysis relies on the fact that the diverging quantity, in our case the second derivative of the ground-state energy $\partial_\theta^2 e_0$, can be obtained for different system sizes by the so-called scaling function Φ via

$$\partial_\theta^2 e_0(\theta) = - \left(\sqrt{N_p} \right)^{\frac{\alpha}{\nu}} \Phi \left(\left(\sqrt{N_p} \right)^{-\frac{1}{\nu}} |\theta - \theta^c| \right), \quad (5.21)$$

where $(\sqrt{N_p})$ is the typical linear length scale of the system [141].

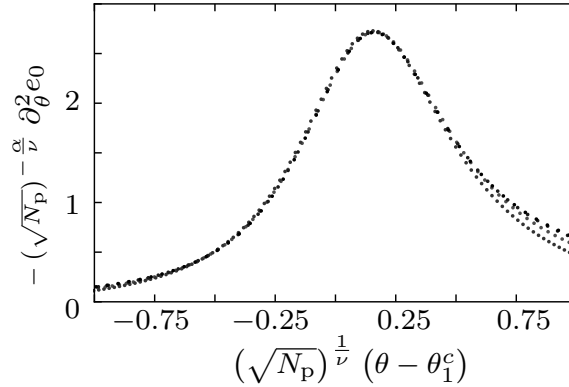


FIGURE 5.13: We perform a data collapse of the exact-diagonalization results for $\partial_\theta^2 e_0$ for the systems with $N_p = 7, 9, 12,$ and 13 plaquettes. After rescaling according to (5.21) with the values $\nu = 0.41$ and $\alpha = 0.78$, the four curves collapse onto one curve in a large range of parameters.

Thus if one rescales the obtained results according to (5.21), the points for different system sizes should fall onto one single curve in the vicinity of θ_c . Since the rescaling depends on the critical exponents ν and α , we vary these to obtain an optimal collapse for all but the smallest system size. The values $\alpha = 0.78$ and $\nu = 0.41$ yield the collapsed data as shown in Figure 5.13.

Assuming that our estimate for the dynamical exponent $z = 1.$ is correct, this yields an estimate $z\nu = 0.41$, which is consistent with the above discussion for the series expansion results. Additionally, the values $\nu = 0.41$, $z = 1.$, and $\alpha = 0.78$ fulfill the hyper-scaling relation (5.14) with good accuracy.

In conclusion, we obtain evidence for a second-order phase transition at $\theta_1^c = 0.255$ with a set of critical exponents, which is consistent with the values $\nu = 0.41$, $z = 1.$, and $\alpha = 0.78$.

5.2.2 Phase transition between topological and τ -phase

We investigate the phase transition between the topological and the τ -phase by the same tools as in Section 5.2.1.

The series expansion of the ground-state energy in the τ -phase is obtained up to order nine, it reads up to order four

$$e_0^\tau = -\sin \theta (0.301316 \cdot t^{-1} - 0.113204 \cdot t^{-2} + 0.028078 \cdot t^{-3} - 0.004508 \cdot t^{-4}). \quad (5.22)$$

Note that the signs of the higher-order coefficients shown in (B.54) do not show a regular sign pattern as it is the case for e_0^{top} and e_0^1 .

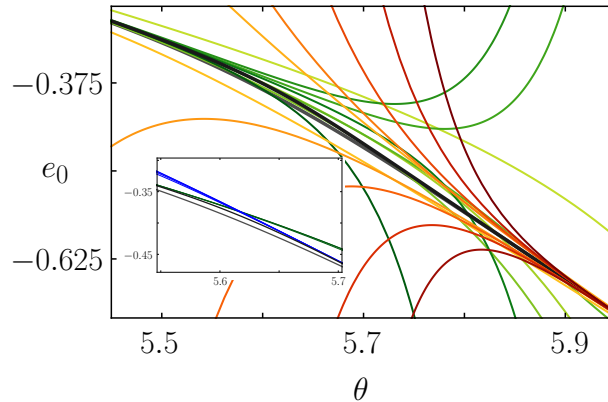


FIGURE 5.14: The series for ground-state energy e_0^{top} is depicted from order one (orange) to ten (dark red) and compared to the series for e_0^τ , depicted from order two (yellow) to nine (green). We show additionally the exact-diagonalization result for the system with $N_p = 9$ (gray) and $N_p = 13$ (black) plaquettes. In the inset, we show Padé extrapolations of the series (blue for e_0^{top} and green e_0^τ), which agree with exact diagonalization data. The respective crossing points of the extrapolations correspond to $\theta_2^c = 5.62$.

We show in Figure 5.14 the series for e_0^τ order by order (light green to dark green) together with the one for e_0^{top} (orange to dark red) as well as the exact-diagonalization results (gray and black).

The alternating series show a good agreement also with the exact diagonalization results for $\theta > 5.9$ and $\theta < 5.5$. In between, the series are dominated by the respective highest-order terms, which leads to deviations from the curve in the limit of infinite order. To compensate for this, we perform Padé extrapolations for e_0^{top} (blue) and e_0^τ (green), which are shown in the inset to agree well with the exact diagonalization result for $N_p = 13$ system. The crossing points of the shown extrapolants are located at $\theta_2^c = 5.62$.

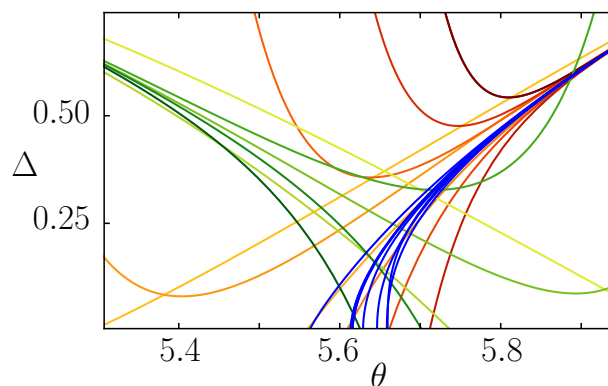


FIGURE 5.15: The series for the gap Δ_{top}^- in topological phase is depicted from order two (orange) to order 10 (dark red), the series for the gap Δ_{top}^+ from order one (yellow) to six (green). As for the ground-state energy, the alternating series do not show a monotonous convergence. We show also dlog-Padé extrapolants for Δ_{top}^- (blue), which signal a gap closing in the region $\theta \in [5.6, 5.7]$. For Δ_{top}^+ , there are no extrapolants, which approximate the series well for values of $\theta > 5.4$ due to its low orders and the alternating behavior of the coefficients.

We consider additionally the gap shown in Figure 5.15. The dispersion in the topological phase is minimized by $\vec{k} = \pm(\frac{2\pi}{3}, -\frac{2\pi}{3})$ and yields the gap Δ_{top}^- , which reads up to order four

$$\Delta_{\text{top}}^- = \cos \theta (1 + 0.829180 \cdot t + 0.114590 \cdot t^2 + 0.511033 \cdot t^3 + 0.404476 \cdot t^4). \quad (5.23)$$

The dispersion in the τ -phase is determined up to order six. It is minimized for $\vec{k} = \pm(\frac{2\pi}{3}, -\frac{2\pi}{3})$ and the gap Δ_{τ}^+ reads up to order four

$$\Delta_{\tau}^+ = -\sin \theta (1 + 0.266874 \cdot t^{-1} - 0.204817 \cdot t^{-2} - 0.075713 \cdot t^{-3} + 0.039643 \cdot t^{-4}). \quad (5.24)$$

We show in Figure 5.15 the series from order two (orange) to order 10 (dark red) for Δ_{top}^- and from order one (yellow) to six (green) for Δ_{τ}^+ . We observe the same alternating behavior as for the ground-state energy. Unbiased dlog-Padé extrapolations (blue) are depicted for Δ_{top}^- . The results for the location of the gap closing θ_2^c shown in Table 5.6 already indicates that the results are compatible with a continuous phase transition at $\theta_2^c = 5.7$. The large uncertainty of θ_2^c also translates to an even larger uncertainty in the critical exponents. We find that also biased extrapolations do not lead to any improvement.

| θ_2^c obtained from Δ_{top}^- | | | |
|--|---------|---------|-----------|
| N | [N/N-1] | [N / N] | [N / N+1] |
| 2 | - | 5.725 | 5.716 |
| 3 | 5.658 | 5.693 | 5.695 |
| 4 | 5.695 | 5.693* | 5.704 |
| 5 | 5.725 | - | - |

| $z\nu$ obtained from Δ_{top}^- | | | | z obtained from Δ_{top}^- | | | |
|--|---------|---------|-----------|---|---------|---------|-----------|
| N | [N/N-1] | [N / N] | [N / N+1] | N | [N/N-1] | [N / N] | [N / N+1] |
| 2 | - | 0.42 | 0.98 | 2 | - | 0.94 | 0.98 |
| 3 | 0.89 | 0.58 | 0.46 | 3 | 1.80 | 1.21 | 1.19 |
| 4 | 0.56 | 0.58* | 0.50 | 4 | 1.12 | - | 1.07 |
| 5 | 0.32 | - | - | 5 | 0.73 | - | - |

TABLE 5.6: The values for the location of the phase transition θ_2^c and the estimates for $z\nu$ and z are obtained by unbiased dlog-Padé extrapolations.

Let us remark here that for the obtained orders, there is no extrapolant for the gap in the τ -phase Δ_{τ}^+ , which approximates the series well even for values of $\theta < 5.4$ due to the low orders and alternating behavior of the series.

Nevertheless, the second derivative of the ground-state energy as shown in Figure 5.16 shows a diverging behavior consistent with a divergence in the region $\theta_2^c \in [5.6, 5.7]$.

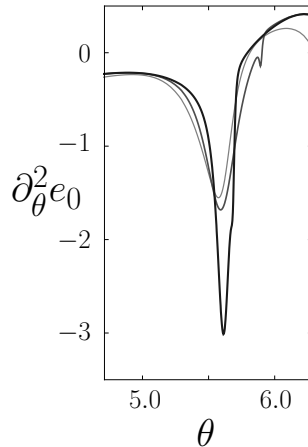


FIGURE 5.16: The second derivative of the ground-state energy e_0 , shown for system sizes $N_p = 4$ (light gray), $N_p = 9$ (dark gray), and $N_p = 13$ (black), diverges with increasing system size. The divergence is located in the region $\theta \in [5.6, 5.7]$. The features of the curves for $\theta > 5.7$ as e.g. the peak for $\partial_\theta^2 e_0 = 0$ stem from level crossings between the four ground states in the topological phase and are thus finite-size effects.

All these results lead us to the conclusion that our data is consistent with a second-order phase transition around $\theta \in [5.6, 5.7]$. However, the obtained orders are not enough to give a quantitatively precise estimate for the critical exponents.

5.2.3 Phase transition between 1- and τ -phase

Let us briefly discuss the phase transition between the two topologically-trivial phases. At the point $\theta = \pi$, the infinitely-many ground states are the flux-full states discussed in Section 3.5.1.3. The perturbation acts within this ground-state manifold, so we expect a splitting of the levels for $\theta \neq \pi$.

We do not have the series expansions, neither from the **1**-phase nor from the τ -phase, which approach the limit $\theta = \pi$ quantitatively. This is due to the fact that this limit corresponds to the value $-\infty$ for the expansion parameter $\pm 1/\tan \theta$ and the orders reached in our expansions are not sufficient to describe the spectrum in a quantitative fashion.

Additionally, we see in Figure 5.7 that perturbative and the exact diagonalization results differ significantly in the region $\theta \in [\frac{\pi}{2}, \frac{3\pi}{2}]$. In the **1**-phase, this is due to the fact that on the finite-size systems, additional low-energy modes are present, which corresponds to closed strings of τ -bonds, which wrap around non-contractible loops of the system. These modes are absent in the thermodynamic limit and thus not described by the series expansions. In the τ -phase, the finite size of the systems impacts the spectrum, as it constrains the effect of the long-range hoppings terms discussed in Section 3.5.1.5.

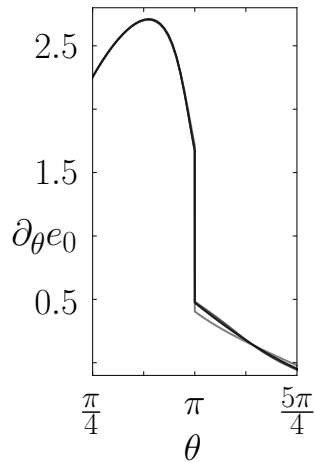


FIGURE 5.17: The first derivative of the ground-state energy $\partial_{\theta}e_0$ is shown for the system sizes from $N_p = 4$ (light gray) to $N_p = 13$ (black). For system sizes larger than four, the curves lie almost on top of each other, suggesting a converged jump of the first derivative.

However, the data from the exact diagonalization does not show any particular features except at the point $\theta = \pi$ itself. We depicted in Figure 5.17 the first derivative of the ground-state energy $\partial_{\theta}e_0$, showing a pronounced jump, which seems to be converges for all considered systems sizes with $N_p > 4$. We thus conclude that the **1**- and the τ -phase are separated by a first-order phase transition at $\theta = \pi$.

5.2.4 Summary of the phase transitions in the Fibonacci model

In the above section, we presented the phase diagram of the perturbed string-net model for Fibonacci anyons. We found that the phase diagram is constituted by the three phases discussed in Section 3.5.1: the topological, the **1**- and the τ -phase.

For the phase transition between the topological and the **1**-phase, we were able to perform a finite-size/order scaling as in Section 5.1.1 and to obtain the location of the phase transition $\theta_1^c = 0.255$. We observe a good agreement between the results obtained by series expansions and exact diagonalization.

The data-collapse results are consistent with a continuous phase transition. Additionally to the analysis of the series, we performed a data-collapse analysis. This allowed us to extract the critical exponents. Our results are $\nu = 0.41$, $z = 1.$, and $\alpha = 0.78$. These findings are consistent with the hyper-scaling relation (5.14) and with the observation that the first derivative of the ground-state energy does not diverge. To our knowledge, even when considering the error estimates discussed in Section 5.1, these values do not correspond to a known universality class that could be related to this system.

For the phase transition between the topological and the τ -phase, we obtained series of lower order than in the just discussed phase transition. This and the fact that coefficients of the series alternate in sign lead to a slow convergence of the series expansions in the vicinity of the phase transition. Therefore, we have to rely on extrapolations to estimate the position of the phase transition $\theta_2^c \in [5.6, 5.7]$. This result is also supported by the data of exact diagonalizations, which displays a divergence of the second derivative of the ground-state energy in this region. Our estimates for the critical exponents are consistent with the values $z\nu = 0.5$ and $z = 1.$, but less precise due to the alternating series.

For the phase transitions between the non-topologically ordered phases, we considered the exact diagonalization results, which show clear evidence for a first-order phase transition at $\theta = \pi$.

5.3 Phase transitions for Ising anyons

For the string-net model with Ising anyons, we found two points with a finite ground-state degeneracy, namely the topological phase for $\theta = 0$ and the $\mathbf{1}$ -phase for $\theta = \frac{\pi}{2}$.

Additionally, we discussed the flux-full case $\theta = \pi$ and the dimer-limit $\theta = \frac{3\pi}{2}$.

For the former, we can read off Eq. (3.72) the ground-state degeneracy, which yields $D_{N_p}^{\text{torus}} = (1 + 6(-1)^{N_p} + 2 \cdot 3^{N_p})$.

For the latter, we can infer its ground-state degeneracy by considering the mapping $\sigma \rightarrow s, \psi \rightarrow \mathbf{1}$, which yields a one-to-one correspondence of the ground states in the dimer limit with the string-net states of the semion model defined on the same lattice. Thus the ground-state degeneracy is in this case given by (3.74), and, in particular, is different from the one for the flux-full case.

As we have only two limits, around which we can perform a perturbative analysis, we rely on the exact diagonalization to determine the global shape of the phase diagram.

In Figure 5.18, we show the ground-state energy and its first and second derivative for system sizes from $N_p = 4$ (light gray) to $N_p = 13$ (black). We observe at the phase boundary between the topological and the $\mathbf{1}$ -phase the same shape of the curves as in the case of the Fibonacci-model. Thus we shall consider the transition as a candidate for a second-order phase transition at the location θ_1^c to be determined in the following.

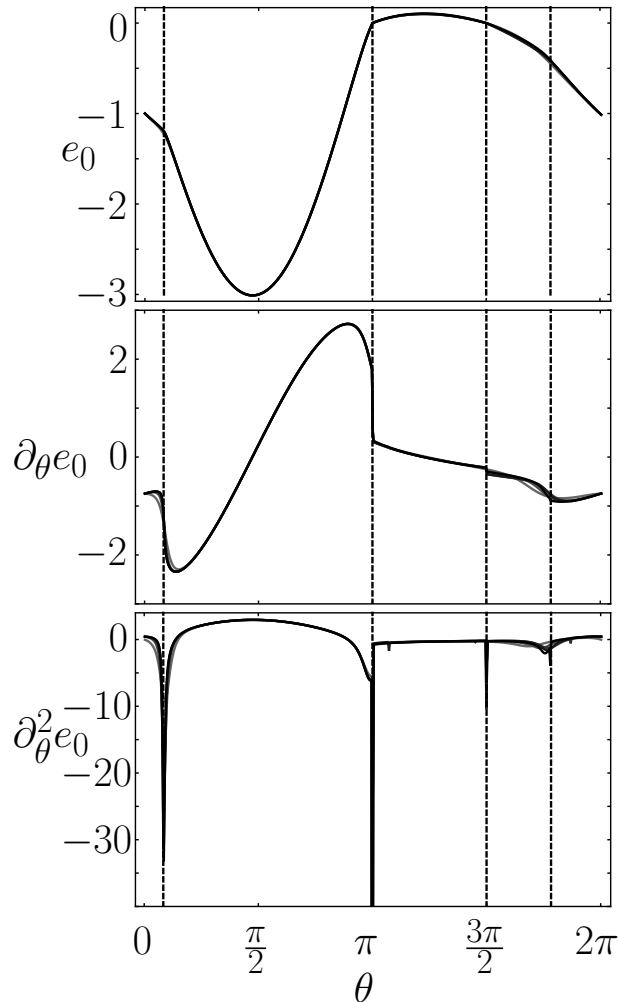


FIGURE 5.18: We show the exact-diagonalization results for the ground-state energy e_0 and its first- and second-order derivative for system sizes from $N_p = 4$ (light gray) to $N_p = 13$ (black). The first derivative shows jumps at $\theta = \pi$ and $\theta = \frac{3\pi}{2}$, indicating a first-order transition. The phase transition out of the topological phase show the characteristics of a second-order phase transition.

Additionally, we clearly observe a discontinuous behavior of the first derivative at $\theta = \pi$ and $\theta = \frac{3\pi}{2}$.⁴ Finally, we see in the region $\theta \in [\frac{3\pi}{2}, 2\pi]$ indications of a divergent second-order derivative at the value θ_2^c to be determined, thus another candidate for a second-order phase transition.

We remark that there are several features in the interval $\theta \in [\pi, \frac{3\pi}{2}]$, but the exact-diagonalization data for the considered system sizes does not provide a conclusive picture. Thus, as we are interested in the phase transitions out of the topological phase, we will restrict our analysis to the phases neighboring the topological phase.

⁴We note that the finite depth of the dip in $\partial_\theta^2 e_0$ at $\theta = \frac{3\pi}{2}$ is just a finite-resolution effect.

5.3.1 The valence-bond crystal

Before discussing the different phase transitions in more detail, let us investigate the phase between $\theta = \frac{3\pi}{2}$ and θ_2^c . In particular, we are interested whether this phase is gapped or gapless, whether it is possibly topologically ordered and what are its characteristics as e.g. the ground-state degeneracy.

The key observation for our analysis is the fact that there are no indications of a phase transition between $\theta = \frac{3\pi}{2}$ and θ_2^c . Thus, we can use insights for the dimer limit to infer properties of the whole phase.

Consequently, we consider the dimer limit $\theta = \frac{3\pi}{2}$ discussed in Section 3.5.2.5 and treat the topological Hamiltonian H_{LW} at first-order degenerate perturbation theory in the infinitely degenerate ground-state manifold. When restricted to this subspace, the Hamiltonian (3.5) in the dimer language H_{dm} reads up to a constant shift

$$H_{\text{dm}} = -\frac{J_{\text{p}}}{4} \sum_{\diamond} \left| \begin{array}{c} \text{hexagon with } \sigma\text{-bonds} \end{array} \right\rangle \left\langle \begin{array}{c} \text{hexagon with } \psi\text{-bonds} \end{array} \right| - \frac{J_{\text{p}}}{8} \sum_{\diamond} \left(\left| \begin{array}{c} \text{hexagon with } \sigma\text{-bonds} \end{array} \right\rangle \left\langle \begin{array}{c} \text{hexagon with } \psi\text{-bonds} \end{array} \right| + \left| \begin{array}{c} \text{hexagon with } \psi\text{-bonds} \end{array} \right\rangle \left\langle \begin{array}{c} \text{hexagon with } \sigma\text{-bonds} \end{array} \right| \right), \quad (5.25)$$

i.e. we have a potential term $\propto \frac{J_{\text{p}}}{4}$ that is diagonal in the bond basis and a kinetic term $\propto \frac{J_{\text{p}}}{8}$ which introduces fluctuations. We see that the coefficient of the kinetic term is smaller than the one of the potential term. Therefore we neglect in a first step the kinetic term and discuss only the potential term in (5.25).

For $J_{\text{p}} > 0$, this term favors hexagons formed by σ -bonds, which consequently have outgoing ψ -bonds. The ground states of this effective Hamiltonian is thus formed by dense-packed σ -hexagons as depicted on the left-hand side in Figure 5.19. Note that this configuration breaks the translational symmetry of the lattice and thus we expect three ground states for $J_{\text{p}} > 0$.

Defects of this configuration as depicted on the right-hand side of Figure 5.19 are the elementary excitations with an energy cost $\frac{3J_{\text{p}}}{4}$, as this configuration lacks three σ -hexagons.

Thus if there was no kinetic term, we would see that the Hamiltonian leads to a threefold degenerate ground state with gapped excitations. If we treat in a next step the kinetic term as a perturbation, we obtain in second-order perturbation theory a gap

$$\Delta_{\text{dm}} = \frac{J_{\text{p}}}{4} \left(3 - \frac{4}{3} \frac{1}{2^2} \right) = \frac{2J_{\text{p}}}{3}, \quad (5.26)$$

i.e., the gap is reduced by the kinetic term, but remains finite. Thus, we can conclude that the topological Hamiltonian opens for $J_{\text{p}} > 0$, i.e. for $\theta > \frac{3\pi}{2}$, a gap in the flux-full

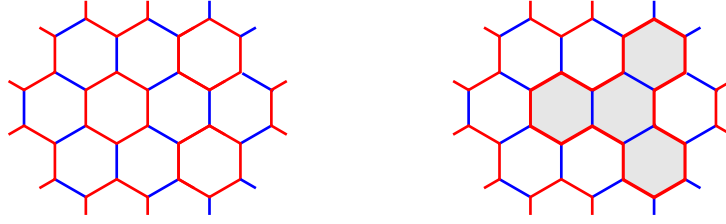


FIGURE 5.19: One ground-state configuration for the diagonal part of the Hamiltonian H_{dm} is depicted on the left-hand side. The other ground states are obtained by translating this configuration by one plaquette. On the right-hand side, we show the elementary excitation above this ground state shaded in gray.

sector of the perturbed string-net model and one obtains a threefold degenerate ground state, which is a valence bond crystal (VBC) formed by ψ -bonds. In particular, the phase between $\theta = \frac{3\pi}{2}$ and θ_2^c is not topologically ordered.

Let us note here that for $J_p < 0$, the analogous reasoning does not apply in this straightforward fashion, as there no state is favored by the dominant part of the Hamiltonian. Thus, we cannot infer the characteristics of the phase between $\theta = \pi$ and $\theta = \frac{3\pi}{2}$ this way.

5.3.2 Phase transition between topological and 1-phase

For the phase transition between the topological and the **1**-phase, we proceed as for the other models. So we consider the series expansions for the ground-state energy e_0 . The series valid in the topological phase is determined up to order ten and reads up to order four

$$e_0^{\text{top}} = \cos \theta \left(-1. - 0.750000 \cdot t - 0.281250 \cdot t^2 - 0.210938 \cdot t^3 - 0.329590 \cdot t^4 \right). \quad (5.27)$$

The ground-state energy in the **1**-phase is determined up to order 18 and reads up to order four

$$e_0^{\mathbf{1}} = \sin \theta \left(-3. - 0.250000 \cdot t^{-1} - 0.312500 \cdot 10^{-1} \cdot t^{-2} - 0.260417 \cdot 10^{-2} \cdot t^{-3} - 0.178543 \cdot 10^{-3} \cdot t^{-4} \right). \quad (5.28)$$

In Figure 5.20 we show, as for the Fibonacci model, the series order by order and the exact-diagonalization results for the ground-state energy. We have qualitatively the same behavior as for the Fibonacci model. The series for the topological phase is well converged, whereas the series for the **1**-phase still shows changes when increasing the

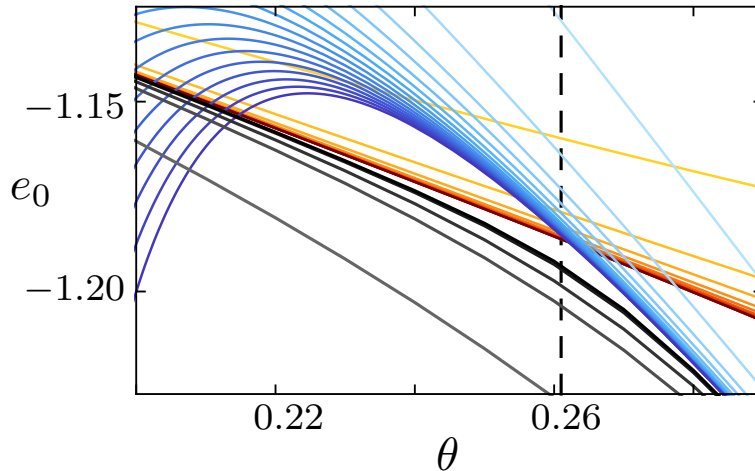


FIGURE 5.20: The perturbative results for the ground-state energy e_0 are shown order by order from order two (light blue) to order 18 (dark blue) for e_0^1 and from order two (orange) to order ten (dark red) for e_0^{top} . There are two intersections of the series for e_0^1 and e_0^{top} , respectively. Additionally we show the results of the exact diagonalization (light gray to dark gray with increasing system size). All data shows a convergent behavior, from which we estimate the location of the critical point indicated by the dashed line by a finite-order/size scaling.

order. The exact-diagonalization results show also convergence for the largest system sizes.

To complete our analysis of the low-energy spectrum, let us turn to the gap. In the topological phase, we have two different excitations: the σ - and the ψ -flux. We determine their dispersion up to order ten. For $\theta > 0$, the dispersion is minimized for $\vec{k} = \vec{0}$ and the gaps $\Delta_{\text{top}}^{\sigma,+}$ and $\Delta_{\text{top}}^{\psi,+}$ read up to order five

$$\begin{aligned} \Delta_{\text{top}}^{\sigma,+} = & 1. - 1.500000 \cdot t - 1.875000 \cdot t^2 \\ & - 2.812500 \cdot t^3 - 7.093750 \cdot t^4 - 16.523356 \cdot t^5, \end{aligned} \quad (5.29)$$

$$\begin{aligned} \Delta_{\text{top}}^{\psi,+} = & 1. - 1.500000 \cdot t - 1.875000 \cdot t^2 \\ & - 2.812500 \cdot t^3 - 7.093750 \cdot t^4 - 16.523681 \cdot t^5. \end{aligned} \quad (5.30)$$

We note that both dispersions agree with each other exactly up to order four. In order five they start to differ and, consequently, also the gaps differ from each other. However the deviations of the coefficients from each other is of the order of 10^{-4} or smaller, so that the difference does not impact the results for the spectrum in any noticeable way for the values of $t \approx 0.3$ considered here.⁵

So we conclude that both achiral excitations condense at the same point, which corresponds to the phase transition to a topological trivial phase described in Section 4.2.3.

⁵Nevertheless, we note that this difference is one of the principal differences to the one-dimensional case of the ladder discussed in Ref. [70], where we find that both dispersions are identical up to high orders.

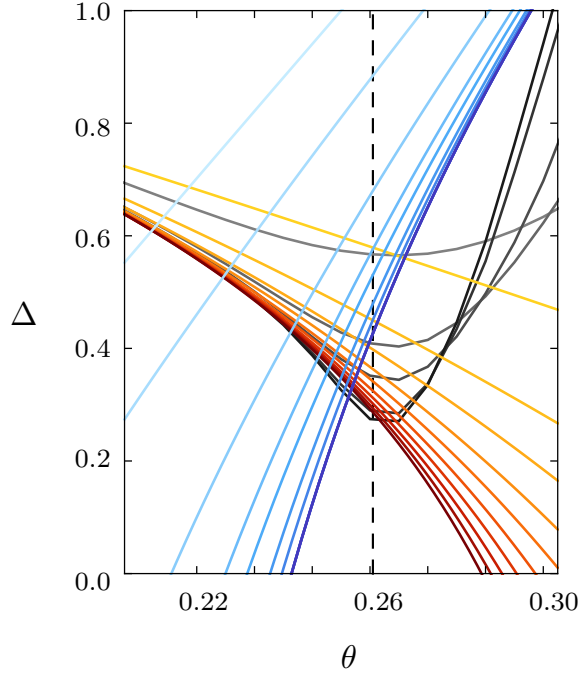


FIGURE 5.21: With the same color-coding as in Figure 5.20, we show the perturbative and exact-diagonalization results for the elementary-excitation gap in the region, where the phase transition between the topological and the **1**-phase occurs. We depict the series for $\Delta_{\text{top}}^{\sigma,+}$ from order one (orange) to ten (dark red) and the series for $\Delta_{\mathbf{1}}$ from order one (light blue) to order eight (dark blue). The picture is qualitatively the same as in semion model shown in Figure 5.10.

However, we see that the σ -gap is strictly below the ψ -gap, thus we use this series for the further analysis.

The series valid in the **1**-phase is determined up to order eight and reads up to order four

$$\Delta_{\mathbf{1}}^+ = \cos \theta \left(6. - 0.500000 \cdot t^{-1} - 0.500000 \cdot 10^{-1} \cdot t^{-2} - 0.151042 \cdot 10^{-1} \cdot t^{-3} - 0.204226 \cdot 10^{-2} \cdot t^{-4} \right). \quad (5.31)$$

We show the series for $\Delta_{\text{top}}^{\sigma,+}$ (orange to dark red) and $\Delta_{\mathbf{1}}$ (light blue to dark blue) as well as the exact-diagonalization results for the gap in Figure 5.21. Let us note that on a system with periodic boundary conditions, there is no single σ -state. Thus the exact-diagonalization gap depicted here corresponds to single ψ -flux states.

A finite-order analysis completely analogous to the one performed in Section 5.2.1 leads finally to the estimate $\theta_{\mathbf{1}}^c = 0.261$.

We perform dlog-Padé extrapolations of $\Delta_{\text{top}}^{\sigma,+}$ to obtain $z\nu = 0.40$ and $z = 1.$, shown in Table 5.7, as estimates for the critical exponents.

| θ_1^c obtained from $\Delta_{\text{top}}^{\sigma,+}$ | | | |
|---|---------|---------|-----------|
| N | [N/N-1] | [N / N] | [N / N+1] |
| 2 | - | 0.274 | 0.274 |
| 3 | 0.273 | 0.289* | 0.267 |
| 4 | 0.267 | 0.272 | 0.269 |
| 5 | 0.269 | - | - |

| $z\nu$ obtained from $\Delta_{\text{top}}^{\sigma,+}$ | | | | z obtained from $\Delta_{\text{top}}^{\sigma,+}$ | | | |
|---|---------|---------|-----------|--|---------|---------|-----------|
| N | [N/N-1] | [N / N] | [N / N+1] | N | [N/N-1] | [N / N] | [N / N+1] |
| 2 | - | 0.46 | 0.46 | 2 | - | 0.99 | 0.99 |
| 3 | 0.45 | 0.31* | 0.36 | 3 | 0.99 | 0.47* | 0.82 |
| 4 | 0.35 | 0.45 | 0.40 | 4 | 0.81 | 1.00 | 0.90 |
| 5 | 0.40 | - | - | 5 | 0.89 | - | - |

TABLE 5.7: The values for the location of the phase transition θ_1^c and the estimates for $z\nu$ and z are obtained by unbiased dlog-Padé extrapolations.

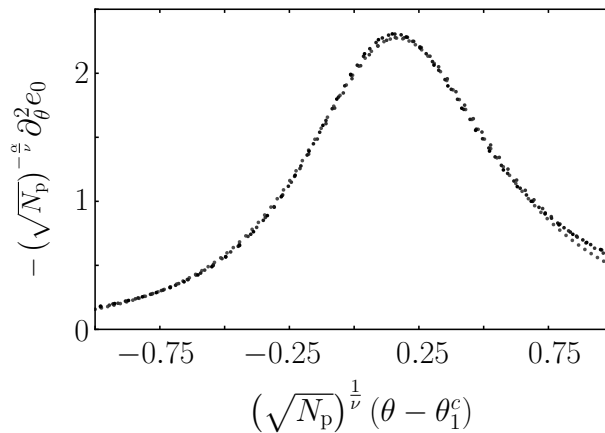


FIGURE 5.22: We perform a data collapse of the exact-diagonalization results for $\partial_\theta^2 e_0$ for the systems with $N_p = 7, 9, 12,$ and 13 plaquettes. After rescaling according to (5.21) with the values $\nu = 0.39$ and $\alpha = 0.83$, the four curves collapse onto one curve in a large range of parameters.

Additionally, we perform a data collapse of the exact-diagonalization results for $\partial_\theta^2 e_0$. For the values $\nu = 0.39$ and $\alpha = 0.83$, we obtain the collapse shown in Figure 5.22.

This leads us to conclude that we find evidence of a second-order phase transition consistent with the simultaneous condensation of σ - and ψ -fluxes at $\theta_1^c = 0.261$. We obtain estimates for the critical exponents $\nu = 0.39$, $z = 1.$, and $\alpha = 0.83$. These values are in the same range as the ones for the corresponding phase transition in the Fibonacci model. However, our estimated accuracy does not allow us to judge, whether these two sets of exponents coincide and thus fall in the same universality class or not.

5.3.3 Phase transition between topological and the VBC

For the investigation of this phase transition, we are in the same situation as in Section 5.1.2: series expansions are only available for the topological phase. Thus, we estimate the phase transition by extrapolating the gap.

The gaps valid for $\theta < 0$ read up to order five

$$\begin{aligned} \Delta_{\text{top}}^{\sigma,-} = & 1. + 0.750000 \cdot t + 0.093750 \cdot t^2 \\ & + 0.421875 \cdot t^3 + 0.369629 \cdot t^4 + 0.680623 \cdot t^5 \end{aligned} \quad (5.32)$$

$$\begin{aligned} \Delta_{\text{top}}^{\psi,-} = & 1. + 0.750000 \cdot t + 0.093750 \cdot t^2 \\ & + 0.421875 \cdot t^3 + 0.369629 \cdot t^4 + 0.680786 \cdot t^5. \end{aligned} \quad (5.33)$$

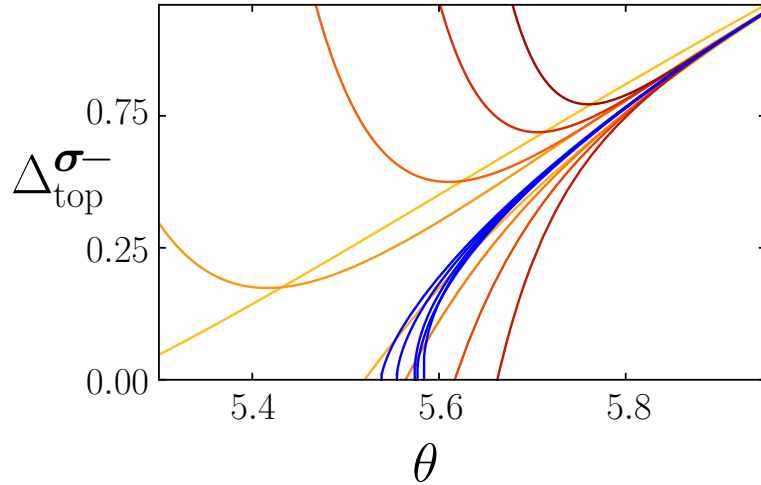


FIGURE 5.23: The series of the gap $\Delta_{\text{top}}^{\sigma,-}$ in the topological phase is depicted from order one (orange) to order ten (dark red). Additionally to the alternating series, we give the dlog-Padé extrapolations (blue), which determine the location of the phase transition θ_2^c at between 5.5 and 5.6.

We see that also for this region, the σ -flux gap $\Delta_{\text{top}}^{\sigma,-}$ is slightly smaller than the ψ -flux gap with a difference in the series beginning at order five.

Thus, we use the series for $\Delta_{\text{top}}^{\sigma,-}$ to extrapolate the gap towards its closing point, as shown in Figure 5.23. The extrapolations yield a gap closing in the region around $\theta_2^c = 5.57$ and estimates for the exponents $z\nu = 0.5$ and $z = 1.$.

The simultaneous condensation of the σ - and the ψ -flux is consistent with the fact that the valence-bond crystal phase found between $\theta = \frac{3\pi}{2}$ and θ_2^c is not topologically ordered.

| θ_2^c obtained from $\Delta_{\text{top}}^{\sigma,-}$ | | | | | | | |
|---|---------|---------|-----------|--|--|--|--|
| N | [N/N-1] | [N / N] | [N / N+1] | | | | |
| 2 | - | 5.58 | 5.61 | | | | |
| 3 | 5.48 | 5.54 | 5.56 | | | | |
| 4 | 5.57 | 5.44* | 5.57 | | | | |
| 5 | 5.58 | - | - | | | | |

| $z\nu$ obtained from $\Delta_{\text{top}}^{\sigma,-}$ | | | | z obtained from $\Delta_{\text{top}}^{\sigma,-}$ | | | |
|---|---------|---------|-----------|--|---------|---------|-----------|
| N | [N/N-1] | [N / N] | [N / N+1] | N | [N/N-1] | [N / N] | [N / N+1] |
| 2 | - | 0.53 | 0.46 | 2 | - | 1.15 | - |
| 3 | 1.13 | 0.68 | 0.59 | 3 | 2.23 | 1.41 | 1.25 |
| 4 | 0.48 | 0.89* | 0.55 | 4 | 1.04 | 0.26* | 1.16 |
| 5 | 0.44 | - | - | 5 | 0.95 | - | - |

TABLE 5.8: The values for the location of the phase transition θ_2^c and the estimates for $z\nu$ and z are obtained by unbiased dlog-Padé extrapolations.

5.3.4 Summary of the phase transitions in the Ising model

For the perturbed string-net model with Ising-anyons, we studied the phase transitions out of the topologically ordered phase.

The phase transition between the topological and the **1**-phase is investigated in the analogous fashion as in the case of the Fibonacci anyons and we find a qualitatively similar picture. We locate the phase transition at $\theta_1^c = 0.261$. Our results are consistent with a second-order phase transition with the exponents $\nu = 0.39$, $z = 1.$, and $\alpha = 0.83$.

We analyze the phase neighboring to the topological phase for $\theta < 0$ by first-order degenerate perturbation theory around the dimer limit $\theta = \frac{3\pi}{2}$. The effective Hamiltonian describes a quantum dimer model. By a perturbative treatment of the kinetic term, we show that the topological Hamiltonian opens a gap in the ground-state manifold for $\theta > \frac{3\pi}{2}$. The ground state is a threefold degenerate valence bond crystal.

The phase transition between the topological and the valence bond crystal phase is investigated in the same fashion as for the semion model. We find the location of the phase transition at $\theta_2^c = 5.57$. Our results are consistent with a second-order phase transition with the exponents $z = 1.$ and $z\nu = 0.5$.

Our findings for the order of the phase transitions are in agreement with the fact that the gaps of both elementary excitations go to zero at the transition point. This corresponds to the condensation-driven phase transition from the D(Ising) to a topologically-trivial phase as discussed in Section 4.2.3.

We note that the estimates for the critical exponents coincide within our estimated uncertainty with the ones obtained for the Fibonacci-anyon case. However, our results

are not precise enough to discriminate whether the obtained exponents are the same or not.

5.4 Comparison between the different models

In the previous sections, we analyzed the phase transitions for the perturbed string-net models for semions, Fibonacci-, and Ising-anyons on the honeycomb lattice. The phase diagrams can be summarized as in Figure 5.24.

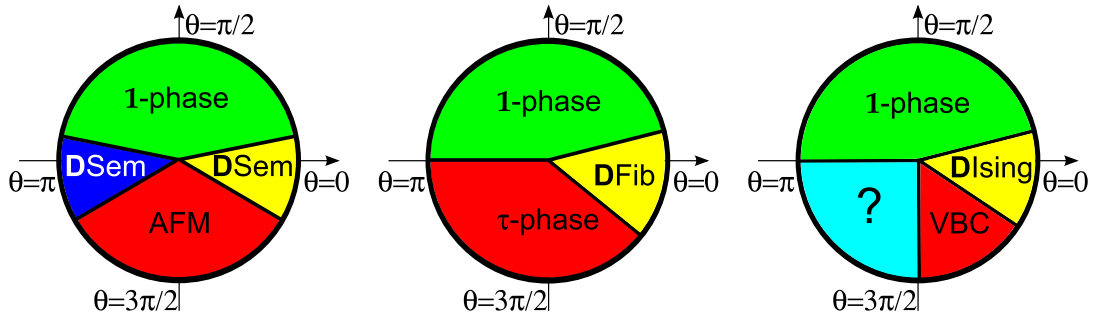


FIGURE 5.24: We show the phase diagrams of the perturbed string-net model for semions (left), Fibonacci- (middle), and Ising-anyons (right) discussed in the previous sections. For the Abelian case, there are two topologically ordered phases, whereas for the non-Abelian cases, there is only one. The extension of this phase for the non-Abelian models is larger than for the Abelian one.

The phase transitions out of the topological phases are found for all three models to be consistent with a second-order transition, which corresponds in the framework of condensate-induced phase transitions discussed in Chapter 5 to a condensation of the achiral fluxes.

The phase transitions between the non-topological phases⁶ are first-order phase transitions, if present in the phase diagram.

We found for the Abelian model of the semions two extended topological phases. The phase around $\theta = 0$ is also present for the non-Abelian models, whereas the phase around $\theta = \pi$ shrinks to a single point.

We list the critical points θ_1^c and θ_2^c in Table 5.9. The location of the phase transition to the different phases at θ_2^c are close to each other, whereas the location of the phase transitions to the 1-phase shows a difference of more than 20% between the models with Abelian and non-Abelian anyons. In this sense the phases harboring non-Abelian excitations are more stable against the local perturbation considered here.

⁶We did not discuss the phase in the region $\theta \in [\pi, \frac{3\pi}{2}]$ for Ising anyons. However we shall assume for the discussion here that it is topologically trivial, as exact-diagonalization results (not shown) suggest a possible gapless phase, which, per definition, is not topologically ordered.

| | θ_2^c | θ_1^c |
|-----------|--------------|--------------|
| Semions | 5.73 | 0.207 |
| Fibonacci | 5.7 | 0.255 |
| Ising | 5.57 | 0.261 |

TABLE 5.9: The location of the phase transitions out of the topological phase for the different models studied in this work.

In our analysis of the non-Abelian models, we find values of the critical exponents, which are close to each other and might coincide within our accuracy estimates. Therefore one can speculate whether the exponents are the same and thus the phase transitions out of a topologically ordered phase with non-Abelian anyons are in the same universality class. However, we will compare in the following the Abelian and non-Abelian cases.

One difference between the appearing phase transitions is that the corresponding critical properties differ significantly between the Abelian and non-Abelian cases. For the phase transitions out of the Abelian phase, the exponent ν of the corresponding $3D$ Ising or $3D$ XY universality classes are 0.63 [138] and 0.67 [142], respectively. Our analysis yields values of ν which are much smaller. We find values in the range 0.36 – 0.5.

The values determined for the dynamical exponent z are compatible with the value 1 for the Abelian and non-Abelian cases. As the combination $d + z$, with d the dimension of the quantum lattice problem, is replaced by the dimension d_{cl} , which is the dimension of a classical model sharing the same critical exponents [137], it may be possible to find three-dimensional classical models, which are in the same universality class and possibly better suited to further investigation.

One can already infer from the hyper-scaling relation (5.14) that the differences in the exponent ν result also in different values of α . For the non-Abelian models, we find large values of $\alpha = 0.78$ (Fibonacci) or $\alpha = 0.83$ (Ising), whereas for the Abelian model, the values of α are small ($\alpha = 0.11$ for the $3D$ Ising class [138] and $\alpha = -0.014$ for the $3D$ XY class [142]). This may have an impact for the detection of phase transitions out of a topologically ordered phase, as the large value of α close to 1 leads to a behavior of the ground-state energy which is similar to the one for a first-order transition. Consequently, the distinction between first- and second-order phase transition might be more complicated than for the Abelian cases.

So, our study reveals that the more complex structure of non-Abelian excitations impacts not only the extension of a topological phase, but also the critical behavior at its boundaries.

5.5 Chapter Summary

In this chapter, we studied the phase diagram and the phase transitions in the perturbed string-net models for semions, Fibonacci-, and Ising-anyons on the honeycomb lattice.

The study of the semion model revealed two topological phases separated by two non-topological phases. These findings are in agreement with the phase diagram of the transverse-field Ising model as discussed in Section 3.5.3. In particular the second-order phase transitions out of the topological phases are driven by the condensation of the anyonic excitations as discussed in Chapter 4.

We determined the locations of the phase transitions and critical properties by analyzing the low-energy spectrum. In particular, we employed a finite-order scaling analysis to obtain the location of the phase transition between the topological and the **1**-phase.

The comparison with known values for the location of the phase transition and the critical exponents of the transverse-field Ising model allowed us to estimate the systematic errors of our approach consisting of a perturbative description of the low-energy physics as well as exact diagonalizations.

The same quantities have been determined for the non-Abelian models. The phase diagram for the perturbed string-net model with Fibonacci anyons consists of three phases. We find by the same methods as for the semions the locations of the phase transitions. We obtain results, which show strong evidence for second-order phase transitions out of the topologically ordered phase. The set of exponents obtained for both transitions differ from each other by more than 10% for the value of $z\nu$, so these phase transitions may belong to different universality classes. However, the corresponding critical exponents do, up to our knowledge, not belong to a known universality class that could be related to the respective models.

We additionally studied the phase transitions in the model with Ising-anyons. Also for this model, we found strong evidence for second-order phase transitions out of the topological phase. The determined critical exponents show similar values as the ones for the Fibonacci theory. However, our accuracy for these quantities does not allow us to decide, whether the exponents are the same or different.

Nevertheless, we presented in this chapter the evidence for second order phase transitions out of topologically ordered phases in a two-dimensional system and provided estimates for critical exponents associated with spectral quantities.

To conclude, we compared the obtained results for the Abelian and non-Abelian cases.

Part II

Series expansion techniques for perturbed string-net models

Methodology

*What from your father you've inherited,
You must earn again, to own it straight.
- Johann Wolfgang von Goethe -*

The study of phase transitions involving topologically ordered phases in two-dimensional lattice systems remains a challenging task even after several years of intensive researches. This is basically due to the fact that the order parameters describing these phases are non-local [10, 16, 53, 88, 99] and thus Landau-theory [1, 2] does not apply.

Also a field-theoretical description for topologically ordered phases including their excitations, which holds in the presence of perturbations, is still missing. These features rule out most of the renormalization group approaches usually used for the study of phase transitions.¹ Additionally, all non-Abelian models, which are the main interest in the context of topological quantum computation and also the focus of this thesis, seem to suffer from the sign-problem, rendering quantum Monte Carlo techniques rather difficult to apply. Also variational methods, which have already been employed successfully in the context of phase transitions out of Abelian topologically ordered phases [82, 86], seem to be rather difficult to implement for the models in question, e.g. because of the large support of the operators (the twelve-link interactions) in the string-net models.

One of the remaining possibilities that has already been applied with some success in the study of Abelian phase transitions, are perturbative techniques, which give access to spectral properties like the ground-state energy or dispersions of elementary excitations [78, 81, 82, 86]. Other local observables and correlation functions are in principle also accessible [144–146], although their investigation is beyond the focus this thesis. The perturbative results are correct in the thermodynamic limit (up to a given order), so finite-size effects are absent for these approaches. However, to capture the physics of the

¹Note that renormalization ansatzes based on entanglement properties are currently developed [143]. However, their numerical accuracy for systems in two or more dimensions is still to be improved.

phase transitions not only qualitatively but also quantitatively, a perturbative treatment up to high orders complemented by suitable extrapolations is necessary.

Nevertheless, a perturbative expansion may miss phase transitions, if the mode driving it is not taken into account. So, we also perform exact (Lanczos-) diagonalization (ED) on finite-size systems. The results obtained by ED are non-perturbative (take into account all modes on the finite system), but subject to finite-size effects. Consequently, ED is a complementary approach to series expansions. In the following, we discuss how the different methods are implemented in order to obtain the results presented in the previous chapter.

6.1 Series expansions

In this section, we present three perturbative techniques, namely perturbative continuous unitary transformations [105, 147], degenerate perturbation theory [106, 148], and a perturbative version of a partitioning approach [107], we used to derive the effective low-energy Hamiltonians H^{eff} and to determine the ground-state energy as well the dispersion presented in Chapter 5. These techniques have in common that they allow to determine the effective Hamiltonian model-independently in operator form. This is in contrast to the approach of typical linked-cluster expansions [129, 149–151], where the effective Hamiltonian is explicitly derived for each of the finite-size systems used to obtain the quantities of interest. The idea here is to separate the tasks of derivation and evaluation to be able to optimize them independently. In this way, we can benefit from the operator form of the effective Hamiltonian to perform a linked-cluster expansion also for non-Abelian anyons.

Here, we will give a short introduction to the derivation of the respective effective Hamiltonians for each approach. Since all effective Hamiltonians are linked to the original one by a unitary transformation, the quantities of interest such as the low-energy spectrum of these Hamiltonians do not depend on the specific approach in the end. However, the different approaches allow to evaluate the effective Hamiltonian in a more or less efficient way depending on the problem at hand. We give a short comparison of the different approaches in order to determine which one to use in which context in Section 6.1.4. Additionally, we briefly present the main features of the different methods that allow to obtain results valid in thermodynamic limit in an efficient way for the different models presented in Chapter 3.

The aim of these methods is to decouple one subspace from all other subspaces in the Hilbert space. The problem of diagonalizing the full Hamiltonian reduces then to

diagonalize the remaining effective Hamiltonian in the smaller (however, in general still infinite-dimensional) subspace. We shall see in Chapter 7, in which way to proceed for the relevant subspaces.

All these approaches have in common that they require the original Hamiltonian to be of the form

$$H = H_0 + V. \quad (6.1)$$

The unperturbed part H_0 has to be diagonal, i.e. represented in its eigenbasis. The (possibly degenerate) eigenspaces of H_0 are coupled with each other via the action of the perturbation V . To decouple the eigenspace with eigenvalue E_0 of H_0 , all of the presented methods require that this subspace has a finite-energy gap towards the rest of the spectrum. The operator V depends linearly on one or more parameters, which are supposed to be small compared to the energy gap of H_0 to allow for a converging perturbative expansion for the effective Hamiltonian. As the effective Hamiltonian H^{eff} is constructed to decouple a degenerate subspace of H_0 from the rest of the Hilbert space, it just couples eigenstates of H_0 with a given unperturbed eigenvalue E_0 .

It is useful for the following discussion to introduce the operator Q , which counts the number of excitations in terms of excited states of H_0 , i.e.

$$Q |n\rangle = n |n\rangle, \quad (6.2)$$

where $|n\rangle$ is an n -particle eigenstate of H_0 . The effective Hamiltonian H^{eff} conserves the number of particles and thus commutes with Q .

6.1.1 Perturbative continuous unitary transformations

In this section, we discuss the perturbative continuous unitary transformation (pCUT) method [147]. It is based on the continuous unitary transformations (CUTs) independently proposed by Wegner [152] and Głazek and Wilson [153]. First, we briefly introduce the idea of CUTs, then describe its perturbative version and finally mention some important properties of the effective Hamiltonian, e.g. that it fulfills a linked-cluster theorem, which is at the heart of the linked-cluster expansion presented in Chapter 8.

6.1.1.1 Continuous unitary transformations

The key idea of CUTs is to decouple a subspace of H not by one unitary transformation U , but to obtain the effective Hamiltonian H^{eff} by the application of an infinite sequence

of transformations. So we consider

$$H(\ell) = U^\dagger(\ell) H U(\ell), \quad (6.3)$$

with $H(0) = H$ and $H(\ell = \infty) = H^{\text{eff}}$. Differentiating equation (6.3) by the so-called flow parameter ℓ , we obtain the flow equation

$$\partial_\ell H(\ell) = \left(\partial_\ell U^\dagger(\ell) \right) H U(\ell) + U^\dagger(\ell) H \left(\partial_\ell U(\ell) \right) \quad (6.4)$$

$$= [\eta(\ell), H(\ell)], \quad (6.5)$$

where we introduced the antiHermitian generator

$$\eta(\ell) = \left(\partial_\ell U^\dagger(\ell) \right) U(\ell). \quad (6.6)$$

So the problem of transforming H into the effective Hamiltonian H^{eff} is shifted from finding the unitary transformation U to the appropriate choice of the generator $\eta(\ell)$. The effective Hamiltonian is then obtained as a solution of the flow equation (6.5) by

$$H^{\text{eff}} = \lim_{\ell \rightarrow \infty} H(\ell). \quad (6.7)$$

Although the effective Hamiltonian (6.7) will not couple different sectors of the Hilbert space, and thus will be of simpler global structure, its form within each decoupled sector will be, generically speaking, more complicated compared to the original Hamiltonian. For example, locality of the operators will usually not be preserved during the flow.

However, the main advantage of this continuous formulation is that one can prove some properties of the effective model by analyzing the behavior of $H(\ell)$ independently of the choice of a specific basis during the flow. For example, Wegner [152] chose the generator

$$\eta^W(\ell) = [H_d(\ell), H(\ell)], \quad (6.8)$$

where H_d is diagonal part of the Hamiltonian H , and has shown that all matrix elements between non-degenerate eigenstates of H vanish in the limit of $\ell \rightarrow \infty$ and thus the resulting Hamiltonian becomes diagonal if no degeneracies appear. However, this result holds just in the limit $\ell \rightarrow \infty$, which can often not be obtained in practice.

Let us mention that the flow equation (6.5) represents in general an infinite set of coupled, non-linear differential equations, which can often not be solved analytically. For a numerical solution, one has then to truncate the set of equations in order to obtain a finite system of equations. There exist several strategies of truncation schemes

based on criteria like the form of the effective terms [154], the extension of their support [155, 156], or perturbative reasonings [157], just to name a few.

In what follows, we consider the analytical solution for the choice of the quasi-particle conserving generator η^Q [105, 158]. Its matrix elements in a common eigenbasis $\{|i\rangle\}$ of H_0 and Q are defined as

$$\eta_{i,j}^Q = \text{sgn}(Q_{i,i} - Q_{j,j}) H_{i,j}(\ell), \quad (6.9)$$

where $O_{i,j} = \langle i|O|j\rangle$ is the matrix element of the operator O .

This generator is also used in the pCUT [105]. Compared to η^W , it has the additional feature that it sorts the eigenvalues according to the eigenvalues n of Q (6.2). In the following, we will consider a special form of H_0 and V in order to solve the resulting flow equation by a model-independent perturbative ansatz that leads us to consider the perturbative continuous unitary transformations.

Let us just mention that this transformation not only decouples one degenerate eigenspace of H_0 from the rest, but it will decouple all of them from each other. For an analytical perturbative treatment, this fact does not represent a complication, however if one wants to solve the flow equations numerically (as e.g. in [157]), one can also choose different generators to only decouple the part of the Hilbert space, in which one is interested, and, consequently, reduce the complexity of the flow equations to be solved [159].

6.1.1.2 Perturbative continuous unitary transformations

In the context of pCUT, we assume for the Hamiltonian (6.1):

- The unperturbed Hamiltonian H_0 has a discrete spectrum bounded from below.

Thus we can label the eigenvalues by ε_i with non-negative integer i . For notational convenience, we denote the excitation energies by $\Delta\varepsilon_i = \varepsilon_i - \varepsilon_0$.

- There is a $\Delta\varepsilon$ such that we have for any excitation energy $\Delta\varepsilon_i = n_i\Delta\varepsilon$ with integer n_i .

By rescaling H_0 , it is then always possible to set $\Delta\varepsilon = 1$, as we do in the following. In this case, H_0 equals then the particle number counting operator Q (6.2) up to a constant.

- It exists an integer N_{\max} such that the perturbation can be written as

$$V = \sum_{m=-N_{\max}}^{N_{\max}} T_m, \quad (6.10)$$

where the operators T_m raise the particle number by m , i.e.

$$[H_0, T_m] = mT_m. \quad (6.11)$$

These assumptions restrict the applicability of the pCUTs. However there are many (effective) models fulfilling these assumptions in the context of low-dimensional (frustrated or unfrustrated) quantum magnets, spin ladders, Hubbard-models, supersolids, nuclear physics, as well as stabilizer codes including topologically ordered spin models [78, 81, 82, 86, 90, 160–168], just to name a few.

In the following, we present a solution of the flow equation (6.5) as detailed in [105, 169]. Therefore, we introduce the multi-index notations

$$\mathbf{m} = (m_1, m_2, m_3, \dots, m_k), \quad (6.12)$$

$$|\mathbf{m}| = k, \quad (6.13)$$

$$M(\mathbf{m}) = \sum_{i=1}^k m_i, \quad (6.14)$$

$$\{\mathbf{m}, \mathbf{m}'\} = (m_1, \dots, m_{|\mathbf{m}|}, m'_1, \dots, m'_{|\mathbf{m}'|}), \quad (6.15)$$

$$T(\mathbf{m}) = T_{m_1} T_{m_2} T_{m_3} \dots T_{m_{|\mathbf{m}|}}. \quad (6.16)$$

With these notations, we choose the following general ansatz for the perturbation (H_0 stays constant during the flow):

$$V(\ell) = \sum_{k=1}^{\infty} \sum_{|\mathbf{m}|=k} F(\ell; \mathbf{m}) T(\mathbf{m}), \quad (6.17)$$

so that the complete ℓ -dependence is absorbed in the functions $F(\ell, \mathbf{m})$. Inserting (6.17) in the definition of the generator (6.9) yields the following form

$$\eta^Q(\ell) = \sum_{k=1}^{\infty} \sum_{|\mathbf{m}|=k} F(\ell; \mathbf{m}) \operatorname{sgn}(M(\mathbf{m})) T(\mathbf{m}), \quad (6.18)$$

where sgn is the sign function defined with $\operatorname{sgn}(0) = 0$.

For the quasi-particle conserving generator (6.9), the flow equation (6.5) reads

$$\frac{\partial}{\partial \ell} H(\ell) = \frac{\partial}{\partial \ell} V(\ell), \quad (6.19)$$

$$= [\eta^Q(\ell), V(\ell)] - [H_0, \eta^Q(\ell)], \quad (6.20)$$

$$= [\eta^Q(\ell), V(\ell)] - \sum_{k=1}^{\infty} \sum_{|\mathbf{m}|=k} F(\ell; \mathbf{m}) \operatorname{sgn}(M(\mathbf{m})) \underbrace{[H_0, T(\mathbf{m})]}_{M(\mathbf{m})T(\mathbf{m})}. \quad (6.21)$$

Now inserting the expressions for $V(\ell)$ (6.17) and $\eta^Q(\ell)$ (6.21) yields:

$$\begin{aligned} \sum_{k=1}^{\infty} \sum_{|\mathbf{m}|=k} \frac{\partial}{\partial \ell} F(\ell; \mathbf{m}) T(\mathbf{m}) &= \sum_{\substack{k_1, k_2 \\ |\mathbf{m}_1|=k_1 \\ |\mathbf{m}_2|=k_2}} F(\ell; \mathbf{m}_1) F(\ell; \mathbf{m}_2) \operatorname{sgn}(M(\mathbf{m}_1)) [T(\mathbf{m}_1), T(\mathbf{m}_2)] \\ &\quad - \sum_{\substack{k \\ |\mathbf{m}|=k}} F(\ell; \mathbf{m}) |M(\mathbf{m})| T(\mathbf{m}). \end{aligned} \quad (6.22)$$

The differential equation for the function $F(\ell; \mathbf{m})$ is then given by the coefficients of $T(\mathbf{m})$ in (6.22) for each \mathbf{m} and reads:

$$\begin{aligned} \frac{d}{d\ell} F(\ell; \mathbf{m}) &= -|M(\mathbf{m})| F(\ell; \mathbf{m}) \\ &\quad + \sum_{\substack{\{\mathbf{m}_1, \mathbf{m}_2\}=\mathbf{m} \\ |\mathbf{m}| \geq 2}} [\operatorname{sgn}(M(\mathbf{m}_1)) - \operatorname{sgn}(M(\mathbf{m}_2))] F(\ell; \mathbf{m}_1) F(\ell; \mathbf{m}_2). \end{aligned} \quad (6.23)$$

Here, one can see a feature of the flow equation due to the choice of η^Q [158]: no terms with $|M(\mathbf{m})| > N_{\max}$ are generated during the flow, since their the coefficient $[\operatorname{sgn}(M(\mathbf{m}_1)) - \operatorname{sgn}(M(\mathbf{m}_2))]$ yields a zero on the right-hand side of (6.23).

In order to simplify (6.23), we define

$$F(\ell; \mathbf{m}) = e^{-|M(\mathbf{m})|\ell} f(\ell; \mathbf{m}). \quad (6.24)$$

Inserting (6.24) in (6.23), the linear term vanishes and we are left with

$$\begin{aligned} \frac{\partial}{\partial \ell} f(\ell; \mathbf{m}) &= \sum_{\substack{\{\mathbf{m}_1, \mathbf{m}_2\}=\mathbf{m} \\ |\mathbf{m}| \geq 2}} e^{(|M(\mathbf{m})| - |M(\mathbf{m}_1)| - |M(\mathbf{m}_2)|)\ell} \\ &\quad \times \{\operatorname{sgn}(M(\mathbf{m}_1)) - \operatorname{sgn}(M(\mathbf{m}_2))\} f(\ell; \mathbf{m}_1) f(\ell; \mathbf{m}_2). \end{aligned} \quad (6.25)$$

In Ref. [105] it has been shown that the $f(\ell; \mathbf{m})$ are bounded functions. Thus we see that $f(\ell; \mathbf{m}) \rightarrow 0$ for $M(\mathbf{m}) \neq 0$ due to the exponential in (6.25). So, the effective Hamiltonian contains only terms with $M(\mathbf{m}) = 0$.

Since the sum on the right-hand side of (6.25) contains only \mathbf{m}_i with $|\mathbf{m}_i| < |\mathbf{m}|$, we can solve the equation (6.25) for every \mathbf{m} recursively. As $|\mathbf{m}|$ corresponds to the order, we obtain a solution of the flow equation order by order in the perturbation parameter. The initial conditions can be determined from (6.17):

$$F(0; \mathbf{m}) = f(0; \mathbf{m}) = \begin{cases} 1, & \text{for } |\mathbf{m}| = 1 \text{ and } T_{m_1} \text{ present in } V = V(\ell = 0) \\ 0, & \text{otherwise} \end{cases}. \quad (6.26)$$

Since we are interested in the limit $\ell \rightarrow \infty$, it is convenient to define coefficients

$$C(\mathbf{m}) = \lim_{\ell \rightarrow \infty} F(\ell; \mathbf{m}). \quad (6.27)$$

One can show by explicitly solving the equations (6.25) that these $C(\mathbf{m})$ are rational numbers [105]. So, in the end, we can write down the effective Hamiltonian as

$$H_{\text{pCUT}}^{\text{eff}} = H_0 + \sum_{k=1}^{\infty} \sum_{\substack{|\mathbf{m}|=k \\ M(\mathbf{m})=0}} C(\mathbf{m})T(\mathbf{m}), \quad (6.28)$$

which reads for the leading orders:

$$\begin{aligned} H_{\text{pCUT}}^{\text{eff}} &= H_0 + T_0 \\ &+ \sum_{n \neq 0} \frac{1}{n} T_n T_{-n} \\ &+ \sum_{n \neq 0, m \neq -n} \frac{1}{n(n+m)} T_{-n-m} T_m T_n - \sum_{n \neq 0} \frac{1}{2n^2} (T_0 T_{-n} T_n + T_{-n} T_n T_0) \\ &+ \dots, \end{aligned} \quad (6.29)$$

where the indices take values $-N_{\text{max}}, \dots, N_{\text{max}}$ if not stated otherwise.

We would like to stress that the coefficients $C(\mathbf{m})$ are independent of any other property of the original Hamiltonian (6.1) and so they can be determined once and for all. This contrasts with alternative approaches with CUTs as presented in Ref. [157] or also in a perturbative framework as in Ref. [150], where the effective Hamiltonian has to be derived explicitly for each specific system in question.

Let us additionally note that we have

$$\begin{aligned} [H_0, H_{\text{pCUT}}^{\text{eff}}] &\stackrel{6.28}{=} [H_0, H_0] + \sum_{k=1}^{\infty} \sum_{\substack{|\mathbf{m}|=k \\ M(\mathbf{m})=0}} C(\mathbf{m}) [H_0, T(\mathbf{m})] \\ &\stackrel{6.11}{=} 0 + \sum_{k=1}^{\infty} \sum_{\substack{|\mathbf{m}|=k \\ M(\mathbf{m})=0}} C(\mathbf{m}) M(\mathbf{m}) T(\mathbf{m}) = 0, \end{aligned} \quad (6.30)$$

so we can still use the quantum numbers of the eigenstates of H_0 to characterize eigenstates of $H_{\text{pCUT}}^{\text{eff}}$, as these are conserved. In the following sections, we discuss two important properties of the effective Hamiltonian (6.28), namely that it is cluster additive and fulfills a linked-cluster theorem. These features allow to relate results obtained on finite clusters with those valid in the thermodynamic limit under certain conditions.

6.1.1.3 Cluster additivity

Cluster additivity is a necessary property of the effective Hamiltonian H^{eff} to obtain results valid for the thermodynamic limit, although H^{eff} is only evaluated on finite-size systems. Formally, an operator M^C defined on a finite- or infinite-size system C is said to be cluster additive, if for any disjoint bipartition A, B such that $C = A \dot{\cup} B$ can be expressed as

$$M^C = M^A \otimes \mathbb{1}^B + \mathbb{1}^A \otimes M^B, \quad (6.31)$$

where M^A and M^B only have support in the subsystems A and B , respectively. Typically, we consider the case of M being an operator of the type $P_m H^{\text{eff}} P_m$, where P_m projects on the m -particle subspace, i.e. $P_m |n\rangle = \delta_{m,n} |n\rangle$ for eigenstates of the particle-counting operator Q (6.2). The meaning of disjoint partition depends on the model considered. However, it is clear that this property is e.g. fulfilled if no operator with support in A acts on the same degrees of freedom as any operator with support in B .

Let us mention that for practical purposes, the definition is often turned around: two subclusters A and B are said to form a disjoint bipartition of C , if (6.31) holds. If the size of these subsystems is bounded, the contributions to a cluster additive operator M for an infinite-size system can be decomposed into the sum of the contributions from finite-size subclusters. The latter can be efficiently evaluated and the value valid for the thermodynamic limit can be obtained by summing up the finite-size contributions. We refer to finite-size systems as clusters or graphs in the following.

Let us note that it is in general not true that the effective Hamiltonian H^{eff} is cluster additive even if the original Hamiltonian H has this property. However, for $H_{\text{pCUT}}^{\text{eff}}$, we can prove that this holds: for this purpose, we show that the cluster additivity is maintained during the flow. We suppose $H(\ell)$ to be cluster additive for a given $\ell \geq 0$, i.e. for a suitable partition $C = A \dot{\cup} B$ one has

$$H(\ell)^C = H(\ell)^A \otimes \mathbb{1}^B + \mathbb{1}^A \otimes H(\ell)^B. \quad (6.32)$$

As the particle counting operator Q (6.2) is cluster additive, we have also cluster additivity for the generator $\eta^Q(\ell)$ (6.9) for this ℓ :

$$\eta^Q(\ell)^C = \eta^Q(\ell)^A \otimes \mathbb{1}^B + \mathbb{1}^A \otimes \eta^Q(\ell)^B. \quad (6.33)$$

Considering the flow equation (6.5), we get

$$\partial_\ell H(\ell)^C = [\eta(\ell)^C, H(\ell)^C] = [\eta(\ell)^A, H(\ell)^A] \otimes \mathbb{1}^B + \mathbb{1}^A \otimes [\eta(\ell)^B, H(\ell)^B]. \quad (6.34)$$

We see that a cluster-additive Hamiltonian is changed by cluster-additive terms during the flow and thus starting with a cluster-additive Hamiltonian at $\ell = 0$ yields a cluster-additive effective Hamiltonian.

The best known consequence of cluster additivity is that the ground-state energy \mathcal{E}_0 , which is the non-zero eigenvalue of the operator $P_0 H P_0$, is an extensive quantity. There are also examples for excited states. For instance, for a general linked-cluster expansion Gelfand showed [149] that the one-particle reduced Hamiltonian

$$H_1 = P_1 \left(H^{\text{eff}} - \mathcal{E}_0 \mathbb{1} \right) P_1 \quad (6.35)$$

is cluster additive provided H is cluster additive and that $P_0 H P_1 = 0$. We have seen above that the cluster additivity of $P_1 \left(H_{\text{pCUT}}^{\text{eff}} - \mathcal{E}_0 \mathbb{1} \right) P_1$ holds even without the latter constraint. This is a very convenient fact, as e.g. the string-net Hamiltonian (3.9) does not meet this constraint in the non-topological phase, but nevertheless, we obtain an expansion for the dispersion of the elementary excitations in this case. Let us note that for this case, alternative linked-cluster approaches need to use cluster-dependent decoupling schemes [150, 151], which increase the necessary computational resources.

Finally, let us point out that the cluster additivity is one of the ingredients of the linked-cluster expansion [151, 170], presented in Chapter 8.

As we shall see in the next section, the upper bound for the needed cluster sizes is provided by another feature of the effective Hamiltonian $H_{\text{pCUT}}^{\text{eff}}$: it fulfills the so-called linked-cluster theorem.

6.1.1.4 Linked-Cluster Theorem

The next ingredient towards an efficient graph expansion is an upper bound on the range of the terms in the effective Hamiltonian. It will on the one hand provide a criterion, which cluster size is large enough to obtain the same result as for the thermodynamic limit and on the other hand allows us to treat also Hamiltonians, which do not possess the

cluster additivity property described in the last section. Therefore, we want to re-express the effective Hamiltonian (6.28) as a sum of nested commutators of the operators T_n . To explain the significance of this rewriting, let us recall that the operators T_m are sums of local terms. As terms which do not act on the same degrees of freedom commute, the commutator structure of the effective Hamiltonian will then tell us that terms, which act on disjoint supports, do have a zero contribution and thus their evaluation can therefore be omitted from the very beginning. Let us emphasize that this result holds for any effective Hamiltonian derived with pCUT, so the linked-cluster theorem is an intrinsic property of this method.

To prove of this result, we argue along the lines of [171], but for a general form of the perturbation V : we consider the flow equation (6.21) and introduce the abbreviations

$$T_m^{(k)}(\ell) = \sum_{\substack{M(\mathbf{m})=m \\ |\mathbf{m}|=k}} F(\ell, \mathbf{m})T(\mathbf{m}), \quad (6.36)$$

$$\tilde{T}_m(\ell) = \sum_k T_m^{(k)}. \quad (6.37)$$

The expressions for the perturbation and the generator read then

$$V(\ell) = \sum_m \tilde{T}_m, \quad (6.38)$$

$$\eta^Q(\ell) = \sum_m \text{sgn}(m) \tilde{T}_m(\ell), \quad (6.39)$$

which leads us finally to the flow equation (6.22) for the $\tilde{T}_m(\ell)$, which reads:

$$\frac{\partial}{\partial \ell} \tilde{T}_m(\ell) = \sum_{\substack{n, n' \\ n+n'=m}} \left[\text{sgn}(n) \tilde{T}_n(\ell), \tilde{T}_{n'}(\ell) \right] - |m| \tilde{T}_m(\ell). \quad (6.40)$$

We see that the flow of the \tilde{T}_m operators and thus the $T(\mathbf{m})$ is governed by commutator terms on the right-hand side of (6.40). Replacing \tilde{T}_m from (6.37) in (6.40) yields

$$\frac{\partial}{\partial \ell} \tilde{T}_m^{(k)}(\ell) = \sum_{\substack{n, n' \\ n+n'=m}} \sum_{q=1}^{k-1} \left[\text{sgn}(n) \tilde{T}_n^{(k-q)}(\ell), \tilde{T}_{n'}^{(q)}(\ell) \right] - |m| \tilde{T}_m^{(k)}(\ell). \quad (6.41)$$

Now, we could solve the flow equations again recursively by sorting the different terms according to their order k . However, it is sufficient for our purpose to state that the replacement of lower order terms just results in a nesting of the different commutators and thus will lead to the structure pointed already out in the beginning of this paragraph.

Here, we give the effective Hamiltonian $H_{\text{pCUT}}^{\text{eff}}$ (6.29) in terms of the commutator expansion (6.28) for the leading orders

$$\begin{aligned}
H_{\text{pCUT}}^{\text{eff}} = & H_0 + T_0 \\
& + \sum_{n>0} \frac{1}{n} [T_n, T_{-n}] \\
& + \sum_{n>0} \frac{1}{2n^2} ([T_n, T_0], T_{-n}) + [T_n, [T_0, T_{-n}]] \\
& + \sum_{\substack{n>0 \\ m \neq -n, 0}} \frac{1}{n+m} \frac{1}{n} ([T_{-n-m}, T_m], T_n) + [T_{-n}, [T_{-m}, T_{n+m}]] \\
& + \dots
\end{aligned} \tag{6.42}$$

Let us emphasize again that due to the above commutator structure of $H_{\text{pCUT}}^{\text{eff}}$, the size of clusters to be taken into account in a perturbative calculation based on pCUT depends basically only on the extension of the perturbation V and not on the unperturbed Hamiltonian H_0 . This means that our series expansions for the topologically ordered phase needs the same cluster sizes as *any* treatment of a topologically trivial phase with a local perturbation as long as the excitation can be localized on the plaquettes of the lattice. As we shall see, these effects of the non-trivial statistics will only change the so-called weights of each cluster in a linked-cluster expansion, but not its general form.

6.1.2 Degenerate perturbation theory

An alternative way to derive an effective Hamiltonian H^{eff} for $H = H_0 + V$ is the degenerate perturbation theory (dpt) described in Ref. [106], which was originally detailed by Kato [148]. Its advantage compared to the pCUT method presented in the previous chapter is on the one hand that it is less restrictive on the form of H_0 and V and thus can be applied to more general Hamiltonians than the pCUT method. On the other hand it has a rather compact structure, which results in faster evaluation of the effective Hamiltonian. However, this method has also some drawbacks, as e.g. the fact that $H_{\text{dpt}}^{\text{eff}}$ does not obey a linked-cluster theorem, resulting in a restricted applicability.

Let us briefly introduce the method by considering a Hamiltonian of the form (6.1) and let us introduce additionally the Hermitian projectors P and \tilde{P} , where P projects onto the (possibly degenerate) eigenspace of H_0 with eigenvalue E_0 and \tilde{P} onto the eigenspace of H with eigenvalue E . We then define the operator

$$\Gamma = \tilde{P} P \left(P \tilde{P} P \right)^{-\frac{1}{2}}. \tag{6.43}$$

We have

$$\Gamma^\dagger \Gamma = \left(P \tilde{P} P \right)^{-\frac{1}{2}} P \tilde{P} \tilde{P} P \left(P \tilde{P} P \right)^{-\frac{1}{2}} = \left(P \tilde{P} P \right)^{-\frac{1}{2}} P \tilde{P} P \left(P \tilde{P} P \right)^{-\frac{1}{2}} = P, \quad (6.44)$$

so the transformation $|\psi\rangle \mapsto \Gamma |\psi\rangle$ is unitary within the subspace, for which we aim at deriving an effective model. The effective Hamiltonian then reads

$$H_{\text{dpt}}^{\text{eff}} = \Gamma^\dagger H \Gamma. \quad (6.45)$$

Now one has to rewrite the projector \tilde{P} in terms of H_0 and V to be able to explicitly write down $H_{\text{dpt}}^{\text{eff}}$. The key idea is to express it via the resolvent of H :

$$\tilde{P} = \frac{1}{2\pi i} \oint_C dz \frac{1}{z - H}, \quad (6.46)$$

where the contour C has to be chosen in the complex plane such that it encircles no other eigenvalue of H_0 than E_0 and also contains the unknown eigenvalues E . Note that the existence of such a contour relies on the existence of a finite energy gap between E_0 and all other eigenvalues of H_0 as well as the assumption that the perturbation is small enough such that all E are still in the vicinity of E_0 . We express the resolvent in (6.46) in terms of a power series in V :

$$\frac{1}{z - H} = \frac{1}{z - (H_0 + V)} = \frac{1}{z - H_0} \frac{1}{\left(1 - \frac{V}{z - H_0}\right)} = \frac{1}{z - H_0} \sum_{n=0}^{\infty} \left(V \frac{1}{z - H_0} \right)^n. \quad (6.47)$$

With (6.47) and using additionally the operator identity

$$\frac{1}{z - H_0} = \frac{P}{z - E_0} + \frac{1 - P}{z - H_0}, \quad (6.48)$$

we get after carrying out the integral in (6.46)

$$\tilde{P} = P - \sum_{n=1}^{\infty} \sum_{\substack{k_1 + \dots + k_{n+1} = n \\ k_i \geq 0}} S^{k_1} V \dots V S^{k_{n+1}}, \quad (6.49)$$

where we introduced the abbreviations

$$S^0 = -P, \quad (6.50)$$

$$S^k = \left(\frac{1 - P}{E_0 - H_0} \right)^k. \quad (6.51)$$

Now we expand the second factor of Γ in (6.43):

$$\left(P \tilde{P} P \right)^{-\frac{1}{2}} = \left(P - P + P \tilde{P} P \right)^{-\frac{1}{2}} \quad (6.52)$$

$$= \left(P - P \left(P - \tilde{P} \right) P \right)^{-\frac{1}{2}} \quad (6.53)$$

$$= P + \sum_{n=1}^{\infty} \frac{(2n-1)!!}{(2n)!!} \left(P - P \left(P - \tilde{P} \right) P \right)^n, \quad (6.54)$$

where we used $(n)!! = \begin{cases} 1 \cdot 3 \cdot \dots \cdot n & n \text{ odd} \\ 2 \cdot 4 \cdot \dots \cdot n & n \text{ even} \end{cases}$. Using the two series expansions (6.49) and (6.54) in the expression for Γ (6.43), we finally evaluate the effective Hamiltonian $H_{\text{dpt}}^{\text{eff}}$ (6.45)

$$H_{\text{dpt}}^{\text{eff}} = E_0 P + \sum_{n \geq 1} \sum_{k_1 + \dots + k_{n-1} = n-1} c_{(k_1, \dots, k_{n-1})} P V S^{k_1} \dots S^{k_{n-1}} V P, \quad (6.55)$$

where the $c_{(k_1, \dots, k_{n-1})}$ are the coefficients stemming from the summation of the fractions in (6.54). Consequently, these coefficients are rational numbers, like the $C(\mathbf{m})$ in (6.28).

The leading orders of the effective Hamiltonian $H_{\text{dpt}}^{\text{eff}}$ are given by:

$$\begin{aligned} H_{\text{dpt}}^{\text{eff}} = & E_0 P \\ & + P V P \\ & + P V S V P \\ & + P V S V S V P - \frac{1}{2} P V P V S^2 V P - \frac{1}{2} P V S^2 V P V P \\ & + \dots \end{aligned} \quad (6.56)$$

Let us note that if we are in a situation, where a pCUT expansion is possible, and replace $V = \sum_n T_n$ in (6.56), we obtain the same expression as (6.29) up to order three. The coefficients start to differ from order four on. This indicates that the two effective models obtained by pCUT and degenerate perturbation theory will differ in general although they are unitarily equivalent. We will discuss this fact in more detail later. Already by comparing the number of terms appearing in (6.29) and (6.56), we see that the total number of terms is always smaller for degenerate perturbation theory compared to pCUT. This already gives a hint that it is faster to evaluate (6.55) than (6.28).

However, the number of intermediate states appearing in the evaluation of each term in (6.55) is in general larger, so that more memory is needed in the computer-based evaluation process. In this sense, degenerate perturbation theory represents a method, which provides a sizable speed-up of the evaluation of the effective Hamiltonian provided that the necessary computational resources are given. However, this speed-up can still be increased for the case of a non-degenerate eigenvalue E_0 , which can be inferred by using partitioning techniques as presented in the next section.

Let us finally remark that due to the appearance of the non-local denominator $E_0 - H_0$ in the operator S , the effective Hamiltonian $H_{\text{dpt}}^{\text{eff}}$ (6.55) typically violates cluster additivity.

6.1.3 Partition technique

In the following, we discuss with the partition technique (pt) a third way to obtain an effective Hamiltonian $H_{\text{pt}}^{\text{eff}}$. Its final expression is very similar to the degenerate perturbation theory in the previous section and it allows us to determine the effective matrix element for a non-degenerate energy level of the unperturbed Hamiltonian. The method, described in large detail in [107], relies on partitioning the Hilbert space into two orthogonal parts. First, we introduce the general idea and afterwards, we will focus on the case of a non-degenerate eigenstate of H_0 , giving us a method to evaluate series expansions for the perturbed eigenvalue E in a faster manner.

We divide the Hilbert space \mathcal{H} into two parts \mathcal{H}_1 and \mathcal{H}_2 and define orthogonal projectors \mathcal{O}_1 and \mathcal{O}_2 , where \mathcal{O}_i projects onto \mathcal{H}_i for $i \in \{1, 2\}$:

$$\mathbb{1} = \mathcal{O}_1 + \mathcal{O}_2, \quad (6.57)$$

$$\mathcal{O}_i^2 = \mathcal{O}_i, \quad \mathcal{O}_i^\dagger = \mathcal{O}_i, \quad i \in \{1, 2\}, \quad (6.58)$$

$$\mathcal{O}_1\mathcal{O}_2 = \mathcal{O}_2\mathcal{O}_1 = 0. \quad (6.59)$$

To shorten notations, let us further define the partial resolvent

$$T = \frac{\mathcal{O}_2}{E - H}, \quad (6.60)$$

which is well-defined if E is not in the spectrum of $H|_{\mathcal{H}_2}$. We assume E to be an (possibly degenerate) eigenvalue of the unperturbed Hamiltonian. In our application to perturbation theory, the well-definedness of T is usually guaranteed by the existence of an energy gap for a sufficiently small perturbation.

One has the following useful relation

$$\mathcal{O}_2(E - H)T = \mathcal{O}_2. \quad (6.61)$$

With these notations, we define the operator

$$\Omega = \mathcal{O}_1 + TH\mathcal{O}_1. \quad (6.62)$$

This operator annihilates obviously all states in \mathcal{H}_2 . Additionally, we have

$$\begin{aligned} \mathcal{O}_2 (H - E) \Omega &\stackrel{6.62}{=} \mathcal{O}_2 (H - E) \mathcal{O}_1 + \mathcal{O}_2 (H - E) T H \mathcal{O}_1 \\ &\stackrel{6.61}{=} \mathcal{O}_2 H \mathcal{O}_1 - \mathcal{O}_2 H \mathcal{O}_1 = 0, \end{aligned} \quad (6.63)$$

which states that we also have $\mathcal{O}_2 H \Omega = E \mathcal{O}_2 \Omega$. So the operator Ω projects by construction onto an eigenstate, if restricted to \mathcal{H}_2 . Next, we show that Ω is an eigenoperator of H , i.e. $H\Omega = E\Omega$, iff the eigenvalue E fulfills an additional condition. One has

$$H\Omega = E\Omega \quad (6.64)$$

$$\begin{aligned} \Leftrightarrow 0 &= (H - E) \Omega = (\mathcal{O}_1 + \mathcal{O}_2) (H - E) \Omega \stackrel{6.63}{=} \mathcal{O}_1 (H - E) \Omega \\ &= \mathcal{O}_1 (H + HTH - E) \mathcal{O}_1 \\ \Leftrightarrow \mathcal{O}_1 E \mathcal{O}_1 &= \mathcal{O}_1 (H + HTH) \mathcal{O}_1. \end{aligned} \quad (6.65)$$

By evaluating the expectation value of (6.65) for a eigenstate $|\psi\rangle$ of H with eigenvalue E , we obtain

$$E = \langle \varphi | H + HTH | \varphi \rangle = \langle \varphi | H + H \frac{\mathcal{O}_2}{E - H} H | \varphi \rangle, \quad (6.66)$$

where $|\varphi\rangle \propto \mathcal{O}_1 |\psi\rangle$ is the normalized component of the eigenstate in \mathcal{H}_1 .

As we can see in (6.66), the problem of determining an eigenvalue of H has now been formally reduced to calculating an expectation value within one part of the Hilbert space. The important fact is that we did not require \mathcal{H}_1 to be an eigenspace, but just that the corresponding eigenfunction has a non-zero component in it. This is naturally fulfilled, if one chooses \mathcal{H}_1 to be an eigenspace of an unperturbed Hamiltonian H_0 and $H = H_0 + V$ as in (6.1) with a small perturbation V .

In the following, we consider only this case and we furthermore assume \mathcal{H}_1 to be spanned by the non-degenerate eigenstate $|\varphi_0\rangle$ of H_0 with unperturbed eigenenergy E_0 . Therefore, one has $\mathcal{O}_1 = P$, $\mathcal{O}_2 = \mathbb{1} - P = \bar{P}$ with the notations from the previous section. Condition (6.65) then simplifies to

$$E = \langle \varphi_0 | H_0 | \varphi_0 \rangle + \langle \varphi_0 | V + V T V | \varphi_0 \rangle = E + \langle t \rangle_0, \quad (6.67)$$

where we defined the so-called reaction operator t , whose expectation value

$$\langle t \rangle_0 = \langle \varphi_0 | t | \varphi_0 \rangle = \langle \varphi_0 | P t P | \varphi_0 \rangle \quad (6.68)$$

gives the energy shift with respect to the unperturbed energy E_0 .

To rewrite the partial resolvent (6.60), we use the operator identity $\frac{1}{A-B} = \frac{1}{A} + \frac{1}{A}B\frac{1}{A-B}$ with $A = \bar{P}(E_0 - H_0)\bar{P}$ and $B = \bar{P}(V - \langle t \rangle_0)\bar{P}$ in (6.60) and obtain

$$\begin{aligned}
 T &= \frac{\bar{P}}{E_0 - H_0 - (V - \langle t \rangle_0)} \\
 &= \frac{\bar{P}}{E_0 - H_0} + \frac{\bar{P}}{E_0 - H_0} (V - \langle t \rangle_0) \frac{\bar{P}}{E_0 - H_0 - (V - \langle t \rangle_0)} \\
 &= S + S(V - \langle t \rangle_0)T \\
 \Leftrightarrow T &= \frac{1}{1 - S(V - \langle t \rangle_0)}S,
 \end{aligned} \tag{6.69}$$

where we employed $S = S^1$ from (6.51). Expanding the right-hand side of (6.69), we get

$$T = \sum_{k=0}^{\infty} (S(V - \langle t \rangle_0))^k S, \tag{6.70}$$

where the requirement for the convergence of the series in (6.70) is fulfilled for a small and regular perturbation. Inserting (6.70) in the equation for the reaction operator (6.67), we obtain

$$t = V + V \sum_{k=0}^{\infty} (S(V - \langle t \rangle_0))^k SV. \tag{6.71}$$

We observe that (6.71) still contains $\langle t \rangle_0$, but as a power series. So if we now express

$$t = \sum_{i=1}^{\infty} t_i, \tag{6.72}$$

with t_i being of order i in the perturbation parameter, we can recursively determine t_n by expanding $\langle t \rangle_0$ on the right-hand side of (6.71) up to order $n - 2$. We thus get

$$\begin{aligned}
 t &= V \\
 &+ VSV \\
 &+ VSVSV - \langle t_1 \rangle_0 VS^2V \\
 &+ VSVSVSV - \langle t_1 \rangle_0 VSVS^2V - \langle t_1 \rangle_0 VS^2VSV - \langle t_2 \rangle_0 VS^2V \\
 &+ \dots
 \end{aligned} \tag{6.73}$$

and finally by using $E_n P = P \langle t_n \rangle_0 = P t_n P$:

$$\begin{aligned}
 H_{\text{pt}}^{\text{eff}} &= EP = E_0 P + P t P = \\
 &E_0 P + P V P
 \end{aligned}$$

$$\begin{aligned}
& + PVSVP \\
& + PVS SV P - E_1 PVS^2 VP \\
& + PVS SV SV P - E_1 PVS SV S^2 VP - E_1 PVS^2 V SV P - E_2 PVS^2 VP \\
& + \dots
\end{aligned} \tag{6.74}$$

If one compares the expressions (6.74) and (6.55), one sees that they are closely related. One can indeed interpret (6.74) as a simplified version of (6.55), where one replaced all terms $P \dots P$ by P and gathered the coefficients to express them in terms of the E_n . This tells us that (6.74) is faster to evaluate than (6.55). However, as the term $PVS SV \dots V SV P$, which contains usually the largest number of intermediate states, appears in both expansions, the maximal computation requirement in terms of memory is exactly the same for both methods.

6.1.4 Efficient perturbation theory

In previous sections, we presented different effective Hamiltonians. Here, we shall now discuss the advantages and drawbacks of the different methods with respect to each other as well as the situations, in which one can easily transform results obtained for one effective Hamiltonian to another one.

In the evaluation of the matrix elements of the different effective Hamiltonians, there are, generically speaking, two limiting factors: computation time and memory resources.

The latter is basically given by the number of intermediate states to store at a given moment during the calculation. Most impact on the computation time has the number of terms in the effective Hamiltonian as well as the number of intermediate states to be acted on by an operator.

To estimate the number of intermediate states involved, one has to compare the operators T_m for the pCUT and V for the other methods. Since $V = \sum_{n=-N_{\max}}^{N_{\max}} T_n$, it is obvious that the degenerate perturbation theory and the partition technique generate much more intermediate states appearing at each step than the pCUT.

Another way to see this, is to realize that all intermediate states appearing in the same step in the pCUT have a well-defined particle number, whereas the action of the operator V in (6.55) or (6.74) generates superpositions of states with different particle numbers. Thus, one can already conclude that dpt and pt are more memory demanding than the pCUT.

In the latter, all intermediate states are also treated within the calculation. However, this is not achieved by the evaluation of one single term², but by several ones.

This is also reflected in the number of terms in the effective Hamiltonian: As can be seen in Table 6.1, the number of terms of $H_{\text{pCUT}}^{\text{eff}}$ is much larger. In conclusion, although each term of $H_{\text{pCUT}}^{\text{eff}}$ can be evaluated faster than a term of $H_{\text{dpt}}^{\text{eff}}$ or $H_{\text{pt}}^{\text{eff}}$ as it involves less intermediate states, combinatorial considerations tell us that the time to evaluate $H_{\text{pCUT}}^{\text{eff}}$ is longer. Additionally, the number of terms in $H_{\text{pCUT}}^{\text{eff}}$ depends exponentially on the parameter N_{max} , so that the runtime difference increases with increasing N_{max} .

| order | pCUT ($N_{\text{max}}=2$) | pCUT ($N_{\text{max}}=6$) | dpt | pt |
|-------|-----------------------------|-----------------------------|-----|----|
| 1 | 1 | 1 | 1 | 1 |
| 2 | 4 | 12 | 1 | 1 |
| 3 | 18 | 126 | 3 | 2 |
| 4 | 84 | 1.468 | 9 | 5 |
| 5 | 380 | 17.150 | 28 | 12 |
| 6 | 1.750 | 204.762 | 94 | 28 |
| 7 | 8.134 | 2.473.324 | 337 | 63 |

TABLE 6.1: Number of terms for the first seven orders for the different methods. The pCUT ($N_{\text{max}}=2$) has to be used for the series expansion in the topological phase, pCUT ($N_{\text{max}}=6$) for the non-topological phase. The number of terms suggests that the degenerate perturbation theory and even more the partition technique shall be employed if possible. However, one has still to keep in mind that the operator V corresponds to $\sum_{n=-N_{\text{max}}}^{N_{\text{max}}} T_n$ and thus will involve a larger number of intermediate states, whereas the pCUT will only involve intermediate states of one particle number n at a time. Thus the need of memory resources has also to be taken into account.

Thus, we can conclude that if sufficient memory is available, the matrix elements of $H_{\text{dpt}}^{\text{eff}}$ and $H_{\text{pt}}^{\text{eff}}$ are faster evaluated than the matrix elements of $H_{\text{pCUT}}^{\text{eff}}$. Thus, in this case, degenerate perturbation theory and the partitioning technique are the methods of choice, especially for large N .

Let us note additionally that in the case of a non-degenerate unperturbed eigenspace, $H_{\text{pt}}^{\text{eff}}$ contains less terms and can thus be evaluated faster than $H_{\text{dpt}}^{\text{eff}}$, provided that the energy contributions of the previous orders are known at the moment of evaluation.

However, it is only $H_{\text{pCUT}}^{\text{eff}}$, for which we are able to prove the linked-cluster expansion. This leads directly to the question, whether and how we can relate efficiently the different effective Hamiltonians.

As the different effective Hamiltonians are all unitarily equivalent to the original one within the eigenspace of H_0 , all effective Hamiltonians can be related by a unitary transformation (Note that the operator Ω in 6.1.3 is not unitary by itself, however

²A term corresponds here to one term of the sums in (6.28) or (6.55)

together with the normalization of the functions φ , it forms a unitary transformation). The unitary transformation, which transform one of the effective Hamiltonians into another is usually dependent on the system, on which these are evaluated.

In general, one has to know both effective Hamiltonians in order to determine the unitary transformation linking them. However, there are some useful exceptions. These allow to evaluate the best suited effective Hamiltonian (usually $H_{\text{dpt}}^{\text{eff}}$ or $H_{\text{pt}}^{\text{eff}}$) and obtain from it the elements of another one (usually $H_{\text{pCUT}}^{\text{eff}}$), which are then in turn used further, i.e. to derive quantities for the thermodynamic limit.

A simple example is the case, in which the unperturbed eigenspace of H_0 is non-degenerate. Then the unitary U connecting the different effective Hamiltonians acts as identity. Consequently, the obtained eigenvalues are the same and all properties proven for one effective Hamiltonian carry over directly to the other ones.

This seems to be rather academic, however it turns out that this is often the case. For example, the ground state of the non-topological phase presented in Chapter 3 is unique and thus the above considerations apply.

Another non-trivial example are the topologically ordered ground states presented in (3.43), which are $(N + 1)^2$ -fold degenerate, but as a consequence of the topological order, these states cannot be coupled by a local perturbation in the thermodynamic limit. Thus one is left with $(N + 1)^2$ decoupled states, for which the different approaches that yield the same energies.

One can also obtain similar results for the one-particle sector: if the cluster, on which the effective Hamiltonian is evaluated, has translational symmetry and there is only one excited state per site/plaquette, Fourier transformation decouples the different eigenmodes of the effective Hamiltonian completely and again one is left with a unique eigenvalue.

One important remark is that the effective Hamiltonians are all translation-invariant and thus commute with the Fourier transformation. As a consequence, not only the dispersion in \vec{k} -space, but also each real-space matrix element coincides. This case is e.g. realized for the excitations in a $N = 1$ string-net model.

For $N > 1$, translational invariance can be used in the same way, however, the Hamiltonian is reduced to an $N \times N$ matrix in \vec{k} -space. As the unitary transformation may in this case be explicitly \vec{k} -dependent, one has to determine all matrix elements of H^{eff} on the given cluster. Having determined e.g. the full $H_{\text{dpt}}^{\text{eff}}$, one still finds a suitable unitary transform such that all real space elements, which shall be zero for $H_{\text{pCUT}}^{\text{eff}}$ due to the linked-cluster theorem, vanish. The resulting Hamiltonian coincides with $H_{\text{pCUT}}^{\text{eff}}$ up to

a local, i.e. \vec{k} -independent, unitary transformation. Thus, the obtained dispersions from the block-diagonalized form coincide.

However, without additional symmetries like translational symmetry or topological order mentioned above, the unitary transformation cannot be determined without determining both effective Hamiltonians. This limits the use of $H_{\text{dpt}}^{\text{eff}}$ and $H_{\text{pt}}^{\text{eff}}$ for linked-cluster expansions for excited states, as the used graphs do not have translational invariance.

Let us finally make a link to another method to perform high-order series expansions [150]. This relies also on decoupling schemes for different sectors of the Hilbert space. The degenerate perturbation theory and the partition technique decouple one eigenspace of the unperturbed Hamiltonian from the rest of the Hilbert space and are thus the analogue of the "two-block decoupling scheme" (TBOT) presented in [150], whereas the pCUT decouples all unperturbed eigenspaces from each other and thus corresponds to the "multi-block decoupling scheme" (MBOT). We remark that the differences for properties like e.g. cluster additivity of the different decoupling schemes correspond directly to the differences of the methods presented in this thesis.

6.1.5 Perturbation theory in the thermodynamic limit

There is a large amount of literature about how to perform series expansions for the low-energy spectrum in such a way that the results are correct in thermodynamic limit, although the actual calculations are performed on finite-size systems, as e.g. presented in [151, 172, 173] just to name a few review works. Most of them are concerned with series expansions for the ground-state energy. As this is an extensive quantity, the effective Hamiltonian is cluster-additive and so it decomposes into a sum of terms, which have bounded support on the lattice for a given maximal order. This allows then for a linked-cluster expansion [129, 173], which consists in first determining the combinatorial weight of each finite-size cluster to the total result and secondly evaluate the contribution for each cluster. We discuss linked-cluster expansions in more detail in Chapter 8.

However let us note that cluster additive quantities can also be evaluated on large clusters with suitable boundary conditions. The linked-cluster theorem presented in Section 6.1.1.4 yields an upper bound on the size of the support of the contributing terms. So, for an expansion of order n one has to consider a cluster, in which all clusters consisting of the joint, connected support of up to n operators can be embedded. To obtain the correct results for the thermodynamic limit, one has in particular to take care that no "wrapping" of the operator support around the finite-size system is possible if periodic boundary conditions are applied.

This “one-cluster” approach yields typically not the highest performance, however, it allows to determine at least the leading orders of an expansion and can thus be used as a valuable check. Note that in cases, where translational invariance decouples completely the excited states, for each real space matrix element, one can choose a translation-invariant cluster, which is optimally shaped for this particular matrix element, as the linked-cluster theorem guarantees its correctness for larger clusters.

6.1.6 Extrapolations

Perturbative expansions approximate a given physical quantity $f(z)$ by a finite order series expansion

$$S_N(z) = \sum_{n=0}^N s_n z^n. \quad (6.75)$$

One expects for a regular f that $S_N(z) \stackrel{N \rightarrow \infty}{\equiv} f(z)$. However in practice, one has to deal with the fact that one can just determine the first N orders of the series expansion (6.75). For a sufficiently small parameter z , $S_N(z)$ and $f(z)$ agree reasonably well, whereas the behavior of S_N for large z is usually dictated only by the highest-order term $s_N z^N$.

This case is rather unfortunate, as e.g. physical quantities are usually bounded, but the functional form of (6.75) is not. Also in the study of second-order phase transitions, the quantities in the vicinity of a critical point are known to show algebraic behavior, which is not reflected in the functional form of (6.75). Nevertheless, to describe qualitatively and also quantitatively the physics, one therefore is often led to extrapolate the obtained series instead of using them directly. As in this work, we want to describe phase transitions, which are a non-perturbative effect, we are notoriously in this situation.

There are several possibilities to extrapolate a series expansion and none of them is optimal for every possible situation.

The approach, we use throughout this work, is based on the so-called Padé approximants [174]. A very detailed discussion of their properties and applications can e.g. be found in Refs. [175, 176].

A Padé approximant $P_{[L/M]}$ is given by

$$P_{[L/M]}(z) = \frac{P_L(z)}{Q_M(z)}, \quad (6.76)$$

with $P_L(z), Q_M(z)$ being polynomials of degree L and M respectively:

$$P_L(z) = \sum_{n=0}^L p_n z^n, \quad (6.77)$$

$$Q_M(z) = \sum_{n=0}^M q_n z^n. \quad (6.78)$$

We set $q_0 = 1$ to avoid ambiguities in the following. The Padé approximants $P_{[L/M]}[S_N]$ are determined via

$$S_N(z)Q_M(z) = P_L(z) + O(z^{L+M+1}), \quad (6.79)$$

which leads to a linear equation system for the $L + 1 + M$ unknown coefficients of P_L and Q_M . Thus, by setting $N \geq L + M$ we get a unique approximant $P_{[L/M]}[S_N]$ for a given S_N . These approximants have by construction the same Taylor series as S_N up to order N and thus agree well with the series in the region of small z . For larger values of z , the rational function $P_{[L/M]}$ typically does not vary as much as $S_N(z)$, so that it seems a reasonable approximation.

Generally speaking, Padé approximants should work well for rational functions, which in turn shall be able to approximate not too strongly varying functions f . For a detailed discussion of the convergence properties, we refer to [175].

One drawback of this method is that the approximants may have poles. The corresponding divergences may or may not be related to physical properties. If we use the Padé extrapolations to extend the range of reliable results, we will not consider approximants showing poles in the relevant parameter regime.

Another drawback of this method is that it does not allow to estimate an error of the extrapolations in a reliable fashion. So one is led to consider several approximants, usually choosing those, which correspond to larger $L + M$, as these incorporate more information.

Nevertheless Padé approximants can also be used to obtain more information from the series expansions S_N . In the vicinity of a quantum critical point at a parameter value z_c , scale invariance tells us that quantities like e.g. the gap behaves algebraically, i.e. for $z \simeq z_c$ there are $A(z)$ and α such that

$$f(z) = A(z) \left(1 - \frac{z}{z_c}\right)^\alpha. \quad (6.80)$$

The rational Padé approximants by themselves are not very good candidates to approximate this behavior. However, taking the logarithmic derivative of (6.80) yields

$$\frac{d}{dz} (\log(f(z))) = \frac{\alpha}{z - z_c} (1 + O(z - z_c)), \quad (6.81)$$

where the corrections stem from the variations of $A(z)$ as well as from corrections to (6.80) away from criticality. The rational form (6.81) is then approximated by a Padé approximant. If one proceeds like this for the series expansion $S_N(z)$, one obtains its logarithmic derivative

$$\tilde{S}_N(z) = \frac{\sum_{n=1}^N n s_{n-1} z^{n-1}}{\sum_{n=0}^N s_n z^n}. \quad (6.82)$$

The corresponding equation for the coefficients p_n, q_n

$$S'_N(z)Q_M(z) = S_N(z)P_L(z) + O(z^{L+M+1}) \quad (6.83)$$

yields a unique solution, if we choose $L + M \leq N - 1$. The approximant of the original physical quantity f is then the so-called dlog-Padé approximant $DP_{[L/M]}$, whose functional form is

$$DP_{[L/M]}(z) [S_N(z)] = S_N(0) \exp \left(\int_0^z dz' P_{[L/M]} [\tilde{S}_N(z')] \right). \quad (6.84)$$

If z_c is a zero of Q_M (and not of P_L), then the exponential function tends to 0 when z approaches z_c and the corresponding critical parameter z_c is given by the zero of the denominator Q_L . The corresponding exponent is obtained as the residuum

$$\alpha = \frac{P_L(z)}{\frac{d}{dz} Q_M(z)} \Big|_{z=z_c}. \quad (6.85)$$

Let us note that it is possible that the physical z_c is not the zero of Q_M , which is closest to $z = 0$. These intermediate zeros of Q_M , which are called “spurious poles” of the approximant, are also (exact or approximate) zeros of the nominator $P_L(z)$ and thus do not impact (severely) the ratio $\frac{P_L}{Q_M}$. The corresponding dlog-Padé $DP_{[L/M]}$ is then called “defective” as it yields the same information as $DP_{[L-1/M-1]}$ and thus cannot be used to obtain new statements about convergence. Results obtained by defective approximants are, in general, marked by an asterisk *.

A convenient feature of the dlog-Padé approximants is that they allow to use already known information to refine the analysis. If e.g. the critical value z_c is already known,

the exponent obtained by the biased approximant is given by

$$\left((z_c - z) P_{[L/M]} \left[\tilde{S}_N(z) \right] \right) \Big|_{z=z_c} = \alpha. \quad (6.86)$$

Let us finally mention that there are a plethora of generalizations of Padé approximants to e.g. two-point Padé approximants [176] for the case that series expansions for several limits are available, differential approximants [177] to smoothen even more the form of the approximant itself, or extensions for the treatment of multi-variate series [178, 179] just to name a few. There exist even more approximant schemes as the self-similar factor approximants [180–182], which have also been applied in the context of topological phase transitions [82]. However for the purpose of this work, we find that the univariate Padé and dlog-Padé approximants and their biased variants are the most stable extrapolations and therefore are used to extract the desired information from the series.

6.2 Exact diagonalization

An alternative way, we use to describe the low-energy spectrum, is (Lanczos-) exact diagonalization on small systems. This method has the advantage that it allows to determine the low-energy spectrum of a given Hamiltonian on a finite-size system without specific assumptions like e.g. the low-energy subspace corresponding to some unperturbed Hamiltonian H_0 as done within the series-expansion framework. In addition, one is not restricted to a certain phase, but can study the whole parameter range in a single setting. One drawback is that the results of the diagonalization are not directly valid in the thermodynamic limit and finite-size scaling is necessary to determine e.g. the order of a phase transition. Exact diagonalization has already been successfully employed in the study of topologically ordered phases and topological phase transitions, e.g. in Refs. [59, 67, 69, 70].

In order to avoid boundary effects due to edges, the systems studied here are chosen to be periodic. As the symmetry of the lattice plays some role (e.g. quasi one-dimensional systems shall show the behavior described in Refs. [67, 69, 70], which is not at all expected in a two-dimensional system), the unit cells are chosen for all sizes such that the corresponding unit vectors form an angle of $\frac{\pi}{3}$. So the shortest non-contractible cycles have all the same length in each direction. Of particular interest are non-contractible cycles of length six, as these have a similar energy as the extended low-energy excitations in the non-topological phase (3.51). The corresponding states are part of the low-energy Hilbert space, but not present in the thermodynamic limit. Thus systems harboring these states will not yield a correct description of the low-energy spectrum

of the thermodynamic limit. As can be seen in Figure 6.1, cycles of the length six are not present in the clusters with $N_p = 12, 13$, so that this particular finite-size effect is absent for these systems.

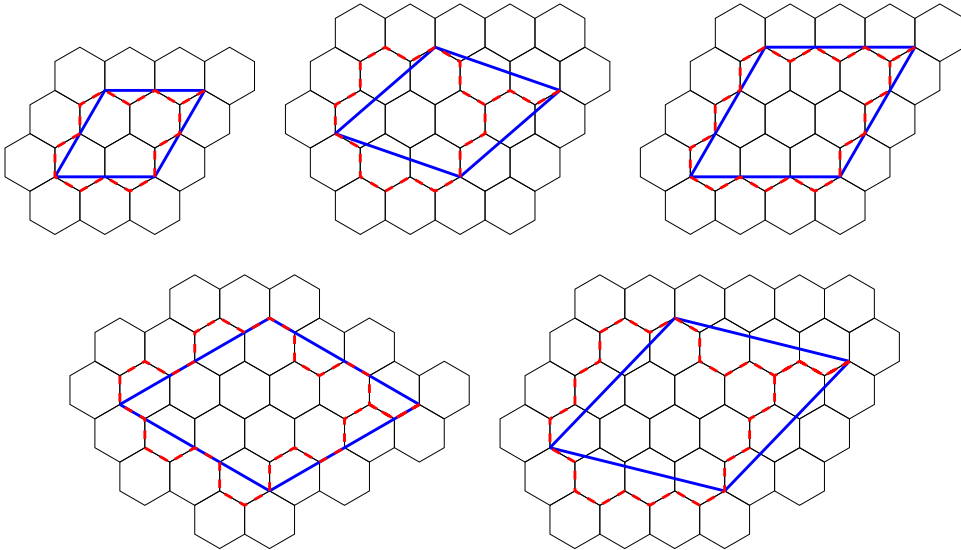


FIGURE 6.1: The different systems, on which the diagonalization is performed. The blue lines indicate unit cells, which have untwisted periodic boundary conditions. The dashed red lines show a deformed unit cell, which allows to count the number of plaquettes $N_p = 4, 7, 9, 12, 13$. The clusters are constructed such that the shortest non-contractible cycles (also indicated by the dashed red lines connecting two corners of the unit cell) are of the same length in each direction.

In order to obtain the low-energy spectrum, we follow a brute force approach:

- First the complete bond-basis for the finite system, i.e. all states not violating the vertex constraints (2.5), is generated. For large systems, this requires an appropriate algorithm.

The way of choice is here to introduce for each plaquette p a “flip operator” F_p , which, when acting on a state, will generate all states, the operator B_p (3.9) generates, storing each string-net configuration in the bond basis separately.

Note that the flip operators do not necessarily commute with each other as the B_p , so maybe one has to act several times with each F_p to generate all states. However, for some theories presented in Chapter 3, this is not sufficient. This is because states, which differ by an odd number of non-contractible loops of non-trivial ($D(\mathbb{Z}_2)$ -theory) or σ -($D(\text{Ising})$) labeled links, cannot be transformed into each other locally as a consequence of the branching rules. So one has to generate the basis for each sector separately. As the Hamiltonian does not couple these four resulting sectors, one can treat each of them separately.

Apart from this, no other symmetries are used to decouple different sectors of the Hilbert space. One can check, whether one has generated the whole basis by

comparing the number of the generated states with the total dimension of the Hilbert space ((3.74),(3.62), or (3.73)) for N_p plaquettes.

- Second, the Hamiltonian is written in this basis as a finite-dimensional matrix. This is trivial for the local term (3.48), as it is diagonal in the bond basis. The string-net Hamiltonian then is written down according to the bond basis. Both parts of the Hamiltonian are stocked separately and then summed up with the coupling constants given by the parameter θ (3.54).
- Third, the eigenvalues of the full Hamiltonian are obtained by using an appropriate Lanczos [183, 184] or power-method [185] routine. For the large systems, i.e. $N_p \geq 9$, the matrix is not fully diagonalized, but only the low-energy spectrum (typically the lowest 20-50 eigenvalues) is computed. Therefore one has to introduce eventually an appropriate spectral shift, so that the low-energy spectrum of the Hamiltonian corresponds to the eigenvalues, which have the largest norm.

The algorithms used to obtain the eigenvalues are chosen by the used MathematicaTM software [186] itself in function of the actual matrix and available computer resources. So, no further optimizations have to be made, which leads to a relatively comfortable use.

Let us mention that the brute-force approach used here is not optimal in the sense that it does not allow to treat the largest possible system for the given computer resources. Nevertheless, it allows to compute the low-energy spectrum for reasonable system sizes (see Table 6.2) on rather short time-scales (5-60 minutes per parameter value) with a rather minimal effort of programming. The prize to pay for the fast evaluation is that one has to stock the full Hamiltonian (in sparse format) in memory to avoid repeated slow read-in processes. Thus, it turns out that in this setting one is restricted to a Hilbert space of typically 30 millions states, if one uses up to 96GB memory.

| N_p | $\mathbf{D}(\mathbb{Z}_2)$ | $\mathbf{D}(\text{Fib})$ | $\mathbf{D}(\text{Ising})$ |
|-------|----------------------------|--------------------------|----------------------------|
| 4 | 8 (32) | 175 | 144 (528) |
| 7 | 64 (256) | 8.125 | 8.320 (32.896) |
| 9 | 256 (1.024) | 106.250 | 131.584 (524.800) |
| 12 | 2.048 (8.192) | 5.031.250 | 8.392.704 (33.558.528) |
| 13 | 4.096 (16.384) | 18.203.125 | 33.562.624 (134.225.920) |
| 16 | 32.768 (131.072) | 862.109.375 | - (8.590.000.128) |

TABLE 6.2: Largest block size of the Hamiltonian on a system with N_p plaquettes and periodic boundary conditions. In parentheses, we show the dimension of the total Hilbert space if it differs from the largest block size.

Note that more involved approaches using (lattice-)symmetries [183, 187] can also be implemented for two-dimensional string-net system. For these, the low-energy spectrum

has been calculated for system sizes up to $N_p = 16$ [59]. These systems harbor a comparable number of local anyonic degrees of freedom, however, the total number of states is about two orders of magnitude larger (cf. Table 6.2).

6.3 Chapter summary

In this chapter, we have presented the methods, which we employ within this thesis. We discussed three different ways to derive an effective Hamiltonian in a perturbative fashion, namely perturbative continuous unitary transformations, degenerate perturbation theory, and the perturbative version of the partition technique. The evaluation of these yield the series expansions presented in the Chapter 5.

We discussed the respective general framework and among other features the linked-cluster theorem, which is of particular interest in the context of the linked-cluster expansion presented in Chapter 8.

The technical details of the implementation are discussed in Chapter 7. In the present chapter, we detailed the extrapolation employed e.g. to obtain estimates for the critical exponents presented in Chapter 5. Additionally, we discussed the details of the exact diagonalizations on finite-size systems.

Implementation of the series expansion

*It isn't the mountain ahead that wears you out;
it's the grain of sand in your shoe.*

- Robert W. Service -

In this section, we discuss the technical details, which are necessary to implement the methods presented in the previous chapter in order to obtain the series expansion results of Chapter 5. Thus, we will discuss the details of the evaluation of the matrix elements of the effective Hamiltonians (6.28), (6.55), and (6.74).

Before we discuss the particularities of the different limits, let us begin with some general remarks that apply whenever one performs computer-based series expansions for the low-energy sector of the Hilbert space under consideration. Then we turn to the implementation details for the different phases. However, we do not discuss in large detail the possible optimizations for different finite-size systems to evaluate the matrix elements of H^{eff} except for the dispersion in the **1**-phase, as we consider the linked-cluster expansion employed for the other cases in Chapter 8.

7.1 General considerations

For the evaluation of H^{eff} it is mandatory to stock the operators T_n or V in some fashion. It is not useful to store the full Hamiltonian, as this requires a large amount of memory and the large amount of information to handle slows down the calculation considerably. Thus, one is often led to a local representation of the perturbation stocked in the memory, which takes much less memory than the full Hamiltonian. However, an efficient implementation of this setup requires that the states are represented in a way that one can easily read the local degrees of freedom necessary to determine the action of the local Hamiltonian. This is trivial for non-topological phases, however we discuss the consequences of this especially for the example of the topological phase.

Another point is to consider the implementation of the actual action of the perturbation operators: as already stated in Ref. [173], instead of determining for each action the actual operator elements $\langle f | H^{\text{eff}} | i \rangle$, it is more efficient to postpone the scalar product of $\langle f |$ and $(H^{\text{eff}} | i \rangle)$ to the end of the calculation and to store for the intermediate steps the result of the actions of H^{eff} on the initial state $|i\rangle$. This saves the calculation time for the intermediate scalar products, which represent an important slow-down factor, if one has to deal with many intermediate states. This reasoning holds even if one works with an orthogonal basis, in which for each basis vector the scalar product is trivial, but the amount of states results in a sizable effort. Thus one reduces the number of actually calculated scalar products to at most one per term of H^{eff} .

There are in principle two useful strategies: either one performs the scalar product in the end, i.e. one calculates

$$\langle f | \left(H^{\text{eff}} | i \rangle \right) \quad (7.1)$$

or one performs it in the middle, i.e. for a term $T_{m_1} T_{m_2} T_{m_3} \dots T_{m_{|m|}}$, one determines the overlap of the left and the right bracket

$$\left(\langle f | T_{m_1} T_{m_2} \dots T_{m_{|m|/2}} \right) \left(T_{m_{|m|/2+1}} \dots T_{m_{|m|}} | i \rangle \right). \quad (7.2)$$

separately. Version (7.1) has the advantage that the final scalar product has not to be calculated for each term separately, which reduces the effort considerably (see Table 6.1 for the number of terms), whereas the latter version (7.2) employs the fact that less actions of the perturbation generate considerably less intermediate states and thus one has not to deal with one superposition with contributions from many basis states, but two superpositions of similar but much smaller number of contributions. However, this way involves a splitting of each term as in (7.2), so that here the scalar product has to be carried out for each term separately. Another disadvantage of the latter way is that for each final state, the calculation has to be carried out explicitly, whereas without the splitting, one can in principle obtain all possible final states at once.

In conclusion, whenever there is a unique final state and an efficient way to carry out the scalar product, we take advantage to split the terms of the effective Hamiltonian as this reduces also the need of memory and allows to evaluate the actions of H^{eff} up to higher orders, as it acts on simpler states. This is typically the case in our development for the non-topological phases, especially for the ground states. Whenever several final states for a given initial state are needed and enough memory resources are available, or the calculation of the scalar product represents a sizable effort, we implement the final

overlap calculation. This will be the case for the graph expansions for the excited states as well as the treatment of the topological phase.

Before considering the specific cases, let us mention another possible simplification, we use to ease the effort of evaluating the effective Hamiltonian. The key observation is that we are interested in operator elements in the low-energy sector and that we can represent the excited states as the ground states almost everywhere except in some region, where the excitations are located. It is therefore extremely recommendable to reduce the effort of evaluating the perturbation on the local ground-state configuration.

One way to achieve this for possibly degenerate unperturbed ground states $|\text{gs}\rangle$ not coupled by the perturbation at order one, i.e. for all limits for which high-order series expansions are obtained within this thesis, is to consider instead of V or T_0 the modified operators

$$\tilde{V} = V - \langle \text{gs} | V | \text{gs} \rangle \mathbb{1}, \quad \tilde{T}_0 = T_0 - \langle \text{gs} | T_0 | \text{gs} \rangle \mathbb{1} \quad (7.3)$$

and treat the first-order contribution separately. By doing so, one sets $\tilde{T}_0|_{\text{gs}}$ as well as $P\tilde{V}P$ for the ground states to zero and thus one assures that the action on the (local) ground state always creates excitations. This removes a sizable number of terms from the sums in (6.28), (6.55), and (6.74). Additionally, the action of the operators in (7.3) on a local ground-state configuration has not to be evaluated, which speeds up the evaluation of the remaining terms.

The spectral shift in (7.3) has no impact on the hopping elements, as it drops out in the difference of excited- and ground-state contributions. For the ground states, the spectral shift is easily determined and constitutes the order one contribution to the series expansion of the ground-state energy. Thus, in the actual calculations, we will always consider the shifted version and thus we will drop the $\tilde{}$ for notational convenience. The spectral shift is determined explicitly in the following discussion for each phase.

7.2 Implementation for the topological phase

In the topological phase, we use the eigenstates of H_{LW} discussed in Chapter 3 to perform the series expansion. We presented two eigenbasis sets, namely the flux basis (3.21) and the dual basis (3.39). The latter is defined purely in terms of the fluxes and their fusion channels. As this represents the minimal information needed to characterize unambiguously a state, it is desirable to choose this basis to perform efficiently a perturbative expansion. One can easily determine the constant spectral shift discussed in (7.3), to

yield per link

$$\begin{aligned}
\langle g_{\text{S}_{\text{top}}} | H_{\text{loc},e} | g_{\text{S}_{\text{top}}} \rangle &= -J_e \left\langle \left| \begin{array}{c} \text{1} \\ \text{e} \\ \text{1} \end{array} \right| \sum_s \frac{d_s}{\mathcal{D}^2} L_e^s \left| \begin{array}{c} \text{1} \\ \text{e} \\ \text{1} \end{array} \right. \right\rangle \\
&= -J_e \sum_s \frac{d_s}{\mathcal{D}^2} \left\langle \left| \begin{array}{c} \text{1} \\ \text{e} \\ \text{1} \end{array} \right| \left| \begin{array}{c} s \\ \text{e} \\ s \end{array} \right. \right\rangle = -J_e \frac{d_1}{\mathcal{D}^2} = -J_e \frac{1}{\mathcal{D}^2}. \quad (7.4)
\end{aligned}$$

However, this basis is intrinsically non-local because it involves for the action on each bond e different R - and F -moves to bring the fusion tree in the form depicted in (7.4). Thus, this basis is not very useful for the series expansion, as the non-locality of the involved transformations prevents an efficient evaluation of local operators as the perturbation H_{loc} . This is necessary to perform a series expansion up to high orders, so we use instead the flux basis for the actual calculations, as it allows to express the eigenstates of H_{LW} in a (quasi-) local way.

The drawback of this choice is that we have to work with an overcomplete and in particular non-orthogonal basis, which requires additional considerations as detailed below. The dual basis is nevertheless a very useful representation as it allows a straightforward calculation of low-order matrix elements by hand, where one can easily figure out the F - and R -moves needed to apply the perturbation.

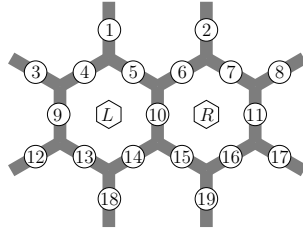


FIGURE 7.1: Labeling of the degrees of freedom necessary to determine the action of H_{loc} on the bond labeled by 10. As detailed in the text, the evaluation of P_{10}^1 involved the nineteen bond variables as well as the flux-variables located at the left (L) and right (R) plaquette. The labels of the outgoing links, which are enumerated here by 1, 2, 3, 8, 12, 17, 18, and 19, are not altered in the representation of the perturbation in the flux basis.

Let us remind that in the flux basis, we deal with the flux-labels $\{b_p\}$ as well as the bond-labels $\{\ell_e\}$. Therefore, we have to express also the local perturbation H_{loc} in terms of the involved quantum numbers, i.e. to determine

$$-J_e \sum_e P_e^1 |\{b_p\}, \{\ell_e\}\rangle. \quad (7.5)$$

With the labeling of Figure 7.1, we can see that for the bond $e = 10$, we have

$$P_{10}^1 = \mathbb{1}_L P_{10}^1 \mathbb{1}_R = \left(\sum_{\alpha', \beta'} P_L^{\alpha'} P_R^{\beta'} \right) P_{10}^1 \left(\sum_{\alpha, \beta} P_L^\alpha P_R^\beta \right), \quad (7.6)$$

where the indices $\alpha, \beta, \alpha', \beta'$ denote the different possible flux labels before and after the action of the perturbation. Thus, we can obtain the desired matrix elements of the perturbation by evaluating

$$\langle \alpha', \beta', \{\ell'_e\} | P_L^{\alpha'} P_R^{\beta'} P_{10}^1 P_L^\alpha P_R^\beta | \alpha, \beta, \{\ell_e\} \rangle \quad (7.7)$$

in the bond basis. The price to pay is that its evaluation and thus also the application within the calculation not only involves the two plaquette variables, but also 19 bond variables, so that we are dealing with 21 variables, which can take $(N+1)$ values each, in total. The need of handling the large resulting number of matrix elements in an efficient manner implies for example the use of hash-lists for the states (which for representations involving less degrees of freedom is usually a slowing-down feature).

Although the number of involved degrees of freedom is large, let us remark that the number of non-zero matrix elements is by far not as large as $(N+1)^{21}$: the labels of the outgoing links of the double plaquette, as depicted in Figure 7.1, are unchanged. Consequently, the Hamiltonian splits into $(N+1)^8$ sub-blocks. The dimension of each block is further reduced by the branching rules of the theory.

Let us note already here that the use of this representation with enlarged support of the perturbation operators does not impact properties as the cluster additivity, as it is solely mediated by the action of the projectors P_p^α that all commute with each other.

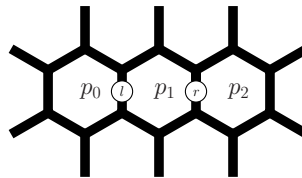


FIGURE 7.2: Labeling of the flux hopping from plaquette p_0 to the next-nearest neighbor plaquette p_2 via the action of H_{loc} on the bonds labeled by l and r . The examples are detailed in (7.8)-(7.11).

The choice of the flux basis therefore forces us to work with an overcomplete basis, which has important consequences. These can already be anticipated by considering for example the states involved in the evaluation of the next-nearest neighbor hopping term for the Fibonacci theory. This process appears at leading order due to the action of the

operator $T_{-2,l}T_{2,r}|\tau_{p_0}\rangle$. It reads with the labeling of Figure 7.2:

$$\left| \begin{array}{c} \tau \\ \mathbf{1} \\ \bullet \\ l \end{array} \right\rangle \xrightarrow{T_{2,r}} \left| \begin{array}{c} \tau \\ \mathbf{1} \\ \bullet \\ l \end{array} \right\rangle \xrightarrow{T_{-2,l}} \left| \begin{array}{c} \tau \\ \mathbf{1} \\ \bullet \\ l \end{array} \right\rangle, \quad (7.8)$$

$$\left| \begin{array}{c} \tau \\ \mathbf{1} \\ \bullet \\ l \end{array} \right\rangle \xrightarrow{T_{2,r}} \left| \begin{array}{c} \tau \\ \mathbf{1} \\ \bullet \\ l \end{array} \right\rangle \xrightarrow{T_{-2,l}} \left| \begin{array}{c} \tau \\ \mathbf{1} \\ \bullet \\ l \end{array} \right\rangle, \quad (7.9)$$

$$\left| \begin{array}{c} \tau \\ \mathbf{1} \\ \bullet \\ l \end{array} \right\rangle \xrightarrow{T_{2,r}} \left| \begin{array}{c} \tau \\ \mathbf{1} \\ \bullet \\ l \end{array} \right\rangle \xrightarrow{T_{-2,l}} \left| \begin{array}{c} \tau \\ \mathbf{1} \\ \bullet \\ l \end{array} \right\rangle, \quad (7.10)$$

$$\dots, \quad (7.11)$$

where the bonds are colored according to their label and the τ denoted plaquettes with a τ -flux. All of these processes represent (among the others summarized by “...” in (7.11)) the same physical processes: a hopping of a τ -flux to a next-nearest neighbor plaquette. As discussed in Chapter 3, one-flux states are unique. Consequently, the final states in (7.8) - (7.10) all coincide up to a weight, which has to be determined by explicitly calculating the respective overlaps.

Another point is that the description of the hopping process, which can be written in the dual basis in a simple fashion as

$$\left| \begin{array}{c} \tau \\ \mathbf{1} \\ \bullet \\ l \end{array} \right\rangle \xrightarrow{T_{2,r}} \left| \begin{array}{c} \tau \\ \mathbf{1} \\ \bullet \\ l \end{array} \right\rangle \xrightarrow{F\text{-move}} \left| \begin{array}{c} \tau \\ \mathbf{1} \\ \bullet \\ l \end{array} \right\rangle \xrightarrow{T_{-2,l}} \left| \begin{array}{c} \mathbf{1} \\ \tau \\ \bullet \\ r \end{array} \right\rangle, \quad (7.12)$$

involves in the flux-basis description basically all possible configurations of the bond variables (hidden in (7.11)). As the number of possible bond configurations (15) for the example (7.8) - (7.11) is larger than the number of flux configurations in the intermediate state, it is obvious that taking into account all states results in avoidable calculations.

Thus the task of performing computer-based series expansions in an efficient manner involves necessarily an implementation of the non-trivial overlap calculation as well as a reduction of the appearing redundancies. These are the implementation issues we detail in the next two sections.

7.2.1 Implementation of the scalar product

Let us recall the definition of a state in the flux basis (3.21).

$$|\{b_p\}, \{\ell_e\}\rangle = \mathcal{N} \prod_p \mathcal{P}_p^{b_p} \prod_e |\ell\rangle_e.$$

Therefore, we have to be able to evaluate the scalar product for two arbitrary states

$$\langle \{b'_p\}, \{\ell'_e\} | \{b_p\}, \{\ell_e\} \rangle = \mathcal{N} \mathcal{N}' \prod_e \langle \ell'_e | \prod_p \mathcal{P}_p^{b'_p} \prod_p \mathcal{P}_p^{b_p} \prod_e |\ell_e\rangle_e \quad (7.13)$$

$$= \mathcal{N} \mathcal{N}' \prod_p \delta_{b_p, b'_p} \prod_e \langle \ell'_e | \prod_p \mathcal{P}_p^{b_p} \prod_e |\ell_e\rangle_e, \quad (7.14)$$

where in the last step we used $\mathcal{P}_p^\alpha \mathcal{P}_p^\beta = \delta_{\alpha, \beta} \mathcal{P}_p^\beta$. So the calculation of the overlap reduces to determining the action of the projectors onto a state represented in the bond-basis $\prod_e \langle \ell'_e | \prod_p \mathcal{P}_p^{b_p} \prod_e |\ell_e\rangle_e$.

Although this looks similar to perform series expansions in the non-topologically ordered phase, there are several differences. The most important one is that one has to act on each plaquette of the given system. This represents a sizable effort for large and, in particular, for periodic systems. Additionally, one cannot introduce a spectral shift to ease the calculation as discussed above, because a determination of the action of the projectors onto arbitrary link-configurations depends in general on the plaquette p .

One conclusion to be drawn is that the overlap calculation represents a sizable effort, which may have an impact on the efficiency of the performed calculation. To avoid, as much as possible, the need of performing scalar products, it is useful to implement the calculation such that the action of H^{eff} on an initial state determined (for all terms) first and afterwards the scalar product with the resulting superposition of final states is performed.

This strategy makes the evaluation of the matrix elements of H^{eff} a feasible task. This is true especially for small and open systems like the graphs discussed in detail in the next chapter. Nevertheless it prevents the splitting of the Hamiltonian H^{eff} as a speed-up mechanism.

7.2.2 Removing the redundancy

As already discussed, the overcompleteness of the flux basis is due to the involved bond degrees of freedom necessary to keep track of the information, in which fusion channel the different fluxes in the system are. The tracking of these fusion channels is not unique, as a fusion channel of two fluxes can be basically encoded in every path through the lattice, which links the two flux degrees of freedom. To reduce the computational effort, it is thus desirable to reduce the redundant number of bond degrees of freedom.

As we perform our calculations by acting with local operators, we cannot remove the redundancies by specifying the overall, i.e. global, fusion configuration. Nevertheless, we

can locally remove the redundancy for a given flux configuration. As we represented in Section 7.2 the perturbation by contributions of the form $\mathcal{P}_L^{\alpha'} \mathcal{P}_R^{\beta'} V_e \mathcal{P}_L^\alpha \mathcal{P}_R^\beta$, we can reduce the number of final (and thus intermediate) states by choosing suitable re-expressions of the form

$$\mathcal{P}_L^{\alpha'} \mathcal{P}_R^{\beta'} | \{ \ell'_1 \dots \ell'_m \} \rangle = \sum_{\{ \ell_1 \dots \ell_m \}} c_{\{ \ell'_1 \dots \ell'_m \}, \{ \ell_1 \dots \ell_m \}}^{\alpha', \beta'} \mathcal{P}_L^{\alpha'} \mathcal{P}_R^{\beta'} | \{ \ell_1 \dots \ell_m \} \rangle. \quad (7.15)$$

We discuss the procedure to find a suitable set $c_{\{ \ell'_1 \dots \ell'_m \}, \{ \ell_1 \dots \ell_m \}}^{\alpha', \beta'}$ in detail by giving an explicit example for the Fibonacci theory. We consider a double-plaquette (see Figure 7.1) in a configuration, where all outgoing links are in state **1**. The state of the outgoing links is not affected by the action of the perturbation. The procedure has to be done for all values of α' and β' in (7.15) as well as for all configurations of the outgoing links separately. Here we discuss the case $\alpha' = \beta' = \tau$. With the projectors (3.19), we can write formally

$$\mathcal{D}^4 \mathcal{P}_L^\tau \mathcal{P}_R^\tau \begin{pmatrix} | \text{ref} \rangle \\ | \text{ref} \rangle \\ | \text{ref} \rangle \\ | \text{ref} \rangle \\ | \text{ref} \rangle \end{pmatrix} = \begin{pmatrix} \varphi^4 & -\varphi^3 & -\varphi^3 & \varphi & \varphi^{3/2} \\ -\varphi^3 & \varphi^2 & \varphi^2 & -1 & -\varphi^{1/2} \\ -\varphi^3 & \varphi^2 & \varphi^2 & -1 & -\varphi^{1/2} \\ \varphi & -1 & -1 & 2\varphi^3 & -3\varphi^{1/2} - \varphi^{3/2} \\ \varphi^{3/2} & -\varphi^{1/2} & -\varphi^{1/2} & -3\varphi^{1/2} - \varphi^{3/2} & 4 + \varphi \end{pmatrix} \begin{pmatrix} | \text{ref} \rangle \\ | \text{ref} \rangle \\ | \text{ref} \rangle \\ | \text{ref} \rangle \\ | \text{ref} \rangle \end{pmatrix}, \quad (7.16)$$

where φ is the golden mean and \mathcal{D} the total quantum dimension of the Fibonacci theory. Note that we sorted the states according to the number of links, which are not in the trivial value, i.e. which differ from the reference state $|\text{ref}\rangle$ (3.30).

Now we multiply (7.16) with $\mathcal{P}_L^\tau \mathcal{P}_R^\tau$ from the left on both sides. Using $(\mathcal{P}_p^\tau)^2 = \mathcal{P}_p^\tau$ and subtracting the left-hand side yields

$$\begin{pmatrix} -6.2361 & -4.2361 & -4.2361 & 1.6180 & 2.0582 \\ -4.2361 & -10.4721 & 2.6180 & -1. & -1.2720 \\ -4.2361 & 2.6180 & -10.4721 & -1. & -1.2720 \\ 1.6180 & -1. & -1. & -4.6180 & -5.8742 \\ 2.0582 & -1.2720 & -1.2720 & -5.8742 & -7.4721 \end{pmatrix} \begin{pmatrix} \mathcal{P}_L^\tau \mathcal{P}_R^\tau | \text{ref} \rangle \\ \mathcal{P}_L^\tau \mathcal{P}_R^\tau | \text{ref} \rangle \\ \mathcal{P}_L^\tau \mathcal{P}_R^\tau | \text{ref} \rangle \\ \mathcal{P}_L^\tau \mathcal{P}_R^\tau | \text{ref} \rangle \\ \mathcal{P}_L^\tau \mathcal{P}_R^\tau | \text{ref} \rangle \end{pmatrix} = 0, \quad (7.17)$$

where we expressed all coefficients as floating point numbers, since the following operations involve division of matrix elements and do not preserve the simple structure in terms of the quantum dimensions as in (7.16). We note that we perform the actual calculations to guarantee a precision of 50 digits for the final result.

We perform backward elimination (with eventual pivotation) and forward substitution, which yields

$$\begin{pmatrix} 0. & 0. & 0. & 0. & 0. \\ 0. & 0. & 0. & 0. & 0. \\ -0.6180 & 0. & -1. & 0. & 0. \\ -0.6180 & 0. & 0. & -1. & 0. \\ 0.4859 & -0.7862 & 0. & 0. & -1. \end{pmatrix} \begin{pmatrix} \mathcal{P}_L^T \mathcal{P}_R^T | \text{state 1} \rangle \\ \mathcal{P}_L^T \mathcal{P}_R^T | \text{state 2} \rangle \\ \mathcal{P}_L^T \mathcal{P}_R^T | \text{state 3} \rangle \\ \mathcal{P}_L^T \mathcal{P}_R^T | \text{state 4} \rangle \\ \mathcal{P}_L^T \mathcal{P}_R^T | \text{state 5} \rangle \end{pmatrix} = 0. \quad (7.18)$$

So by considering the non-trivial lines of (7.18), we have finally

$$\mathcal{P}_L^T \mathcal{P}_R^T | \text{state 3} \rangle = -0.6180 \mathcal{P}_L^T \mathcal{P}_R^T | \text{state 1} \rangle, \quad (7.19)$$

$$\mathcal{P}_L^T \mathcal{P}_R^T | \text{state 4} \rangle = -0.6180 \mathcal{P}_L^T \mathcal{P}_R^T | \text{state 2} \rangle, \quad (7.20)$$

$$\mathcal{P}_L^T \mathcal{P}_R^T | \text{state 5} \rangle = 0.4859 \mathcal{P}_L^T \mathcal{P}_R^T | \text{state 1} \rangle - 0.7862 \mathcal{P}_L^T \mathcal{P}_R^T | \text{state 2} \rangle, \quad (7.21)$$

and thus, we can express all final states in terms of the two states $\mathcal{P}_L^T \mathcal{P}_R^T | \text{state 1} \rangle$ and $\mathcal{P}_L^T \mathcal{P}_R^T | \text{state 2} \rangle$, which have not been replaced by the above procedure.

Due to our initial sorting of the states, we retain the states having maximal number of links in the state **1**. This speeds up the final overlap calculation, and it also reduces the necessity of keeping track of a growing number of non-trivial string-net configurations during the calculation. Note that this procedure eliminates the need of taking into account processes as for example depicted in (7.10), as the intermediate state has been eliminated by the above procedure. However, processes, whose non-trivial bond values arise due to the fact that intermediate loops cannot be annihilated as depicted in (7.9), are still to be taken into account, so that one has still to perform an overlap calculation at the end.

Let us also note that the coincidence of the number of the remaining states and the number of fusion channels of the two τ -fluxes on the plaquettes is by far not accidental, but is reflecting the fact that the local perturbation acts within a subspace spanned by the possible fusion outcomes of the local flux labels.

For the case of an Abelian theory, the positions of fluxes specify completely a state. Thus the above procedure reduces the number of final states always to one state for each sector given by values α' , β' , and the outgoing link variables. If one selects this state to yield the reference state in the definition of the flux basis (3.21) when embedded into the lattice, one thus sees that the link degrees of freedom are not necessary at all to describe the physics of the topological phase. The matrix elements are completely determined by the plaquette (dual) variables.

7.2.3 Implementation details of the calculations

As our representation of states in the overcomplete flux basis involves many intermediate states, we reduce the need of memory by evaluating $H_{\text{pCUT}}^{\text{eff}}$ (6.28) instead of $H_{\text{dpt}}^{\text{eff}}$ or $H_{\text{pt}}^{\text{eff}}$ for the ground-state energy and the dispersion.

The overlap calculation is performed in the end of each calculation. This also allows for a more convenient book keeping in the linked-cluster expansion detailed in the next chapter. Indeed, for one initial state all possible final states are determined in one calculation and thus the effort of tracking all possible matrix elements is reduced.

7.3 The non-topological phases

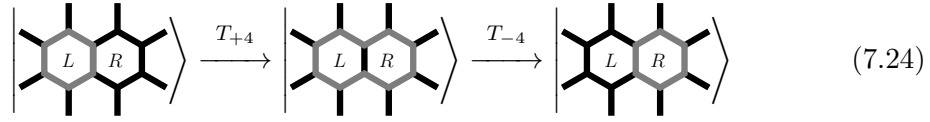
In our discussion of the implementation of the series expansion for the non-topological phases, we give first the details for the **1**-phase, which is present in all of the considered models within this thesis. Afterwards, we give details for the τ -phase, which is only present for the Fibonacci-theory. The other models do not have a finite ground-state degeneracy in the analogue parameter regime and are therefore not treated by high-order series expansions.

However, let us mention before we enter the detailed discussion that within the non-topological phases, we represent the eigenstates of the unperturbed Hamiltonian in the bond basis, which is an orthonormal product basis. Thus all considerations of the previous section resulting from the need to deal with an overcomplete basis are absent.

7.3.1 Implementation in the **1**-phase

Let us recall that in the **1**-phase of any $(N + 1)$ string-net model, the ground state $|\text{gs}_{\text{loc},1}\rangle$ is given by (3.50). One can easily determine the spectral shift discussed in

where processes like



contribute. The linked-cluster theorem 6.1.1.4 assures that for a hopping over n plaquettes, the perturbation not only acts on the initial and final location of the excitation, but also on the $n - 1$ intermediate plaquettes. As we consider here the action of the shifted perturbation, any action on the intermediate plaquettes creates excitations on typically all internal links of the plaquettes. These excitations have to be annihilated again by a second action of the perturbation to yield a non vanishing contribution for the whole process. Thus, to obtain non-vanishing hopping elements for a hopping over n plaquettes, we have to perform the perturbative expansion up to order $2 + 2 \cdot (n - 1) = 2n$. Consequently, we have to consider periodic clusters without non-contractible loops of length n to obtain hopping elements valid for the thermodynamic limit up to order $2n$. Note that a similar result for the ground-state energy on open clusters is discussed in Section 8.2.1.

Let us emphasize that the calculation of the respective hopping elements can be done on different cluster shapes such that at least the considered hopping element is determined correctly in the thermodynamic limit (and other hopping elements on this cluster may have contributions from non-contractible loops). By shaping an optimal, i.e. smallest possible, cluster for each hopping element, one is typically able to determine higher-order contributions (typically two to three orders more) than by only considering one cluster sufficiently large to obtain all hopping elements correctly for the thermodynamic limit. The hopping elements are determined by the evaluation of $H_{\text{dpt}}^{\text{eff}}$, which involves many intermediate states at the same time. Therefore, we evaluate $H_{\text{dpt}}^{\text{eff}}$ by the use of the splitting strategy discussed in Section 7.1, mainly to reduce the need of memory resources, which can still reach up to several tens of gigabytes per hopping element.

However, the straightforward calculation of the hopping elements for the thermodynamic limit via the evaluation of $H_{\text{dpt}}^{\text{eff}}$ works only if $H_{\text{pCUT}}^{\text{eff}}$ and $H_{\text{dpt}}^{\text{eff}}$ coincide. This is necessarily the case, if there is only one elementary excitation per plaquette, i.e. for the $N = 1$ theories for semions and Fibonacci-anyons. However, for the Ising theory, the effective Hamiltonians for the elementary excitation sector do not need to coincide. It turns out that they do not. In particular, $H_{\text{dpt}}^{\text{eff}}$ contains also terms, which violate the linked-cluster theorem valid for $H_{\text{pCUT}}^{\text{eff}}$. According to the discussion in Section 6.1.4, the unitary transformation which rotates away these terms (which depend also on the specific cluster, on which $H_{\text{dpt}}^{\text{eff}}$ is evaluated) yields $H_{\text{pCUT}}^{\text{eff}}$ up to a local and thus irrelevant transformation, as we are only interested in the spectrum of the effective Hamiltonian.

In order to determine the unitary transformation, all matrix elements of $H_{\text{dpt}}^{\text{eff}}$ have to be determined on the same cluster. This reduces the maximal order reached (eight for Ising anyons instead of eleven for the Fibonacci theory).

Let us remark that for the ladder geometry, the reduction of the cluster size for a given order does not apply, as the excitations are located on single rungs of the ladder and thus are not extended objects.

7.3.2 Implementation of the τ -phase in the Fibonacci theory

This section deals with the implementation details of the τ -phase in the Fibonacci model, as the other considered models do not have a finite ground-state degeneracy in the limit $\theta = \frac{3\pi}{2}$. Although the perturbation is the same for the $\mathbf{1}$ - and the τ -phase, the different unperturbed Hamiltonians result in some differences. These can already be observed in the calculation of the spectral shift, which yields per plaquette

$$\begin{aligned} \langle \text{gs}_{\text{loc},\tau} | H_{\text{LW},p} | \text{gs}_{\text{loc},\tau} \rangle &= -J_p \left\langle \text{Diagram}_p \left| \sum_s \frac{d_s}{\mathcal{D}^2} B_p^s \right| \text{Diagram}_p \right\rangle \\ &= -J_p \left(\frac{d_1}{\mathcal{D}^2} + \frac{d_\tau}{\mathcal{D}^2} d_\tau^{-6} \right) = -J_p \frac{1 + d_\tau^{-5}}{\mathcal{D}^2}, \end{aligned} \quad (7.25)$$

where the second term in (7.25) stems from the diagonal contribution of the operator B_p^τ to the ground state. This already shows that in this limit, the structure of the perturbation is more involved than in the other cases discussed in this thesis. The differences manifest themselves not only in the diagonal contribution of the perturbation to the ground-state energy, but also in the action onto the unperturbed ground state. As the perturbation acting on the ground state can generate excitations on each of the internal bonds of the plaquette, there are much more intermediate states (there are 17 non-zero local matrix elements for the action of H_{LW} on $|\text{gs}_{\text{loc},\tau}\rangle$) and this already at low orders. As the elementary excitations in the τ -phase are localized on links, and thus not extended as the excitations in the $\mathbf{1}$ -phase, we do not have an ‘‘acting-twice’’ property in this case.

Consequently, the necessary cluster sizes to obtain hopping elements valid for the thermodynamic limit grow rapidly. Thus, we choose to perform a linked-cluster expansion to obtain the ground-state energy and the dispersion, as detailed in the next chapter. This however restricts the highest order reached especially for the hopping elements, as the evaluation of $H_{\text{pCUT}}^{\text{eff}}$ involves among other challenges the large number of terms shown in the second column of Table 6.1.

7.4 Chapter Summary

In this chapter, we presented the technical details of our implementation to perform the high-order computer-based series expansions. The main focus is on the topological phases. To be able to perform the linked-cluster expansion presented in the next chapter, we have to choose the overcomplete flux-basis. The overcompleteness leads us to consider explicitly the evaluation of the non-trivial scalar products, as well as a prescription to reduce locally the number of basis states to be taken into account. These steps enable us to perform the graph expansion to obtain reasonably high orders for the series expansions also for the quantities of the two-dimensional systems.

Additionally, we discussed the details of the series expansions in the non-topological phases with finite ground-state degeneracy. The structure of the perturbation is more involved for the two-dimensional systems in the sense that $H_{\text{pCUT}}^{\text{eff}}$ contains too many terms to be efficiently evaluated up to high orders. Consequently, we choose to evaluate the hopping elements for the elementary excitations in the $\mathbf{1}$ -phase on periodic clusters. The fact that these excitations are extended reduces the size of the involved clusters, so that nevertheless reasonable orders are obtained.

For the τ -phase of the Fibonacci theory, this feature is absent and we are thus led to perform a linked-cluster expansion for the hopping elements due to the otherwise rapidly growing size of the periodic clusters.

For the ground-state energies of the non-topological phases with unique ground states, we are able to perform a linked-cluster expansion as detailed in the next chapter.

Linked-cluster expansion

*Nothing is particularly hard
if you divide it into small jobs.
- Henry Ford -*

Linked-cluster or graph-expansions are intimately related, but not limited to, the use of series expansion techniques for lattice systems.

The key idea is to treat the model Hamiltonian defined on an infinite, or finite-size but large, system by identifying suitable smaller subsystems and decompose the full Hamiltonian as a sum over contributions from these subsystems. The details of this decomposition depend on the model, the lattice and the particular form of the desired decomposition.

Let us mention here the main difference between various approaches as used in either perturbative [151, 173], or purely numerical [156, 188, 189] treatments and the one used throughout this thesis: for the former, the effective Hamiltonian, i.e. the Hamiltonian, which does not couple the subspace of interest to the rest of the Hilbert space, is derived for each subsystem and the obtained results are then combined in order to yield an effective Hamiltonian in the thermodynamic limit. The underlying assumption that the corresponding subspace of the subsystem Hilbert spaces can be meaningfully embedded in the Hilbert space of the large system is not necessarily true in general. However, it turns out that it holds in many cases. In particular this embedding is perturbatively exact for gapped systems [173] and thus also holds at least perturbatively for the non-perturbative approaches.

In our approach, we determined with the effective Hamiltonian $H_{\text{pCUT}}^{\text{eff}}$ (6.28)¹ already an operator expansion directly valid for the thermodynamic limit. Our interest is therefore to evaluate the matrix elements of $H_{\text{pCUT}}^{\text{eff}}$. Since $H_{\text{pCUT}}^{\text{eff}}$ is given as a sum over products

¹Since we aim at a local expansion, we consider $H_{\text{dpt}}^{\text{eff}}$ and $H_{\text{pt}}^{\text{eff}}$ only in the sense of Section 6.1.4, as the involved resolvent is a non-local quantity.

of the (quasi-) local operators $T_n = \sum_{\{i\}} T_{n,\{i\}}$, where the i corresponds to the location of the degrees of freedom, our idea is to reorganize (6.28) as a sum of contributions stemming from different subclusters, as e.g. also performed in Ref. [164]. Thus there is no further approximation in our decomposition, as long as all subclusters needed to obtain the correct result up to a given order are taken into account.

Despite this difference, the concept coincides for the different approaches and can be summarized by the following steps:

1. Choose a suitable family of subclusters, in which one decomposes the original lattice. This choice is usually driven by the size of the subclusters necessary to obtain all contributions for a given order correctly as well as the number of the subclusters involved.
2. Identify equivalent subclusters, such that the quantity of interest q has the same contribution on each of these subclusters. This reduces the number of subclusters, on which one has actually to perform an explicit evaluation. A representative of each class of subclusters is called a graph g . The number of equivalent subclusters contributes to the weight of the graph $w_q(g)$.
3. Determine the quantity of interest $q(g)$ for each graph g .
4. Sum up the contributions $q(g)$ according to

$$q = \sum_g w_q(g) q(g) \quad (8.1)$$

in order to obtain the desired quantity q .

Step 4 is trivial, if all ingredients of (8.1) are known. For Step 3, we evaluate the effective Hamiltonian (6.28) or its reduced one-particle version (6.35). Within this chapter, we will be concerned mainly with the first two steps, as well as the determination of the weights $w_q(g)$ of the different graphs g .

There are several strategies to choose a family of subclusters. The trivial one is to choose the cluster itself or a sufficiently large subcluster in the sense of Section 6.1.5 and perform all calculations on a unique cluster.

A more involved choice for the family of subclusters are the variants of rectangular-shaped subclusters, which were introduced for the finite-lattice method [190] on a square lattice in the context of classical statistical physics. This method is also applied successfully in the context of quantum many body systems [163, 171]. This choice allows to identify easily equivalent clusters, which are simply those with identical shape. Also

the number of graphs grows slowly, i.e. quadratically with the maximal order M of the perturbative expansion. Note that the adaption to the triangular lattice is also already known in the literature [191].

In this approach, the size of the largest graph involved grows also quadratically with the order, i.e. the largest graph contains for this choice roughly M^2 plaquettes. As discussed in Section 6.1.4, the effort of an evaluation does strongly depend on the system size. We are thus interested here to reduce the maximal size of the graph as much as possible. This can be achieved by choosing subclusters, which contain at most the joint support of M local perturbation operators $T_{n,i}$, so in our case roughly M plaquettes. The price to pay is that the number of graphs then grows exponentially with M . We compensate this by parallelizing the evaluation of the effective Hamiltonian on different graphs.

As the important features like the determination of contributing graphs, their weights and reduced contributions usually depend on the details of the model, let us discuss the different limits of presented in Chapter 3 separately in the following sections. Let us however mention already here that graphs are systems with open boundaries, and consequently we will for simplicity always assume to evaluate $H_{\text{pCUT}}^{\text{eff}}$ on an infinitely extended plane in order to avoid notational difficulties caused by the non-local fluxes e.g. present on a torus.

8.1 Graph decomposition in the topological phase

For the evaluation of $H_{\text{pCUT}}^{\text{eff}}$, let us introduce the pictorial notations as in Figure 8.1. The flux degrees of freedom, which determine the eigenvalues of the unperturbed Hamil-

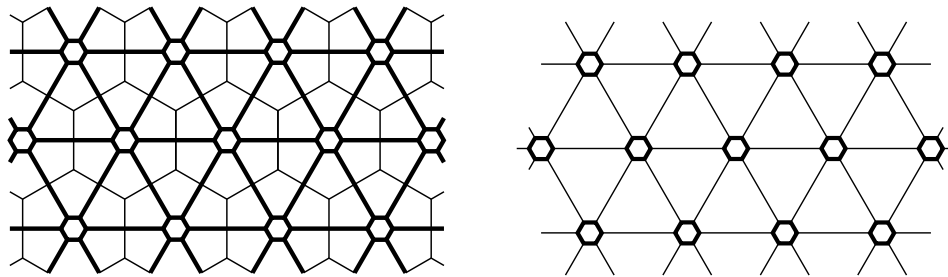


FIGURE 8.1: For the topological phase we consider instead of the hexagonal lattice, (thin lines left), the dual triangular lattice (thick lines left, or right). The degrees of freedom, which are measured by the particle-counting operator Q reside then on the sites of the triangular lattice. The perturbation acts on bonds linking the corresponding sites. we can use the same labeling also for the **1**-phase, as the (barycenter of the) elementary excitations are also located on plaquettes.

tonian, are denoted as small hexagonal sites. The perturbation acts on the bonds of the

dual lattice linking the adjacent sites. A subcluster is then a collection of a finite number of bonds as depicted in Figure 8.2. This representation is useful in the context of developing a graph expansion, the actual calculations are in the end carried out in the setting already discussed in Chapter 7.

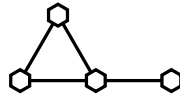


FIGURE 8.2: A subcluster is a finite collection of effective sites representing the locations of the degrees of freedom and of bonds linking them. These bonds can form closed loops as the triangle or branches as the bond linking the site not being part of the triangle.

Additionally, we define

$$\langle \text{gs} | H^{\text{eff}} \Big|_{\triangle} | \text{gs} \rangle = \text{Diagram} \quad (8.2)$$

$$\langle \text{gs} | H^{\text{eff}} \Big|_{\triangle} | \text{gs} \rangle = \text{Diagram} \quad (8.3)$$

$$\langle j | H^{\text{eff}} \Big|_{\triangle} | i \rangle = \text{Diagram} \quad (8.4)$$

where in (8.2) the Hamiltonian acts on arbitrary links of the given subcluster (here the one depicted in Figure 8.2), in (8.3) the Hamiltonian has acted on all links depicted by doubled lines, and (8.4) represents the hopping element $t_{i,j}$ on the finite cluster.² Note that the contribution to the local hopping element $t_{i,i}$ reads for this subcluster

$$t_{ii} = \text{Diagram} - \text{Diagram} \quad (8.5)$$

Bonds not acted on by the perturbation are represented by dotted lines. The reduced contribution $\bar{q}(g)$ of a subcluster g is the contribution, which cannot be expressed by the contributions of smaller subclusters. As we take into account all subclusters up to a given number of bonds, the reduced contributions of a cluster are thus yielded by non-trivial action of the effective Hamiltonian on all bonds of this cluster. So, the reduced contribution e.g. for the cluster depicted in 8.2 is given by (8.3).

²One-particle states cannot change their label via the action of the perturbation in the topological phase. We thus drop the anyon label for the hopping elements here.

For the following reasoning, it is useful to consider the dual basis, as it deals only with the involved flux degrees of freedom and contains no additional local degrees of freedom. Thus, it is closest to the pictorial representation (8.2)-(8.4). As the flux basis contains also the flux quantum numbers explicitly, all considerations can be carried over for the actual calculation, i.e. vanishing reduced contributions in the dual basis are also zero in the flux basis, in which the actual calculations are performed.

A key observation for reducing further the number of contributing subclusters, is that subclusters with M bonds do not necessarily contribute at order M . One simple example is

$$\text{---}\bigcirc\text{---}\bigcirc\text{---}\bigcirc = \mathcal{O}(J_e^4), \quad (8.10)$$

i.e. a cluster with two connected bonds contributes to the ground-state energy from order four on. Note that is a direct consequence of treating the first-order contribution in the ground-state sector apart in the actual calculation as detailed in Section 7.1.

The reason for the higher leading order of the contribution is that due to the fact that the action on a bond will create excitations on adjacent sites, if these were unoccupied before. These excitations have then to be annihilated again to yield a non-vanishing contribution to the operator element. Thus each site of the cluster has to be acted on at least twice. This can be achieved by acting twice on the same bond or by acting on another bond linking the same site. The former is necessarily the case if the site is the endpoint of a branch as the outer sites in (8.10) or as shown in Figure 8.2. This yields that the leading order in (8.10) has to be at least four. The fact that one cannot annihilate single excitations allows to generalize the argument to branches of arbitrary length, i.e.

$$\underbrace{\text{---}\bigcirc\text{---}\bigcirc\text{---}\bigcirc\text{---}\bigcirc\text{---}\bigcirc}_{n \text{ bonds}} = \mathcal{O}(J_e^{2n}). \quad (8.11)$$

Another possibility of acting on the same site is to act with the perturbation on another bond, provided the considered site is not the endpoint of a branch. Then each bond has only to be acted on once. This is possible in a loop, so e.g.

$$\text{---}\bigcirc\text{---}\bigcirc\text{---}\bigcirc = \mathcal{O}(J_e^3). \quad (8.12)$$

Consequently, as a general rule, bonds forming a branch have to be acted upon twice, bonds being part of a loop just once. The minimal order, from which a cluster can

contribute, is therefore given by the sum of these numbers, e.g.

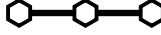
$$\begin{array}{c} \circ \\ \diagup \quad \diagdown \\ \circ \text{---} \circ \text{---} \circ \end{array} = \mathcal{O}(J_e^{2 \cdot 1 + 1 \cdot 3}) = \mathcal{O}(J_e^5). \quad (8.13)$$

Furthermore, let us mention that e.g. the contribution of the dumbbell-like shaped cluster

$$\begin{array}{c} \circ \quad \circ \\ \diagup \quad \diagdown \quad \diagup \quad \diagdown \\ \circ \text{---} \circ \text{---} \circ \text{---} \circ \end{array} = \mathcal{O}(J_e^7), \quad (8.14)$$

and not, as a naive counting may yield, $\mathcal{O}(J_e^8)$. This is due to the fact that the middle bond takes formally part of a loop, since the perturbation, also contains two-particle interaction terms.

A similar reasoning as for contributions to the ground-state energy can also be applied to the hopping elements. The major difference is that the bonds along the paths connecting initial and final position of the excitation have not to be acted on twice, which reduces the minimal order at which a cluster can contribute.

However, the minimal order of the contribution depends, for a given graph, on the actual initial and final position. For example, one has on the same cluster  for the leading orders of the hopping elements

$$\begin{array}{c} \otimes \text{---} \circ \text{---} \odot \\ \circ \text{---} \otimes \text{---} \odot \\ \circ \text{---} \otimes \text{---} \circ \end{array} = \mathcal{O}(J_e^2), \quad \circ \text{---} \otimes \text{---} \odot = \mathcal{O}(J_e^3), \quad \circ \text{---} \otimes \text{---} \circ = \mathcal{O}(J_e^4). \quad (8.15)$$

This type of reasoning is based on purely local particle-number counting and properties of the perturbation and thus also holds for anyonic excitations. Let us mention that the above considered properties of a cluster, i.e. whether its links form loops or branches, can all be obtained easily from local connectivity properties of the sites of the cluster. So the adjacency matrix of the sites of the cluster, as defined below, can be used to characterize this property.

Finally, we discuss here an important class of clusters, which have a non-zero contribution only for non-Abelian anyons, e.g. one has

$$\begin{array}{c} \circ \quad \circ \\ \diagup \quad \diagdown \quad \diagup \quad \diagdown \\ \otimes \\ \diagdown \quad \diagup \quad \diagdown \quad \diagup \\ \circ \quad \circ \end{array} = \mathcal{O}(J_e^6) \neq 0. \quad (8.16)$$

This is not in contradiction to the linked-cluster theorem, as there is no perturbation acting on the seemingly disconnected site in the middle of the loop. So, closed loops

around a particle, which is not acted on at all, also contribute in a non-trivial manner to the dispersion, manifesting the non-trivial braiding statistics directly in the graph expansion.

Up to now, we discussed clusters yielding a priori a vanishing contribution. Let us turn now to the task, which turns a linked-cluster expansion into a graph expansion: the identification of subclusters that yield the same reduced contribution. It is clear that clusters, which are mapped onto each other by the action of a symmetry of the underlying triangular lattice, yield the same result. These global symmetries are translations (T), inversion at one site (I), rotation about one site (C), and reflection about an axis of the lattice ($R_{1,2}$). For example, for the subcluster depicted in Figure 8.3, we have

$$\begin{array}{ccccccc}
 \begin{array}{c} \text{---} \\ \diagup \quad \diagdown \\ \text{---} \\ \diagdown \quad \diagup \\ \text{---} \end{array} & \equiv & \begin{array}{c} \text{---} \\ \diagdown \quad \diagup \\ \text{---} \\ \diagup \quad \diagdown \\ \text{---} \end{array} & \equiv & \begin{array}{c} \text{---} \\ \diagdown \quad \diagup \\ \text{---} \\ \diagdown \quad \diagup \\ \text{---} \end{array} \\
 \begin{array}{c} \text{---} \\ \diagdown \quad \diagup \\ \text{---} \\ \diagup \quad \diagdown \\ \text{---} \end{array} & \equiv & \begin{array}{c} \text{---} \\ \diagup \quad \diagdown \\ \text{---} \\ \diagdown \quad \diagup \\ \text{---} \end{array} & \equiv & \begin{array}{c} \text{---} \\ \diagdown \quad \diagup \\ \text{---} \\ \diagup \quad \diagdown \\ \text{---} \end{array} & \equiv & \begin{array}{c} \text{---} \\ \diagdown \quad \diagup \\ \text{---} \\ \diagdown \quad \diagup \\ \text{---} \end{array}
 \end{array} \quad (8.17)$$

However, apart from these global symmetries, there are also local ones like

$$\begin{array}{c} \text{---} \\ \diagup \quad \diagdown \\ \text{---} \\ \diagdown \quad \diagup \\ \text{---} \end{array} = \begin{array}{c} \text{---} \\ \diagdown \quad \diagup \\ \text{---} \\ \diagup \quad \diagdown \\ \text{---} \end{array} . \quad (8.18)$$

Since the perturbation is local, its contributions when acting on a bond is entirely determined by the two fluxes labels residing on the adjacent plaquettes as well as their (local) fusion channel. Consequently, these local deformations do not change the final contribution.

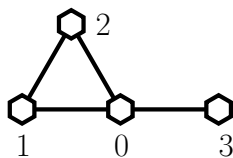


FIGURE 8.3: The enumeration of the sites of the shown graph g is chosen such that the site with the maximal number of links is assigned the lowest label 0. The sites 1 and 2 are equivalent, as their exchange does not alter the maximized adjacency matrix A_g to be discussed in Eq. (8.20). The sites labeled by 0 and 3 cannot be equivalent to any other site of the graph due to their different number of links.

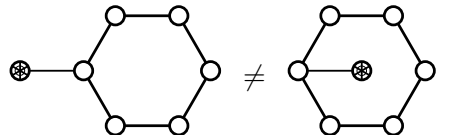
Note that local deformations as depicted in (8.18) leave the adjacency matrix A_c of the cluster c invariant. The adjacency matrix is defined as

$$(A_c)_{s,s'} = \begin{cases} 1 & \text{if sites } s \text{ and } s' \text{ are linked by a bond} \\ 0 & \text{otherwise} \end{cases} \quad (8.19)$$

and is, due to this invariance, a suitable tool to distinguish inequivalent clusters. Permutations of site enumeration may change A_c so that one has to fix a convention. We choose a permutation of the site ordering which maximizes the matrix elements $(A_c)_{s,s'}$ in the increasing order $s' = 0, \dots, S_c - 1$, $s = 0, \dots, S_c - 1$, where S_c is the number of sites of cluster c . Permutations leaving the maximized A_c invariant will map labels of equivalent sites onto each other. For the example depicted in Figure 8.3, the maximized adjacency matrix reads

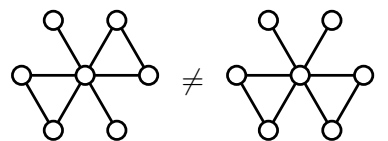
$$A_g = \begin{pmatrix} 0 & 1 & 1 & 1 \\ 1 & 0 & 1 & 0 \\ 1 & 1 & 0 & 0 \\ 1 & 0 & 0 & 0 \end{pmatrix}. \quad (8.20)$$

Identifying all subclusters with the same maximized A_c works for standard lattice models, which do not involve non-Abelian anyonic excitations. However, if non-Abelian anyons are involved, it is clear that



$$\text{Cluster 1} \neq \text{Cluster 2}, \quad (8.21)$$

since on the right cluster, one encircles a non-Abelian excitation in contrast to the left one. This braiding effect of non-Abelian anyons manifests itself also in differences of contributions to the ground-state energy, e.g



$$\text{Cluster 1} \neq \text{Cluster 2}. \quad (8.22)$$

This difference can be understood if one considers the eigenbasis of the unperturbed Hamiltonian in the dual basis. In order to apply the perturbation to one bond, one has eventually to perform R - or F -moves as mentioned in Section 3.2, such that the direct fusion channel of the sites adjacent to the bond acted on is obtained. As different R -moves do not commute with each other for excited states (braiding with flux-free states is still trivial), the contribution from the local perturbation will in general differ.

As a consequence, two clusters cannot be identified with the same graph, if only their maximized adjacency matrix coincides, but additionally, this inequivalent braidings have been taken into account. In our setting, this is achieved by introducing an ordering of the neighboring sites, e.g. for the cluster in (8.22) a labeling of the sites maximizing the adjacency matrix is given by Figure 8.4. The neighboring order $\{n(s)\}$ of a site s

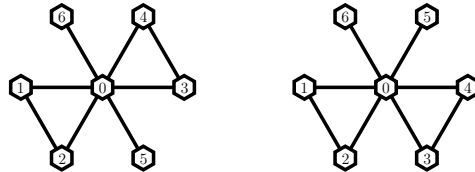


FIGURE 8.4: We depict one labeling, which maximizes the adjacency matrix of the given subclusters, respectively. As the contributions of these two subclusters differ, we have to take into account not only the adjacency matrix, which coincides for the given clusters, but also the order of the neighbors of sites with more than two links. As global symmetries like reflections change the orientation, we have to consider both counterclockwise and clockwise order of the linked neighboring sites. This differs for these two clusters, as one can infer by following the neighbors of site 0 in the middle. Permuting the labels of the right cluster so that they take the labels of the left one yields the same neighboring order, however, the adjacency matrix for this configuration is not maximized. Consequently, we can use the adjacency matrix combined with the neighboring order to classify the clusters.

is then given by the counterclockwise order of the sites linked with s , i.e. for the left $n^{\text{left}}(0) = \langle 1, 2, 5, 3, 4, 6 \rangle$ and for the right $n^{\text{right}}(0) = \langle 1, 2, 3, 4, 5, 6 \rangle$, where we dropped all neighbor orders for sites with less than three neighbors. Note that improper rotations change the orientation and will thus reverse the order of the neighbor order for all sites. Thus, we will identify the contribution from clusters, sharing the same maximized adjacency matrix and the same or globally (i.e. for all sites) reversed neighbor order.

For the identification of hopping elements $t_{i,j}$, we have to consider equivalent sites. This means that the contributions $t_{i,j}^{c_1}$ will equal $t_{k,l}^{c_2}$, if c_1 and c_2 are equivalent subclusters and additionally there has to be a permutation σ of the site labels of c_2 , which leaves the maximized adjacency matrix A_{c_2} invariant, yields an equivalent neighbor order n^{c_2} and additionally fulfills $\sigma(k) = i$, $\sigma(l) = j$. Moreover, we take into account the fact that the Hamiltonian is real, so that we have $t_{i,j} = t_{j,i}$.

After having detailed how to identify identical contributions, let us determine the weight of each reduced contribution for each graph $w_{\bar{q}(g)}$. We define a graph as a representation of equivalent subclusters. Thus the weight of a graph depends on how many equivalent subclusters can be embedded in the large or finite cluster.

This number could e.g. be obtained by considering a large cluster, choosing one site in its bulk as the origin and determining all linked subclusters containing the origin. By doing so, one can count the number of equivalent subclusters per graph $N(g)$, which

yields $w_{\bar{e}_0}(g)$. As a graph with S_g sites contributes to the ground-state energy of S_g plaquettes in the original lattice, one has for the weight of the reduced contribution to the ground-state energy per plaquette

$$w_{\bar{e}_0} = \frac{N(g)}{S_g} \quad (8.23)$$

So the graph-expansion for the ground-state energy per plaquette reads

$$e_0 = \frac{6}{2} \times \text{---} \text{---} + \frac{6}{3} \times \text{---} \text{---} \text{---} + \frac{45}{3} \times \text{---} \text{---} \text{---} \text{---} + \frac{12}{4} \times \text{---} \text{---} \text{---} \text{---} + \mathcal{O}(J_e^5), \quad (8.24)$$

where the leading order of the contributions from different graphs are two, three, four, and four respectively.

Note that effects of the non-Abelian statistics start to play a role at order eight with the distinction of the contributions

$$\text{---} \text{---} \text{---} \text{---} \text{---} \text{---} \neq \text{---} \text{---} \text{---} \text{---} \text{---} \text{---} = \mathcal{O}(J_e^8). \quad (8.25)$$

For the hopping elements, each cluster containing the initial site i and the final site f contributes with weight 1 to $t_{i,f}$. Thus the weight of each graph is given by $w_{\bar{t}_{i,j}} = N(g)$ up to simplifications due to equivalent sites. Identifying the positions \vec{r}_i (\vec{r}_f) of the site i (f) in the lattice, one finds for the respective hopping element $t_{\vec{r}_f - \vec{r}_i}$:

$$t_{\vec{0}} = 6 \times \left(\text{---} \text{---} - \text{---} \text{---} \right) + 6 \times \left(\text{---} \text{---} \text{---} - \text{---} \text{---} \text{---} \right) + \mathcal{O}(J_e^4), \quad (8.26)$$

$$t_{\vec{n}_1} = 1 \times \text{---} \text{---} + 2 \times \text{---} \text{---} \text{---} + 10 \times \text{---} \text{---} \text{---} \text{---} + 2 \times \text{---} \text{---} + 4 \times \text{---} \text{---} \text{---} \text{---} + \mathcal{O}(J_e^4), \quad (8.27)$$

$$t_{2\vec{n}_1} = 1 \times \text{---} \text{---} \text{---} + 6 \times \text{---} \text{---} \text{---} \text{---} + \mathcal{O}(J_e^4), \quad (8.28)$$

$$t_{3\vec{n}_1} = 1 \times \text{---} \text{---} \text{---} \text{---} + \mathcal{O}(J_e^4), \quad (8.29)$$

$$t_{\vec{n}_1 + \vec{n}_2} = 2 \times \text{---} \text{---} \text{---} + 6 \times \text{---} \text{---} \text{---} \text{---} + \mathcal{O}(J_e^4), \quad (8.30)$$

$$t_{2\vec{n}_1 + \vec{n}_2} = 3 \times \text{---} \text{---} \text{---} \text{---} + \mathcal{O}(J_e^4). \quad (8.31)$$

For the determination of these six hopping elements up to order three, one has to evaluate the contributions from four graphs. This involves in total seven initial states.

However, the way mentioned above to obtain all contributing clusters is not well suited for practical use, as it will generate all subclusters and thus a large overhead of unneeded information. It is more efficient to consider a separately generated set of graphs and embed each graph in a sufficiently large cluster.

Therefore, one identifies sites of the graph with sites of the cluster. We start by choosing the first site of the graph and identify it with the site at the origin of the large cluster. Successively, the remaining sites are embedded according to their links to already embedded sites. This procedure is then repeated for all inequivalent sites of the graph. It turns out that a list of graphs only distinguished by the adjacency matrix (also referred to as topologically equivalent graphs in the literature [151]) is most conveniently generated.

The neighbor order is then determined for each embedded cluster. After the embedding, the different clusters are identified yielding the final list of graphs and initial states, for which operator elements of the effective Hamiltonians have to be determined. We show in Table 8.1 a list of the number of graphs and initial states needed for a given order.

| max. order | no. graphs for e_0 | no. graphs for 1qp | no. of initial states for 1qp |
|------------|----------------------|--------------------|-------------------------------|
| 1 | - | 1 | 1 |
| 2 | 1 | 2 | 3 |
| 3 | 2 | 4 | 7 |
| 4 | 4 | 8 | 15 |
| 5 | 7 | 16 | 33 |
| 6 | 13 | 33 | 78 |
| 7 | 24 | 75 | 203 |
| 8 | 52 | 188 | 580 |
| 9 | 114 | 515 | 1770 |
| 10 | 282 | 1507 | 5765 |
| 11 | 713 | 4711 | 19659 |

TABLE 8.1: Number of graphs and initial states needed to calculate the ground-state energy per plaquette e_0 or the one quasi-particle dispersion inside the topologically ordered phase. Note that for the ground-state energy, there is one initial state per graph. The obtained numbers take into account already all global and local symmetries.

Let us finally mention how the reduced contribution is obtained directly. During the calculation, we track the links on which the perturbation has already acted. Final contributions are only added to the reduced quantity, if the perturbation has acted on all links. This additional information not only saves one from constructing a subtraction scheme but can also be used to reduce the computational effort by suppressing actions of the perturbation, which cannot yield a non-zero reduced contribution in the end. For example, for a contribution of a graph with M bonds at order M , excluding any second action of the perturbation on a bond does not alter the final reduced contribution and

additionally reduces the number of the intermediate states. This eases the computational effort and outweighs the effort of tracking the location of perturbation-actions whenever the number of bonds is close to the order up to which one calculates.

Let us finally remark that in order to minimize the number of initial states to act on, we can use again the symmetry $t_{i,j} = t_{j,i}$. We conclude with a Table 8.1 of the number of graphs and initial states necessary to obtain the ground-state energy and the quasi-particle dispersion up to a given order.

It is not obvious to give a good estimate of the runtime for each graph due to the different shapes of each individual graph and also due to the difference of the computers used for the calculation. As a rule of thumb, the most challenging calculations of one graph for one initial state take for the maximal order contribution determined about 40-60 hours, so that the parallelization of the calculation is mandatory.

8.2 Graph expansions for non-topological phases

For non-topological phases, we do not face challenges like the determination of the possibly contributing graphs, as excitations in these limits are purely bosonic and the unperturbed basis is given by simple, orthogonal product states. As we see in the following, challenges for a graph expansion rise due to the extended support of the perturbation. We first consider the clusters for the graph expansion for the **1**-phase, i.e. about the limit $\theta = \frac{\pi}{2}$. Afterwards we turn to the limit of the τ -phase, i.e. $\theta = \frac{3\pi}{2}$.

8.2.1 Graph expansions in the 1-phase

Let us define in complete analogy to (8.2)-(8.4) the full and reduced contribution on a single plaquette by

$$\langle \text{gs} | H^{\text{eff}} \Big|_{\star} | \text{gs} \rangle = \text{Diagram 1} , \quad (8.32)$$

$$\langle \text{gs} | H^{\text{eff}} \Big|_{\star} | \text{gs} \rangle = \text{Diagram 2} . \quad (8.33)$$

As the number of terms in $H_{\text{pCUT}}^{\text{eff}}$ is too large for an efficient evaluation for order larger than seven, we aim to evaluate not $H_{\text{pCUT}}^{\text{eff}}$ but determine the contribution via evaluation of $H_{\text{pt}}^{\text{eff}}$ for the ground-state energy. We thus do not attempt a graph expansion for the excited states, but determine the hopping elements on large periodic clusters.

Let us also remark that we represent not all twelve link degrees of freedom, but only the six, which can be changed by the action of the perturbation. This is just a notational convenience as the perturbation cannot link two plaquettes sharing only one external link, as the corresponding operators commute. So again, the linked-cluster theorem tells us that only linked clusters, i.e. clusters formed by plaquettes sharing their internal bonds, can contribute.

Due to the fact that the perturbation creates a single, six-particle excitation, one cannot reduce the number of contributing clusters in the same way as for the topological phase.

However, this is largely compensated by another feature: the fact that on open clusters, each plaquette, has to be acted on at least twice to contribute to the ground-state energy. This can be understood by the following reasoning: consider a plaquette at the boundary of a cluster, i.e. at least one of the internal links of the plaquette is not an internal link of another plaquette. When the perturbation acts on this plaquette, it will introduce an excitation on this link. In order to contribute to the ground-state energy, this excitation has to be annihilated again. This is only possible if the same plaquette is acted on again by the perturbation.

This argument can be extended to the bulk of the cluster by the statement that plaquettes, which have been acted on once, are surrounded by a non-trivial string as depicted in Figure 8.5. The outermost string cannot be annihilated by actions on plaquettes

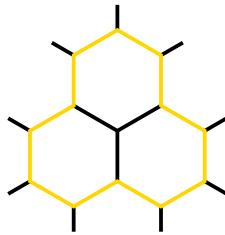


FIGURE 8.5: A region, in which every plaquette has been acted on once by the perturbation, is bounded by a string. On open clusters, one has to act inside this region to annihilate this string again.

outside the enclosed area, as this action would move the string outwards. So this string forms effectively a boundary in the sense that, to be annihilated, the plaquettes within the encircled area have to be acted on again. Consequently, for the determination of the reduced contributions up to order $2M$, we need only to consider clusters up to M plaquettes.

If one considers the question of identifying clusters yielding the same contribution, it should be clear that

$$\text{Diagram 1} \neq \text{Diagram 2} \neq \text{Diagram 3} . \quad (8.34)$$

Note that the difference between the first two contributions stems only from the different configurations of the not-coupled links of the middle plaquette. In order to take into account this feature, we characterize a cluster not only by the adjacency matrix of the involved plaquettes, where two plaquettes are defined as being linked if they share an internal link, i.e. if they can contribute to a non-vanishing contribution in the sense of the linked-cluster theorem.

Additionally, we consider a neighbor order in analogy to the one for the topological phase. However, as the relative positions of the neighbors matter in this case, we introduce a label “-1” for absent plaquettes. For example, the three clusters

$$\text{cl1} = \text{Diagram 1}, \text{cl2} = \text{Diagram 2}, \text{cl3} = \text{Diagram 3} \quad (8.35)$$

are then characterized by

$$A_{\text{cl1}} = \begin{pmatrix} 0 & 1 & 1 \\ 1 & 0 & 0 \\ 1 & 0 & 0 \end{pmatrix}, \quad n^{\text{cl1}}(0) = \langle -1, -1, 1, -1, -1, 2 \rangle \quad (8.36)$$

$$A_{\text{cl2}} = \begin{pmatrix} 0 & 1 & 1 \\ 1 & 0 & 0 \\ 1 & 0 & 0 \end{pmatrix}, \quad n^{\text{cl2}}(0) = \langle -1, -1, -1, 1, -1, 2 \rangle \quad (8.37)$$

$$A_{\text{cl3}} = \begin{pmatrix} 0 & 1 & 1 \\ 1 & 0 & 1 \\ 1 & 1 & 0 \end{pmatrix}, \quad \begin{aligned} n^{\text{cl3}}(0) &= \langle -1, -1, 1, -1, -1, 2 \rangle \\ n^{\text{cl3}}(1) &= \langle -1, -1, -1, -1, 2, 0 \rangle \\ n^{\text{cl3}}(2) &= \langle -1, -1, -1, -1, 0, 1 \rangle \end{aligned} \quad (8.38)$$

As for the topological phase, our considerations are based on the triangular lattice formed by plaquettes. This avoids the effort to track the numerous link degrees of freedom coupled by the perturbation separately (what would e.g. give an adjacency tensor of rank six) as well as to discuss issues like identifying clusters by considering about 50 degrees of freedom. With the above convention of the cluster identification,

the relevant information can be obtained from ~ 10 plaquettes, which represents a considerable effort.

A consequence of our treatment is that lattice symmetries of the triangular lattice map equivalent clusters onto each other. The impact of the extended support of the perturbation manifests itself in the fact that no local deformations of a cluster as in (8.35) yield an equivalent cluster.

As we have seen previously, we need for order $2M$ only clusters with up to M plaquettes. Thus, the way to obtain the reduced contributions presented in the previous section, is not the optimal one. The tracking of the plaquettes already acted on is a nearly useless effort, since it cannot be compensated by ruling out efficiently intermediate states not contributing to the final one.

So, we shall determine the reduced contributions via a subtraction scheme as detailed in Refs. [171, 173]. From the definition of the reduced contribution (8.33), we see that we can express the full contribution of a cluster as the sum over the reduced contributions of all subclusters. here, we do not discuss abstract (and problem specific) formulas, but we give as an example of the clusters contributing to the ground-state energy up to order seven:

$$\begin{array}{c} \text{Diagram 1} \\ \text{Diagram 2} \end{array} = \begin{array}{c} \text{Diagram 3} \\ \text{Diagram 4} \end{array}, \quad (8.39)$$

$$\begin{array}{c} \text{Diagram 5} \\ \text{Diagram 6} \end{array} = \begin{array}{c} \text{Diagram 7} \\ \text{Diagram 8} \end{array} + 2 \times \begin{array}{c} \text{Diagram 9} \\ \text{Diagram 10} \end{array}, \quad (8.40)$$

$$\begin{array}{c} \text{Diagram 11} \\ \text{Diagram 12} \end{array} = \begin{array}{c} \text{Diagram 13} \\ \text{Diagram 14} \end{array} + 2 \times \begin{array}{c} \text{Diagram 15} \\ \text{Diagram 16} \end{array} + 3 \times \begin{array}{c} \text{Diagram 17} \\ \text{Diagram 18} \end{array}, \quad (8.41)$$

$$\begin{array}{c} \text{Diagram 19} \\ \text{Diagram 20} \end{array} = \begin{array}{c} \text{Diagram 21} \\ \text{Diagram 22} \end{array} + 2 \times \begin{array}{c} \text{Diagram 23} \\ \text{Diagram 24} \end{array} + 3 \times \begin{array}{c} \text{Diagram 25} \\ \text{Diagram 26} \end{array}, \quad (8.42)$$

$$\begin{array}{c} \text{Diagram 27} \\ \text{Diagram 28} \end{array} = \begin{array}{c} \text{Diagram 29} \\ \text{Diagram 30} \end{array} + 3 \times \begin{array}{c} \text{Diagram 31} \\ \text{Diagram 32} \end{array} + 3 \times \begin{array}{c} \text{Diagram 33} \\ \text{Diagram 34} \end{array}, \quad (8.43)$$

where we already identified subclusters yielding the same contribution due to symmetries.

The full contribution can be determined by evaluating H^{eff} without any further restrictions or tracking procedures.

To obtain the reduced contribution, for which the weights can be determined as in the topological phase, we invert the above equations to get:

$$\begin{array}{c} \text{Diagram 35} \\ \text{Diagram 36} \end{array} = \begin{array}{c} \text{Diagram 37} \\ \text{Diagram 38} \end{array}, \quad (8.44)$$

$$\begin{array}{c} \text{Diagram 1} \\ \text{Diagram 2} \end{array} = \begin{array}{c} \text{Diagram 3} \\ \text{Diagram 4} \end{array} - 2 \times \begin{array}{c} \text{Diagram 5} \\ \text{Diagram 6} \end{array}, \quad (8.45)$$

$$\begin{array}{c} \text{Diagram 7} \\ \text{Diagram 8} \end{array} = \begin{array}{c} \text{Diagram 9} \\ \text{Diagram 10} \end{array} - 2 \times \begin{array}{c} \text{Diagram 11} \\ \text{Diagram 12} \end{array} - 3 \times \begin{array}{c} \text{Diagram 13} \\ \text{Diagram 14} \end{array}, \quad (8.46)$$

$$\begin{array}{c} \text{Diagram 15} \\ \text{Diagram 16} \end{array} = \begin{array}{c} \text{Diagram 17} \\ \text{Diagram 18} \end{array} - 2 \times \begin{array}{c} \text{Diagram 19} \\ \text{Diagram 20} \end{array} - 3 \times \begin{array}{c} \text{Diagram 21} \\ \text{Diagram 22} \end{array}, \quad (8.47)$$

$$\begin{array}{c} \text{Diagram 23} \\ \text{Diagram 24} \end{array} = \begin{array}{c} \text{Diagram 25} \\ \text{Diagram 26} \end{array} - 3 \times \begin{array}{c} \text{Diagram 27} \\ \text{Diagram 28} \end{array} - 3 \times \begin{array}{c} \text{Diagram 29} \\ \text{Diagram 30} \end{array}. \quad (8.48)$$

We see that these expressions still contain reduced contributions on the right-hand-side, but only those of smaller subclusters. We can therefore obtain the reduced contributions in terms of the full contributions by replacing iteratively the reduced contributions on the right-hand side using the above expressions (Note that the full contribution equals the reduced contribution on the smallest cluster.).

This yields

$$\begin{array}{c} \text{Diagram 31} \\ \text{Diagram 32} \end{array} = \begin{array}{c} \text{Diagram 33} \\ \text{Diagram 34} \end{array}, \quad (8.49)$$

$$\begin{array}{c} \text{Diagram 35} \\ \text{Diagram 36} \end{array} = \begin{array}{c} \text{Diagram 37} \\ \text{Diagram 38} \end{array} - 2 \times \begin{array}{c} \text{Diagram 39} \\ \text{Diagram 40} \end{array}, \quad (8.50)$$

$$\begin{array}{c} \text{Diagram 41} \\ \text{Diagram 42} \end{array} = \begin{array}{c} \text{Diagram 43} \\ \text{Diagram 44} \end{array} - 2 \times \left(\begin{array}{c} \text{Diagram 45} \\ \text{Diagram 46} \end{array} - 2 \times \begin{array}{c} \text{Diagram 47} \\ \text{Diagram 48} \end{array} \right) - 3 \times \begin{array}{c} \text{Diagram 49} \\ \text{Diagram 50} \end{array} \\ = \begin{array}{c} \text{Diagram 51} \\ \text{Diagram 52} \end{array} - 2 \times \begin{array}{c} \text{Diagram 53} \\ \text{Diagram 54} \end{array} + 1 \times \begin{array}{c} \text{Diagram 55} \\ \text{Diagram 56} \end{array}, \quad (8.51)$$

$$\begin{array}{c} \text{Diagram 57} \\ \text{Diagram 58} \end{array} = \begin{array}{c} \text{Diagram 59} \\ \text{Diagram 60} \end{array} - 2 \times \begin{array}{c} \text{Diagram 61} \\ \text{Diagram 62} \end{array} + 1 \times \begin{array}{c} \text{Diagram 63} \\ \text{Diagram 64} \end{array}, \quad (8.52)$$

$$\begin{array}{c} \text{Diagram 65} \\ \text{Diagram 66} \end{array} = \begin{array}{c} \text{Diagram 67} \\ \text{Diagram 68} \end{array} - 3 \times \begin{array}{c} \text{Diagram 69} \\ \text{Diagram 70} \end{array} + 3 \times \begin{array}{c} \text{Diagram 71} \\ \text{Diagram 72} \end{array}. \quad (8.53)$$

By this subtraction, we can thus determine the reduced contributions and then via (8.6) one obtains the ground-state energy. Note that the weights for the reduced contributions are independent of the order and can thus be determined once and for all, whereas the weights of the full contribution depend on the maximal order. Consequently, in this setting it is more convenient to obtain the weights and subtraction scheme in two separate steps.

The weights for the reduced contributions are determined in the same fashion as in 8.1.

We finally obtain the ground-state energy per plaquette

$$e_0 = \frac{1}{1} \times \begin{array}{c} \text{Diagram 73} \\ \text{Diagram 74} \end{array} + \frac{6}{2} \times \begin{array}{c} \text{Diagram 75} \\ \text{Diagram 76} \end{array} + \frac{9}{3} \times \begin{array}{c} \text{Diagram 77} \\ \text{Diagram 78} \end{array}$$

| max. order | no. graphs |
|------------|------------|
| 2 | 1 |
| 4 | 2 |
| 6 | 5 |
| 8 | 12 |
| 10 | 34 |
| 12 | 116 |
| 14 | 449 |
| 16 | 1897 |
| 18 | 8469 |
| 20 | 38959 |

TABLE 8.2: Number of graphs and thus initial states to calculate the ground-state energy per plaquette e_0 about the limit $\theta = \frac{\pi}{2}$. The obtained numbers take into account already all global symmetries. The relatively high orders achieved are due to the “act-twice” property. The large number of graphs originates from the fact that no local deformations can be used due to the large support of the perturbation operator.

$$+ \frac{18}{3} \times \begin{array}{c} \text{---} \circ \text{---} \\ \diagup \quad \diagdown \\ \circ \quad \circ \\ \diagdown \quad \diagup \\ \text{---} \circ \text{---} \end{array} + \frac{6}{3} \times \begin{array}{c} \text{---} \circ \text{---} \\ \diagup \quad \diagdown \\ \circ \quad \circ \\ \diagdown \quad \diagup \\ \text{---} \circ \text{---} \end{array} + \mathcal{O}(J_p^8). \quad (8.54)$$

We give the number of graphs for a given maximal order $2M$ in Table 8.2. Due to the “act-twice” property, graphs needed for maximal order $2M + 1$, are identical to the ones needed for order $2M$.

Again, it is not evident how to give a universal time estimate for the calculation. Roughly speaking, the time to calculate the contribution of the maximal order performed within this thesis takes about 1-2 hours. This relatively short timescale for this large maximal order is on one hand due to the fact that the sizes of the involved clusters are small and on the other hand that the perturbation generates relatively few states when acting in the low-energy sector (e.g. just two states when acting on a local ground state).

8.2.2 Graph expansions in the τ -phase

This limit shares a lot of details with the **1**-phase, apart from one important fact: the perturbation can create and annihilate (among others) single excitations on one link. Consequently, one does not have the “act-twice” property discussed for the other limit, which arose due to the fact that acting on a ground state always affects more than one link.

Additionally, one cannot use local deformations to identify different equivalent clusters. So one is left to calculate on linked clusters with up to M plaquettes for a calculation of order M for the ground-state energy as well as for the hopping elements.

We define analogously to (8.32)

$$\langle \text{gs} | H^{\text{eff}} \Big|_{\star} | \text{gs} \rangle = \text{Diagram 1}, \quad (8.55)$$

$$\langle \text{gs} | H^{\text{eff}} \Big|_{\star} | \text{gs} \rangle = \text{Diagram 2}, \quad (8.56)$$

$$\langle j | H^{\text{eff}} \Big|_{\star} | i \rangle = \text{Diagram 3}, \quad (8.57)$$

where for this limit, we also explicitly consider the external links to be able to represent correctly the impact of the excited states.

The graphs for this limit are the same as for the other non-topological limit, as the perturbation is the same. We also consider hopping elements, since the one-cluster approach suffers from the fact that the necessary cluster sizes become too large. The hopping elements describe the hopping from one link to another caused by the perturbation, which involves twelve links. Consequently, the number of hopping elements to determine grows rapidly with the order.

Additional computational effort arises as the perturbation has not only one non-trivial matrix element when acting on the local ground state, but 17, as it can generate any configuration of excitations on the internal links of plaquette acted on. Thus a considerable number of states is generated after a few applications of operators.

In order to deal with these challenges, we discuss the determination of the reduced contributions for the ground-state energy and the hopping elements separately. We determine the reduced contributions for the ground-state energy as for the other non-topological phase with the same subtraction scheme and we reach order nine in this limit.

For the hopping elements, we calculate the reduced hopping element directly, taking advantage of avoiding the generation of unnecessary contributions.

We obtain the expansion for the ground state energy per plaquette

$$e_0 = \frac{1}{1} \times \text{Diagram 4} + \frac{6}{2} \text{Diagram 5} + \mathcal{O}(J_p^3). \quad (8.58)$$

For the non-topological phases, we detailed the most important features of our implementation to be able to deal with the large extension of the support of the perturbation operators. The key idea is to express all quantities of interest (e.g. adjacency matrices) not directly in terms of the unperturbed degrees of freedom, but first in terms of the support of the perturbation, i.e. in plaquettes, and then to determine all supplementary information from this.

We also discussed two different implementations to obtain reduced quantities for each graph. The direct evaluation requires tracking of the locations, where the perturbation has acted. It allows to suppress unnecessary intermediate states. We presented briefly also the idea of the subtraction method, which allows to determine the reduced contributions without any further information and is thus particularly useful for intrinsic checks of the graph expansion as well as in the situation, where not many contributions can be sorted out during the calculation.

Summary and Outlook

*Begin at the beginning
and go on to the end; then stop.
- Lewis Carroll -*

Within this thesis, we studied phase transitions between several time-reversal invariant topologically ordered and topologically trivial phases.

Therefore, we considered the topologically ordered phases realized for the string-net Hamiltonian introduced by Levin and Wen [56]. In particular, we studied the topologically-ordered phases described by the topological quantum field theory for the Abelian doubled semions and the non-Abelian doubled Fibonacci and doubled Ising anyons. The phase transitions studied here are induced by a local perturbation, which drives the system into the topologically trivial phase.

Our investigation of the phase transitions reveals the first evidence for continuous phase transitions between topologically ordered phases featuring non-Abelian anyons and topologically trivial phases in two dimensions [104]. Thus our findings open the possibility to study the critical behavior of systems featuring non-Abelian anyons in dimensions that are of interest for the possible implementation of a topological quantum computer.

Additionally, the deduced critical exponents for the phase transitions out of the non-Abelian phases seem to not correspond to any known universality class. This indicates that the critical properties of these phase transitions may be distinct to the ones known for conventional phases transitions characterized by local order parameters.

To study further the critical properties in the context of topologically ordered phases, the investigation of other examples may yield further insights. In one spatial dimension, similar studies for chiral systems described by the quantum groups $SU(2)_k$ for larger values of k revealed a rich variety of different phase transitions [68]. Along the same lines,

an investigation for two-dimensional systems described by different quantum groups [54, 55, 65, 102] may provide more examples of different topological phases as well as examples of phase transitions out of topologically ordered phases. The setting proposed in this thesis is flexible enough to realize different doubled phases and thus allows for such an analysis.

Further investigation of the hypothesis of universal behavior in phase transitions out of topological phases can be performed beyond the study of different string-net models by the consideration of other models realizing the same phase. For example, string-net and toric code models are distinct but may realize the same topological phases. The study of critical properties for these models, which are defined on different lattices and from different microscopic degrees of freedom, may reveal whether there are universal properties of the phase transitions.

The methods developed in this thesis, especially the linked-cluster expansion presented in Chapter 8, allow for an investigation of different models featuring excitations with Abelian or non-Abelian exchange statistics and thus are suitable for more general investigations if suitable starting points of the quasi-particle picture are identified. For example, studies in analogy to the ones performed for quantum dimers models in Ref. [192] can be carried out in order to reveal the properties as the low-energy spectrum beyond the special case of string-net models.

Nevertheless, there are still open questions for the string-net models discussed within this thesis. A characterization of the respective topological phases in terms of the S -matrix, proposed in [16, 193], is possible at least for small perturbations. This can lead to more insights about the interplay between the properties of the topological quantum field theory and the entanglement properties.

In the study presented in the thesis, we considered the ground states and the single-excitation states to derive effective low-energy models. With this approach, we are able to investigate continuous phase transitions in agreement with the framework of condensate-induced phase transitions. However, the condensate-induced phase transitions rely on the condensation of single excitations. In order to verify this underlying statement, the role of interactions has to be investigated. This can be achieved by the investigation of low-energy multi-particle states. Analog studies have been performed for Abelian anyons [136] and revealed the existence of bound states in special cases. An investigation of this part of the low-energy spectrum would allow to infer the validity of the condensation picture for the phase transition.

The study of topologically ordered phases has been substantially helped by the study of one- and quasi one-dimensional systems as ladder geometries revealed some properties of two-dimensional systems [67, 71, 72]. A study of crossover between one and two dimensions by investigation of these ladder geometries for different ladder-widths with the methods presented in this thesis may even lead to further insights as larger system sizes (ladder widths) can be investigated and thus the impact of the boundaries on topologically ordered systems can be studied also on a quantitative level.

Another question in the context of condensate-induced phase transitions is whether there are phase transitions driven by the condensation of chiral particles. The charges in the string-net model are such chiral excitations and thus by investigating the impact of suitable perturbations, one may study the possibility of their condensation.

Of particular interest for the detection of topological order in experimental realizations are quantities like spectral densities, as these are accessible by spectroscopy experiments. These quantities have already been determined for the toric code in magnetic field [194] and Kitaev's honeycomb model [195] and may lead to more insights in the detection of non-Abelian topological order in real systems.

We have seen in Chapter 4.2.3 that there are two possibilities for a condensate-induced phase transition for the string-net model described by the doubled Ising anyons. By modifying the local perturbation, it is actually possible to drive the phase transition to a doubled \mathbb{Z}_2 phase [101]. Interpolating between the different perturbations may lead to multi-critical behavior similar to the case of the toric code in parallel fields [77–79] and thus lead to another example of multi-criticality in the context of topological phases.

All the points mentioned above, ranging from general considerations as universality in the absence of local order parameters to more specific ones as the investigation of particular phase transitions in specific models, show that the study of quantum critical behavior in the context of topological order is just at its beginning. Quantitative results as the ones obtained in this thesis yield further insights and thus stimulate further investigation of this fast moving and rich field at the interface of quantum information, condensed matter and mathematical physics.

Appendix A

Series expansions for the semion model

In the following, we give the series expansions for the various quantities discussed Section 5.1.

For notational convenience, we set $t = \tan \theta$. We give the numerical coefficient of the series with 24 digits.

A.1 Series expansions for the topological phase

ground-state energy e_0

For the topological phase ($\theta = 0$), we obtain the following expression for the ground-state energy per plaquette

$$\begin{aligned}
 \frac{e_0}{\cos \theta} &= -1. - 1.50000000000000000000000000000000 \cdot t - 0.37500000000000000000000000000000 \cdot t^2 \\
 &\quad - 0.3750000000000000000000000000000000 \cdot t^3 - 0.67968750000000000000000000000000 \cdot t^4 \\
 &\quad - 1.5468750000000000000000000000000000 \cdot t^5 - 4.17773437500000000000000000000000 \cdot t^6 \\
 &\quad - 12.33398437500000000000000000000000 \cdot t^7 - 39.063629150390625000000000000000 \cdot t^8 \\
 &\quad - 130.1117248535156250000000 \cdot t^9 - 451.023448944091796875000 \cdot t^{10} \\
 &\quad - 1613.77437404791514078776 \cdot t^{11} \\
 &= -1 - \frac{3}{2} \cdot t - \frac{3}{8} \cdot t^2 - \frac{3}{8} \cdot t^3 - \frac{87}{128} \cdot t^4 - \frac{99}{64} \cdot t^5 - \frac{2139}{512} \cdot t^6 - \frac{6315}{512} \cdot t^7 \\
 &\quad - \frac{1280037}{32768} \cdot t^8 - \frac{4263501}{32768} \cdot t^9 - \frac{118233091}{262144} \cdot t^{10} - \frac{40611961873}{25165824} \cdot t^{11}.
 \end{aligned} \tag{A.1}$$

This series coincides with the one obtained in Ref. [129] via

$$e_0^{\text{He}} = 2 \cdot e_0|_{t=x} + 2 + \frac{3}{2}x. \tag{A.2}$$

hopping elements and dispersion

With the definitions of Fig. 5.1, we obtain the hopping elements

$$\begin{aligned}
t_{\vec{0}} = & 1. + 0.75000000000000000000000000000000 \cdot t^2 + 1.50000000000000000000000000000000 \cdot t^3 \\
& + 3.23437500000000000000000000000000 \cdot t^4 + 9.46875000000000000000000000000000 \cdot t^5 \\
& + 30.09375000000000000000000000000000 \cdot t^6 + 104.285156250000000000000000000000 \cdot t^7 \\
& + 374.5241088867187500000000 \cdot t^8 + 1403.146270751953125000000 \cdot t^9 \\
& + 5383.30179977416992187500 \cdot t^{10} + 21149.4260612328847249349 \cdot t^{11}
\end{aligned} \tag{A.3}$$

$$\begin{aligned}
t_{\vec{n}_2} = & -0.50000000000000000000000000000000 \cdot t - 0.25000000000000000000000000000000 \cdot t^2 \\
& + 0.06250000000000000000000000000000 \cdot t^3 + 0.28125000000000000000000000000000 \cdot t^4 \\
& + 1.16406250000000000000000000000000 \cdot t^5 + 3.60937500000000000000000000000000 \cdot t^6 \\
& + 13.010498046875000000000000 \cdot t^7 + 44.696777343750000000000000 \cdot t^8 \\
& + 164.428810119628906250000 \cdot t^9 + 605.546660582224527994792 \cdot t^{10} \\
& + 2306.28812142213185628255 \cdot t^{11}
\end{aligned} \tag{A.4}$$

$$\begin{aligned}
t_{2\vec{n}_2} = & -0.12500000000000000000000000000000 \cdot t^2 - 0.37500000000000000000000000000000 \cdot t^3 \\
& - 0.64062500000000000000000000000000 \cdot t^4 - 1.14062500000000000000000000000000 \cdot t^5 \\
& - 2.17089843750000000000000000 \cdot t^6 - 3.907714843750000000000000 \cdot t^7 \\
& - 5.639038085937500000000000 \cdot t^8 + 3.16546249389648437500000 \cdot t^9 \\
& + 76.5140865643819173177083 \cdot t^{10} + 498.552775965796576605903 \cdot t^{11}
\end{aligned} \tag{A.5}$$

$$\begin{aligned}
t_{3\vec{n}_2} = & -0.06250000000000000000000000000000 \cdot t^3 - 0.46875000000000000000000000000000 \cdot t^4 \\
& - 1.4882812500000000000000000000 \cdot t^5 - 4.24218750000000000000000000000000 \cdot t^6 \\
& - 12.097778320312500000000000 \cdot t^7 - 35.455627441406250000000000 \cdot t^8 \\
& - 106.436784744262695312500 \cdot t^9 - 326.464408556620279947917 \cdot t^{10} \\
& - 1012.68701063262091742622 \cdot t^{11}
\end{aligned} \tag{A.6}$$

$$\begin{aligned}
t_{4\vec{n}_2} = & -0.03906250000000000000000000000000 \cdot t^4 - 0.54687500000000000000000000000000 \cdot t^5 \\
& - 2.7109375000000000000000000000 \cdot t^6 - 10.4318847656250000000000 \cdot t^7 \\
& - 37.115875244140625000000000 \cdot t^8 - 129.222908020019531250000 \cdot t^9 \\
& - 449.400380770365397135417 \cdot t^{10} - 1572.80865471892886691623 \cdot t^{11}
\end{aligned} \tag{A.7}$$

$$\begin{aligned}
t_{5\vec{n}_2} = & -0.02734375000000000000000000000000 \cdot t^5 - 0.61523437500000000000000000000000 \cdot t^6 \\
& - 4.4125976562500000000000000000 \cdot t^7 - 21.8605651855468750000000 \cdot t^8 \\
& - 93.8983821868896484375000 \cdot t^9 - 377.987742424011230468750 \cdot t^{10} \\
& - 1477.1400665479236178928 \cdot t^{11}
\end{aligned} \tag{A.8}$$

$$\begin{aligned}
t_{6\vec{n}_2} = & -0.020507812500000000000000000000 \cdot t^6 - 0.67675781250000000000000000000000 \cdot t^7 \\
& - 6.669799804687500000000000 \cdot t^8 - 41.4899940490722656250000 \cdot t^9 \\
& - 211.558639526367187500000 \cdot t^{10} - 973.772403717041015625000 \cdot t^{11}
\end{aligned} \tag{A.9}$$

$$\begin{aligned}
t_{7\vec{n}_2} = & -0.016113281250000000000000000000 \cdot t^7 - 0.73315429687500000000000000000000 \cdot t^8 \\
& - 9.54661560058593750000000 \cdot t^9 - 73.2607340812683105468750 \cdot t^{10} \\
& - 438.539537936449050903320 \cdot t^{11}
\end{aligned} \tag{A.10}$$

$$\begin{aligned}
t_{8\vec{n}_2} = & -0.01309204101562500000000000 \cdot t^8 - 0.78552246093750000000000000000000 \cdot t^9 \\
& - 13.0996780395507812500000 \cdot t^{10} - 122.200531065464019775391 \cdot t^{11}
\end{aligned} \tag{A.11}$$

$$\begin{aligned}
t_{9\vec{n}_2} = & -0.01091003417968750000000000 \cdot t^9 - 0.834617614746093750000000 \cdot t^{10} \\
& - 17.3805027008056640625000 \cdot t^{11}
\end{aligned} \tag{A.12}$$

$$t_{10\vec{n}_2} = -0.00927352905273437500000000 \cdot t^{10} - 0.880985260009765625000000 \cdot t^{11} \tag{A.13}$$

$$t_{11\vec{n}_2} = -0.00800895690917968750000000 \cdot t^{11} \tag{A.14}$$

$$\begin{aligned}
t_{\vec{n}_1+\vec{n}_2} = & -0.25000000000000000000000000000000 \cdot t^2 - 0.37500000000000000000000000000000 \cdot t^3 \\
& - 0.50000000000000000000000000000000 \cdot t^4 - 0.73437500000000000000000000000000 \cdot t^5
\end{aligned}$$

$$\begin{aligned}
& - 1.011718750000000000000000 \cdot t^6 - 0.359863281250000000000000 \cdot t^7 \\
& + 5.406188964843750000000000 \cdot t^8 + 39.2456626892089843750000 \cdot t^9 \\
& + 195.897086461385091145833 \cdot t^{10} + 905.313535816139645046658 \cdot t^{11}
\end{aligned} \tag{A.15}$$

$$\begin{aligned}
t_{\vec{n}_1+2\vec{n}_2} = & - 0.187500000000000000000000 \cdot t^3 - 0.6250000000000000000000 \cdot t^4 \\
& - 1.593750000000000000000000 \cdot t^5 - 4.0351562500000000000000 \cdot t^6 \\
& - 10.6092529296875000000000 \cdot t^7 - 29.0416259765625000000000 \cdot t^8 \\
& - 80.8363075256347656250000 \cdot t^9 - 227.717893759409586588542 \cdot t^{10} \\
& - 629.395159383614857991536 \cdot t^{11}
\end{aligned} \tag{A.16}$$

$$\begin{aligned}
t_{\vec{n}_1+3\vec{n}_2} = & - 0.156250000000000000000000 \cdot t^4 - 0.9570312500000000000000 \cdot t^5 \\
& - 3.583984375000000000000000 \cdot t^6 - 12.0117187500000000000000 \cdot t^7 \\
& - 39.2326660156250000000000 \cdot t^8 - 128.676366806030273437500 \cdot t^9 \\
& - 427.447437763214111328125 \cdot t^{10} - 1439.60862997836536831326 \cdot t^{11}
\end{aligned} \tag{A.17}$$

$$\begin{aligned}
t_{\vec{n}_1+4\vec{n}_2} = & - 0.136718750000000000000000 \cdot t^5 - 1.3535156250000000000000 \cdot t^6 \\
& - 6.948730468750000000000000 \cdot t^7 - 29.2557067871093750000000 \cdot t^8 \\
& - 113.533174514770507812500 \cdot t^9 - 426.75170898437500000000 \cdot t^{10} \\
& - 1585.90241499079598320855 \cdot t^{11}
\end{aligned} \tag{A.18}$$

$$\begin{aligned}
t_{\vec{n}_1+5\vec{n}_2} = & - 0.123046875000000000000000 \cdot t^6 - 1.8046875000000000000000 \cdot t^7 \\
& - 12.2636718750000000000000 \cdot t^8 - 63.2041854858398437500000 \cdot t^9 \\
& - 286.543255805969238281250 \cdot t^{10} - 1217.66795808076858520508 \cdot t^{11}
\end{aligned} \tag{A.19}$$

$$\begin{aligned}
t_{\vec{n}_1+6\vec{n}_2} = & - 0.112792968750000000000000 \cdot t^7 - 2.3041992187500000000000 \cdot t^8 \\
& - 20.1859130859375000000000 \cdot t^9 - 125.385822727979736328125 \cdot t^{10} \\
& - 657.463814467191696166992 \cdot t^{11}
\end{aligned} \tag{A.20}$$

$$\begin{aligned}
t_{\vec{n}_1+7\vec{n}_2} = & - 0.104736328125000000000000 \cdot t^8 - 2.8475189208984375000000 \cdot t^9 \\
& - 31.4438095092773437500000 \cdot t^{10} - 232.755758762359619140625 \cdot t^{11}
\end{aligned} \tag{A.21}$$

$$\begin{aligned}
t_{\vec{n}_1+8\vec{n}_2} = & - 0.098190307617187500000000 \cdot t^9 - 3.4312057495117187500000 \cdot t^{10} \\
& - 46.8299579620361328125000 \cdot t^{11}
\end{aligned} \tag{A.22}$$

$$t_{\vec{n}_1+9\vec{n}_2} = - 0.092735290527343750000000 \cdot t^{10} - 4.0525321960449218750000 \cdot t^{11} \tag{A.23}$$

$$t_{\vec{n}_1+10\vec{n}_2} = - 0.088098526000976562500000 \cdot t^{11} \tag{A.24}$$

$$\begin{aligned}
t_{2\vec{n}_1+2\vec{n}_2} = & - 0.234375000000000000000000 \cdot t^4 - 1.0937500000000000000000 \cdot t^5 \\
& - 3.837890625000000000000000 \cdot t^6 - 12.3198242187500000000000 \cdot t^7 \\
& - 39.1840820312500000000000 \cdot t^8 - 125.973030090332031250000 \cdot t^9 \\
& - 411.775950113932291666667 \cdot t^{10} - 1367.05790572696261935764 \cdot t^{11}
\end{aligned} \tag{A.25}$$

$$\begin{aligned}
t_{2\vec{n}_1+3\vec{n}_2} = & - 0.273437500000000000000000 \cdot t^5 - 1.8457031250000000000000 \cdot t^6 \\
& - 8.370605468750000000000000 \cdot t^7 - 32.7843627929687500000000 \cdot t^8 \\
& - 121.609603881835937500000 \cdot t^9 - 442.748262882232666015625 \cdot t^{10} \\
& - 1606.17204455865754021539 \cdot t^{11}
\end{aligned} \tag{A.26}$$

$$\begin{aligned}
t_{2\vec{n}_1+4\vec{n}_2} = & - 0.307617187500000000000000 \cdot t^6 - 2.9326171875000000000000 \cdot t^7 \\
& - 16.7292480468750000000000 \cdot t^8 - 78.2688560485839843750000 \cdot t^9 \\
& - 333.422058105468750000000 \cdot t^{10} - 1356.67053508758544921875 \cdot t^{11}
\end{aligned} \tag{A.27}$$

$$\begin{aligned}
t_{2\vec{n}_1+5\vec{n}_2} = & - 0.338378906250000000000000 \cdot t^7 - 4.3989257812500000000000 \cdot t^8 \\
& - 31.1006469726562500000000 \cdot t^9 - 171.519048213958740234375 \cdot t^{10} \\
& - 832.120862156152725219727 \cdot t^{11}
\end{aligned} \tag{A.28}$$

$$\begin{aligned}
t_{2\vec{n}_1+6\vec{n}_2} = & - 0.366577148437500000000000 \cdot t^8 - 6.2841796875000000000000 \cdot t^9 \\
& - 54.4121589660644531250000 \cdot t^{10} - 350.486615896224975585938 \cdot t^{11}
\end{aligned} \tag{A.29}$$

$$\begin{aligned}
t_{2\vec{n}_1+7\vec{n}_2} = & - 0.392761230468750000000000 \cdot t^9 - 8.6243820190429687500000 \cdot t^{10} \\
& - 90.4114532470703125000000 \cdot t^{11}
\end{aligned} \tag{A.30}$$

$$t_{2\vec{n}_1+8\vec{n}_2} = -0.417308807373046875000000 \cdot t^{10} - 11.4528083801269531250000 \cdot t^{11} \quad (\text{A.31})$$

$$t_{2\vec{n}_1+9\vec{n}_2} = -0.440492630004882812500000 \cdot t^{11} \quad (\text{A.32})$$

$$t_{3\vec{n}_1+3\vec{n}_2} = -0.410156250000000000000000 \cdot t^6 - 3.383789062500000000000000 \cdot t^7 \\ - 18.395507812500000000000000 \cdot t^8 - 83.4729766845703125000000 \cdot t^9 \\ - 348.776204109191894531250 \cdot t^{10} - 1399.64360278844833374023 \cdot t^{11} \quad (\text{A.33})$$

$$t_{3\vec{n}_1+4\vec{n}_2} = -0.563964843750000000000000 \cdot t^7 - 5.865234375000000000000000 \cdot t^8 \\ - 37.89138793945312500000000 \cdot t^9 - 197.860380649566650390625 \cdot t^{10} \\ - 926.142159551382064819336 \cdot t^{11} \quad (\text{A.34})$$

$$t_{3\vec{n}_1+5\vec{n}_2} = -0.733154296875000000000000 \cdot t^8 - 9.622650146484375000000000 \cdot t^9 \\ - 73.49217224121093750000000 \cdot t^{10} - 439.152867794036865234375 \cdot t^{11} \quad (\text{A.35})$$

$$t_{3\vec{n}_1+6\vec{n}_2} = -0.916442871093750000000000 \cdot t^9 - 15.0231170654296875000000 \cdot t^{10} \\ - 135.048494338989257812500 \cdot t^{11} \quad (\text{A.36})$$

$$t_{3\vec{n}_1+7\vec{n}_2} = -1.112823486328125000000000 \cdot t^{10} - 22.4651241302490234375000 \cdot t^{11} \quad (\text{A.37})$$

$$t_{3\vec{n}_1+8\vec{n}_2} = -1.321477890014648437500000 \cdot t^{11} \quad (\text{A.38})$$

$$t_{4\vec{n}_1+4\vec{n}_2} = -0.916442871093750000000000 \cdot t^8 - 10.9973144531250000000000 \cdot t^9 \\ - 80.87608337402343750000000 \cdot t^{10} - 471.840214133262634277344 \cdot t^{11} \quad (\text{A.39})$$

$$t_{4\vec{n}_1+5\vec{n}_2} = -1.374664306640625000000000 \cdot t^9 - 19.4744110107421875000000 \cdot t^{10} \\ - 163.324848175048828125000 \cdot t^{11} \quad (\text{A.40})$$

$$t_{4\vec{n}_1+6\vec{n}_2} = -1.947441101074218750000000 \cdot t^{10} - 32.7726516723632812500000 \cdot t^{11} \quad (\text{A.41})$$

$$t_{4\vec{n}_1+7\vec{n}_2} = -2.642955780029296875000000 \cdot t^{11} \quad (\text{A.42})$$

$$t_{5\vec{n}_1+5\vec{n}_2} = -2.336929321289062500000000 \cdot t^{10} - 37.0013809204101562500000 \cdot t^{11} \quad (\text{A.43})$$

$$t_{5\vec{n}_1+6\vec{n}_2} = -3.700138092041015625000000 \cdot t^{11}. \quad (\text{A.44})$$

The remaining hopping elements are related by lattice symmetries of the underlying triangular lattice and can be obtained via the relations

$$t_{\vec{r}} = t_{-\vec{r}}, \quad (\text{A.45})$$

$$t_{n_2\vec{n}_1+n_1\vec{n}_2} = t_{n_1\vec{n}_1+n_2\vec{n}_2}, \quad (\text{A.46})$$

$$t_{-n_2\vec{n}_1+(n_1+n_2)\vec{n}_2} = t_{n_1\vec{n}_1+n_2\vec{n}_2}, \quad (\text{A.47})$$

$$t_{(-n_1-n_2)\vec{n}_1+n_1\vec{n}_2} = t_{n_1\vec{n}_1+n_2\vec{n}_2}. \quad (\text{A.48})$$

The dispersion $\omega(\vec{k})$ has for $\theta > 0$ its minimum at $\vec{k} = 0$ and thus we obtain the gap

$$\frac{\Delta^+}{\cos \theta} = 1 - 3.000000000000000000000000 \cdot t - 3.000000000000000000000000 \cdot t^2 \\ - 5.250000000000000000000000 \cdot t^3 - 15.750000000000000000000000 \cdot t^4 \\ - 49.265625000000000000000000 \cdot t^5 - 173.3554687500000000000000 \cdot t^6 \\ - 627.6027832031250000000000 \cdot t^7 - 2397.71850585937500000000 \cdot t^8 \\ - 9328.93494415283203125000 \cdot t^9 - 37313.6442575454711914062 \cdot t^{10} \\ - 151392.490055541197458903 \cdot t^{11} \quad (\text{A.49})$$

$$= 1 - 3 \cdot t - 3 \cdot t^2 - \frac{21}{4} \cdot t^3 - \frac{63}{4} \cdot t^4 - \frac{3153}{64} \cdot t^5 - \frac{44379}{256} \cdot t^6 - \frac{2570661}{4096} \cdot t^7 \\ - \frac{9821055}{4096} \cdot t^8 - \frac{1222762161}{131072} \cdot t^9 - \frac{39126191841}{1048576} \cdot t^{10} - \frac{7619833519319}{50331648} \cdot t^{11}, \quad (\text{A.50})$$

whereas for $\theta < 0$, the minimum is located at $\vec{k} = \pm(\frac{2\pi}{3}, -\frac{2\pi}{3})$ and thus we obtain the gap

$$\frac{\Delta^-}{\cos \theta} = 1 + 1.500000000000000000000000 \cdot t + 0.375000000000000000000000 \cdot t^2$$

$$\begin{aligned}
& + 0.93750000000000000000000000000000 \cdot t^3 + 1.89843750000000000000000000000000 \cdot t^4 \\
& + 6.52734375000000000000000000000000 \cdot t^5 + 21.752929687500000000000000000000 \cdot t^6 \\
& + 79.519042968750000000000000000000 \cdot t^7 + 296.0393371582031250000000 \cdot t^8 \\
& + 1135.80865287780761718750 \cdot t^9 + 4438.45324659347534179688 \cdot t^{10} \\
& + 17653.5536835690339406331 \cdot t^{11}
\end{aligned} \tag{A.51}$$

$$\begin{aligned}
= & 1 + \frac{3}{2} \cdot t + \frac{3}{8} \cdot t^2 + \frac{15}{16} \cdot t^3 + \frac{243}{128} \cdot t^4 + \frac{1671}{256} \cdot t^5 + \frac{22275}{1024} \cdot t^6 + \frac{162855}{2048} \cdot t^7 \\
& + \frac{9700617}{32768} \cdot t^8 + \frac{595490847}{524288} \cdot t^9 + \frac{9308111103}{2097152} \cdot t^{10} + \frac{1777064899901}{100663296} \cdot t^{11}.
\end{aligned} \tag{A.52}$$

The coefficients of the series for Δ^+ (A.50) coincide with the ones given in Ref. [129] after the rescaling $\Delta^{\text{He}} = 2 \cdot \Delta^+$ up to the obvious error in the order nine coefficient. The coefficients of the series for Δ^- (A.52) coincide with the ones given in Ref. [133] for $t \rightarrow -2x$.

A.2 Series expansions for the 1-phase

ground-state energy e_0

For the topological phase ($\theta = \frac{\pi}{2}$), we obtain the following expression for the ground-state energy per plaquette

$$\begin{aligned}
\frac{e_0}{\sin \theta} = & -3. - 0.50000000000000000000000000000000 \cdot t^{-1} - 0.416666666666666666666666666667 \cdot 10^{-1} \cdot t^{-2} \\
& - 0.578703703703703703703704 \cdot 10^{-4} \cdot t^{-4} - 7.80790711346266901822457 \cdot 10^{-7} \cdot t^{-6} \\
& - 1.23107823611105556599804 \cdot 10^{-8} \cdot t^{-8} - 2.62701489676216894225737 \cdot 10^{-10} \cdot t^{-10} \\
& - 6.38456088193761406424490 \cdot 10^{-12} \cdot t^{-12} - 1.85303547423302779835841 \cdot 10^{-13} \cdot t^{-14} \\
& - 4.99918130665435430856152 \cdot 10^{-15} \cdot t^{-16} - 1.57645891633032307544926 \cdot 10^{-16} \cdot t^{-18}.
\end{aligned} \tag{A.53}$$

This series coincides with one given in Ref. [130].

hopping elements and dispersion

We give here the hopping elements up to order seven. Higher orders for the gap can be found e.g. in Ref. [130]. The other hopping elements can be obtained by the symmetry relations (A.48).

$$t_{\vec{0}} = 6 - \frac{1}{24} \cdot t^{-2} - \frac{7}{27648} \cdot t^{-4} + \frac{125663}{6967296000} \cdot t^{-6} + \mathcal{O}(t^{-8}) \tag{A.54}$$

$$t_{\vec{n}_2} = -\frac{1}{48} \cdot t^{-2} - \frac{1}{3456} \cdot t^{-4} + \frac{9499}{1592524800} \cdot t^{-6} + \mathcal{O}(t^{-8}) \tag{A.55}$$

$$t_{2\vec{n}_2} = -\frac{1}{55296} \cdot t^{-4} + \frac{67}{796262400} \cdot t^{-6} + \mathcal{O}(t^{-8}) \tag{A.56}$$

$$t_{3\vec{n}_2} = -\frac{217}{1592524800} \cdot t^{-6} + \mathcal{O}(t^{-8}) \tag{A.57}$$

$$t_{\vec{n}_1 + \vec{n}_2} = -\frac{1}{27648} \cdot t^{-4} - \frac{2791}{796262400} \cdot t^{-6} + \mathcal{O}(t^{-8}) \tag{A.58}$$

$$t_{\vec{n}_1 + 2\vec{n}_2} = -\frac{217}{530841600} \cdot t^{-6} + \mathcal{O}(t^{-8}). \tag{A.59}$$

The dispersion $\omega(\vec{k})$ has for $\theta > 0$ and $\theta < 0$ its minimum at $\vec{k} = 0$ and thus we obtain the gap

$$\frac{\Delta}{\sin \theta} = 6 - \frac{1}{6} \cdot t^{-2} - \frac{1}{432} \cdot t^{-4} + \frac{1501}{54432000} \cdot t^{-6} + \mathcal{O}(t^{-8}). \tag{A.60}$$

Appendix B

Series expansions for Fibonacci anyons

In the following, we give the series expansions for the various quantities discussed Section 5.2.

B.1 Series expansions for the topological phase

ground-state energy e_0

For the topological phase ($\theta = 0$), we obtain the following expression for the ground-state energy per plaquette.

$$\begin{aligned} \frac{e_0}{\cos \theta} = & -1. - 0.829179606750063091077248 \cdot t - 0.30000000000000000000000000000000 \cdot t^2 \\ & - 0.232917960675006309107725 \cdot t^3 - 0.375835921350012618215450 \cdot t^4 \\ & - 0.693462236992136224686426 \cdot t^5 - 1.51775783113839717794778 \cdot t^6 \\ & - 3.61589688790508917832884 \cdot t^7 - 9.25748294775309355458362 \cdot t^8 \\ & - 24.8964621013594868463679 \cdot t^9 - 69.6365374734577493488629 \cdot t^{10} \\ & - 200.825369723026929491604 \cdot t^{11}. \end{aligned} \tag{B.1}$$

hopping elements and dispersion

With the definitions of Fig. 5.1, we obtain the hopping elements

$$\begin{aligned} t_{\vec{0}} = & 1. - 0.141640786499873817845504 \cdot t^2 - 0.466252583997981085528067 \cdot 10^{-1} \cdot t^3 \\ & - 0.306594202199646689967412 \cdot t^4 - 0.507724231194690093317687 \cdot t^5 \\ & - 1.98261113839699255548697 \cdot t^6 - 5.17250789491702409870602 \cdot t^7 \\ & - 17.8773252365141724161415 \cdot t^8 - 53.9302405061167652662779 \cdot t^9 \\ & - 183.079533841477778644822 \cdot t^{10} \\ t_{\vec{n}_2} = & -0.276393202250021030359083 \cdot t - 0.20000000000000000000000000000000 \cdot t^2 \\ & - 0.258246851112416930081624 \cdot t^3 - 0.551755592679035927934370 \cdot t^4 \\ & - 1.10155425426524371553296 \cdot t^5 - 3.07765763344458978337354 \cdot t^6 \\ & - 7.88729182075149400723644 \cdot t^7 - 24.0328898739467053254430 \cdot t^8 \end{aligned} \tag{B.2}$$

$$- 69.4424027886691217299854 \cdot t^9 - 219.323166494970746856176 \cdot t^{10} \quad (\text{B.3})$$

$$\begin{aligned} t_{2\bar{n}_2} = & - 0.381966011250105151795413 \cdot 10^{-1} \cdot t^2 - 0.804257247250441637540735 \cdot 10^{-1} \cdot t^3 \\ & - 0.161720870791705222324985 \cdot t^4 - 0.425847962035092974389786 \cdot t^5 \\ & - 1.28036432183705022118028 \cdot t^6 - 3.52082396268926344921981 \cdot t^7 \\ & - 11.0299913871715386189683 \cdot t^8 - 32.3808443887924141916060 \cdot t^9 \\ & - 104.198135759730335478727 \cdot t^{10} \end{aligned} \quad (\text{B.4})$$

$$\begin{aligned} t_{3\bar{n}_2} = & - 0.105572809000084121436331 \cdot 10^{-1} \cdot t^3 - 0.563597022584167537576944 \cdot 10^{-1} \cdot t^4 \\ & - 0.173717721305049995419165 \cdot t^5 - 0.540756550613346027059142 \cdot t^6 \\ & - 1.56242415201506815048037 \cdot t^7 - 4.88424515549049707041029 \cdot t^8 \\ & - 14.6189236725596756548611 \cdot t^9 - 46.7837080838554814645440 \cdot t^{10} \end{aligned} \quad (\text{B.5})$$

$$\begin{aligned} t_{4\bar{n}_2} = & - 0.364745084375788638465599 \cdot 10^{-2} \cdot t^4 - 0.3308497748598430794444810 \cdot 10^{-1} \cdot t^5 \\ & - 0.142057373159266152205821 \cdot t^6 - 0.546196466900145178778252 \cdot t^7 \\ & - 1.98185880470609954783192 \cdot t^8 - 6.84738550844484565834790 \cdot t^9 \\ & - 23.5978561963701904055989 \cdot t^{10} \end{aligned} \quad (\text{B.6})$$

$$\begin{aligned} t_{5\bar{n}_2} = & - 0.141138286625809668824681 \cdot 10^{-2} \cdot t^5 - 0.201158426782593063342408 \cdot 10^{-1} \cdot t^6 \\ & - 0.115353483310139997768118 \cdot t^7 - 0.524473364555857824181961 \cdot t^8 \\ & - 2.13985018746450841732523 \cdot t^9 - 8.26682620877668321951283 \cdot t^{10} \end{aligned} \quad (\text{B.7})$$

$$\begin{aligned} t_{6\bar{n}_2} = & - 0.585144945008832750814706 \cdot 10^{-3} \cdot t^6 - 0.119176882843235126137407 \cdot 10^{-1} \cdot t^7 \\ & - 0.892119640111350012887621 \cdot 10^{-1} \cdot t^8 - 0.482875434922475978431369 \cdot t^9 \\ & - 2.25523734083541099322585 \cdot t^{10} \end{aligned} \quad (\text{B.8})$$

$$\begin{aligned} t_{7\bar{n}_2} = & - 0.254147276635063026821040 \cdot 10^{-3} \cdot t^7 - 0.703106100515988441002700 \cdot 10^{-2} \cdot t^8 \\ & - 0.666721604247304515044548 \cdot 10^{-1} \cdot t^9 - 0.424976581727582208856755 \cdot t^{10} \end{aligned} \quad (\text{B.9})$$

$$\begin{aligned} t_{8\bar{n}_2} = & - 0.114147441902466406560965 \cdot 10^{-3} \cdot t^8 - 0.411327815923552151027176 \cdot 10^{-2} \cdot t^9 \\ & - 0.484059136028509012304455 \cdot 10^{-1} \cdot t^{10} \end{aligned} \quad (\text{B.10})$$

$$t_{9\bar{n}_2} = - 0.157747884980354614220636 \cdot 10^{-3} \cdot t^9 - 0.478752360185602711803169 \cdot 10^{-2} \cdot t^{10} \quad (\text{B.11})$$

$$t_{10\bar{n}_2} = - 0.172948424208956557050026 \cdot 10^{-3} \cdot t^{10} \quad (\text{B.12})$$

$$\begin{aligned} t_{\bar{n}_1 + \bar{n}_2} = & - 0.763932022500210303590826 \cdot 10^{-1} \cdot t^2 - 0.975077640500378546463487 \cdot 10^{-1} \cdot t^3 \\ & - 0.272525735941566421955039 \cdot t^4 - 0.600371970898235799201321 \cdot t^5 \\ & - 1.73248177878844941997509 \cdot t^6 - 4.58294446149620266843477 \cdot t^7 \\ & - 14.2421041531861767801670 \cdot t^8 - 41.4649422871111522899885 \cdot t^9 \\ & - 132.304893340465256326020 \cdot t^{10} \end{aligned} \quad (\text{B.13})$$

$$\begin{aligned} t_{\bar{n}_1 + 2\bar{n}_2} = & - 0.316718427000252364308992 \cdot 10^{-1} \cdot t^3 - 0.961300899000925335799636 \cdot 10^{-1} \cdot t^4 \\ & - 0.253772375728318742183049 \cdot t^5 - 0.727564859149058832148180 \cdot t^6 \\ & - 2.01623520935345068394831 \cdot t^7 - 6.23491046308452615972553 \cdot t^8 \\ & - 18.3968412033347749770463 \cdot t^9 - 59.0999146932450267921766 \cdot t^{10} \end{aligned} \quad (\text{B.14})$$

$$\begin{aligned} t_{\bar{n}_1 + 3\bar{n}_2} = & - 0.145898033750315455386239 \cdot 10^{-1} \cdot t^4 - 0.688276809623228808068173 \cdot 10^{-1} \cdot t^5 \\ & - 0.260769110241328306661252 \cdot t^6 - 0.898462908385217026687590 \cdot t^7 \\ & - 3.05594603897855257039047 \cdot t^8 - 9.91304325640091125119255 \cdot t^9 \\ & - 32.7971889309124860778559 \cdot t^{10} \end{aligned} \quad (\text{B.15})$$

$$\begin{aligned} t_{\bar{n}_1 + 4\bar{n}_2} = & - 0.705691433129048344123407 \cdot 10^{-2} \cdot t^5 - 0.514270380105545806027688 \cdot 10^{-1} \cdot t^6 \\ & - 0.233054149087808156595000 \cdot t^7 - 0.945387931955848508118029 \cdot t^8 \\ & - 3.56789739160315633182691 \cdot t^9 - 13.0984732593139931634285 \cdot t^{10} \end{aligned} \quad (\text{B.16})$$

$$\begin{aligned} t_{\bar{n}_1 + 5\bar{n}_2} = & - 0.351086967005299650488824 \cdot 10^{-2} \cdot t^6 - 0.359255109770322519274984 \cdot 10^{-1} \cdot t^7 \\ & - 0.205712112222701764953352 \cdot t^8 - 0.969913825530281937670501 \cdot t^9 \\ & - 4.12056409640547979130013 \cdot t^{10} \end{aligned} \quad (\text{B.17})$$

$$t_{\bar{n}_1 + 6\bar{n}_2} = - 0.177903093644544118774728 \cdot 10^{-2} \cdot t^7 - 0.245615795851864470530205 \cdot 10^{-1} \cdot t^8$$

$$-0.171548870929062166427230 \cdot t^9 - 0.934837844078137167580934 \cdot t^{10} \quad (\text{B.18})$$

$$t_{\vec{n}_1+7\vec{n}_2} = -0.913179535219731252487721 \cdot 10^{-3} \cdot t^8 - 0.163426973509469375890074 \cdot 10^{-1} \cdot t^9 \\ - 0.138545341101261472560514 \cdot t^{10} \quad (\text{B.19})$$

$$t_{\vec{n}_1+8\vec{n}_2} = -0.141973096482319152798572 \cdot 10^{-2} \cdot t^9 - 0.213456248018639911759962 \cdot 10^{-1} \cdot t^{10} \quad (\text{B.20})$$

$$t_{\vec{n}_1+9\vec{n}_2} = -0.172948424208956557050026 \cdot 10^{-2} \cdot t^{10} \quad (\text{B.21})$$

$$t_{2\vec{n}_1+2\vec{n}_2} = -0.218847050625473183079359 \cdot 10^{-1} \cdot t^4 - 0.855992356152581126071409 \cdot 10^{-1} \cdot t^5 \\ - 0.322723201834968487591958 \cdot t^6 - 1.05861680184552551450558 \cdot t^7 \\ - 3.53188052243374435692284 \cdot t^8 - 11.1870369835744048458532 \cdot t^9 \\ - 36.5463370044321783454247 \cdot t^{10} \quad (\text{B.22})$$

$$t_{2\vec{n}_1+3\vec{n}_2} = -0.141138286625809668824681 \cdot 10^{-1} \cdot t^5 - 0.782779883307381856713200 \cdot 10^{-1} \cdot t^6 \\ - 0.325839772267923332367724 \cdot t^7 - 1.25818071366651594466509 \cdot t^8 \\ - 4.60117467542154252927394 \cdot t^9 - 16.5122399092724910779658 \cdot t^{10} \quad (\text{B.23})$$

$$t_{2\vec{n}_1+4\vec{n}_2} = -0.877717417513249126222059 \cdot 10^{-2} \cdot t^6 - 0.649073443323444531902840 \cdot 10^{-1} \cdot t^7 \\ - 0.333022836821848716470200 \cdot t^8 - 1.45124809904342637222716 \cdot t^9 \\ - 5.85935689475067270101426 \cdot t^{10} \quad (\text{B.24})$$

$$t_{2\vec{n}_1+5\vec{n}_2} = -0.533709280933632356324184 \cdot 10^{-2} \cdot t^7 - 0.517684299102857910993563 \cdot 10^{-1} \cdot t^8 \\ - 0.310501425140458593358384 \cdot t^9 - 1.55004238456344598333016 \cdot t^{10} \quad (\text{B.25})$$

$$t_{2\vec{n}_1+6\vec{n}_2} = -0.319612837326905938370702 \cdot 10^{-2} \cdot t^8 - 0.394528036680243874617043 \cdot 10^{-1} \cdot t^9 \\ - 0.280054208256104914145310 \cdot t^{10} \quad (\text{B.26})$$

$$t_{2\vec{n}_1+7\vec{n}_2} = -0.567892385929276611194288 \cdot 10^{-2} \cdot t^9 - 0.582048896889056485961234 \cdot 10^{-1} \cdot t^{10} \quad (\text{B.27})$$

$$t_{2\vec{n}_1+8\vec{n}_2} = -0.778267908940304506725119 \cdot 10^{-2} \cdot t^{10} \quad (\text{B.28})$$

$$t_{3\vec{n}_1+3\vec{n}_2} = -0.117028989001766550162941 \cdot 10^{-1} \cdot t^6 - 0.782409814063805453775581 \cdot 10^{-1} \cdot t^7 \\ - 0.390314474796729130272594 \cdot t^8 - 1.65539340079026540964864 \cdot t^9 \\ - 6.58023611241411782848196 \cdot t^{10} \quad (\text{B.29})$$

$$t_{3\vec{n}_1+4\vec{n}_2} = -0.889515468222720593873640 \cdot 10^{-2} \cdot t^7 - 0.734962030240667476307657 \cdot 10^{-1} \cdot t^8 \\ - 0.414203488408062479246243 \cdot t^9 - 1.98545003708950221274601 \cdot t^{10} \quad (\text{B.30})$$

$$t_{3\vec{n}_1+5\vec{n}_2} = -0.639225674653811876741405 \cdot 10^{-2} \cdot t^8 - 0.647082976878168596435513 \cdot 10^{-1} \cdot t^9 \\ - 0.421008277480882308155368 \cdot t^{10} \quad (\text{B.31})$$

$$t_{3\vec{n}_1+6\vec{n}_2} = -0.132508223383497875945334 \cdot 10^{-1} \cdot t^9 - 0.108633799755562863949760 \cdot t^{10} \quad (\text{B.32})$$

$$t_{3\vec{n}_1+7\vec{n}_2} = -0.207538109050747868460032 \cdot 10^{-1} \cdot t^{10} \quad (\text{B.33})$$

$$t_{4\vec{n}_1+4\vec{n}_2} = -0.799032093317264845926756 \cdot 10^{-2} \cdot t^8 - 0.759163137328899042064891 \cdot 10^{-1} \cdot t^9 \\ - 0.481308995651267623265606 \cdot t^{10} \quad (\text{B.34})$$

$$t_{4\vec{n}_1+5\vec{n}_2} = -0.198762335075246813918001 \cdot 10^{-1} \cdot t^9 \\ - 0.146644133922214106259923 \cdot t^{10} \quad (\text{B.35})$$

$$t_{4\vec{n}_1+6\vec{n}_2} = -0.363191690838808769805056 \cdot 10^{-1} \cdot t^{10} \quad (\text{B.36})$$

$$t_{5\vec{n}_1+5\vec{n}_2} = -0.435830029006570523766067 \cdot 10^{-1} \cdot t^{10}. \quad (\text{B.37})$$

The other hopping elements can be obtained by the symmetry relations (A.48).

The dispersion $\omega(\vec{k})$ has for $\theta > 0$ its minimum at $\vec{k} = 0$ and thus we obtain the gap

$$\frac{\Delta^+}{\cos \theta} = 1. - 1.65835921350012618215450 \cdot t - 2.02917960675006309107725 \cdot t^2 \\ - 3.10711309552514510947767 \cdot t^3 - 8.04259726696331282337854 \cdot t^4 \\ - 19.1624988542355849837791 \cdot t^5 - 58.3172040905260665826176 \cdot t^6 \\ - 164.442125764749511128228 \cdot t^7 - 528.531811101441199058830 \cdot t^8 \\ - 1615.45332802511250829292 \cdot t^9 - 5311.99645899926157253121 \cdot t^{10}, \quad (\text{B.38})$$

whereas for $\theta < 0$, the minimum is located at $\vec{k} = \pm(\frac{2\pi}{3}, -\frac{2\pi}{3})$ and thus we obtain the gap

$$\begin{aligned} \frac{\Delta^-}{\cos \theta} = & 1. + 0.829179606750063091077248 \cdot t + 0.114589803375031545538624 \cdot t^2 \\ & + 0.511033255612458990799789 \cdot t^3 + 0.404476040819411930552126 \cdot t^4 \\ & + 0.955438271995633484922172 \cdot t^5 + 1.78475247774001720568886 \cdot t^6 \\ & + 4.52396192042311525049865 \cdot t^7 + 11.1729466330618734690580 \cdot t^8 \\ & + 31.2002068100911363913816 \cdot t^9 + 89.4189513764563181889883 \cdot t^{10}. \end{aligned} \quad (\text{B.39})$$

B.2 Series expansions for the 1-phase

ground-state energy e_0

For the **1** phase ($\theta = \frac{\pi}{2}$), we obtain the following expression for the ground-state energy per plaquette.

$$\begin{aligned} \frac{e_0}{\sin \theta} = & -3. - 0.276393202250021030359083 \cdot t^{-1} - 0.33333333333333333333333333333333 \cdot 10^{-1} \cdot t^{-2} \\ & - 0.248451997499976632934353 \cdot 10^{-2} \cdot t^{-3} - 0.147309011464659210318636 \cdot 10^{-3} \cdot t^{-4} \\ & - 0.176251645032083273480020 \cdot 10^{-4} \cdot t^{-5} - 0.311482915054660249657726 \cdot 10^{-5} \cdot t^{-6} \\ & - 4.97495483230338463651490 \cdot 10^{-7} \cdot t^{-7} - 8.71294202575369519247181 \cdot 10^{-8} \cdot t^{-8} \\ & - 1.68047083130372398695520 \cdot 10^{-8} \cdot t^{-9} - 3.25279806074299317941897 \cdot 10^{-9} \cdot t^{-10} \\ & - 6.45224770766780340870601 \cdot 10^{-10} \cdot t^{-11} - 1.32894291749439876426994 \cdot 10^{-10} \cdot t^{-12} \\ & - 2.78653124402744019389761 \cdot 10^{-11} \cdot t^{-13} - 5.92393131555246254099121 \cdot 10^{-12} \cdot t^{-14} \\ & - 1.28029068152250493791582 \cdot 10^{-12} \cdot t^{-15} - 2.80343262342032185562862 \cdot 10^{-13} \cdot t^{-16} \\ & - 6.20299568622746687211081 \cdot 10^{-14} \cdot t^{-17} - 1.38624823359624468944367 \cdot 10^{-14} \cdot t^{-18} \\ & - 3.12554096212216427348799 \cdot 10^{-15} \cdot t^{-19} - 7.10025660183991072598726 \cdot 10^{-16} \cdot t^{-20}. \end{aligned} \quad (\text{B.40})$$

hopping elements and dispersion

With the definitions of Fig. 5.1, we obtain the hopping elements

$$\begin{aligned} t_{\vec{0}} = & 6. - 1. \cdot t^{-1} + 0.187435299583017877947094 \cdot 10^{-1} \cdot t^{-2} - 0.578842089590388187162962 \cdot 10^{-1} \cdot t^{-3} \\ & - 0.149146653743505240470545 \cdot 10^{-1} \cdot t^{-4} - 0.695912354451466808606340 \cdot 10^{-3} \cdot t^{-5} \\ & - 0.211566860915465138527270 \cdot 10^{-2} \cdot t^{-6} - 0.749385915953240835199622 \cdot 10^{-4} \cdot t^{-7} \\ & - 0.294739505503116743244296 \cdot 10^{-3} \cdot t^{-8} + .117236929525346125606034 \cdot 10^{-3} \cdot t^{-9} \\ & - 0.967859450032886842513143 \cdot 10^{-4} \cdot t^{-10} + .261994518488941101334499 \cdot 10^{-4} \cdot t^{-11} \end{aligned} \quad (\text{B.41})$$

$$\begin{aligned} t_{2\vec{n}_2} = & - 0.524316338958385909231040 \cdot 10^{-1} \cdot t^{-2} - 0.189066274190990623786420 \cdot 10^{-1} \cdot t^{-3} \\ & - 0.470391128699895065039709 \cdot 10^{-2} \cdot t^{-4} - 0.147613660837969425456556 \cdot 10^{-2} \cdot t^{-5} \\ & - 0.933392501538059637010548 \cdot 10^{-3} \cdot t^{-6} - 0.193865812848346541101498 \cdot 10^{-3} \cdot t^{-7} \\ & - 0.649791057279814650873279 \cdot 10^{-4} \cdot t^{-8} - 0.267955925966750967609429 \cdot 10^{-5} \cdot t^{-9} \\ & - 0.166317860657325408512926 \cdot 10^{-4} \cdot t^{-10} - 0.499957378474017175706321 \cdot 10^{-5} \cdot t^{-11} \end{aligned} \quad (\text{B.42})$$

$$t_{2\vec{n}_2} = - 0.139727107396835243038338 \cdot 10^{-3} \cdot t^{-4} - 0.134280203717502119723759 \cdot 10^{-3} \cdot t^{-5}$$

$$\begin{aligned}
& -0.492458712721092650153558 \cdot 10^{-4} \cdot t^{-6} - 0.323883447447409509227056 \cdot 10^{-4} \cdot t^{-7} \\
& -0.105734911316938641307931 \cdot 10^{-4} \cdot t^{-8} - 0.140344768573218682341937 \cdot 10^{-4} \cdot t^{-9} \\
& -0.740870447975950092526239 \cdot 10^{-5} \cdot t^{-10} - 0.707152002941310774152446 \cdot 10^{-5} \cdot t^{-11} \quad (\text{B.43})
\end{aligned}$$

$$\begin{aligned}
t_{3\bar{n}_2} = & -0.208536299987985784787439 \cdot 10^{-5} \cdot t^{-6} - 0.273670375295580569788355 \cdot 10^{-5} \cdot t^{-7} \\
& -0.260613497570593627354210 \cdot 10^{-5} \cdot t^{-8} - 0.165186003053570302418776 \cdot 10^{-5} \cdot t^{-9} \\
& -0.131707182609010001055197 \cdot 10^{-5} \cdot t^{-10} - 0.625339087885252907319405 \cdot 10^{-6} \cdot t^{-11} \quad (\text{B.44})
\end{aligned}$$

$$\begin{aligned}
t_{4\bar{n}_2} = & -0.101349121653913759767228 \cdot 10^{-7} \cdot t^{-8} - 0.241335022369316833346293 \cdot 10^{-7} \cdot t^{-9} \\
& -0.209894265060151254797359 \cdot 10^{-7} \cdot t^{-10} - 0.231615914030353046566143 \cdot 10^{-7} \cdot t^{-11} \quad (\text{B.45})
\end{aligned}$$

$$t_{5\bar{n}_2} = -0.258104894335177400542058 \cdot 10^{-9} \cdot t^{-10} - 0.563550589226373529676399 \cdot 10^{-9} \cdot t^{-11} \quad (\text{B.46})$$

$$\begin{aligned}
t_{\bar{n}_1+\bar{n}_2} = & -0.279454214793670486076675 \cdot 10^{-3} \cdot t^{-4} - 0.268560407435004239447518 \cdot 10^{-3} \cdot t^{-5} \\
& -0.120417923847500007846082 \cdot 10^{-3} \cdot t^{-6} - 0.101412926310923299853054 \cdot 10^{-3} \cdot t^{-7} \\
& -0.485510043217187014412262 \cdot 10^{-4} \cdot t^{-8} - 0.348804779168664799584680 \cdot 10^{-4} \cdot t^{-9} \\
& -0.952006899037934518443172 \cdot 10^{-5} \cdot t^{-10} - 0.832316956699560118517686 \cdot 10^{-5} \cdot t^{-11} \quad (\text{B.47})
\end{aligned}$$

$$\begin{aligned}
t_{\bar{n}_1+2\bar{n}_2} = & -0.625608899963957354362318 \cdot 10^{-5} \cdot t^{-6} - 0.821011125886741709365064 \cdot 10^{-5} \cdot t^{-7} \\
& -0.693557796656057604154798 \cdot 10^{-5} \cdot t^{-8} - 0.322286468281330202712094 \cdot 10^{-5} \cdot t^{-9} \\
& -0.215079017024405358708527 \cdot 10^{-5} \cdot t^{-10} - 0.692492851313765924432534 \cdot 10^{-6} \cdot t^{-11} \quad (\text{B.48})
\end{aligned}$$

$$\begin{aligned}
t_{\bar{n}_1+3\bar{n}_2} = & -0.405396486615655039068914 \cdot 10^{-7} \cdot t^{-8} - 0.965340089477267333385173 \cdot 10^{-7} \cdot t^{-9} \\
& -0.879703162772606638824929 \cdot 10^{-7} \cdot t^{-10} - 0.101623030855691290434328 \cdot 10^{-6} \cdot t^{-11} \quad (\text{B.49})
\end{aligned}$$

$$t_{\bar{n}_1+4\bar{n}_2} = -0.129052447167588700271029 \cdot 10^{-8} \cdot t^{-10} - 0.281775294613186764838200 \cdot 10^{-8} \cdot t^{-11} \quad (\text{B.50})$$

$$\begin{aligned}
t_{2\bar{n}_1+2\bar{n}_2} = & -0.608094729923482558603370 \cdot 10^{-7} \cdot t^{-8} - 0.144801013421590100007776 \cdot 10^{-6} \cdot t^{-9} \\
& -0.136542828485842850810935 \cdot 10^{-6} \cdot t^{-10} - 0.162558384797575706852191 \cdot 10^{-6} \cdot t^{-11} \quad (\text{B.51})
\end{aligned}$$

$$t_{2\bar{n}_1+3\bar{n}_2} = -0.258104894335177400542058 \cdot 10^{-8} \cdot t^{-10} - 0.563550589226373529676399 \cdot 10^{-8} \cdot t^{-11}. \quad (\text{B.52})$$

The other hopping elements can be obtained by the symmetry relations (A.48).

The dispersion $\omega(\vec{k})$ has for $\theta < \frac{\pi}{2}$ and $\theta > \frac{\pi}{2}$ its minimum at $\vec{k} = 0$ and thus we obtain the gap

$$\begin{aligned}
\frac{\Delta}{\sin \theta} = & 6. - 0.447213595499957939281835 \cdot t^{-1} - 0.591692546833459515487829 \cdot 10^{-1} \cdot t^{-2} \\
& - 0.153236820344965837350024 \cdot 10^{-1} \cdot t^{-3} - 0.182612884117949049296508 \cdot 10^{-2} \cdot t^{-4} \\
& - 0.214121856617765481253763 \cdot 10^{-3} \cdot t^{-5} - 0.705727330807649509929227 \cdot 10^{-4} \cdot t^{-6} \\
& - 0.771312026051760919224748 \cdot 10^{-5} \cdot t^{-7} - 0.182261920022292588988498 \cdot 10^{-5} \cdot t^{-8} \\
& - 0.173939403418595455023298 \cdot 10^{-6} \cdot t^{-9} - 0.106851219217155477742849 \cdot 10^{-6} \cdot t^{-10} \\
& - 0.158373280142416397082900 \cdot 10^{-7} \cdot t^{-11} \quad (\text{B.53})
\end{aligned}$$

B.3 Series expansions for the τ -phase

ground-state energy e_0

For the τ phase ($\theta = \frac{3\pi}{2}$), we obtain the following expression for the ground-state energy per plaquette

$$\frac{e_0}{-\sin \theta} = 0.301315561749642483895595 \cdot t^{-1} - 0.113204493325481999275817 \cdot t^{-2}$$

$$\begin{aligned}
& + 0.0280779746071996264677079 \cdot t^{-3} - 0.00450780949097200145030589 \cdot t^{-4} \\
& - 0.00303798844679437916619015 \cdot t^{-5} + 0.00459675253275435560375994 \cdot t^{-6} \\
& - 0.00163366937441387847322281 \cdot t^{-7} - 0.00228871711566844098308512 \cdot t^{-8} \\
& + 0.00381264213049307331396524 \cdot t^{-9}.
\end{aligned} \tag{B.54}$$

hopping elements and dispersion

With the definitions of Fig. 5.1, we obtain the hopping elements

$$t_{-5\vec{n}_1-\vec{n}_2}^{xx} = -0.181723785297851315000999 \cdot 10^{-5} \cdot t^{-6} \tag{B.55}$$

$$t_{-5\vec{n}_1}^{xx} = 0.529549932959660053710220 \cdot 10^{-5} \cdot t^{-6} \tag{B.56}$$

$$t_{-5\vec{n}_1+\vec{n}_2}^{xx} = 0.961775368330065795258258 \cdot 10^{-5} \cdot t^{-6} \tag{B.57}$$

$$t_{-5\vec{n}_1+2\vec{n}_2}^{xx} = -0.103449005689306208778332 \cdot 10^{-4} \cdot t^{-6} \tag{B.58}$$

$$t_{-5\vec{n}_1+3\vec{n}_2}^{xx} = -0.103449005689306208778332 \cdot 10^{-4} \cdot t^{-6} \tag{B.59}$$

$$t_{-5\vec{n}_1+4\vec{n}_2}^{xx} = 0.961775368330065795258258 \cdot 10^{-5} \cdot t^{-6} \tag{B.60}$$

$$t_{-5\vec{n}_1+5\vec{n}_2}^{xx} = 0.529549932959660053710220 \cdot 10^{-5} \cdot t^{-6} \tag{B.61}$$

$$t_{-5\vec{n}_1+6\vec{n}_2}^{xx} = -0.181723785297851315000999 \cdot 10^{-5} \cdot t^{-6} \tag{B.62}$$

$$t_{-4\vec{n}_1-2\vec{n}_2}^{xx} = -0.908618926489256575004996 \cdot 10^{-5} \cdot t^{-6} \tag{B.63}$$

$$t_{-4\vec{n}_1-\vec{n}_2}^{xx} = 0.114754160039893426049055 \cdot 10^{-4} \cdot t^{-5} + 0.361933210817370581410633 \cdot 10^{-4} \cdot t^{-6} \tag{B.64}$$

$$t_{-4\vec{n}_1}^{xx} = -0.447627643570088142536093 \cdot 10^{-4} \cdot t^{-5} - 0.121954072428841706377138 \cdot 10^{-6} \cdot t^{-6} \tag{B.65}$$

$$t_{-4\vec{n}_1+\vec{n}_2}^{xx} = -0.176154236726482919602624 \cdot 10^{-4} \cdot t^{-5} + 0.738993312915439904793731 \cdot 10^{-4} \cdot t^{-6} \tag{B.66}$$

$$t_{-4\vec{n}_1+2\vec{n}_2}^{xx} = 0.772455133766997297965047 \cdot 10^{-4} \cdot t^{-5} - 0.249410428512881467064340 \cdot 10^{-3} \cdot t^{-6} \tag{B.67}$$

$$t_{-4\vec{n}_1+3\vec{n}_2}^{xx} = -0.176154236726482919602624 \cdot 10^{-4} \cdot t^{-5} + 0.738993312915439904793731 \cdot 10^{-4} \cdot t^{-6} \tag{B.68}$$

$$t_{-4\vec{n}_1+4\vec{n}_2}^{xx} = -0.447627643570088142536093 \cdot 10^{-4} \cdot t^{-5} - 0.121954072428841706377138 \cdot 10^{-6} \cdot t^{-6} \tag{B.69}$$

$$t_{-4\vec{n}_1+5\vec{n}_2}^{xx} = 0.114754160039893426049055 \cdot 10^{-4} \cdot t^{-5} + 0.361933210817370581410633 \cdot 10^{-4} \cdot t^{-6} \tag{B.70}$$

$$t_{-4\vec{n}_1+6\vec{n}_2}^{xx} = -0.908618926489256575004996 \cdot 10^{-5} \cdot t^{-6} \tag{B.71}$$

$$t_{-3\vec{n}_1-3\vec{n}_2}^{xx} = -0.181723785297851315000999 \cdot 10^{-4} \cdot t^{-6} \tag{B.72}$$

$$t_{-3\vec{n}_1-2\vec{n}_2}^{xx} = 0.459016640159573704196219 \cdot 10^{-4} \cdot t^{-5} + 0.604137277311930870001592 \cdot 10^{-4} \cdot t^{-6} \tag{B.73}$$

$$\begin{aligned}
t_{-3\vec{n}_1-\vec{n}_2}^{xx} &= -0.776405003785464634873963 \cdot 10^{-4} \cdot t^{-4} - 0.180185105474197158838274 \cdot 10^{-3} \cdot t^{-5} \\
& + 0.286386194984530231538305 \cdot 10^{-3} \cdot t^{-6}
\end{aligned} \tag{B.74}$$

$$\begin{aligned}
t_{-3\vec{n}_1}^{xx} &= 0.373413500113866978664719 \cdot 10^{-3} \cdot t^{-4} - 0.195946957259888759173168 \cdot 10^{-3} \cdot t^{-5} \\
& - 0.625896065788473410302023 \cdot 10^{-3} \cdot t^{-6}
\end{aligned} \tag{B.75}$$

$$\begin{aligned}
t_{-3\vec{n}_1+\vec{n}_2}^{xx} &= -0.238035580603681576666227 \cdot 10^{-3} \cdot t^{-4} + 0.362402612311765078704201 \cdot 10^{-3} \cdot t^{-5} \\
& - 0.898017682089430936195628 \cdot 10^{-4} \cdot t^{-6}
\end{aligned} \tag{B.76}$$

$$\begin{aligned}
t_{-3\vec{n}_1+2\vec{n}_2}^{xx} &= -0.238035580603681576666227 \cdot 10^{-3} \cdot t^{-4} + 0.362402612311765078704201 \cdot 10^{-3} \cdot t^{-5} \\
& - 0.898017682089430936195628 \cdot 10^{-4} \cdot t^{-6}
\end{aligned} \tag{B.77}$$

$$\begin{aligned}
t_{-3\vec{n}_1+3\vec{n}_2}^{xx} &= 0.373413500113866978664719 \cdot 10^{-3} \cdot t^{-4} - 0.195946957259888759173168 \cdot 10^{-3} \cdot t^{-5} \\
& - 0.625896065788473410302023 \cdot 10^{-3} \cdot t^{-6}
\end{aligned} \tag{B.78}$$

$$\begin{aligned}
t_{-3\vec{n}_1+4\vec{n}_2}^{xx} &= -0.776405003785464634873963 \cdot 10^{-4} \cdot t^{-4} - 0.180185105474197158838274 \cdot 10^{-3} \cdot t^{-5} \\
& + 0.286386194984530231538305 \cdot 10^{-3} \cdot t^{-6}
\end{aligned} \tag{B.79}$$

$$t_{-3\vec{n}_1+5\vec{n}_2}^{xx} = 0.459016640159573704196219 \cdot 10^{-4} \cdot t^{-5} + 0.604137277311930870001592 \cdot 10^{-4} \cdot t^{-6} \tag{B.80}$$

$$t_{-3\vec{n}_1+6\vec{n}_2}^{xx} = -0.181723785297851315000999 \cdot 10^{-4} \cdot t^{-6} \tag{B.81}$$

$$t_{-2\vec{n}_1-4\vec{n}_2}^{xx} = -0.181723785297851315000999 \cdot 10^{-4} \cdot t^{-6} \quad (\text{B.82})$$

$$t_{-2\vec{n}_1-3\vec{n}_2}^{xx} = 0.688524960239360556294329 \cdot 10^{-4} \cdot t^{-5} + 0.554525655720858586617909 \cdot 10^{-4} \cdot t^{-6} \quad (\text{B.83})$$

$$t_{-2\vec{n}_1-2\vec{n}_2}^{xx} = -0.232921501135639390462189 \cdot 10^{-3} \cdot t^{-4} - 0.181083506430596661823657 \cdot 10^{-3} \cdot t^{-5} \\ + 0.365322440833618684178375 \cdot 10^{-3} \cdot t^{-6} \quad (\text{B.84})$$

$$t_{-2\vec{n}_1-\vec{n}_2}^{xx} = 0.588337100159830729028012 \cdot 10^{-3} \cdot t^{-3} + 0.346398377708810642111611 \cdot 10^{-3} \cdot t^{-4} \\ - 0.351152446156008408494839 \cdot 10^{-3} \cdot t^{-5} - 0.682907473392500010424202 \cdot 10^{-3} \cdot t^{-6} \quad (\text{B.85})$$

$$t_{-2\vec{n}_1}^{xx} = -0.327251092267193924955251 \cdot 10^{-2} \cdot t^{-3} + 0.323733521689035669814616 \cdot 10^{-2} \cdot t^{-4} \\ - 0.149586777640616038787487 \cdot 10^{-2} \cdot t^{-5} - 0.119309261351886905246614 \cdot 10^{-2} \cdot t^{-6} \quad (\text{B.86})$$

$$t_{-2\vec{n}_1+\vec{n}_2}^{xx} = 0.477227060701572778996641 \cdot 10^{-2} \cdot t^{-3} - 0.746990011236562397693934 \cdot 10^{-2} \cdot t^{-4} \\ + 0.639024181690310554303429 \cdot 10^{-2} \cdot t^{-5} - 0.362795530457435173874305 \cdot 10^{-2} \cdot t^{-6} \quad (\text{B.87})$$

$$t_{-2\vec{n}_1+2\vec{n}_2}^{xx} = -0.327251092267193924955251 \cdot 10^{-2} \cdot t^{-3} + 0.323733521689035669814616 \cdot 10^{-2} \cdot t^{-4} \\ - 0.149586777640616038787487 \cdot 10^{-2} \cdot t^{-5} - 0.119309261351886905246614 \cdot 10^{-2} \cdot t^{-6} \quad (\text{B.88})$$

$$t_{-2\vec{n}_1+3\vec{n}_2}^{xx} = 0.588337100159830729028012 \cdot 10^{-3} \cdot t^{-3} + 0.346398377708810642111611 \cdot 10^{-3} \cdot t^{-4} \\ - 0.351152446156008408494839 \cdot 10^{-3} \cdot t^{-5} - 0.682907473392500010424202 \cdot 10^{-3} \cdot t^{-6} \quad (\text{B.89})$$

$$t_{-2\vec{n}_1+4\vec{n}_2}^{xx} = -0.232921501135639390462189 \cdot 10^{-3} \cdot t^{-4} - 0.181083506430596661823657 \cdot 10^{-3} \cdot t^{-5} \\ + 0.365322440833618684178375 \cdot 10^{-3} \cdot t^{-6} \quad (\text{B.90})$$

$$t_{-2\vec{n}_1+5\vec{n}_2}^{xx} = 0.688524960239360556294329 \cdot 10^{-4} \cdot t^{-5} + 0.554525655720858586617909 \cdot 10^{-4} \cdot t^{-6} \quad (\text{B.91})$$

$$t_{-2\vec{n}_1+6\vec{n}_2}^{xx} = -0.181723785297851315000999 \cdot 10^{-4} \cdot t^{-6} \quad (\text{B.92})$$

$$t_{-\vec{n}_1-5\vec{n}_2}^{xx} = -0.908618926489256575004996 \cdot 10^{-5} \cdot t^{-6} \quad (\text{B.93})$$

$$t_{-\vec{n}_1-4\vec{n}_2}^{xx} = 0.459016640159573704196219 \cdot 10^{-4} \cdot t^{-5} + 0.388735463646651204517965 \cdot 10^{-4} \cdot t^{-6} \quad (\text{B.94})$$

$$t_{-\vec{n}_1-3\vec{n}_2}^{xx} = -0.232921501135639390462189 \cdot 10^{-3} \cdot t^{-4} - 0.155970356379276811360361 \cdot 10^{-3} \cdot t^{-5} \\ + 0.311055042433497000599563 \cdot 10^{-3} \cdot t^{-6} \quad (\text{B.95})$$

$$t_{-\vec{n}_1-2\vec{n}_2}^{xx} = 0.117667420031966145805602 \cdot 10^{-2} \cdot t^{-3} + 0.213503988724726916954670 \cdot 10^{-3} \cdot t^{-4} \\ - 0.163569339246820384226204 \cdot 10^{-2} \cdot t^{-5} + 0.718667639479322988988327 \cdot 10^{-3} \cdot t^{-6} \quad (\text{B.96})$$

$$t_{-\vec{n}_1-\vec{n}_2}^{xx} = -0.557280900008412143633053 \cdot 10^{-2} \cdot t^{-2} - 0.419735359449249455919311 \cdot 10^{-3} \cdot t^{-3} \\ - 0.227023316877688790456058 \cdot 10^{-2} \cdot t^{-4} + 0.477180093825364496364849 \cdot 10^{-2} \cdot t^{-5} \\ - 0.473705986999049906338227 \cdot 10^{-2} \cdot t^{-6} \quad (\text{B.97})$$

$$t_{-\vec{n}_1}^{xx} = 0.951949424901157312311624 \cdot 10^{-2} \cdot t^{-2} - 0.747624257671281075055057 \cdot 10^{-2} \cdot t^{-3} \\ - 0.105683535487409915924913 \cdot 10^{-2} \cdot t^{-4} + 0.317422583970608684720011 \cdot 10^{-2} \cdot t^{-5} \\ - 0.524079045120963932991959 \cdot 10^{-2} \cdot t^{-6} \quad (\text{B.98})$$

$$t_{-\vec{n}_1+\vec{n}_2}^{xx} = 0.951949424901157312311624 \cdot 10^{-2} \cdot t^{-2} - 0.747624257671281075055057 \cdot 10^{-2} \cdot t^{-3} \\ - 0.105683535487409915924913 \cdot 10^{-2} \cdot t^{-4} + 0.317422583970608684720011 \cdot 10^{-2} \cdot t^{-5} \\ - 0.524079045120963932991959 \cdot 10^{-2} \cdot t^{-6} \quad (\text{B.99})$$

$$t_{-\vec{n}_1+2\vec{n}_2}^{xx} = -0.557280900008412143633053 \cdot 10^{-2} \cdot t^{-2} - 0.419735359449249455919311 \cdot 10^{-3} \cdot t^{-3} \\ - 0.227023316877688790456058 \cdot 10^{-2} \cdot t^{-4} + 0.477180093825364496364849 \cdot 10^{-2} \cdot t^{-5} \\ - 0.473705986999049906338227 \cdot 10^{-2} \cdot t^{-6} \quad (\text{B.100})$$

$$t_{-\vec{n}_1+3\vec{n}_2}^{xx} = 0.117667420031966145805602 \cdot 10^{-2} \cdot t^{-3} + 0.213503988724726916954670 \cdot 10^{-3} \cdot t^{-4} \\ - 0.163569339246820384226204 \cdot 10^{-2} \cdot t^{-5} + 0.718667639479322988988327 \cdot 10^{-3} \cdot t^{-6} \quad (\text{B.101})$$

$$t_{-\vec{n}_1+4\vec{n}_2}^{xx} = -0.232921501135639390462189 \cdot 10^{-3} \cdot t^{-4} - 0.155970356379276811360361 \cdot 10^{-3} \cdot t^{-5} \\ + 0.311055042433497000599563 \cdot 10^{-3} \cdot t^{-6} \quad (\text{B.102})$$

$$t_{-\vec{n}_1+5\vec{n}_2}^{xx} = 0.459016640159573704196219 \cdot 10^{-4} \cdot t^{-5} + 0.388735463646651204517965 \cdot 10^{-4} \cdot t^{-6} \quad (\text{B.103})$$

$$t_{-\vec{n}_1+6\vec{n}_2}^{xx} = -0.908618926489256575004996 \cdot 10^{-5} \cdot t^{-6} \quad (\text{B.104})$$

$$t_{-6\vec{n}_2}^{xx} = -0.181723785297851315000999 \cdot 10^{-5} \cdot t^{-6} \quad (\text{B.105})$$

$$t_{-5\vec{n}_2}^{xx} = 0.114754160039893426049055 \cdot 10^{-4} \cdot t^{-5} + 0.385069750673932543615370 \cdot 10^{-5} \cdot t^{-6} \quad (\text{B.106})$$

$$t_{-4\bar{n}_2}^{xx} = -0.776405003785464634873963 \cdot 10^{-4} \cdot t^{-4} - 0.644075270499111237017463 \cdot 10^{-4} \cdot t^{-5} \\ + 0.103872962092428672078990 \cdot 10^{-3} \cdot t^{-6} \quad (\text{B.107})$$

$$t_{-3\bar{n}_2}^{xx} = 0.588337100159830729028012 \cdot 10^{-3} \cdot t^{-3} + 0.110660224382454286956223 \cdot 10^{-3} \cdot t^{-4} \\ - 0.147852419912244622637577 \cdot 10^{-3} \cdot t^{-5} - 0.143923159259271323547389 \cdot 10^{-2} \cdot t^{-6} \quad (\text{B.108})$$

$$t_{-2\bar{n}_2}^{xx} = -0.557280900008412143633053 \cdot 10^{-2} \cdot t^{-2} - 0.430452856461170362514866 \cdot 10^{-2} \cdot t^{-3} \\ + 0.414293336781008673731188 \cdot 10^{-2} \cdot t^{-4} - 0.129643993879778321553960 \cdot 10^{-2} \cdot t^{-5} \\ - 0.143608789139510590723459 \cdot 10^{-2} \cdot t^{-6} \quad (\text{B.109})$$

$$t_{-\bar{n}_2}^{xx} = 0.105572809000084121436331 \cdot t^{-1} - 0.366891015028180681170728 \cdot 10^{-1} \cdot t^{-2} \\ - 0.232445691056920962382703 \cdot 10^{-1} \cdot t^{-3} + 0.144322573584726778543351 \cdot 10^{-1} \cdot t^{-4} \\ - 0.216830618787032024986157 \cdot 10^{-2} \cdot t^{-5} - 0.450239404872368613385934 \cdot 10^{-2} \cdot t^{-6} \quad (\text{B.110})$$

$$t_0^{xx} = 1 - 0.180339887498948482045868 \cdot t^{-1} + 0.981984037163864760662581 \cdot 10^{-1} \cdot t^{-2} \\ - 0.149188223162105760410718 \cdot t^{-3} + 0.555480182906295683843826 \cdot 10^{-1} \cdot t^{-4} \\ + 0.578104903547281459136771 \cdot 10^{-1} \cdot t^{-5} - 0.105103788127556625909095 \cdot t^{-6} \quad (\text{B.111})$$

$$t_{\bar{n}_2}^{xx} = 0.105572809000084121436331 \cdot t^{-1} - 0.366891015028180681170728 \cdot 10^{-1} \cdot t^{-2} \\ - 0.232445691056920962382703 \cdot 10^{-1} \cdot t^{-3} + 0.144322573584726778543351 \cdot 10^{-1} \cdot t^{-4} \\ - 0.216830618787032024986157 \cdot 10^{-2} \cdot t^{-5} - 0.450239404872368613385934 \cdot 10^{-2} \cdot t^{-6} \quad (\text{B.112})$$

$$t_{2\bar{n}_2}^{xx} = -0.557280900008412143633053 \cdot 10^{-2} \cdot t^{-2} - 0.430452856461170362514866 \cdot 10^{-2} \cdot t^{-3} \\ + 0.414293336781008673731188 \cdot 10^{-2} \cdot t^{-4} - 0.129643993879778321553960 \cdot 10^{-2} \cdot t^{-5} \\ - 0.143608789139510590723459 \cdot 10^{-2} \cdot t^{-6} \quad (\text{B.113})$$

$$t_{3\bar{n}_2}^{xx} = 0.588337100159830729028012 \cdot 10^{-3} \cdot t^{-3} + 0.110660224382454286956223 \cdot 10^{-3} \cdot t^{-4} \\ - 0.147852419912244622637577 \cdot 10^{-3} \cdot t^{-5} - 0.143923159259271323547389 \cdot 10^{-2} \cdot t^{-6} \quad (\text{B.114})$$

$$t_{4\bar{n}_2}^{xx} = -0.776405003785464634873963 \cdot 10^{-4} \cdot t^{-4} - 0.644075270499111237017463 \cdot 10^{-4} \cdot t^{-5} \\ + 0.103872962092428672078990 \cdot 10^{-3} \cdot t^{-6} \quad (\text{B.115})$$

$$t_{5\bar{n}_2}^{xx} = 0.114754160039893426049055 \cdot 10^{-4} \cdot t^{-5} + 0.385069750673932543615370 \cdot 10^{-5} \cdot t^{-6} \quad (\text{B.116})$$

$$t_{6\bar{n}_2}^{xx} = -0.181723785297851315000999 \cdot 10^{-5} \cdot t^{-6} \quad (\text{B.117})$$

$$t_{\bar{n}_1-6\bar{n}_2}^{xx} = -0.908618926489256575004996 \cdot 10^{-5} \cdot t^{-6} \quad (\text{B.118})$$

$$t_{\bar{n}_1-5\bar{n}_2}^{xx} = 0.459016640159573704196219 \cdot 10^{-4} \cdot t^{-5} + 0.388735463646651204517965 \cdot 10^{-4} \cdot t^{-6} \quad (\text{B.119})$$

$$t_{\bar{n}_1-4\bar{n}_2}^{xx} = -0.232921501135639390462189 \cdot 10^{-3} \cdot t^{-4} - 0.155970356379276811360361 \cdot 10^{-3} \cdot t^{-5} \\ + 0.311055042433497000599563 \cdot 10^{-3} \cdot t^{-6} \quad (\text{B.120})$$

$$t_{\bar{n}_1-3\bar{n}_2}^{xx} = 0.117667420031966145805602 \cdot 10^{-2} \cdot t^{-3} + 0.213503988724726916954670 \cdot 10^{-3} \cdot t^{-4} \\ - 0.163569339246820384226204 \cdot 10^{-2} \cdot t^{-5} + 0.718667639479322988988327 \cdot 10^{-3} \cdot t^{-6} \quad (\text{B.121})$$

$$t_{\bar{n}_1-2\bar{n}_2}^{xx} = -0.557280900008412143633053 \cdot 10^{-2} \cdot t^{-2} - 0.419735359449249455919311 \cdot 10^{-3} \cdot t^{-3} \\ - 0.227023316877688790456058 \cdot 10^{-2} \cdot t^{-4} + 0.477180093825364496364849 \cdot 10^{-2} \cdot t^{-5} \\ - 0.473705986999049906338227 \cdot 10^{-2} \cdot t^{-6} \quad (\text{B.122})$$

$$t_{\bar{n}_1-\bar{n}_2}^{xx} = 0.951949424901157312311624 \cdot 10^{-2} \cdot t^{-2} - 0.747624257671281075055057 \cdot 10^{-2} \cdot t^{-3} \\ - 0.105683535487409915924913 \cdot 10^{-2} \cdot t^{-4} + 0.317422583970608684720011 \cdot 10^{-2} \cdot t^{-5} \\ - 0.524079045120963932991959 \cdot 10^{-2} \cdot t^{-6} \quad (\text{B.123})$$

$$t_{\bar{n}_1}^{xx} = 0.951949424901157312311624 \cdot 10^{-2} \cdot t^{-2} - 0.747624257671281075055057 \cdot 10^{-2} \cdot t^{-3} \\ - 0.105683535487409915924913 \cdot 10^{-2} \cdot t^{-4} + 0.317422583970608684720011 \cdot 10^{-2} \cdot t^{-5} \\ - 0.524079045120963932991959 \cdot 10^{-2} \cdot t^{-6} \quad (\text{B.124})$$

$$t_{\bar{n}_1+\bar{n}_2}^{xx} = -0.557280900008412143633053 \cdot 10^{-2} \cdot t^{-2} - 0.419735359449249455919311 \cdot 10^{-3} \cdot t^{-3} \\ - 0.227023316877688790456058 \cdot 10^{-2} \cdot t^{-4} + 0.477180093825364496364849 \cdot 10^{-2} \cdot t^{-5} \\ - 0.473705986999049906338227 \cdot 10^{-2} \cdot t^{-6} \quad (\text{B.125})$$

$$t_{\bar{n}_1+2\bar{n}_2}^{xx} = 0.117667420031966145805602 \cdot 10^{-2} \cdot t^{-3} + 0.213503988724726916954670 \cdot 10^{-3} \cdot t^{-4} \\ - 0.163569339246820384226204 \cdot 10^{-2} \cdot t^{-5} + 0.718667639479322988988327 \cdot 10^{-3} \cdot t^{-6} \quad (\text{B.126})$$

$$t_{\vec{n}_1+3\vec{n}_2}^{xx} = -0.232921501135639390462189 \cdot 10^{-3} \cdot t^{-4} - 0.155970356379276811360361 \cdot 10^{-3} \cdot t^{-5} + 0.311055042433497000599563 \cdot 10^{-3} \cdot t^{-6} \quad (\text{B.127})$$

$$t_{\vec{n}_1+4\vec{n}_2}^{xx} = 0.459016640159573704196219 \cdot 10^{-4} \cdot t^{-5} + 0.388735463646651204517965 \cdot 10^{-4} \cdot t^{-6} \quad (\text{B.128})$$

$$t_{\vec{n}_1+5\vec{n}_2}^{xx} = -0.908618926489256575004996 \cdot 10^{-5} \cdot t^{-6} \quad (\text{B.129})$$

$$t_{2\vec{n}_1-6\vec{n}_2}^{xx} = -0.181723785297851315000999 \cdot 10^{-4} \cdot t^{-6} \quad (\text{B.130})$$

$$t_{2\vec{n}_1-5\vec{n}_2}^{xx} = 0.688524960239360556294329 \cdot 10^{-4} \cdot t^{-5} + 0.554525655720858586617909 \cdot 10^{-4} \cdot t^{-6} \quad (\text{B.131})$$

$$t_{2\vec{n}_1-4\vec{n}_2}^{xx} = -0.232921501135639390462189 \cdot 10^{-3} \cdot t^{-4} - 0.181083506430596661823657 \cdot 10^{-3} \cdot t^{-5} + 0.365322440833618684178375 \cdot 10^{-3} \cdot t^{-6} \quad (\text{B.132})$$

$$t_{2\vec{n}_1-3\vec{n}_2}^{xx} = 0.588337100159830729028012 \cdot 10^{-3} \cdot t^{-3} + 0.346398377708810642111611 \cdot 10^{-3} \cdot t^{-4} - 0.351152446156008408494839 \cdot 10^{-3} \cdot t^{-5} - 0.682907473392500010424202 \cdot 10^{-3} \cdot t^{-6} \quad (\text{B.133})$$

$$t_{2\vec{n}_1-2\vec{n}_2}^{xx} = -0.327251092267193924955251 \cdot 10^{-2} \cdot t^{-3} + 0.323733521689035669814616 \cdot 10^{-2} \cdot t^{-4} - 0.149586777640616038787487 \cdot 10^{-2} \cdot t^{-5} - 0.119309261351886905246614 \cdot 10^{-2} \cdot t^{-6} \quad (\text{B.134})$$

$$t_{2\vec{n}_1-\vec{n}_2}^{xx} = 0.477227060701572778996641 \cdot 10^{-2} \cdot t^{-3} - 0.746990011236562397693934 \cdot 10^{-2} \cdot t^{-4} + 0.639024181690310554303429 \cdot 10^{-2} \cdot t^{-5} - 0.362795530457435173874305 \cdot 10^{-2} \cdot t^{-6} \quad (\text{B.135})$$

$$t_{2\vec{n}_1}^{xx} = -0.327251092267193924955251 \cdot 10^{-2} \cdot t^{-3} + 0.323733521689035669814616 \cdot 10^{-2} \cdot t^{-4} - 0.149586777640616038787487 \cdot 10^{-2} \cdot t^{-5} - 0.119309261351886905246614 \cdot 10^{-2} \cdot t^{-6} \quad (\text{B.136})$$

$$t_{2\vec{n}_1+\vec{n}_2}^{xx} = 0.588337100159830729028012 \cdot 10^{-3} \cdot t^{-3} + 0.346398377708810642111611 \cdot 10^{-3} \cdot t^{-4} - 0.351152446156008408494839 \cdot 10^{-3} \cdot t^{-5} - 0.682907473392500010424202 \cdot 10^{-3} \cdot t^{-6} \quad (\text{B.137})$$

$$t_{2\vec{n}_1+2\vec{n}_2}^{xx} = -0.232921501135639390462189 \cdot 10^{-3} \cdot t^{-4} - 0.181083506430596661823657 \cdot 10^{-3} \cdot t^{-5} + 0.365322440833618684178375 \cdot 10^{-3} \cdot t^{-6} \quad (\text{B.138})$$

$$t_{2\vec{n}_1+3\vec{n}_2}^{xx} = 0.688524960239360556294329 \cdot 10^{-4} \cdot t^{-5} + 0.554525655720858586617909 \cdot 10^{-4} \cdot t^{-6} \quad (\text{B.139})$$

$$t_{2\vec{n}_1+4\vec{n}_2}^{xx} = -0.181723785297851315000999 \cdot 10^{-4} \cdot t^{-6} \quad (\text{B.140})$$

$$t_{3\vec{n}_1-6\vec{n}_2}^{xx} = -0.181723785297851315000999 \cdot 10^{-4} \cdot t^{-6} \quad (\text{B.141})$$

$$t_{3\vec{n}_1-5\vec{n}_2}^{xx} = 0.459016640159573704196219 \cdot 10^{-4} \cdot t^{-5} + 0.604137277311930870001592 \cdot 10^{-4} \cdot t^{-6} \quad (\text{B.142})$$

$$t_{3\vec{n}_1-4\vec{n}_2}^{xx} = -0.776405003785464634873963 \cdot 10^{-4} \cdot t^{-4} - 0.180185105474197158838274 \cdot 10^{-3} \cdot t^{-5} + 0.286386194984530231538305 \cdot 10^{-3} \cdot t^{-6} \quad (\text{B.143})$$

$$t_{3\vec{n}_1-3\vec{n}_2}^{xx} = 0.373413500113866978664719 \cdot 10^{-3} \cdot t^{-4} - 0.195946957259888759173168 \cdot 10^{-3} \cdot t^{-5} - 0.625896065788473410302023 \cdot 10^{-3} \cdot t^{-6} \quad (\text{B.144})$$

$$t_{3\vec{n}_1-2\vec{n}_2}^{xx} = -0.238035580603681576666227 \cdot 10^{-3} \cdot t^{-4} + 0.362402612311765078704201 \cdot 10^{-3} \cdot t^{-5} - 0.898017682089430936195628 \cdot 10^{-4} \cdot t^{-6} \quad (\text{B.145})$$

$$t_{3\vec{n}_1-\vec{n}_2}^{xx} = -0.238035580603681576666227 \cdot 10^{-3} \cdot t^{-4} + 0.362402612311765078704201 \cdot 10^{-3} \cdot t^{-5} - 0.898017682089430936195628 \cdot 10^{-4} \cdot t^{-6} \quad (\text{B.146})$$

$$t_{3\vec{n}_1}^{xx} = 0.373413500113866978664719 \cdot 10^{-3} \cdot t^{-4} - 0.195946957259888759173168 \cdot 10^{-3} \cdot t^{-5} - 0.625896065788473410302023 \cdot 10^{-3} \cdot t^{-6} \quad (\text{B.147})$$

$$t_{3\vec{n}_1+\vec{n}_2}^{xx} = -0.776405003785464634873963 \cdot 10^{-4} \cdot t^{-4} - 0.180185105474197158838274 \cdot 10^{-3} \cdot t^{-5} + 0.286386194984530231538305 \cdot 10^{-3} \cdot t^{-6} \quad (\text{B.148})$$

$$t_{3\vec{n}_1+2\vec{n}_2}^{xx} = 0.459016640159573704196219 \cdot 10^{-4} \cdot t^{-5} + 0.604137277311930870001592 \cdot 10^{-4} \cdot t^{-6} \quad (\text{B.149})$$

$$t_{3\vec{n}_1+3\vec{n}_2}^{xx} = -0.181723785297851315000999 \cdot 10^{-4} \cdot t^{-6} \quad (\text{B.150})$$

$$t_{4\vec{n}_1-6\vec{n}_2}^{xx} = -0.908618926489256575004996 \cdot 10^{-5} \cdot t^{-6} \quad (\text{B.151})$$

$$t_{4\vec{n}_1-5\vec{n}_2}^{xx} = 0.114754160039893426049055 \cdot 10^{-4} \cdot t^{-5} + 0.361933210817370581410633 \cdot 10^{-4} \cdot t^{-6} \quad (\text{B.152})$$

$$t_{4\vec{n}_1-4\vec{n}_2}^{xx} = -0.447627643570088142536093 \cdot 10^{-4} \cdot t^{-5} - 0.121954072428841706377138 \cdot 10^{-6} \cdot t^{-6} \quad (\text{B.153})$$

$$t_{4\vec{n}_1-3\vec{n}_2}^{xx} = -0.176154236726482919602624 \cdot 10^{-4} \cdot t^{-5} + 0.738993312915439904793731 \cdot 10^{-4} \cdot t^{-6} \quad (\text{B.154})$$

$$t_{4\vec{n}_1-2\vec{n}_2}^{xx} = 0.772455133766997297965047 \cdot 10^{-4} \cdot t^{-5} - 0.249410428512881467064340 \cdot 10^{-3} \cdot t^{-6} \quad (\text{B.155})$$

$$t_{4\vec{n}_1-\vec{n}_2}^{xx} = -0.176154236726482919602624 \cdot 10^{-4} \cdot t^{-5} + 0.738993312915439904793731 \cdot 10^{-4} \cdot t^{-6} \quad (\text{B.156})$$

$$t_{4\vec{n}_1}^{xx} = -0.447627643570088142536093 \cdot 10^{-4} \cdot t^{-5} - 0.121954072428841706377138 \cdot 10^{-6} \cdot t^{-6} \quad (\text{B.157})$$

$$t_{4\vec{n}_1+\vec{n}_2}^{xx} = 0.114754160039893426049055 \cdot 10^{-4} \cdot t^{-5} + 0.361933210817370581410633 \cdot 10^{-4} \cdot t^{-6} \quad (\text{B.158})$$

$$t_{4\vec{n}_1+2\vec{n}_2}^{xx} = -0.908618926489256575004996 \cdot 10^{-5} \cdot t^{-6} \quad (\text{B.159})$$

$$t_{5\vec{n}_1-6\vec{n}_2}^{xx} = -0.181723785297851315000999 \cdot 10^{-5} \cdot t^{-6} \quad (\text{B.160})$$

$$t_{5\vec{n}_1-5\vec{n}_2}^{xx} = 0.529549932959660053710220 \cdot 10^{-5} \cdot t^{-6} \quad (\text{B.161})$$

$$t_{5\vec{n}_1-4\vec{n}_2}^{xx} = 0.961775368330065795258258 \cdot 10^{-5} \cdot t^{-6} \quad (\text{B.162})$$

$$t_{5\vec{n}_1-3\vec{n}_2}^{xx} = -0.103449005689306208778332 \cdot 10^{-4} \cdot t^{-6} \quad (\text{B.163})$$

$$t_{5\vec{n}_1-2\vec{n}_2}^{xx} = -0.103449005689306208778332 \cdot 10^{-4} \cdot t^{-6} \quad (\text{B.164})$$

$$t_{5\vec{n}_1-\vec{n}_2}^{xx} = 0.961775368330065795258258 \cdot 10^{-5} \cdot t^{-6} \quad (\text{B.165})$$

$$t_{5\vec{n}_1}^{xx} = 0.529549932959660053710220 \cdot 10^{-5} \cdot t^{-6} \quad (\text{B.166})$$

$$t_{5\vec{n}_1+\vec{n}_2}^{xx} = -0.181723785297851315000999 \cdot 10^{-5} \cdot t^{-6} \quad (\text{B.167})$$

$$t_{-5\vec{n}_1-\vec{n}_2}^{xy} = -0.181723785297851315000999 \cdot 10^{-5} \cdot t^{-6} \quad (\text{B.168})$$

$$t_{-5\vec{n}_1}^{xy} = -0.189534496764798260647388 \cdot 10^{-5} \cdot t^{-6} \quad (\text{B.169})$$

$$t_{-5\vec{n}_1+\vec{n}_2}^{xy} = 0.877376080621468792419441 \cdot 10^{-5} \cdot t^{-6} \quad (\text{B.170})$$

$$t_{-5\vec{n}_1+2\vec{n}_2}^{xy} = 0.177037358417683147613166 \cdot 10^{-4} \cdot t^{-6} \quad (\text{B.171})$$

$$t_{-5\vec{n}_1+3\vec{n}_2}^{xy} = 0.877376080621468792419441 \cdot 10^{-5} \cdot t^{-6} \quad (\text{B.172})$$

$$t_{-5\vec{n}_1+4\vec{n}_2}^{xy} = -0.189534496764798260647388 \cdot 10^{-5} \cdot t^{-6} \quad (\text{B.173})$$

$$t_{-5\vec{n}_1+5\vec{n}_2}^{xy} = -0.181723785297851315000999 \cdot 10^{-5} \cdot t^{-6} \quad (\text{B.174})$$

$$t_{-4\vec{n}_1-2\vec{n}_2}^{xy} = -0.908618926489256575004996 \cdot 10^{-5} \cdot t^{-6} \quad (\text{B.175})$$

$$t_{-4\vec{n}_1-\vec{n}_2}^{xy} = 0.114754160039893426049055 \cdot 10^{-4} \cdot t^{-5} + 0.200220092942381917886085 \cdot 10^{-4} \cdot t^{-6} \quad (\text{B.176})$$

$$t_{-4\vec{n}_1}^{xy} = 0.569449829474278083006311 \cdot 10^{-6} \cdot t^{-5} + 0.114014191569625057146409 \cdot 10^{-4} \cdot t^{-6} \quad (\text{B.177})$$

$$t_{-4\vec{n}_1+\vec{n}_2}^{xy} = -0.556687305315238787755085 \cdot 10^{-4} \cdot t^{-5} + 0.786929251879297688085574 \cdot 10^{-4} \cdot t^{-6} \quad (\text{B.178})$$

$$t_{-4\vec{n}_1+2\vec{n}_2}^{xy} = -0.556687305315238787755085 \cdot 10^{-4} \cdot t^{-5} + 0.825966964378827609775518 \cdot 10^{-4} \cdot t^{-6} \quad (\text{B.179})$$

$$t_{-4\vec{n}_1+3\vec{n}_2}^{xy} = 0.569449829474278083006311 \cdot 10^{-6} \cdot t^{-5} - 0.181648856174406830339212 \cdot 10^{-5} \cdot t^{-6} \quad (\text{B.180})$$

$$t_{-4\vec{n}_1+4\vec{n}_2}^{xy} = 0.114754160039893426049055 \cdot 10^{-4} \cdot t^{-5} + 0.100911746228232087451572 \cdot 10^{-4} \cdot t^{-6} \quad (\text{B.181})$$

$$t_{-4\vec{n}_1+5\vec{n}_2}^{xy} = -0.189534496764798260647388 \cdot 10^{-5} \cdot t^{-6} \quad (\text{B.182})$$

$$t_{-3\vec{n}_1-3\vec{n}_2}^{xy} = -0.181723785297851315000999 \cdot 10^{-4} \cdot t^{-6} \quad (\text{B.183})$$

$$t_{-3\vec{n}_1-2\vec{n}_2}^{xy} = 0.459016640159573704196219 \cdot 10^{-4} \cdot t^{-5} + 0.496436370479291037259778 \cdot 10^{-4} \cdot t^{-6} \quad (\text{B.184})$$

$$t_{-3\vec{n}_1-\vec{n}_2}^{xy} = -0.776405003785464634873963 \cdot 10^{-4} \cdot t^{-4} - 0.122296316262054141270010 \cdot 10^{-3} \cdot t^{-5} \\ + 0.203523580864738729690733 \cdot 10^{-3} \cdot t^{-6} \quad (\text{B.185})$$

$$t_{-3\vec{n}_1}^{xy} = 0.702459994891137941012653 \cdot 10^{-4} \cdot t^{-4} - 0.488919937266819365796534 \cdot 10^{-4} \cdot t^{-5} \\ - 0.139469056620406891732139 \cdot 10^{-3} \cdot t^{-6} \quad (\text{B.186})$$

$$t_{-3\vec{n}_1+\vec{n}_2}^{xy} = 0.295772999735320515177323 \cdot 10^{-3} \cdot t^{-4} - 0.454280811558875829447012 \cdot 10^{-3} \cdot t^{-5} \\ + 0.621598916746433812504030 \cdot 10^{-4} \cdot t^{-6} \quad (\text{B.187})$$

$$t_{-3\vec{n}_1+2\vec{n}_2}^{xy} = 0.702459994891137941012653 \cdot 10^{-4} \cdot t^{-4} - 0.712729126173902816148407 \cdot 10^{-4} \cdot t^{-5} \\ - 0.282245480976858719259202 \cdot 10^{-3} \cdot t^{-6} \quad (\text{B.188})$$

$$t_{-3\vec{n}_1+3\vec{n}_2}^{xy} = -0.776405003785464634873963 \cdot 10^{-4} \cdot t^{-4} - 0.176105720598616376180864 \cdot 10^{-4} \cdot t^{-5} \\ + 0.213566087526141996248093 \cdot 10^{-3} \cdot t^{-6} \quad (\text{B.189})$$

$$t_{-3\vec{n}_1+4\vec{n}_2}^{xy} = 0.569449829474278083006311 \cdot 10^{-6} \cdot t^{-5} - 0.181648856174406830339212 \cdot 10^{-5} \cdot t^{-6} \quad (\text{B.190})$$

$$t_{-3\vec{n}_1+5\vec{n}_2}^{xy} = 0.877376080621468792419441 \cdot 10^{-5} \cdot t^{-6} \quad (\text{B.191})$$

$$t_{-2\vec{n}_1-4\vec{n}_2}^{xy} = -0.181723785297851315000999 \cdot 10^{-4} \cdot t^{-6} \quad (\text{B.192})$$

$$t_{-2\vec{n}_1-3\vec{n}_2}^{xy} = 0.688524960239360556294329 \cdot 10^{-4} \cdot t^{-5} + 0.554525655720858586617909 \cdot 10^{-4} \cdot t^{-6} \quad (\text{B.193})$$

$$t_{-2\bar{n}_1-2\bar{n}_2}^{xy} = -0.232921501135639390462189 \cdot 10^{-3} \cdot t^{-4} - 0.168526931404936736592009 \cdot 10^{-3} \cdot t^{-5} + 0.324718043066997273466999 \cdot 10^{-3} \cdot t^{-6} \quad (\text{B.194})$$

$$t_{-2\bar{n}_1-\bar{n}_2}^{xy} = 0.588337100159830729028012 \cdot 10^{-3} \cdot t^{-3} + 0.228529301045632464533917 \cdot 10^{-3} \cdot t^{-4} - 0.434615398787199701739313 \cdot 10^{-3} \cdot t^{-5} - 0.448700051594377304562255 \cdot 10^{-3} \cdot t^{-6} \quad (\text{B.195})$$

$$t_{-2\bar{n}_1}^{xy} = -0.104791836117613889574824 \cdot 10^{-2} \cdot t^{-3} + 0.848168284701203959635441 \cdot 10^{-3} \cdot t^{-4} + 0.130170278593171370938895 \cdot 10^{-3} \cdot t^{-5} - 0.223958562151266240767136 \cdot 10^{-3} \cdot t^{-6} \quad (\text{B.196})$$

$$t_{-2\bar{n}_1+\bar{n}_2}^{xy} = -0.104791836117613889574824 \cdot 10^{-2} \cdot t^{-3} + 0.191933951155773081014763 \cdot 10^{-2} \cdot t^{-4} - 0.121207250223094324279363 \cdot 10^{-2} \cdot t^{-5} - 0.948698322174021075536699 \cdot 10^{-3} \cdot t^{-6} \quad (\text{B.197})$$

$$t_{-2\bar{n}_1+2\bar{n}_2}^{xy} = 0.588337100159830729028012 \cdot 10^{-3} \cdot t^{-3} - 0.716104703501151355371451 \cdot 10^{-3} \cdot t^{-4} + 0.724485682687886637054834 \cdot 10^{-3} \cdot t^{-5} - 0.210364626416704553400221 \cdot 10^{-3} \cdot t^{-6} \quad (\text{B.198})$$

$$t_{-2\bar{n}_1+3\bar{n}_2}^{xy} = 0.702459994891137941012653 \cdot 10^{-4} \cdot t^{-4} - 0.712729126173902816148407 \cdot 10^{-4} \cdot t^{-5} - 0.282245480976858719259202 \cdot 10^{-3} \cdot t^{-6} \quad (\text{B.199})$$

$$t_{-2\bar{n}_1+4\bar{n}_2}^{xy} = -0.556687305315238787755085 \cdot 10^{-4} \cdot t^{-5} + 0.825966964378827609775518 \cdot 10^{-4} \cdot t^{-6} \quad (\text{B.200})$$

$$t_{-2\bar{n}_1+5\bar{n}_2}^{xy} = 0.177037358417683147613166 \cdot 10^{-4} \cdot t^{-6} \quad (\text{B.201})$$

$$t_{-\bar{n}_1-5\bar{n}_2}^{xy} = -0.908618926489256575004996 \cdot 10^{-5} \cdot t^{-6} \quad (\text{B.202})$$

$$t_{-\bar{n}_1-4\bar{n}_2}^{xy} = 0.459016640159573704196219 \cdot 10^{-4} \cdot t^{-5} + 0.496436370479291037259778 \cdot 10^{-4} \cdot t^{-6} \quad (\text{B.203})$$

$$t_{-\bar{n}_1-3\bar{n}_2}^{xy} = -0.232921501135639390462189 \cdot 10^{-3} \cdot t^{-4} - 0.168526931404936736592009 \cdot 10^{-3} \cdot t^{-5} + 0.324718043066997273466999 \cdot 10^{-3} \cdot t^{-6} \quad (\text{B.204})$$

$$t_{-\bar{n}_1-2\bar{n}_2}^{xy} = 0.117667420031966145805602 \cdot 10^{-2} \cdot t^{-3} + 0.213503988724726916954670 \cdot 10^{-3} \cdot t^{-4} - 0.135702625373352364606986 \cdot 10^{-2} \cdot t^{-5} + 0.118451844517147120630783 \cdot 10^{-2} \cdot t^{-6} \quad (\text{B.205})$$

$$t_{-\bar{n}_1-\bar{n}_2}^{xy} = -0.557280900008412143633053 \cdot 10^{-2} \cdot t^{-2} - 0.236213196203047654053398 \cdot 10^{-2} \cdot t^{-3} + 0.702765346756813227778462 \cdot 10^{-2} \cdot t^{-4} - 0.206506034006256052274364 \cdot 10^{-2} \cdot t^{-5} - 0.373671320503437343621277 \cdot 10^{-2} \cdot t^{-6} \quad (\text{B.206})$$

$$t_{-\bar{n}_1}^{xy} = 0.137767414994532106638515 \cdot 10^{-1} \cdot t^{-2} - 0.865348988319435525887061 \cdot 10^{-2} \cdot t^{-3} - 0.132622387204069425441341 \cdot 10^{-2} \cdot t^{-4} + 0.312673425116414530905777 \cdot 10^{-2} \cdot t^{-5} - 0.236686021309884611528280 \cdot 10^{-2} \cdot t^{-6} \quad (\text{B.207})$$

$$t_{-\bar{n}_1+\bar{n}_2}^{xy} = -0.557280900008412143633053 \cdot 10^{-2} \cdot t^{-2} + 0.531461638264693552159016 \cdot 10^{-2} \cdot t^{-3} - 0.670565994231402390842320 \cdot 10^{-2} \cdot t^{-4} + 0.525379281796400113746666 \cdot 10^{-2} \cdot t^{-5} - 0.500519938535582839435800 \cdot 10^{-3} \cdot t^{-6} \quad (\text{B.208})$$

$$t_{-\bar{n}_1+2\bar{n}_2}^{xy} = -0.104791836117613889574824 \cdot 10^{-2} \cdot t^{-3} + 0.191933951155773081014763 \cdot 10^{-2} \cdot t^{-4} - 0.121207250223094324279363 \cdot 10^{-2} \cdot t^{-5} - 0.948698322174021075536699 \cdot 10^{-3} \cdot t^{-6} \quad (\text{B.209})$$

$$t_{-\bar{n}_1+3\bar{n}_2}^{xy} = 0.295772999735320515177323 \cdot 10^{-3} \cdot t^{-4} - 0.454280811558875829447012 \cdot 10^{-3} \cdot t^{-5} + 0.621598916746433812504030 \cdot 10^{-4} \cdot t^{-6} \quad (\text{B.210})$$

$$t_{-\bar{n}_1+4\bar{n}_2}^{xy} = -0.556687305315238787755085 \cdot 10^{-4} \cdot t^{-5} + 0.786929251879297688085574 \cdot 10^{-4} \cdot t^{-6} \quad (\text{B.211})$$

$$t_{-\bar{n}_1+5\bar{n}_2}^{xy} = 0.877376080621468792419441 \cdot 10^{-5} \cdot t^{-6} \quad (\text{B.212})$$

$$t_{-6\bar{n}_2}^{xy} = -0.181723785297851315000999 \cdot 10^{-5} \cdot t^{-6} \quad (\text{B.213})$$

$$t_{-5\bar{n}_2}^{xy} = 0.114754160039893426049055 \cdot 10^{-4} \cdot t^{-5} + 0.200220092942381917886085 \cdot 10^{-4} \cdot t^{-6} \quad (\text{B.214})$$

$$t_{-4\bar{n}_2}^{xy} = -0.776405003785464634873963 \cdot 10^{-4} \cdot t^{-4} - 0.122296316262054141270010 \cdot 10^{-3} \cdot t^{-5} + 0.203523580864738729690733 \cdot 10^{-3} \cdot t^{-6} \quad (\text{B.215})$$

$$t_{-3\bar{n}_2}^{xy} = 0.588337100159830729028012 \cdot 10^{-3} \cdot t^{-3} + 0.228529301045632464533917 \cdot 10^{-3} \cdot t^{-4} - 0.434615398787199701739313 \cdot 10^{-3} \cdot t^{-5} - 0.448700051594377304562255 \cdot 10^{-3} \cdot t^{-6} \quad (\text{B.216})$$

$$t_{-2\bar{n}_2}^{xy} = -0.557280900008412143633053 \cdot 10^{-2} \cdot t^{-2} - 0.236213196203047654053398 \cdot 10^{-2} \cdot t^{-3} + 0.702765346756813227778462 \cdot 10^{-2} \cdot t^{-4} - 0.206506034006256052274364 \cdot 10^{-2} \cdot t^{-5}$$

$$-0.373671320503437343621277 \cdot 10^{-2} \cdot t^{-6} \quad (\text{B.217})$$

$$\begin{aligned} t_{-\vec{n}_2}^{xy} = & 0.105572809000084121436331 \cdot t^{-1} - 0.289876688775131279103747 \cdot 10^{-1} \cdot t^{-2} \\ & - 0.199186554087748061154480 \cdot 10^{-1} \cdot t^{-3} + 0.135649359157411725628515 \cdot 10^{-1} \cdot t^{-4} \\ & - 0.349010482426959712643653 \cdot 10^{-2} \cdot t^{-5} + 0.142312604981261396382189 \cdot 10^{-2} \cdot t^{-6} \end{aligned} \quad (\text{B.218})$$

$$\begin{aligned} t_{\vec{0}}^{xy} = & -0.652475842498527874864216 \cdot 10^{-1} \cdot t^{-1} + 0.664445218705310486949405 \cdot 10^{-1} \cdot t^{-2} \\ & - 0.181424380744510864458450 \cdot 10^{-1} \cdot t^{-3} - 0.127689991799532110388965 \cdot 10^{-1} \cdot t^{-4} \\ & + 0.121266651669238410233434 \cdot 10^{-1} \cdot t^{-5} - 0.800395520818859059765532 \cdot 10^{-2} \cdot t^{-6} \end{aligned} \quad (\text{B.219})$$

$$\begin{aligned} t_{\vec{n}_2}^{xy} = & 0.137767414994532106638515 \cdot 10^{-1} \cdot t^{-2} - 0.865348988319435525887061 \cdot 10^{-2} \cdot t^{-3} \\ & - 0.132622387204069425441341 \cdot 10^{-2} \cdot t^{-4} + 0.312673425116414530905777 \cdot 10^{-2} \cdot t^{-5} \\ & - 0.236686021309884611528280 \cdot 10^{-2} \cdot t^{-6} \end{aligned} \quad (\text{B.220})$$

$$\begin{aligned} t_{2\vec{n}_2}^{xy} = & -0.104791836117613889574824 \cdot 10^{-2} \cdot t^{-3} + 0.848168284701203959635441 \cdot 10^{-3} \cdot t^{-4} \\ & + 0.130170278593171370938895 \cdot 10^{-3} \cdot t^{-5} - 0.223958562151266240767136 \cdot 10^{-3} \cdot t^{-6} \end{aligned} \quad (\text{B.221})$$

$$\begin{aligned} t_{3\vec{n}_2}^{xy} = & 0.702459994891137941012653 \cdot 10^{-4} \cdot t^{-4} - 0.488919937266819365796534 \cdot 10^{-4} \cdot t^{-5} \\ & - 0.139469056620406891732139 \cdot 10^{-3} \cdot t^{-6} \end{aligned} \quad (\text{B.222})$$

$$t_{4\vec{n}_2}^{xy} = 0.569449829474278083006311 \cdot 10^{-6} \cdot t^{-5} + 0.114014191569625057146409 \cdot 10^{-4} \cdot t^{-6} \quad (\text{B.223})$$

$$t_{5\vec{n}_2}^{xy} = -0.189534496764798260647388 \cdot 10^{-5} \cdot t^{-6} \quad (\text{B.224})$$

$$t_{\vec{n}_1 - 6\vec{n}_2}^{xy} = -0.189534496764798260647388 \cdot 10^{-5} \cdot t^{-6} \quad (\text{B.225})$$

$$t_{\vec{n}_1 - 5\vec{n}_2}^{xy} = 0.569449829474278083006311 \cdot 10^{-6} \cdot t^{-5} + 0.114014191569625057146409 \cdot 10^{-4} \cdot t^{-6} \quad (\text{B.226})$$

$$\begin{aligned} t_{\vec{n}_1 - 4\vec{n}_2}^{xy} = & 0.702459994891137941012653 \cdot 10^{-4} \cdot t^{-4} - 0.488919937266819365796534 \cdot 10^{-4} \cdot t^{-5} \\ & - 0.139469056620406891732139 \cdot 10^{-3} \cdot t^{-6} \end{aligned} \quad (\text{B.227})$$

$$\begin{aligned} t_{\vec{n}_1 - 3\vec{n}_2}^{xy} = & -0.104791836117613889574824 \cdot 10^{-2} \cdot t^{-3} + 0.848168284701203959635441 \cdot 10^{-3} \cdot t^{-4} \\ & + 0.130170278593171370938895 \cdot 10^{-3} \cdot t^{-5} - 0.223958562151266240767136 \cdot 10^{-3} \cdot t^{-6} \end{aligned} \quad (\text{B.228})$$

$$\begin{aligned} t_{\vec{n}_1 - 2\vec{n}_2}^{xy} = & 0.137767414994532106638515 \cdot 10^{-1} \cdot t^{-2} - 0.865348988319435525887061 \cdot 10^{-2} \cdot t^{-3} \\ & - 0.132622387204069425441341 \cdot 10^{-2} \cdot t^{-4} + 0.312673425116414530905777 \cdot 10^{-2} \cdot t^{-5} \\ & - 0.236686021309884611528280 \cdot 10^{-2} \cdot t^{-6} \end{aligned} \quad (\text{B.229})$$

$$\begin{aligned} t_{\vec{n}_1 - \vec{n}_2}^{xy} = & -0.652475842498527874864216 \cdot 10^{-1} \cdot t^{-1} + 0.664445218705310486949405 \cdot 10^{-1} \cdot t^{-2} \\ & - 0.181424380744510864458450 \cdot 10^{-1} \cdot t^{-3} - 0.127689991799532110388965 \cdot 10^{-1} \cdot t^{-4} \\ & + 0.121266651669238410233434 \cdot 10^{-1} \cdot t^{-5} - 0.800395520818859059765532 \cdot 10^{-2} \cdot t^{-6} \end{aligned} \quad (\text{B.230})$$

$$\begin{aligned} t_{\vec{n}_1}^{xy} = & 0.105572809000084121436331 \cdot t^{-1} - 0.289876688775131279103747 \cdot 10^{-1} \cdot t^{-2} \\ & - 0.199186554087748061154480 \cdot 10^{-1} \cdot t^{-3} + 0.135649359157411725628515 \cdot 10^{-1} \cdot t^{-4} \\ & - 0.349010482426959712643653 \cdot 10^{-2} \cdot t^{-5} + 0.142312604981261396382189 \cdot 10^{-2} \cdot t^{-6} \end{aligned} \quad (\text{B.231})$$

$$\begin{aligned} t_{\vec{n}_1 + \vec{n}_2}^{xy} = & -0.557280900008412143633053 \cdot 10^{-2} \cdot t^{-2} - 0.236213196203047654053398 \cdot 10^{-2} \cdot t^{-3} \\ & + 0.702765346756813227778462 \cdot 10^{-2} \cdot t^{-4} - 0.206506034006256052274364 \cdot 10^{-2} \cdot t^{-5} \\ & - 0.373671320503437343621277 \cdot 10^{-2} \cdot t^{-6} \end{aligned} \quad (\text{B.232})$$

$$\begin{aligned} t_{\vec{n}_1 + 2\vec{n}_2}^{xy} = & 0.588337100159830729028012 \cdot 10^{-3} \cdot t^{-3} + 0.228529301045632464533917 \cdot 10^{-3} \cdot t^{-4} \\ & - 0.434615398787199701739313 \cdot 10^{-3} \cdot t^{-5} - 0.448700051594377304562255 \cdot 10^{-3} \cdot t^{-6} \end{aligned} \quad (\text{B.233})$$

$$\begin{aligned} t_{\vec{n}_1 + 3\vec{n}_2}^{xy} = & -0.776405003785464634873963 \cdot 10^{-4} \cdot t^{-4} - 0.122296316262054141270010 \cdot 10^{-3} \cdot t^{-5} \\ & + 0.203523580864738729690733 \cdot 10^{-3} \cdot t^{-6} \end{aligned} \quad (\text{B.234})$$

$$t_{\vec{n}_1 + 4\vec{n}_2}^{xy} = 0.114754160039893426049055 \cdot 10^{-4} \cdot t^{-5} + 0.200220092942381917886085 \cdot 10^{-4} \cdot t^{-6} \quad (\text{B.235})$$

$$t_{\vec{n}_1 + 5\vec{n}_2}^{xy} = -0.181723785297851315000999 \cdot 10^{-5} \cdot t^{-6} \quad (\text{B.236})$$

$$t_{2\vec{n}_1 - 6\vec{n}_2}^{xy} = 0.877376080621468792419441 \cdot 10^{-5} \cdot t^{-6} \quad (\text{B.237})$$

$$t_{2\vec{n}_1 - 5\vec{n}_2}^{xy} = -0.556687305315238787755085 \cdot 10^{-4} \cdot t^{-5} + 0.786929251879297688085574 \cdot 10^{-4} \cdot t^{-6} \quad (\text{B.238})$$

$$\begin{aligned} t_{2\vec{n}_1 - 4\vec{n}_2}^{xy} = & 0.295772999735320515177323 \cdot 10^{-3} \cdot t^{-4} - 0.454280811558875829447012 \cdot 10^{-3} \cdot t^{-5} \\ & + 0.621598916746433812504030 \cdot 10^{-4} \cdot t^{-6} \end{aligned} \quad (\text{B.239})$$

$$t_{2\vec{n}_1-3\vec{n}_2}^{xy} = -0.104791836117613889574824 \cdot 10^{-2} \cdot t^{-3} + 0.191933951155773081014763 \cdot 10^{-2} \cdot t^{-4} \\ - 0.121207250223094324279363 \cdot 10^{-2} \cdot t^{-5} - 0.948698322174021075536699 \cdot 10^{-3} \cdot t^{-6} \quad (\text{B.240})$$

$$t_{2\vec{n}_1-2\vec{n}_2}^{xy} = -0.557280900008412143633053 \cdot 10^{-2} \cdot t^{-2} + 0.531461638264693552159016 \cdot 10^{-2} \cdot t^{-3} \\ - 0.670565994231402390842320 \cdot 10^{-2} \cdot t^{-4} + 0.525379281796400113746666 \cdot 10^{-2} \cdot t^{-5} \\ - 0.500519938535582839435800 \cdot 10^{-3} \cdot t^{-6} \quad (\text{B.241})$$

$$t_{2\vec{n}_1-\vec{n}_2}^{xy} = 0.137767414994532106638515 \cdot 10^{-1} \cdot t^{-2} - 0.865348988319435525887061 \cdot 10^{-2} \cdot t^{-3} \\ - 0.132622387204069425441341 \cdot 10^{-2} \cdot t^{-4} + 0.312673425116414530905777 \cdot 10^{-2} \cdot t^{-5} \\ - 0.236686021309884611528280 \cdot 10^{-2} \cdot t^{-6} \quad (\text{B.242})$$

$$t_{2\vec{n}_1}^{xy} = -0.557280900008412143633053 \cdot 10^{-2} \cdot t^{-2} - 0.236213196203047654053398 \cdot 10^{-2} \cdot t^{-3} \\ + 0.702765346756813227778462 \cdot 10^{-2} \cdot t^{-4} - 0.206506034006256052274364 \cdot 10^{-2} \cdot t^{-5} \\ - 0.373671320503437343621277 \cdot 10^{-2} \cdot t^{-6} \quad (\text{B.243})$$

$$t_{2\vec{n}_1+\vec{n}_2}^{xy} = 0.117667420031966145805602 \cdot 10^{-2} \cdot t^{-3} + 0.213503988724726916954670 \cdot 10^{-3} \cdot t^{-4} \\ - 0.135702625373352364606986 \cdot 10^{-2} \cdot t^{-5} + 0.118451844517147120630783 \cdot 10^{-2} \cdot t^{-6} \quad (\text{B.244})$$

$$t_{2\vec{n}_1+2\vec{n}_2}^{xy} = -0.232921501135639390462189 \cdot 10^{-3} \cdot t^{-4} - 0.168526931404936736592009 \cdot 10^{-3} \cdot t^{-5} \\ + 0.324718043066997273466999 \cdot 10^{-3} \cdot t^{-6} \quad (\text{B.245})$$

$$t_{2\vec{n}_1+3\vec{n}_2}^{xy} = 0.459016640159573704196219 \cdot 10^{-4} \cdot t^{-5} + 0.496436370479291037259778 \cdot 10^{-4} \cdot t^{-6} \quad (\text{B.246})$$

$$t_{2\vec{n}_1+4\vec{n}_2}^{xy} = -0.908618926489256575004996 \cdot 10^{-5} \cdot t^{-6} \quad (\text{B.247})$$

$$t_{3\vec{n}_1-6\vec{n}_2}^{xy} = 0.177037358417683147613166 \cdot 10^{-4} \cdot t^{-6} \quad (\text{B.248})$$

$$t_{3\vec{n}_1-5\vec{n}_2}^{xy} = -0.556687305315238787755085 \cdot 10^{-4} \cdot t^{-5} + 0.825966964378827609775518 \cdot 10^{-4} \cdot t^{-6} \quad (\text{B.249})$$

$$t_{3\vec{n}_1-4\vec{n}_2}^{xy} = 0.702459994891137941012653 \cdot 10^{-4} \cdot t^{-4} - 0.712729126173902816148407 \cdot 10^{-4} \cdot t^{-5} \\ - 0.282245480976858719259202 \cdot 10^{-3} \cdot t^{-6} \quad (\text{B.250})$$

$$t_{3\vec{n}_1-3\vec{n}_2}^{xy} = 0.588337100159830729028012 \cdot 10^{-3} \cdot t^{-3} - 0.716104703501151355371451 \cdot 10^{-3} \cdot t^{-4} \\ + 0.724485682687886637054834 \cdot 10^{-3} \cdot t^{-5} - 0.210364626416704553400221 \cdot 10^{-3} \cdot t^{-6} \quad (\text{B.251})$$

$$t_{3\vec{n}_1-2\vec{n}_2}^{xy} = -0.104791836117613889574824 \cdot 10^{-2} \cdot t^{-3} + 0.191933951155773081014763 \cdot 10^{-2} \cdot t^{-4} \\ - 0.121207250223094324279363 \cdot 10^{-2} \cdot t^{-5} - 0.948698322174021075536699 \cdot 10^{-3} \cdot t^{-6} \quad (\text{B.252})$$

$$t_{3\vec{n}_1-\vec{n}_2}^{xy} = -0.104791836117613889574824 \cdot 10^{-2} \cdot t^{-3} + 0.848168284701203959635441 \cdot 10^{-3} \cdot t^{-4} \\ + 0.130170278593171370938895 \cdot 10^{-3} \cdot t^{-5} - 0.223958562151266240767136 \cdot 10^{-3} \cdot t^{-6} \quad (\text{B.253})$$

$$t_{3\vec{n}_1}^{xy} = 0.588337100159830729028012 \cdot 10^{-3} \cdot t^{-3} + 0.228529301045632464533917 \cdot 10^{-3} \cdot t^{-4} \\ - 0.434615398787199701739313 \cdot 10^{-3} \cdot t^{-5} - 0.448700051594377304562255 \cdot 10^{-3} \cdot t^{-6} \quad (\text{B.254})$$

$$t_{3\vec{n}_1+\vec{n}_2}^{xy} = -0.232921501135639390462189 \cdot 10^{-3} \cdot t^{-4} - 0.168526931404936736592009 \cdot 10^{-3} \cdot t^{-5} \\ + 0.324718043066997273466999 \cdot 10^{-3} \cdot t^{-6} \quad (\text{B.255})$$

$$t_{3\vec{n}_1+2\vec{n}_2}^{xy} = 0.688524960239360556294329 \cdot 10^{-4} \cdot t^{-5} + 0.554525655720858586617909 \cdot 10^{-4} \cdot t^{-6} \quad (\text{B.256})$$

$$t_{3\vec{n}_1+3\vec{n}_2}^{xy} = -0.181723785297851315000999 \cdot 10^{-4} \cdot t^{-6} \quad (\text{B.257})$$

$$t_{4\vec{n}_1-6\vec{n}_2}^{xy} = 0.877376080621468792419441 \cdot 10^{-5} \cdot t^{-6} \quad (\text{B.258})$$

$$t_{4\vec{n}_1-5\vec{n}_2}^{xy} = 0.569449829474278083006311 \cdot 10^{-6} \cdot t^{-5} - 0.181648856174406830339212 \cdot 10^{-5} \cdot t^{-6} \quad (\text{B.259})$$

$$t_{4\vec{n}_1-4\vec{n}_2}^{xy} = -0.776405003785464634873963 \cdot 10^{-4} \cdot t^{-4} - 0.176105720598616376180864 \cdot 10^{-4} \cdot t^{-5} \\ + 0.213566087526141996248093 \cdot 10^{-3} \cdot t^{-6} \quad (\text{B.260})$$

$$t_{4\vec{n}_1-3\vec{n}_2}^{xy} = 0.702459994891137941012653 \cdot 10^{-4} \cdot t^{-4} - 0.712729126173902816148407 \cdot 10^{-4} \cdot t^{-5} \\ - 0.282245480976858719259202 \cdot 10^{-3} \cdot t^{-6} \quad (\text{B.261})$$

$$t_{4\vec{n}_1-2\vec{n}_2}^{xy} = 0.295772999735320515177323 \cdot 10^{-3} \cdot t^{-4} - 0.454280811558875829447012 \cdot 10^{-3} \cdot t^{-5} \\ + 0.621598916746433812504030 \cdot 10^{-4} \cdot t^{-6} \quad (\text{B.262})$$

$$t_{4\vec{n}_1-\vec{n}_2}^{xy} = 0.702459994891137941012653 \cdot 10^{-4} \cdot t^{-4} - 0.488919937266819365796534 \cdot 10^{-4} \cdot t^{-5} \\ - 0.139469056620406891732139 \cdot 10^{-3} \cdot t^{-6} \quad (\text{B.263})$$

$$t_{4\vec{n}_1}^{xy} = -0.776405003785464634873963 \cdot 10^{-4} \cdot t^{-4} - 0.122296316262054141270010 \cdot 10^{-3} \cdot t^{-5}$$

$$+ 0.203523580864738729690733 \cdot 10^{-3} \cdot t^{-6} \quad (\text{B.264})$$

$$t_{4\vec{n}_1+\vec{n}_2}^{xy} = 0.459016640159573704196219 \cdot 10^{-4} \cdot t^{-5} + 0.496436370479291037259778 \cdot 10^{-4} \cdot t^{-6} \quad (\text{B.265})$$

$$t_{4\vec{n}_1+2\vec{n}_2}^{xy} = -0.181723785297851315000999 \cdot 10^{-4} \cdot t^{-6} \quad (\text{B.266})$$

$$t_{5\vec{n}_1-6\vec{n}_2}^{xy} = -0.189534496764798260647388 \cdot 10^{-5} \cdot t^{-6} \quad (\text{B.267})$$

$$t_{5\vec{n}_1-5\vec{n}_2}^{xy} = 0.114754160039893426049055 \cdot 10^{-4} \cdot t^{-5} + 0.100911746228232087451572 \cdot 10^{-4} \cdot t^{-6} \quad (\text{B.268})$$

$$t_{5\vec{n}_1-4\vec{n}_2}^{xy} = 0.569449829474278083006311 \cdot 10^{-6} \cdot t^{-5} - 0.181648856174406830339212 \cdot 10^{-5} \cdot t^{-6} \quad (\text{B.269})$$

$$t_{5\vec{n}_1-3\vec{n}_2}^{xy} = -0.556687305315238787755085 \cdot 10^{-4} \cdot t^{-5} + 0.825966964378827609775518 \cdot 10^{-4} \cdot t^{-6} \quad (\text{B.270})$$

$$t_{5\vec{n}_1-2\vec{n}_2}^{xy} = -0.556687305315238787755085 \cdot 10^{-4} \cdot t^{-5} + 0.786929251879297688085574 \cdot 10^{-4} \cdot t^{-6} \quad (\text{B.271})$$

$$t_{5\vec{n}_1-\vec{n}_2}^{xy} = 0.569449829474278083006311 \cdot 10^{-6} \cdot t^{-5} + 0.114014191569625057146409 \cdot 10^{-4} \cdot t^{-6} \quad (\text{B.272})$$

$$t_{5\vec{n}_1}^{xy} = 0.114754160039893426049055 \cdot 10^{-4} \cdot t^{-5} + 0.200220092942381917886085 \cdot 10^{-4} \cdot t^{-6} \quad (\text{B.273})$$

$$t_{5\vec{n}_1+\vec{n}_2}^{xy} = -0.908618926489256575004996 \cdot 10^{-5} \cdot t^{-6} \quad (\text{B.274})$$

$$t_{6\vec{n}_1-6\vec{n}_2}^{xy} = -0.181723785297851315000999 \cdot 10^{-5} \cdot t^{-6} \quad (\text{B.275})$$

$$t_{6\vec{n}_1-5\vec{n}_2}^{xy} = -0.189534496764798260647388 \cdot 10^{-5} \cdot t^{-6} \quad (\text{B.276})$$

$$t_{6\vec{n}_1-4\vec{n}_2}^{xy} = 0.877376080621468792419441 \cdot 10^{-5} \cdot t^{-6} \quad (\text{B.277})$$

$$t_{6\vec{n}_1-3\vec{n}_2}^{xy} = 0.177037358417683147613166 \cdot 10^{-4} \cdot t^{-6} \quad (\text{B.278})$$

$$t_{6\vec{n}_1-2\vec{n}_2}^{xy} = 0.877376080621468792419441 \cdot 10^{-5} \cdot t^{-6} \quad (\text{B.279})$$

$$t_{6\vec{n}_1-\vec{n}_2}^{xy} = -0.189534496764798260647388 \cdot 10^{-5} \cdot t^{-6} \quad (\text{B.280})$$

$$t_{6\vec{n}_1}^{xy} = -0.181723785297851315000999 \cdot 10^{-5} \cdot t^{-6}. \quad (\text{B.281})$$

The remaining hopping elements can be obtained via

$$t_{\vec{r}}^{\alpha,\beta} = t_{-\vec{r}}^{\beta,\alpha}, \quad (\text{B.282})$$

$$t_{(-n_1-n_2)\vec{n}_1+n_1\vec{n}_2}^{yy} = t_{n_1\vec{n}_1+n_2\vec{n}_2}^{xx}, \quad t_{(-n_1-n_2)\vec{n}_1+n_1\vec{n}_2}^{yz} = t_{n_1\vec{n}_1+n_2\vec{n}_2}^{xy}, \quad (\text{B.283})$$

$$t_{(-n_1-n_2)\vec{n}_1+n_1\vec{n}_2}^{zx} = t_{n_1\vec{n}_1+n_2\vec{n}_2}^{yz}, \quad t_{(-n_1-n_2)\vec{n}_1+n_1\vec{n}_2}^{zz} = t_{n_1\vec{n}_1+n_2\vec{n}_2}^{yy}. \quad (\text{B.284})$$

The resulting 3×3 matrix is diagonalized and yields the dispersion $\omega(\vec{k})$. It has for $\theta > \frac{3\pi}{2}$ its minimum at $\vec{k} = (\frac{2\pi}{3}, -\frac{2\pi}{3})$ and thus we obtain the gap

$$\begin{aligned} \frac{\Delta^+}{-\sin \theta} &= 1 + 0.2668737080010094572359664 \cdot t^{-1} - 0.2048165955279984180586789 \cdot t^{-2} \\ &\quad - 0.0757131589365322021180094 \cdot t^{-3} + 0.0396426295787896197316898 \cdot t^{-4} \\ &\quad + 0.0725795604533690748525843 \cdot t^{-5} - 0.0669114965805065886277518 \cdot t^{-6}, \end{aligned} \quad (\text{B.285})$$

whereas for $\theta < \frac{3\pi}{2}$, the minimum is located at $\vec{k} = (0, \pi)$ and thus we obtain the gap

$$\begin{aligned} \frac{\Delta^-}{-\sin \theta} &= 1 - 0.733126291998990542764034 \cdot t^{-1} + 0.262751550219625151364984 \cdot t^{-2} \\ &\quad - 0.101655673067985331255221 \cdot t^{-3} + 0.019666525219269891934356 \cdot t^{-4} \\ &\quad - 0.070704236450894509987165 \cdot t^{-5} + 0.109851689895068525044349 \cdot t^{-6}. \end{aligned} \quad (\text{B.286})$$

Appendix C

Series expansions for Ising Anyons

C.1 Series expansions for the topological phase

ground-state energy e_0

For the topological phase ($\theta = 0$), we obtain the following expression for the ground-state energy per plaquette.

$$\begin{aligned} \frac{e_0}{\cos \theta} = & -1. - 0.75000000000000000000000000000000 \cdot t - 0.28125000000000000000000000000000 \cdot t^2 \\ & - 0.21093750000000000000000000000000 \cdot t^3 - 0.32958984375000000000000000000000 \cdot t^4 \\ & - 0.59118652343750000000000000000000 \cdot t^5 - 1.24871826171875000000000000000000 \cdot t^6 \\ & - 2.87764098909166124131944 \cdot t^7 - 7.11423802596551400643808 \cdot t^8 \\ & - 18.4883434620674377606239 \cdot t^9 - 49.9704000152212494807969 \cdot t^{10} \\ & - 139.288404143044065389608 \cdot t^{11}. \end{aligned} \tag{C.1}$$

hopping elements and dispersion

With the definitions of Fig. 5.1, we obtain the hopping elements

$$\begin{aligned} t_0^\sigma = & 1. - 0.18750000000000000000000000000000 \cdot t^2 - 0.14062500000000000000000000000000 \cdot t^3 \\ & - 0.48339843750000000000000000000000 \cdot t^4 - 0.96907552083333333333333333333333 \cdot t^5 \\ & - 2.966410319010416666666667 \cdot t^6 - 7.99696258262351707175926 \cdot t^7 \\ & - 24.6591871829680454583816 \cdot t^8 - 73.6930784793449527442210 \cdot t^9 \\ & - 232.406474699677368025557 \cdot t^{10} \end{aligned} \tag{C.2}$$

$$\begin{aligned} t_{n_2}^\sigma = & -0.25000000000000000000000000000000 \cdot t - 0.18750000000000000000000000000000 \cdot t^2 \\ & - 0.25000000000000000000000000000000 \cdot t^3 - 0.54231770833333333333333333333333 \cdot t^4 \\ & - 1.097140842013888888888889 \cdot t^5 - 2.93842456958912037037037 \cdot t^6 \\ & - 7.56501314375135633680556 \cdot t^7 - 22.0559009867931099094972 \cdot t^8 \\ & - 63.5154320213767931131015 \cdot t^9 - 193.526018469661293669711 \cdot t^{10} \end{aligned} \tag{C.3}$$

$$\begin{aligned}
t_{2\vec{n}_2}^\sigma &= -0.31250000000000000000 \cdot 10^{-1} \cdot t^2 - 0.62500000000000000000 \cdot 10^{-1} \cdot t^3 \\
&\quad - 0.124348958333333333333333 \cdot t^4 - 0.3179524739583333333333 \cdot t^5 \\
&\quad - 0.959633721245659722222222 \cdot t^6 - 2.66618647398772063078704 \cdot t^7 \\
&\quad - 8.17693404452300366060233 \cdot t^8 - 24.1561720857944017575111 \cdot t^9 \\
&\quad - 75.7219948366463259305374 \cdot t^{10}
\end{aligned} \tag{C.4}$$

$$\begin{aligned}
t_{3\vec{n}_2}^\sigma &= -0.78125000000000000000 \cdot 10^{-2} \cdot t^3 - 0.3971354166666666666667 \cdot 10^{-1} \cdot t^4 \\
&\quad - 0.121120876736111111111111 \cdot t^5 - 0.373268975151909722222222 \cdot t^6 \\
&\quad - 1.06758766998479395736883 \cdot t^7 - 3.24839635508541217066133 \cdot t^8 \\
&\quad - 9.66504388275072080771782 \cdot t^9 - 30.2390387051390908968519 \cdot t^{10}
\end{aligned} \tag{C.5}$$

$$\begin{aligned}
t_{4\vec{n}_2}^\sigma &= -0.2441406250000000000000 \cdot 10^{-2} \cdot t^4 - 0.2072482638888888888889 \cdot 10^{-1} \cdot t^5 \\
&\quad - 0.866928100585937500000000 \cdot 10^{-1} \cdot t^6 - 0.326612225285282841435185 \cdot t^7 \\
&\quad - 1.16846712167861530319653 \cdot t^8 - 3.98588897340459588133259 \cdot t^9 \\
&\quad - 13.5936608585814984151638 \cdot t^{10}
\end{aligned} \tag{C.6}$$

$$\begin{aligned}
t_{5\vec{n}_2}^\sigma &= -0.8544921875000000000000 \cdot 10^{-3} \cdot t^5 - 0.113468876591435185185185 \cdot 10^{-1} \cdot t^6 \\
&\quad - 0.629194813010133342978395 \cdot 10^{-1} \cdot t^7 - 0.279303494843926449371463 \cdot t^8 \\
&\quad - 1.11270097276116676618369 \cdot t^9 - 4.21923662473906511223692 \cdot t^{10}
\end{aligned} \tag{C.7}$$

$$\begin{aligned}
t_{6\vec{n}_2}^\sigma &= -0.3204345703125000000000 \cdot 10^{-3} \cdot t^6 - 0.604850863233024691358025 \cdot 10^{-2} \cdot t^7 \\
&\quad - 0.434483781518268977663645 \cdot 10^{-1} \cdot t^8 - 0.228664498798068822329591 \cdot t^9 \\
&\quad - 1.04398789479137642311625 \cdot t^{10}
\end{aligned} \tag{C.8}$$

$$\begin{aligned}
t_{7\vec{n}_2}^\sigma &= -0.125885009765625000000000 \cdot 10^{-3} \cdot t^7 - 0.321764612394105259773663 \cdot 10^{-2} \cdot t^8 \\
&\quad - 0.291049056935580179033947 \cdot 10^{-1} \cdot t^9 - 0.179595340019241009447528 \cdot t^{10}
\end{aligned} \tag{C.9}$$

$$\begin{aligned}
t_{8\vec{n}_2}^\sigma &= -0.511407852172851562500000 \cdot 10^{-4} \cdot t^8 - 0.169818456934966831704390 \cdot 10^{-2} \cdot t^9 \\
&\quad - 0.189676017536763416941328 \cdot 10^{-1} \cdot t^{10}
\end{aligned} \tag{C.10}$$

$$t_{9\vec{n}_2}^\sigma = -0.213086605072021484375000 \cdot 10^{-4} \cdot t^9 - 0.892141865413920433487476 \cdot 10^{-3} \cdot t^{10} \tag{C.11}$$

$$t_{10\vec{n}_2}^\sigma = -0.905618071556091308593750 \cdot 10^{-5} \cdot t^{10} \tag{C.12}$$

$$\begin{aligned}
t_{\vec{n}_1+\vec{n}_2}^\sigma &= -0.62500000000000000000 \cdot 10^{-1} \cdot t^2 - 0.78125000000000000000 \cdot 10^{-1} \cdot t^3 \\
&\quad - 0.2180989583333333333333 \cdot t^4 - 0.4951714409722222222222 \cdot t^5 \\
&\quad - 1.39795656557436342592593 \cdot t^6 - 3.71651159686806761188272 \cdot t^7 \\
&\quad - 11.1881601875210985725309 \cdot t^8 - 32.7324682939972406552162 \cdot t^9 \\
&\quad - 101.568299548126852534163 \cdot t^{10}
\end{aligned} \tag{C.13}$$

$$\begin{aligned}
t_{\vec{n}_1+2\vec{n}_2}^\sigma &= -0.23437500000000000000 \cdot 10^{-1} \cdot t^3 - 0.70312500000000000000 \cdot 10^{-1} \cdot t^4 \\
&\quad - 0.1844482421875000000000 \cdot t^5 - 0.518719143337673611111111 \cdot t^6 \\
&\quad - 1.42020679403234411168981 \cdot t^7 - 4.26164043219491778087224 \cdot t^8 \\
&\quad - 12.5095777036430536474220 \cdot t^9 - 39.1007119235713741770606 \cdot t^{10}
\end{aligned} \tag{C.14}$$

$$\begin{aligned}
t_{\vec{n}_1+3\vec{n}_2}^\sigma &= -0.97656250000000000000 \cdot 10^{-2} \cdot t^4 - 0.4444715711805555555556 \cdot 10^{-1} \cdot t^5 \\
&\quad - 0.165432400173611111111111 \cdot t^6 - 0.564412935280505521797840 \cdot t^7 \\
&\quad - 1.89547157832133917160976 \cdot t^8 - 6.12645983715617035315034 \cdot t^9 \\
&\quad - 20.0749443747607201583101 \cdot t^{10}
\end{aligned} \tag{C.15}$$

$$\begin{aligned}
t_{\vec{n}_1+4\vec{n}_2}^\sigma &= -0.4272460937500000000000 \cdot 10^{-2} \cdot t^5 - 0.298179343894675925925926 \cdot 10^{-1} \cdot t^6 \\
&\quad - 0.132032871246337890625000 \cdot t^7 - 0.523569408022327187620563 \cdot t^8 \\
&\quad - 1.92930186326918288022893 \cdot t^9 - 6.95990859563730973929208 \cdot t^{10}
\end{aligned} \tag{C.16}$$

$$\begin{aligned}
t_{\vec{n}_1+5\vec{n}_2}^\sigma &= -0.1922607421875000000000 \cdot 10^{-2} \cdot t^6 - 0.186671504267939814814815 \cdot 10^{-1} \cdot t^7 \\
&\quad - 0.103778195233992588372878 \cdot t^8 - 0.477884756279457743766377 \cdot t^9 \\
&\quad - 1.99171805620503751965598 \cdot t^{10}
\end{aligned} \tag{C.17}$$

$$t_{\vec{n}_1+6\vec{n}_2}^\sigma = -0.881195068359375000000000 \cdot 10^{-3} \cdot t^7 - 0.114771132606537744341564 \cdot 10^{-1} \cdot t^8$$

$$-0.773933085655111344262896 \cdot 10^{-1} \cdot t^9 - 0.410204415941156981794813 \cdot t^{10} \quad (\text{C.18})$$

$$t_{\vec{n}_1+7\vec{n}_2}^\sigma = -0.409126281738281250000000 \cdot 10^{-3} \cdot t^8 - 0.687324849502866977853867 \cdot 10^{-2} \cdot t^9 \\ - 0.559710753028918522702650 \cdot 10^{-1} \cdot t^{10} \quad (\text{C.19})$$

$$t_{\vec{n}_1+8\vec{n}_2}^\sigma = -0.191777944564819335937500 \cdot 10^{-3} \cdot t^9 - 0.404455727387848214357478 \cdot 10^{-2} \cdot t^{10} \quad (\text{C.20})$$

$$t_{\vec{n}_1+9\vec{n}_2}^\sigma = -0.905618071556091308593750 \cdot 10^{-4} \cdot t^{10} \quad (\text{C.21})$$

$$t_{2\vec{n}_1+2\vec{n}_2}^\sigma = -0.146484375000000000000000 \cdot 10^{-1} \cdot t^4 - 0.559895833333333333333333 \cdot 10^{-1} \cdot t^5 \\ - 0.207502011899594907407407 \cdot t^6 - 0.679816822946807484567901 \cdot t^7 \\ - 2.23510979938899538644547 \cdot t^8 - 7.07468902868702905495307 \cdot t^9 \\ - 22.8623097034992499402194 \cdot t^{10} \quad (\text{C.22})$$

$$t_{2\vec{n}_1+3\vec{n}_2}^\sigma = -0.854492187500000000000000 \cdot 10^{-2} \cdot t^5 - 0.461776168258101851851852 \cdot 10^{-1} \cdot t^6 \\ - 0.188378993375801745756173 \cdot t^7 - 0.710630058996961931142297 \cdot t^8 \\ - 2.54038479923731832674338 \cdot t^9 - 8.98024584896679734278881 \cdot t^{10} \quad (\text{C.23})$$

$$t_{2\vec{n}_1+4\vec{n}_2}^\sigma = -0.480651855468750000000000 \cdot 10^{-2} \cdot t^6 - 0.343311451099537037037037 \cdot 10^{-1} \cdot t^7 \\ - 0.171912640087889055165734 \cdot t^8 - 0.734671442071678543614098 \cdot t^9 \\ - 2.91172527007669786176128 \cdot t^{10} \quad (\text{C.24})$$

$$t_{2\vec{n}_1+5\vec{n}_2}^\sigma = -0.264358520507812500000000 \cdot 10^{-2} \cdot t^7 - 0.246123090202425733024691 \cdot 10^{-1} \cdot t^8 \\ - 0.143504170164343260933833 \cdot t^9 - 0.698859938329543064978224 \cdot t^{10} \quad (\text{C.25})$$

$$t_{2\vec{n}_1+6\vec{n}_2}^\sigma = -0.143194198608398437500000 \cdot 10^{-2} \cdot t^8 - 0.168646968114196191272291 \cdot 10^{-1} \cdot t^9 \\ - 0.115911826556723072586618 \cdot t^{10} \quad (\text{C.26})$$

$$t_{2\vec{n}_1+7\vec{n}_2}^\sigma = -0.767111778259277343750000 \cdot 10^{-3} \cdot t^9 - 0.111973297019554263770335 \cdot 10^{-1} \cdot t^{10} \quad (\text{C.27})$$

$$t_{2\vec{n}_1+8\vec{n}_2}^\sigma = -0.407528132200241088867188 \cdot 10^{-3} \cdot t^{10} \quad (\text{C.28})$$

$$t_{3\vec{n}_1+3\vec{n}_2}^\sigma = -0.640869140625000000000000 \cdot 10^{-2} \cdot t^6 - 0.416626164942611882716049 \cdot 10^{-1} \cdot t^7 \\ - 0.203075303462307149000129 \cdot t^8 - 0.846265290707186252819004 \cdot t^9 \\ - 3.30091622796906631015783 \cdot t^{10} \quad (\text{C.29})$$

$$t_{3\vec{n}_1+4\vec{n}_2}^\sigma = -0.440597534179687500000000 \cdot 10^{-2} \cdot t^7 - 0.352927470894016846707819 \cdot 10^{-1} \cdot t^8 \\ - 0.193859300625974258768215 \cdot t^9 - 0.908028422496739347394220 \cdot t^{10} \quad (\text{C.30})$$

$$t_{3\vec{n}_1+5\vec{n}_2}^\sigma = -0.286388397216796875000000 \cdot 10^{-2} \cdot t^8 - 0.279760552858946581763332 \cdot 10^{-1} \cdot t^9 \\ - 0.176946337471933712630060 \cdot t^{10} \quad (\text{C.31})$$

$$t_{3\vec{n}_1+6\vec{n}_2}^\sigma = -0.178992748260498046875000 \cdot 10^{-2} \cdot t^9 - 0.211462032443374926824792 \cdot 10^{-1} \cdot t^{10} \quad (\text{C.32})$$

$$t_{3\vec{n}_1+7\vec{n}_2}^\sigma = -0.108674168586730957031250 \cdot 10^{-2} \cdot t^{10} \quad (\text{C.33})$$

$$t_{4\vec{n}_1+4\vec{n}_2}^\sigma = -0.357985496520996093750000 \cdot 10^{-2} \cdot t^8 - 0.329564006894377196930727 \cdot 10^{-1} \cdot t^9 \\ - 0.203350027212208783348565 \cdot t^{10} \quad (\text{C.34})$$

$$t_{4\vec{n}_1+5\vec{n}_2}^\sigma = -0.268489122390747070312500 \cdot 10^{-2} \cdot t^9 - 0.287307652303711377053594 \cdot 10^{-1} \cdot t^{10} \quad (\text{C.35})$$

$$t_{4\vec{n}_1+6\vec{n}_2}^\sigma = -0.190179795026779174804688 \cdot 10^{-2} \cdot t^{10} \quad (\text{C.36})$$

$$t_{5\vec{n}_1+5\vec{n}_2}^\sigma = -0.228215754032135009765625 \cdot 10^{-2} \cdot t^{10} \quad (\text{C.37})$$

$$t_0^\psi = 1 - 0.187500000000000000000000 \cdot t^2 - 0.1406250000000000000000 \cdot t^3 \\ - 0.483398437500000000000000 \cdot t^4 - 0.969075520833333333333333 \cdot t^5 \\ - 2.969875759548611111111111 \cdot t^6 - 7.99989707381637008101852 \cdot t^7 \\ - 24.6819336605660709334008 \cdot t^8 - 73.7497251815143436070823 \cdot t^9 \\ - 232.621863558620319220101 \cdot t^{10} \quad (\text{C.38})$$

$$t_{\vec{n}_2}^\psi = -0.250000000000000000000000 \cdot t - 0.1875000000000000000000 \cdot t^2 \\ - 0.250000000000000000000000 \cdot t^3 - 0.542317708333333333333333 \cdot t^4 \\ - 1.097195095486111111111111 \cdot t^5 - 2.938374837239583333333333 \cdot t^6 \\ - 7.56226872809139298804012 \cdot t^7 - 22.0524087334856574918017 \cdot t^8$$

$$- 63.4936561822250424098576 \cdot t^9 - 193.469729914308153007692 \cdot t^{10} \quad (\text{C.39})$$

$$\begin{aligned} t_{2\vec{n}_2}^\psi &= - 0.31250000000000000000000000000000 \cdot 10^{-1} \cdot t^2 - 0.62500000000000000000000000000000 \cdot 10^{-1} \cdot t^3 \\ &\quad - 0.12434895833333333333333333333333 \cdot t^4 - 0.3179524739583333333333333333 \cdot t^5 \\ &\quad - 0.9596811930338541666666667 \cdot t^6 - 2.66628848181830512152778 \cdot t^7 \\ &\quad - 8.17810664517889297548145 \cdot t^8 - 24.1580036464611525725272 \cdot t^9 \\ &\quad - 75.7335422265733671845178 \cdot t^{10} \end{aligned} \quad (\text{C.40})$$

$$\begin{aligned} t_{3\vec{n}_2}^\psi &= - 0.78125000000000000000000000000000 \cdot 10^{-2} \cdot t^3 - 0.3971354166666666666666667 \cdot 10^{-1} \cdot t^4 \\ &\quad - 0.12112087673611111111111111111111 \cdot t^5 - 0.3732689751519097222222222 \cdot t^6 \\ &\quad - 1.06760102142522364486883 \cdot t^7 - 3.24848327249165915657954 \cdot t^8 \\ &\quad - 9.66498233694414543026269 \cdot t^9 - 30.2390998920468604136778 \cdot t^{10} \end{aligned} \quad (\text{C.41})$$

$$\begin{aligned} t_{4\vec{n}_2}^\psi &= - 0.24414062500000000000000000000000 \cdot 10^{-2} \cdot t^4 - 0.2072482638888888888888889 \cdot 10^{-1} \cdot t^5 \\ &\quad - 0.8669281005859375000000000 \cdot 10^{-1} \cdot t^6 \\ &\quad - 0.326612225285282841435185 \cdot t^7 \\ &\quad - 1.16847226092354260354376 \cdot t^8 - 3.98593470181089369848432 \cdot t^9 \\ &\quad - 13.5939267668929640893583 \cdot t^{10} \end{aligned} \quad (\text{C.42})$$

$$\begin{aligned} t_{5\vec{n}_2}^\psi &= - 0.85449218750000000000000000000000 \cdot 10^{-3} \cdot t^5 - 0.113468876591435185185185 \cdot 10^{-1} \cdot t^6 \\ &\quad - 0.629194813010133342978395 \cdot 10^{-1} \cdot t^7 - 0.279303494843926449371463 \cdot t^8 \\ &\quad - 1.11270319220634236093738 \cdot t^9 - 4.21926829410846433276502 \cdot t^{10} \end{aligned} \quad (\text{C.43})$$

$$\begin{aligned} t_{6\vec{n}_2}^\psi &= - 0.32043457031250000000000000000000 \cdot 10^{-3} \cdot t^6 - 0.604850863233024691358025 \cdot 10^{-2} \cdot t^7 \\ &\quad - 0.434483781518268977663645 \cdot 10^{-1} \cdot t^8 - 0.228664498798068822329591 \cdot t^9 \\ &\quad - 1.04398887547404749321512 \cdot t^{10} \end{aligned} \quad (\text{C.44})$$

$$\begin{aligned} t_{7\vec{n}_2}^\psi &= - 0.12588500976562500000000000000000 \cdot 10^{-3} \cdot t^7 - 0.321764612394105259773663 \cdot 10^{-2} \cdot t^8 \\ &\quad - 0.291049056935580179033947 \cdot 10^{-1} \cdot t^9 - 0.179595340019241009447528 \cdot t^{10} \end{aligned} \quad (\text{C.45})$$

$$\begin{aligned} t_{8\vec{n}_2}^\psi &= - 0.51140785217285156250000000000000 \cdot 10^{-4} \cdot t^8 - 0.169818456934966831704390 \cdot 10^{-2} \cdot t^9 \\ &\quad - 0.189676017536763416941328 \cdot 10^{-1} \cdot t^{10} \end{aligned} \quad (\text{C.46})$$

$$t_{9\vec{n}_2}^\psi = - 0.213086605072021484375000 \cdot 10^{-4} \cdot t^9 - 0.892141865413920433487476 \cdot 10^{-3} \cdot t^{10} \quad (\text{C.47})$$

$$t_{10\vec{n}_2}^\psi = - 0.905618071556091308593750 \cdot 10^{-5} \cdot t^{10} \quad (\text{C.48})$$

$$\begin{aligned} t_{\vec{n}_1+\vec{n}_2}^\psi &= - 0.62500000000000000000000000000000 \cdot 10^{-1} \cdot t^2 - 0.78125000000000000000000000000000 \cdot 10^{-1} \cdot t^3 \\ &\quad - 0.21809895833333333333333333333333 \cdot t^4 - 0.4951714409722222222222222 \cdot t^5 \\ &\quad - 1.39803116409866898148148 \cdot t^6 - 3.71647076547881703317901 \cdot t^7 \\ &\quad - 11.1900493504088601948302 \cdot t^8 - 32.7352555611782767318077 \cdot t^9 \\ &\quad - 101.586238102227245011611 \cdot t^{10} \end{aligned} \quad (\text{C.49})$$

$$\begin{aligned} t_{\vec{n}_1+2\vec{n}_2}^\psi &= - 0.23437500000000000000000000000000 \cdot 10^{-1} \cdot t^3 - 0.70312500000000000000000000000000 \cdot 10^{-1} \cdot t^4 \\ &\quad - 0.18444824218750000000000000000000 \cdot t^5 - 0.5187191433376736111111111 \cdot t^6 \\ &\quad - 1.42024303365636754918981 \cdot t^7 - 4.26175564547134525000804 \cdot t^8 \\ &\quad - 12.5089659191752861883742 \cdot t^9 - 39.0993581152697313946570 \cdot t^{10} \end{aligned} \quad (\text{C.50})$$

$$\begin{aligned} t_{\vec{n}_1+3\vec{n}_2}^\psi &= - 0.97656250000000000000000000000000 \cdot 10^{-2} \cdot t^4 - 0.4444715711805555555555556 \cdot 10^{-1} \cdot t^5 \\ &\quad - 0.16543240017361111111111111111111 \cdot t^6 - 0.564412935280505521797840 \cdot t^7 \\ &\quad - 1.89549046637099466206115 \cdot t^8 - 6.12654282364222656715717 \cdot t^9 \\ &\quad - 20.0755549295504620468229 \cdot t^{10} \end{aligned} \quad (\text{C.51})$$

$$\begin{aligned} t_{\vec{n}_1+4\vec{n}_2}^\psi &= - 0.42724609375000000000000000000000 \cdot 10^{-2} \cdot t^5 - 0.298179343894675925925926 \cdot 10^{-1} \cdot t^6 \\ &\quad - 0.132032871246337890625000 \cdot t^7 - 0.523569408022327187620563 \cdot t^8 \\ &\quad - 1.92931227007459220572264 \cdot t^9 - 6.95998152394272867380673 \cdot t^{10} \end{aligned} \quad (\text{C.52})$$

$$t_{\vec{n}_1+5\vec{n}_2}^\psi = - 0.19226074218750000000000000000000 \cdot 10^{-2} \cdot t^6 - 0.186671504267939814814815 \cdot 10^{-1} \cdot t^7$$

$$\begin{aligned}
& -0.103778195233992588372878 \cdot t^8 - 0.477884756279457743766377 \cdot t^9 \\
& - 1.99172363575858204098777 \cdot t^{10}
\end{aligned} \tag{C.53}$$

$$\begin{aligned}
t_{\vec{n}_1+6\vec{n}_2}^\psi &= -0.881195068359375000000000 \cdot 10^{-3} \cdot t^7 - 0.114771132606537744341564 \cdot 10^{-1} \cdot t^8 \\
& - 0.773933085655111344262896 \cdot 10^{-1} \cdot t^9 - 0.410204415941156981794813 \cdot t^{10}
\end{aligned} \tag{C.54}$$

$$\begin{aligned}
t_{\vec{n}_1+7\vec{n}_2}^\psi &= -0.409126281738281250000000 \cdot 10^{-3} \cdot t^8 - 0.687324849502866977853867 \cdot 10^{-2} \cdot t^9 \\
& - 0.559710753028918522702650 \cdot 10^{-1} \cdot t^{10}
\end{aligned} \tag{C.55}$$

$$t_{\vec{n}_1+8\vec{n}_2}^\psi = -0.191777944564819335937500 \cdot 10^{-3} \cdot t^9 - 0.404455727387848214357478 \cdot 10^{-2} \cdot t^{10} \tag{C.56}$$

$$t_{\vec{n}_1+9\vec{n}_2}^\psi = -0.905618071556091308593750 \cdot 10^{-4} \cdot t^{10} \tag{C.57}$$

$$\begin{aligned}
t_{2\vec{n}_1+2\vec{n}_2}^\psi &= -0.146484375000000000000000 \cdot 10^{-1} \cdot t^4 - 0.559895833333333333333333 \cdot 10^{-1} \cdot t^5 \\
& - 0.207502011899594907407407 \cdot t^6 - 0.679816822946807484567901 \cdot t^7 \\
& - 2.23513729699845176665381 \cdot t^8 - 7.07478435845736449965070 \cdot t^9 \\
& - 22.8631245699911716870647 \cdot t^{10}
\end{aligned} \tag{C.58}$$

$$\begin{aligned}
t_{2\vec{n}_1+3\vec{n}_2}^\psi &= -0.854492187500000000000000 \cdot 10^{-2} \cdot t^5 - 0.461776168258101851851852 \cdot 10^{-1} \cdot t^6 \\
& - 0.188378993375801745756173 \cdot t^7 - 0.710630058996961931142297 \cdot t^8 \\
& - 2.54040492242766832945605 \cdot t^9 - 8.98034534391086969301479 \cdot t^{10}
\end{aligned} \tag{C.59}$$

$$\begin{aligned}
t_{2\vec{n}_1+4\vec{n}_2}^\psi &= -0.480651855468750000000000 \cdot 10^{-2} \cdot t^6 - 0.343311451099537037037037 \cdot 10^{-1} \cdot t^7 \\
& - 0.171912640087889055165734 \cdot t^8 - 0.734671442071678543614098 \cdot t^9 \\
& - 2.91173876214683631619853 \cdot t^{10}
\end{aligned} \tag{C.60}$$

$$\begin{aligned}
t_{2\vec{n}_1+5\vec{n}_2}^\psi &= -0.264358520507812500000000 \cdot 10^{-2} \cdot t^7 - 0.246123090202425733024691 \cdot 10^{-1} \cdot t^8 \\
& - 0.143504170164343260933833 \cdot t^9 - 0.698859938329543064978224 \cdot t^{10}
\end{aligned} \tag{C.61}$$

$$\begin{aligned}
t_{2\vec{n}_1+6\vec{n}_2}^\psi &= -0.143194198608398437500000 \cdot 10^{-2} \cdot t^8 - 0.168646968114196191272291 \cdot 10^{-1} \cdot t^9 \\
& - 0.115911826556723072586618 \cdot t^{10}
\end{aligned} \tag{C.62}$$

$$t_{2\vec{n}_1+7\vec{n}_2}^\psi = -0.767111778259277343750000 \cdot 10^{-3} \cdot t^9 - 0.111973297019554263770335 \cdot 10^{-1} \cdot t^{10} \tag{C.63}$$

$$t_{2\vec{n}_1+8\vec{n}_2}^\psi = -0.407528132200241088867188 \cdot 10^{-3} \cdot t^{10} \tag{C.64}$$

$$\begin{aligned}
t_{3\vec{n}_1+3\vec{n}_2}^\psi &= -0.640869140625000000000000 \cdot 10^{-2} \cdot t^6 - 0.416626164942611882716049 \cdot 10^{-1} \cdot t^7 \\
& - 0.203075303462307149000129 \cdot t^8 - 0.846265290707186252819004 \cdot t^9 \\
& - 3.30093401436759631656652 \cdot t^{10}
\end{aligned} \tag{C.65}$$

$$\begin{aligned}
t_{3\vec{n}_1+4\vec{n}_2}^\psi &= -0.440597534179687500000000 \cdot 10^{-2} \cdot t^7 - 0.352927470894016846707819 \cdot 10^{-1} \cdot t^8 \\
& - 0.193859300625974258768215 \cdot t^9 - 0.908028422496739347394220 \cdot t^{10}
\end{aligned} \tag{C.66}$$

$$\begin{aligned}
t_{3\vec{n}_1+5\vec{n}_2}^\psi &= -0.286388397216796875000000 \cdot 10^{-2} \cdot t^8 - 0.279760552858946581763332 \cdot 10^{-1} \cdot t^9 \\
& - 0.176946337471933712630060 \cdot t^{10}
\end{aligned} \tag{C.67}$$

$$t_{3\vec{n}_1+6\vec{n}_2}^\psi = -0.178992748260498046875000 \cdot 10^{-2} \cdot t^9 - 0.211462032443374926824792 \cdot 10^{-1} \cdot t^{10} \tag{C.68}$$

$$t_{3\vec{n}_1+7\vec{n}_2}^\psi = -0.108674168586730957031250 \cdot 10^{-2} \cdot t^{10} \tag{C.69}$$

$$\begin{aligned}
t_{4\vec{n}_1+4\vec{n}_2}^\psi &= -0.357985496520996093750000 \cdot 10^{-2} \cdot t^8 - 0.329564006894377196930727 \cdot 10^{-1} \cdot t^9 \\
& - 0.203350027212208783348565 \cdot t^{10}
\end{aligned} \tag{C.70}$$

$$\begin{aligned}
t_{4\vec{n}_1+5\vec{n}_2}^\psi &= -0.268489122390747070312500 \cdot 10^{-2} \cdot t^9 \\
& - 0.287307652303711377053594 \cdot 10^{-1} \cdot t^{10}
\end{aligned} \tag{C.71}$$

$$t_{4\vec{n}_1+6\vec{n}_2}^\psi = -0.190179795026779174804688 \cdot 10^{-2} \cdot t^{10} \tag{C.72}$$

$$t_{5\vec{n}_1+5\vec{n}_2}^\psi = -0.228215754032135009765625 \cdot 10^{-2} \cdot t^{10}. \tag{C.73}$$

The other hopping elements can be obtained by the symmetry relations (A.48).

The dispersion $\omega(\vec{k})$ has for $\theta > 0$ its minimum at $\vec{k} = 0$ and thus we obtain the gaps for the σ - and the ψ -particle which read

$$\begin{aligned} \Delta_{\text{top}}^{\sigma,+} = & 1. - 1.50000000000000000000000000000000 \cdot t - 1.87500000000000000000000000000000 \cdot t^2 \\ & - 2.81250000000000000000000000000000 \cdot t^3 - 7.09375000000000000000000000000000 \cdot t^4 \\ & - 16.523356119791666666666667 \cdot t^5 - 48.0582529703776041666667 \cdot t^6 \\ & - 133.183396869235568576389 \cdot t^7 - 409.210126276516620023751 \cdot t^8 \\ & - 1231.46193224709772278743 \cdot t^9 - 3900.73520870614524506574 \cdot t^{10}, \end{aligned} \quad (\text{C.74})$$

$$\begin{aligned} \Delta_{\text{top}}^{\psi,+} = & 1. - 1.50000000000000000000000000000000 \cdot t - 1.87500000000000000000000000000000 \cdot t^2 \\ & - 2.81250000000000000000000000000000 \cdot t^3 - 7.09375000000000000000000000000000 \cdot t^4 \\ & - 16.52368164062500000000000000000000 \cdot t^5 - 48.0621524386935763888889 \cdot t^6 \\ & - 133.170746909247504340278 \cdot t^7 - 409.232616357008616129557 \cdot t^8 \\ & - 1231.41014805650330865334 \cdot t^9 - 3900.79031518243977848558 \cdot t^{10}, \end{aligned} \quad (\text{C.75})$$

whereas for $\theta < 0$, the minimum is located at $\vec{k} = \pm(\frac{2\pi}{3}, -\frac{2\pi}{3})$ and thus we obtain the gaps

$$\begin{aligned} \Delta_{\text{top}}^{\sigma,-} = & 1. + 0.75000000000000000000000000000000 \cdot t + 0.09375000000000000000000000000000 \cdot t^2 \\ & + 0.42187500000000000000000000000000 \cdot t^3 + 0.36962890625000000000000000000000 \cdot t^4 \\ & + 0.68062337239583333333333333333333 \cdot t^5 + 1.17367808024088541666667 \cdot t^6 \\ & + 2.56743341022067599826389 \cdot t^7 + 5.44571827679504582911362 \cdot t^8 \\ & + 12.5039242965188413981057 \cdot t^9 + 29.5149245166312660434282 \cdot t^{10}, \end{aligned} \quad (\text{C.76})$$

$$\begin{aligned} \Delta_{\text{top}}^{\psi,-} = & 1. + 0.75000000000000000000000000000000 \cdot t + 0.09375000000000000000000000000000 \cdot t^2 \\ & + 0.42187500000000000000000000000000 \cdot t^3 + 0.36962890625000000000000000000000 \cdot t^4 \\ & + 0.68078613281250000000000000000000 \cdot t^5 + 1.16975826687282986111111 \cdot t^6 \\ & + 2.55695401297675238715278 \cdot t^7 + 5.40481139951282077365451 \cdot t^8 \\ & + 12.3674853651670148833789 \cdot t^9 + 29.0485813856350017816278 \cdot t^{10}. \end{aligned} \quad (\text{C.77})$$

C.2 Series expansions for the 1-phase

ground-state energy e_0

For the **1** phase ($\theta = \frac{\pi}{2}$), we obtain the following expression for the ground-state energy per plaquette

$$\begin{aligned} \frac{e_0}{\sin \theta} = & -3. - 0.25000000000000000000000000000000 \cdot t^{-1} - 0.31250000000000000000000000000000 \cdot 10^{-1} \cdot t^{-2} \\ & - 0.260416666666666666666667 \cdot 10^{-2} \cdot t^{-3} - 0.1785432449494949494949 \cdot 10^{-3} \cdot t^{-4} \\ & - 0.200349254859198041016223 \cdot 10^{-4} \cdot t^{-5} - 0.351865673699176518563571 \cdot 10^{-5} \cdot t^{-6} \\ & - 6.00264240296590775496022 \cdot 10^{-7} \cdot t^{-7} - 1.06268022747234966299366 \cdot 10^{-7} \cdot t^{-8} \\ & - 2.06668586434339172411199 \cdot 10^{-8} \cdot t^{-9} - 4.14287313184869848904055 \cdot 10^{-9} \cdot t^{-10} \\ & - 8.43173702806333463560174 \cdot 10^{-10} \cdot t^{-11} - 1.76732327215558302458088 \cdot 10^{-10} \cdot t^{-12} \\ & - 3.79308366811706943893733 \cdot 10^{-11} \cdot t^{-13} - 8.26205982070386673481900 \cdot 10^{-12} \cdot t^{-14} \\ & - 1.82493536446614742320773 \cdot 10^{-12} \cdot t^{-15} - 4.08506096403231715115396 \cdot 10^{-13} \cdot t^{-16} \\ & - 9.24547845254661430097976 \cdot 10^{-14} \cdot t^{-17} - 2.11245497716661431781268 \cdot 10^{-14} \cdot t^{-18}. \end{aligned} \quad (\text{C.78})$$

$$t_{\vec{n}_1+2\vec{n}_2}^{\psi,\sigma} = -0.160734204149900231351128 \cdot 10^{-7} \cdot t^{-6} - 0.105835868487557790234729 \cdot 10^{-7} \cdot t^{-7} \\ - 0.439646964049689424904645 \cdot 10^{-8} \cdot t^{-8} \quad (\text{C.94})$$

$$t_{\vec{n}_1+3\vec{n}_2}^{\psi,\sigma} = -0.206417975197758833167057 \cdot 10^{-10} \cdot t^{-8} \quad (\text{C.95})$$

$$t_{2\vec{n}_1+2\vec{n}_2}^{\psi,\sigma} = -0.309626962796638249750585 \cdot 10^{-10} \cdot t^{-8} \quad (\text{C.96})$$

$$t_0^{\psi,\psi} = 6. - 0.14583333333333333333333333333333 \cdot 10^{-1} \cdot t^{-2} - 0.71527777777777777777777777777778 \cdot 10^{-2} \cdot t^{-3} \\ - 0.100903731323653198653199 \cdot 10^{-2} \cdot t^{-4} - 0.143564259077916156514641 \cdot 10^{-3} \cdot t^{-5} \\ - 0.367516624901264042252227 \cdot 10^{-4} \cdot t^{-6} - 0.719451830392257893828678 \cdot 10^{-5} \cdot t^{-7} \\ - 0.158412500886427996629716 \cdot 10^{-5} \cdot t^{-8} \quad (\text{C.97})$$

$$t_{\vec{n}_2}^{\psi,\psi} = -0.52083333333333333333333333333333 \cdot 10^{-2} \cdot t^{-2} - 0.10069444444444444444444444444444 \cdot 10^{-2} \cdot t^{-3} \\ - 0.142071759259259259259259259 \cdot 10^{-3} \cdot t^{-4} - 0.255563241464120370370370 \cdot 10^{-4} \cdot t^{-5} \\ - 0.664474826538919669525862 \cdot 10^{-5} \cdot t^{-6} - 0.126798446353039813793559 \cdot 10^{-5} \cdot t^{-7} \\ - 0.253083575170257517205245 \cdot 10^{-6} \cdot t^{-8} \quad (\text{C.98})$$

$$t_{2\vec{n}_2}^{\psi,\psi} = -0.17089843750000000000000000000000 \cdot 10^{-5} \cdot t^{-4} - 0.703352730624142661179698 \cdot 10^{-6} \cdot t^{-5} \\ - 0.112935384081475495562108 \cdot 10^{-6} \cdot t^{-6} - 0.247826608740329661828209 \cdot 10^{-7} \cdot t^{-7} \\ - 0.119657531341479734686412 \cdot 10^{-8} \cdot t^{-8} \quad (\text{C.99})$$

$$t_{3\vec{n}_2}^{\psi,\psi} = -0.427783156025441483099662 \cdot 10^{-8} \cdot t^{-6} - 0.284855754487624569035530 \cdot 10^{-8} \cdot t^{-7} \\ - 0.129761000554291166071617 \cdot 10^{-8} \cdot t^{-8} \quad (\text{C.100})$$

$$t_{4\vec{n}_2}^{\psi,\psi} = -0.363988538622799799397385 \cdot 10^{-11} \cdot t^{-8} \quad (\text{C.101})$$

$$t_{\vec{n}_1+\vec{n}_2}^{\psi,\psi} = -0.34179687500000000000000000000000 \cdot 10^{-5} \cdot t^{-4} - 0.140670546124828532235940 \cdot 10^{-5} \cdot t^{-5} \\ - 0.298104288949203891815775 \cdot 10^{-6} \cdot t^{-6} - 0.113366444542163287718662 \cdot 10^{-6} \cdot t^{-7} \\ - 0.300709276699838492703622 \cdot 10^{-7} \cdot t^{-8} \quad (\text{C.102})$$

$$t_{\vec{n}_1+2\vec{n}_2}^{\psi,\psi} = -0.128334946807632444929899 \cdot 10^{-7} \cdot t^{-6} - 0.854567263462873707106591 \cdot 10^{-8} \cdot t^{-7} \\ - 0.356290737892094392075796 \cdot 10^{-8} \cdot t^{-8} \quad (\text{C.103})$$

$$t_{\vec{n}_1+3\vec{n}_2}^{\psi,\psi} = -0.145595415449119919758954 \cdot 10^{-10} \cdot t^{-8} \quad (\text{C.104})$$

$$t_{2\vec{n}_1+2\vec{n}_2}^{\psi,\psi} = -0.218393123173679879638431 \cdot 10^{-10} \cdot t^{-8}. \quad (\text{C.105})$$

The other hopping elements can be obtained by the symmetry relations (A.48).

The dispersion is minimized by $\vec{k} = \vec{0}$ and the gap Δ_1^+ for $\theta < \frac{\pi}{2}$ reads

$$\frac{\Delta_1^+}{\cos \theta} = 6. - 0.50000000000000000000000000000000 \cdot t^{-1} - 0.50000000000000000000000000000000 \cdot 10^{-1} \cdot t^{-2} \\ - 0.15104166666666666666666666666667 \cdot 10^{-1} \cdot t^{-3} - 0.204225852272727272727272727273 \cdot 10^{-2} \cdot t^{-4} \\ - 0.240913223439413070094888 \cdot 10^{-3} \cdot t^{-5} - 0.720772401045415442646247 \cdot 10^{-4} \cdot t^{-6} \\ - 0.107328311801088484023827 \cdot 10^{-4} \cdot t^{-7} - 0.242154849905598009927503 \cdot 10^{-5} \cdot t^{-8}, \quad (\text{C.106})$$

whereas the gap Δ_1^- for $\theta > \frac{\pi}{2}$ reads

$$\frac{\Delta_1^-}{\cos \theta} = 6. + 0.25000000000000000000000000000000 \cdot t^{-1} - 0.43750000000000000000000000000000 \cdot 10^{-1} \cdot t^{-2} \\ - 0.12239583333333333333333333333333 \cdot 10^{-1} \cdot t^{-3} - 0.181721511994949494949495 \cdot 10^{-2} \cdot t^{-4} \\ - 0.343887217941727884909703 \cdot 10^{-3} \cdot t^{-5} - 0.828596996337660161192464 \cdot 10^{-4} \cdot t^{-6} \\ - 0.182601329879976380714328 \cdot 10^{-4} \cdot t^{-7} - 0.380068651931927143552667 \cdot 10^{-5} \cdot t^{-8} \quad (\text{C.107})$$

Bibliography

- [1] L. D. LANDAU. *Theory of phase transformations. I.* *Phys. Z. Sowjetunion* **11**, 26 (1937)
- [2] L. D. LANDAU. *Theory of phase transformations. II.* *Phys. Z. Sowjetunion* **11**, 545 (1937)
- [3] D. C. TSUI, H. L. STORMER, A. C. GOSSARD. *Two-Dimensional Magnetotransport in the Extreme Quantum Limit.* *Phys. Rev. Lett.* **48**, 1559 (1982)
- [4] R. B. LAUGHLIN. *Anomalous Quantum Hall Effect: An Incompressible Quantum Fluid with Fractionally Charged Excitations.* *Phys. Rev. Lett.* **50**, 1395 (1983)
- [5] R. B. LAUGHLIN. *The Relationship Between High-Temperature Superconductivity and the Fractional Quantum Hall Effect.* *Science* **242**, 525 (1988)
- [6] X. G. WEN, F. WILCZEK, A. ZEE. *Chiral spin states and superconductivity.* *Phys. Rev. B* **39**, 11413 (1989)
- [7] X. G. WEN. *Vacuum degeneracy of chiral spin states in compactified space.* *Phys. Rev. B* **40**, 7387 (1989)
- [8] X. G. WEN, Q. NIU. *Ground-state degeneracy of the fractional quantum Hall states in the presence of a random potential and on high-genus Riemann surfaces.* *Phys. Rev. B* **41**, 9377 (1990)
- [9] E. WITTEN. *Topological quantum field theory.* *Commun. Math. Phys.* **117**, 353 (1988)
- [10] X. G. WEN. *Quantum Field Theory of Many-Body Systems.* Oxford University Press, (2004)
- [11] Z. WANG. *Topological Quantum Computation.* American Mathematical Society (2008)
- [12] Z. NUSSINOV, G. ORTIZ. *Sufficient symmetry conditions for Topological Quantum Order.* *Proc. Natl. Acad. Sci. U.S.A.* **106**, 16944 (2009)
- [13] Z. NUSSINOV, G. ORTIZ. *A symmetry principle for topological quantum order.* *Ann. Phys.* **324**, 977 (2009)
- [14] S. BRAVYI, M. B. HASTINGS, S. MICHALAKIS. *Topological quantum order: stability under local perturbations.* *J. Math. Phys.* **51**, 093512 (2010)
- [15] X.-G. WEN. *Quantum order from string-net condensations and the origin of light and massless fermions.* *Phys. Rev. D* **68**, 065003 (2003)
- [16] F. A. BAIS, J. C. ROMERS. *The modular S-matrix as order parameter for topological phase transitions.* *New J. Phys.* **14**, 035024 (2012)
- [17] A. KITAEV, J. PRESKILL. *Topological Entanglement Entropy.* *Phys. Rev. Lett.* **96**, 110404 (2006)
- [18] M. LEVIN, X.-G. WEN. *Detecting Topological Order in a Ground State Wave Function.* *Phys. Rev. Lett.* **96**, 110405 (2006)

- [19] F. A. BAIS, J. K. SLINGERLAND. *Condensate-induced transitions between topologically ordered phases.* *Phys. Rev. B* **79**, 045316 (2009)
- [20] B. I. HALPERIN. *Statistics of Quasiparticles and the Hierarchy of Fractional Quantized Hall States.* *Phys. Rev. Lett.* **52**, 1583 (1984)
- [21] G. MOORE, N. READ. *Nonabelions in the fractional quantum Hall effect.* *Nucl. Phys. B* **360**, 362 (1991)
- [22] F. WILCZEK. *Quantum Mechanics of Fractional-Spin Particles.* *Phys. Rev. Lett.* **49**, 957 (1982)
- [23] M. OSHIKAWA, T. SENTHIL. *Fractionalization, Topological Order, and Quasiparticle Statistics.* *Phys. Rev. Lett.* **96**, 060601 (2006)
- [24] J. S. XIA, W. PAN, C. L. VICENTE, E. D. ADAMS, N. S. SULLIVAN, H. L. STORMER, D. C. TSUI, L. N. PFEIFFER, K. W. BALDWIN, K. W. WEST. *Electron Correlation in the Second Landau Level: A Competition Between Many Nearly Degenerate Quantum Phases.* *Phys. Rev. Lett.* **93**, 176809 (2004)
- [25] R. L. WILLETT, L. N. PFEIFFER, K. W. WEST. *Measurement of filling factor $5/2$ quasiparticle interference with observation of charge $e/4$ and $e/2$ period oscillations.* *Proc. Natl. Acad. Sci. U.S.A.* **106**, 8853 (2009)
- [26] R. L. WILLETT, L. N. PFEIFFER, K. W. WEST. *Alternation and interchange of $e/4$ and $e/2$ period interference oscillations consistent with filling factor $5/2$ non-Abelian quasiparticles.* *Phys. Rev. B* **82**, 205301 (2010)
- [27] R. L. WILLETT, C. NAYAK, K. SHTENDEL, L. N. PFEIFFER, K. W. WEST. *Magnetic field-tuned Aharonov-Bohm oscillations and evidence for non-Abelian anyons at $\nu=5/2$.* *Phys. Rev. Lett.* **111**, 186401 (2013)
- [28] A. Y. KITAEV. *Fault-tolerant quantum computation by anyons.* *Ann. Phys.* **303**, 2 (2003)
- [29] J. PRESKILL. *Lecture notes.* <http://www.theory.caltech.edu/people/preskill/ph229/> (2004)
- [30] C. NAYAK, S. H. SIMON, A. STERN, M. FREEDMAN, S. DAS SARMA. *Non-Abelian anyons and topological quantum computation.* *Rev. Mod. Phys.* **80**, 1083 (2008)
- [31] G. K. BRENNEN, J. K. PACHOS. *Why should anyone care about computing with anyons?* *Proc. Roy. Soc. A* **464**, 1 (2008)
- [32] L. HORMOZI, N. E. BONESTEEL, S. H. SIMON. *Topological Quantum Computing with Read-Rezayi States.* *Phys. Rev. Lett.* **103**, 160501 (2009)
- [33] R. KOENIG, G. KUPERBERG, B. W. REICHARDT. *Quantum computation with Turaev-Viro codes.* *Ann. Phys.* **325**, 2707 (2010)
- [34] X.-L. QI, S.-C. ZHANG. *Topological insulators and superconductors.* *Rev. Mod. Phys.* **83**, 1057 (2011)
- [35] A. ROTH, C. BRÜNE, H. BUHMANN, L. W. MOLENKAMP, J. MACIEJKO, X.-L. QI, S.-C. ZHANG. *Nonlocal Transport in the Quantum Spin Hall State.* *Science* **325**, 294 (2009)
- [36] A. ALTLAND, M. R. ZIRNBAUER. *Nonstandard symmetry classes in mesoscopic normal-superconducting hybrid structures.* *Phys. Rev. B* **55**, 1142 (1997)
- [37] A. P. SCHNYDER, S. RYU, A. FURUSAKI, A. W. W. LUDWIG. *Classification of topological insulators and superconductors in three spatial dimensions.* *Phys. Rev. B* **78**, 195125 (2008)
- [38] X.-L. QI, T. L. HUGHES, S.-C. ZHANG. *Topological field theory of time-reversal invariant insulators.* *Phys. Rev. B* **78**, 195424 (2008)

- [39] K. DUIVENVOORDEN, T. QUELLA. *Discriminating string order parameter for topological phases of gapped $SU(N)$ spin chains.* *Phys. Rev. B* **86**, 235142 (2012)
- [40] F. POLLMANN, A. M. TURNER. *Detection of symmetry-protected topological phases in one dimension.* *Phys. Rev. B* **86**, 125441 (2012)
- [41] X. CHEN, Z.-C. GU, X.-G. WEN. *Classification of gapped symmetric phases in one-dimensional spin systems.* *Phys. Rev. B* **83**, 035107 (2011)
- [42] A. Y. KITAEV. *Unpaired Majorana fermions in quantum wires.* *Physics-Uspekhi* **44**, 131 (2001)
- [43] J. ALICEA, Y. OREG, G. REFEAL, F. VON OPPEN, M. P. FISHER. *Non-Abelian statistics and topological quantum information processing in 1D wire networks.* *Nat. Phys.* **7**, 412 (2011)
- [44] B. VAN HECK, A. R. AKHMEROV, F. HASSLER, M. BURRELLO, C. W. J. BEENAKKER. *Coulomb-assisted braiding of Majorana fermions in a Josephson junction array.* *New J. Phys.* **14**, 035019 (2012)
- [45] V. MOURIK, K. ZUO, S. M. FROLOV, S. R. PLISSARD, E. P. A. M. BAKKERS, L. P. KOUWENHOVEN. *Signatures of Majorana Fermions in Hybrid Superconductor-Semiconductor Nanowire Devices.* *Science* **336**, 1003 (2012)
- [46] P. W. ANDERSON. *Resonating valence bonds: A new kind of insulator?* *Mater. Res. Bull.* **8**, 153 (1973)
- [47] C. CASTELNOVO, C. CHAMON. *Entanglement and topological entropy of the toric code at finite temperature.* *Phys. Rev. B* **76**, 184442 (2007)
- [48] D. S. ROKHSAR, S. A. KIVELSON. *Superconductivity and the Quantum Hard-Core Dimer Gas.* *Phys. Rev. Lett.* **61**, 2376 (1988)
- [49] R. MOESSNER, S. L. SONDHI, P. CHANDRA. *Phase diagram of the hexagonal lattice quantum dimer model.* *Phys. Rev. B* **64**, 144416 (2001)
- [50] G. MISGUICH, D. SERBAN, V. PASQUIER. *Quantum Dimer Model on the Kagome Lattice: Solvable Dimer-Liquid and Ising Gauge Theory.* *Phys. Rev. Lett.* **89**, 137202 (2002)
- [51] M. TROYER, S. TREBST, K. SHTENDEL, C. NAYAK. *Local Interactions and Non-Abelian Quantum Loop Gases.* *Phys. Rev. Lett.* **101**, 230401 (2008)
- [52] P. FENDLEY. *Topological order from quantum loops and nets.* *Ann. Phys.* **323**, 3113 (2008)
- [53] A. KITAEV. *Anyons in an exactly solved model and beyond.* *Ann. Phys.* **321**, 2 (2006)
- [54] F. A. BAIS, P. VAN DRIEL, M. DE WILD PROPITIUS. *Quantum symmetries in discrete gauge theories.* *Phys. Lett. B* **280**, 63 (1992)
- [55] F. A. BAIS, P. VAN DRIEL, M. DE WILD PROPITIUS. *Anyons in discrete gauge theories with Chern-Simons terms.* *Nucl. Phys. B* **393**, 547 (1993)
- [56] M. A. LEVIN, X.-G. WEN. *String-net condensation: A physical mechanism for topological phases.* *Phys. Rev. B* **71**, 045110 (2005)
- [57] P. FENDLEY, E. FRADKIN. *Realizing non-Abelian statistics in time-reversal-invariant systems.* *Phys. Rev. B* **72**, 024412 (2005)
- [58] L. FIDKOWSKI, M. FREEDMAN, C. NAYAK, K. WALKER, Z. WANG. *From String Nets to Nonabelions.* *Commun. Math. Phys.* **287**, 805 (2009)
- [59] P. FENDLEY, S. V. ISAKOV, M. TROYER. *Fibonacci topological order from quantum nets.* *Phys. Rev. Lett.* **110**, 260408 (2013)

- [60] P. FINCH, H. FRAHM, J. LINKS. *Ground-state phase diagram for a system of interacting, non-Abelian anyons.* *Nucl. Phys. B* **844**, 129 (2011)
- [61] P. E. FINCH, H. FRAHM. *Collective states of interacting $D(D3)$ -non-Abelian anyons.* *J. Stat. Mech.: Theory Exp.*, L05001 (2012)
- [62] P. E. FINCH, H. FRAHM. *The $D(D3)$ -anyon chain: integrable boundary conditions and excitation spectra.* *New J. Phys.* **15**, 053035 (2013)
- [63] P. E. FINCH. *From spin to anyon notation: the XXZ Heisenberg model as a $D 3$ (or $su(2)_4$) anyon chain.* *J. Phys. A* **46**, 055305 (2013)
- [64] A. FEIGUIN, S. TREBST, A. W. W. LUDWIG, M. TROYER, A. KITAEV, Z. WANG, M. H. FREEDMAN. *Interacting Anyons in Topological Quantum Liquids: The Golden Chain.* *Phys. Rev. Lett.* **98**, 160409 (2007)
- [65] C. GILS, E. ARDONNE, S. TREBST, A. W. W. LUDWIG, M. TROYER, Z. WANG. *Collective States of Interacting Anyons, Edge States, and the Nucleation of Topological Liquids.* *Phys. Rev. Lett.* **103**, 070401 (2009)
- [66] E. ARDONNE, J. GUKELBERGER, A. W. W. LUDWIG, S. TREBST, M. TROYER. *Microscopic models of interacting Yang-Lee anyons.* *New J. Phys.* **13**, 045006 (2011)
- [67] D. POILBLANC, A. W. W. LUDWIG, S. TREBST, M. TROYER. *Quantum spin ladders of non-Abelian anyons.* *Phys. Rev. B* **83**, 134439 (2011)
- [68] C. GILS, E. ARDONNE, S. TREBST, D. A. HUSE, A. W. W. LUDWIG, M. TROYER, Z. WANG. *Anyonic quantum spin chains: Spin-1 generalizations and topological stability.* *Phys. Rev. B* **87**, 235120 (2013)
- [69] C. GILS, S. TREBST, A. KITAEV, A. W. W. LUDWIG, M. TROYER, Z. WANG. *Topology-driven quantum phase transitions in time-reversal-invariant anyonic quantum liquids.* *Nat. Phys.* **5**, 834 (2009)
- [70] C. GILS. *Ashkin-Teller universality in a quantum double model of Ising anyons.* *J. Stat. Mech.: Theory Exp.*, P07019 (2009)
- [71] S. TREBST, E. ARDONNE, A. FEIGUIN, D. A. HUSE, A. W. W. LUDWIG, M. TROYER. *Collective States of Interacting Fibonacci Anyons.* *Phys. Rev. Lett.* **101**, 050401 (2008)
- [72] A. W. W. LUDWIG, D. POILBLANC, S. TREBST, M. TROYER. *Two-dimensional quantum liquids from interacting non-Abelian anyons.* *New J. Phys.* **13**, 045014 (2011)
- [73] S. GLADCHENKO, D. OLAYA, E. DUPONT-FERRIER, B. DOUÇOT, L. B. IOFFE, G. M.E. *Superconducting nanocircuits for topologically protected qubits.* *Nat. Phys.* **5**, 48 (2009)
- [74] S. TREBST, P. WERNER, M. TROYER, K. SHTENDEL, C. NAYAK. *Breakdown of a Topological Phase: quantum Phase Transition in a Loop Gas Model with Tension.* *Phys. Rev. Lett.* **98**, 070602 (2007)
- [75] A. HAMMA, D. A. LIDAR. *Adiabatic Preparation of Topological Order.* *Phys. Rev. Lett.* **100**, 030502 (2008)
- [76] C. CASTELNOVO, M. TROYER, S. TREBST. *Understanding Quantum Phase Transitions*, chapter Topological Order and Quantum Criticality, pp. 167–192. CRC Press, (2010)
- [77] I. S. TUPITSYN, A. KITAEV, N. V. PROKOF'EV, P. C. E. STAMP. *Topological multicritical point in the phase diagram of the toric code model and three-dimensional lattice gauge Higgs model.* *Phys. Rev. B* **82**, 085114 (2010)

- [78] J. VIDAL, S. DUSUEL, K. P. SCHMIDT. *Low-energy effective theory of the toric code model in a parallel magnetic field.* *Phys. Rev. B* **79**, 033109 (2009)
- [79] F. WU, Y. DENG, N. PROKOF'EV. *Phase diagram of the toric code model in a parallel magnetic field.* *Phys. Rev. B* **85**, 195104 (2012)
- [80] K. P. SCHMIDT. *Persisting topological order via geometric frustration.* *Phys. Rev. B* **88**, 035118 (2013)
- [81] J. VIDAL, R. THOMALE, K. P. SCHMIDT, S. DUSUEL. *Self-duality and bound states of the toric code model in a transverse field.* *Phys. Rev. B* **80**, 081104 (2009)
- [82] S. DUSUEL, M. KAMFOR, R. ORÚS, K. P. SCHMIDT, J. VIDAL. *Robustness of a Perturbed Topological Phase.* *Phys. Rev. Lett.* **106**, 107203 (2011)
- [83] C. STARK, L. POLLET, A. M. C. IMAMOĞLU, R. RENNER. *Localization of Toric Code Defects.* *Phys. Rev. Lett.* **107**, 030504 (2011)
- [84] J. R. WOOTTON, J. K. PACHOS. *Bringing Order through Disorder: localization of Errors in Topological Quantum Memories.* *Phys. Rev. Lett.* **107**, 030503 (2011)
- [85] S. S. BULLOCK, G. K. BRENNEN. *Qudit surface codes and gauge theory with finite cyclic groups.* *J. Phys. A* **40**, 3481 (2007)
- [86] M. D. SCHULZ, S. DUSUEL, R. ORÚS, J. VIDAL, K. P. SCHMIDT. *Breakdown of a perturbed Z_N topological phase.* *New J. Phys.* **14**, 025005 (2012)
- [87] M. KOCH-JANUSZ, M. LEVIN, A. STERN. *Exactly soluble lattice models for non-Abelian states of matter in two dimensions.* *Phys. Rev. B* **88**, 115133 (2013)
- [88] F. A. BAIS, J. C. ROMERS. *Anyonic order parameters for discrete gauge theories on the lattice.* *Ann. Phys.* **324**, 1168 (2009)
- [89] V. LAHTINEN, G. KELLS, A. CAROLLO, T. STITT, J. VALA, J. K. PACHOS. *Spectrum of the non-Abelian phase in Kitaev's honeycomb lattice model.* *Ann. Phys.* **323**, 2286 (2008)
- [90] M. KAMFOR, S. DUSUEL, J. VIDAL, K. P. SCHMIDT. *Kitaev model and dimer coverings on the honeycomb lattice.* *J. Stat. Mech.: Theory Exp.*, P08010 (2010)
- [91] M. KAMFOR, S. DUSUEL, K. P. SCHMIDT, J. VIDAL. *Fate of Dirac points in a vortex superlattice.* *Phys. Rev. B* **84**, 153404 (2011)
- [92] V. LAHTINEN, A. W. W. LUDWIG, J. K. PACHOS, S. TREBST. *Topological liquid nucleation induced by vortex-vortex interactions in Kitaev's honeycomb model.* *Phys. Rev. B* **86**, 075115 (2012)
- [93] H.-C. JIANG, Z.-C. GU, X.-L. QI, S. TREBST. *Possible proximity of the Mott insulating iridate Na_2IrO_3 to a topological phase: Phase diagram of the Heisenberg-Kitaev model in a magnetic field.* *Phys. Rev. B* **83**, 245104 (2011)
- [94] C. KASSEL. *Quantum Groups.* Graduate Texts in Mathematics 155. Springer, (1994)
- [95] P. BONDERSON. *Non-Abelian Anyons and Interferometry.* Ph.D. thesis, California Institute of Technology (2007)
- [96] L.-Y. HUNG, Y. WAN. *String-net models with Z_N fusion algebra.* *Phys. Rev. B* **86**, 235132 (2012)
- [97] C. W. VON KEYSERLINGK, F. J. BURNELL, S. H. SIMON. *Three-dimensional topological lattice models with surface anyons.* *Phys. Rev. B* **87**, 045107 (2013)
- [98] F. J. BURNELL, S. H. SIMON. *Space-time geometry of topological phases.* *Ann. Phys.* **325**, 2550 (2010)

- [99] F. J. BURNELL, S. H. SIMON. *A Wilson line picture of the Levin-Wen partition functions.* *New J. Phys.* **13**, 065001 (2011)
- [100] F. J. BURNELL, S. H. SIMON, J. K. SLINGERLAND. *Condensation of achiral simple currents in topological lattice models: Hamiltonian study of topological symmetry breaking.* *Phys. Rev. B* **84**, 125434 (2011)
- [101] F. J. BURNELL, S. H. SIMON, J. K. SLINGERLAND. *Phase transitions in topological lattice models via topological symmetry breaking.* *New J. Phys.* **14**, 015004 (2012)
- [102] E. ROWELL, R. STONG, Z. WANG. *On Classification of Modular Tensor Categories.* *Commun. Math. Phys.* **292**, 343 (2009)
- [103] R. N. C. PFEIFER, O. BUERSCHAPER, S. TREBST, A. W. W. LUDWIG, M. TROYER, G. VIDAL. *Translation invariance, topology, and protection of criticality in chains of interacting anyons.* *Phys. Rev. B* **86**, 155111 (2012)
- [104] M. D. SCHULZ, S. DUSUEL, K. P. SCHMIDT, J. VIDAL. *Topological Phase Transitions in the Golden String-Net Model.* *Phys. Rev. Lett.* **110**, 147203 (2013)
- [105] C. KNETTER, G. S. UHRIG. *Perturbation theory by flow equations: dimerized and frustrated $S = 1/2$ chain.* *Eur. Phys. J. B* **13**, 209 (2000)
- [106] M. TAKAHASHI. *Half-filled Hubbard model at low temperature.* *J. Phys. C* **10**, 1289 (1977)
- [107] P.-O. LÖWDIN. *Studies in Perturbation Theory. IV. Solution of Eigenvalue Problem by Projection Operator Formalism.* *J. Math. Phys.* **3**, 969 (1962)
- [108] J. M. LEINAAS, J. MYRHEIM. *On the theory of identical particles.* *Il Nuovo Cimento B* **37**, 1 (1977)
- [109] G. MOORE, N. SEIBERG. *Classical and quantum conformal field theory.* *Commun. Math. Phys.* **123**, 177 (1989)
- [110] V. G. TURAEV. *Quantum Invariants of Knots and 3-Manifolds.* De Gruyter, (2010)
- [111] P. DI FRANCESCO, P. MATHIEU, D. SÉNÉCHAL. *Conformal Field Theory.* Springer Berlin Heidelberg (1997)
- [112] W. PAULI. *The Connection Between Spin and Statistics.* *Phys. Rev.* **58**, 716 (1940)
- [113] E. ARDONNE, J. SLINGERLAND. *Clebsch-Gordan and 6j-coefficients for rank 2 quantum groups.* *J. Phys. A* **43**, 395205 (2010)
- [114] S. H. SIMON, P. FENDLEY. *Exactly solvable lattice models with crossing symmetry.* *J. Phys. A* **46**, 105002 (2013)
- [115] Y. HU, S. D. STIRLING, Y.-S. WU. *Ground-state degeneracy in the Levin-Wen model for topological phases.* *Phys. Rev. B* **85**, 075107 (2012)
- [116] V. PASQUIER. *Two-dimensional critical systems labelled by Dynkin diagrams.* *Nucl. Phys. B* **285**, 162 (1987)
- [117] T. MANSOUR, S. SEVERINI. *Counting paths in Bratteli diagrams for $SU(2)_k$.* *Europhys. Lett.* **86**, 33001 (2009)
- [118] H. YAO, S. A. KIVELSON. *Exact Spin Liquid Ground States of the Quantum Dimer Model on the Square and Honeycomb Lattices.* *Phys. Rev. Lett.* **108**, 247206 (2012)
- [119] E. FRADKIN, S. H. SHENKER. *Phase diagrams of lattice gauge theories with Higgs fields.* *Phys. Rev. D* **19**, 3682 (1979)

- [120] Z. NUSSINOV, E. FRADKIN. *Discrete sliding symmetries, dualities, and self-dualities of quantum orbital compass models and $p + ip$ superconducting arrays*. *Phys. Rev. B* **71**, 195120 (2005)
- [121] L. D. LANDAU, E. M. LIFSCHITZ. *Statistische Physik*. In *Lehrbuch der Theoretischen Physik*, edited by G. HEBER, volume 5. Akademie Verlag Berlin (1970)
- [122] M. TINKHAM. *Group theory and quantum mechanics*. Dover (1964)
- [123] A. KITAEV, L. KONG. *Models for Gapped Boundaries and Domain Walls*. *Commun. Math. Phys.* **313**, 351 (2012)
- [124] S. ELITZUR. *Impossibility of spontaneously breaking local symmetries*. *Phys. Rev. D* **12**, 3978 (1975)
- [125] P. W. HIGGS. *Broken Symmetries and the Masses of Gauge Bosons*. *Phys. Rev. Lett.* **13**, 508 (1964)
- [126] F. ENGLERT, R. BROUT. *Broken Symmetry and the Mass of Gauge Vector Mesons*. *Phys. Rev. Lett.* **13**, 321 (1964)
- [127] G. S. GURALNIK, C. R. HAGEN, T. W. B. KIBBLE. *Global Conservation Laws and Massless Particles*. *Phys. Rev. Lett.* **13**, 585 (1964)
- [128] T. MÅNSSON, V. LAHTINEN, J. SUORSA, E. ARDONNE. *Condensate-induced transitions and critical spin chains*. *Phys. Rev. B* **88**, 041403 (2013)
- [129] H. X. HE, C. J. HAMER, J. OITMAA. *High-temperature series expansions for the (2+1)-dimensional Ising model*. *J. Phys. A* **23**, 1775 (1990)
- [130] J. OITMAA, C. J. HAMER, Z. WEIHONG. *Low-temperature series expansions for the (2+1)-dimensional Ising model*. *J. Phys. A* **24**, 2863 (1991)
- [131] K. A. PENSON, R. JULLIEN, P. PFEUTY. *Triangular antiferromagnetic Ising model with a transverse field at zero temperature*. *J. Phys. C* **12**, 3967 (1979)
- [132] S. V. ISAKOV, R. MOESSNER. *Interplay of quantum and thermal fluctuations in a frustrated magnet*. *Phys. Rev. B* **68**, 104409 (2003)
- [133] M. POWALSKI, K. COESTER, R. MOESSNER, K. P. SCHMIDT. *Disorder by disorder and flat bands in the kagome transverse field Ising model*. *Phys. Rev. B* **87**, 054404 (2013)
- [134] S. SACHDEV. *Quantum Phase Transitions*. Cambridge University Press (2011)
- [135] M. HASENBUSCH. *Finite size scaling study of lattice models in the three-dimensional Ising universality class*. *Phys. Rev. B* **82**, 174433 (2010)
- [136] M. KAMFOR. *Robustness and spectroscopy of the toric code in a magnetic field*. Ph.D. thesis, TU Dortmund (2013)
- [137] M. CONTINENTINO. *Quantum Scaling in Many-body Systems*. World Scientific lecture notes in physics. World Scientific (2001)
- [138] H. W. J. BLÖTE, E. LUIJTEN, J. R. HERINGA. *Ising universality in three dimensions: a Monte Carlo study*. *J. Phys. A* **28**, 6289 (1995)
- [139] H. KLEINERT. *Critical exponents from seven-loop strong-coupling φ^4 theory in three dimensions*. *Phys. Rev. D* **60**, 085001 (1999)
- [140] A. GOTTLÖB, M. HASENBUSCH. *The XY model and the three-state antiferromagnetic Potts model in three dimensions: Critical properties from fluctuating boundary conditions*. *J. Stat. Phys.* **77**, 919 (1994)
- [141] J. CARDY. *Scaling and Renormalization in Statistical Physics*. Cambridge University Press (1996)

- [142] M. CAMPOSTRINI, M. HASENBUSCH, A. PELISSETTO, P. ROSSI, E. VICARI. *Critical behavior of the three-dimensional XY universality class*. *Phys. Rev. B* **63**, 214503 (2001)
- [143] G. VIDAL. *Entanglement Renormalization*. *Phys. Rev. Lett.* **99**, 220405 (2007)
- [144] C. KNETTER, K. P. SCHMIDT, G. S. UHRIG. *The structure of operators in effective particle-conserving models*. *J. Phys. A* **36**, 7889 (2003)
- [145] C. KNETTER. *Perturbative continuous unitary transformations: spectral properties of low dimensional spin systems*. Ph.D. thesis, Universität zu Köln (2003)
- [146] K. P. SCHMIDT. *Spectral properties of quasi one-dimensional quantum antiferromagnets. Perturbative continuous unitary transformations*. Ph.D. thesis, Universität zu Köln (2004)
- [147] C. KNETTER. *Störungstheorie mit Hilfe von Flußgleichungen angewendet auf dimerisierte Spinmodelle*. Master's thesis, Universität zu Köln (1999)
- [148] T. KATO. *On the Convergence of the Perturbation Method. I*. *Prog. Theor. Phys.* **4**, 514 (1949)
- [149] M. GELFAND, R. R. P. SINGH, D. HUSE. *Perturbation expansions for quantum many-body systems*. *J. Stat. Phys.* **59**, 1093 (1990)
- [150] W. ZHENG, C. J. HAMER, R. R. P. SINGH, S. TREBST, H. MONIEN. *Linked cluster series expansions for two-particle bound states*. *Phys. Rev. B* **63**, 144410 (2001)
- [151] J. OITMAA, C. HAMER, W. ZHENG. *Series Expansion Methods for Strongly Interacting Lattice Models*. Cambridge University Press, (2006)
- [152] F. WEGNER. *Flow-equations for Hamiltonians*. *Ann. Phys. (Leipzig)* **506**, 77 (1994)
- [153] S. D. GLAZEK, K. G. WILSON. *Renormalization of Hamiltonians*. *Phys. Rev. D* **48**, 5863 (1993)
- [154] A. REISCHL, E. MÜLLER-HARTMANN, G. S. UHRIG. *Systematic mapping of the Hubbard model to the generalized t - J model*. *Phys. Rev. B* **70**, 245124 (2004)
- [155] S. A. HAMERLA, S. DUFFE, G. S. UHRIG. *Derivation of the t - J model for finite doping*. *Phys. Rev. B* **82**, 235117 (2010)
- [156] H. Y. YANG, K. P. SCHMIDT. *Effective models for gapped phases of strongly correlated quantum lattice models*. *Europhys. Lett.* **94**, 17004 (2011)
- [157] H. KRULL, N. A. DRESCHER, G. S. UHRIG. *Enhanced perturbative continuous unitary transformations*. *Phys. Rev. B* **86**, 125113 (2012)
- [158] A. MIELKE. *Flow equations for band-matrices*. *Eur. Phys. J. B* **5**, 605 (1998)
- [159] T. FISCHER, S. DUFFE, G. S. UHRIG. *Adapted continuous unitary transformation to treat systems with quasi-particles of finite lifetime*. *New J. Phys.* **12**, 033048 (2010)
- [160] C. KNETTER, A. BÜHLER, E. MÜLLER-HARTMANN, G. S. UHRIG. *Dispersion and Symmetry of Bound States in the Shastry-Sutherland Model*. *Phys. Rev. Lett.* **85**, 3958 (2000)
- [161] C. KNETTER, K. P. SCHMIDT, M. GRÜNINGER, G. S. UHRIG. *Fractional and Integer Excitations in Quantum Antiferromagnetic Spin $1/2$ Ladders*. *Phys. Rev. Lett.* **87**, 167204 (2001)
- [162] C. KNETTER, K. P. SCHMIDT, G. S. UHRIG. *High order perturbation theory for spectral densities of multi-particle excitations: $S = 1/2$ two-leg Heisenberg ladder*. *Eur. Phys. J. B* **36**, 525 (2003)
- [163] S. DUSUEL, J. VIDAL. *Continuous unitary transformations and finite-size scaling exponents in the Lipkin-Meshkov-Glick model*. *Phys. Rev. B* **71**, 224420 (2005)
- [164] H.-Y. YANG, A. M. LÄUCHLI, F. MILA, K. P. SCHMIDT. *Effective Spin Model for the Spin-Liquid Phase of the Hubbard Model on the Triangular Lattice*. *Phys. Rev. Lett.* **105**, 267204 (2010)

- [165] K. P. SCHMIDT, S. DUSUEL, J. VIDAL. *Emergent Fermions and Anyons in the Kitaev Model*. *Phys. Rev. Lett.* **100**, 057208 (2008)
- [166] K. P. SCHMIDT, J. DORIER, A. M. LÄUCHLI, F. MILA. *Supersolid Phase Induced by Correlated Hopping in Spin-1/2 Frustrated Quantum Magnets*. *Phys. Rev. Lett.* **100**, 090401 (2008)
- [167] J. VIDAL, K. P. SCHMIDT, S. DUSUEL. *Perturbative approach to an exactly solved problem: Kitaev honeycomb model*. *Phys. Rev. B* **78**, 245121 (2008)
- [168] M. KARGARIAN, H. BOMBIN, M. A. MARTIN-DELGADO. *Topological color codes and two-body quantum lattice Hamiltonians*. *New J. Phys.* **12**, 025018 (2010)
- [169] J. STEIN. *Flow equations and the strong-coupling expansion for the Hubbard model*. *J. Stat. Phys.* **88**, 487 (1997)
- [170] R. R. P. SINGH, M. P. GELFAND, D. A. HUSE. *Ground States of Low-Dimensional Quantum Antiferromagnets*. *Phys. Rev. Lett.* **61**, 2484 (1988)
- [171] S. DUSUEL, M. KAMFOR, K. P. SCHMIDT, R. THOMALE, J. VIDAL. *Bound states in two-dimensional spin systems near the Ising limit: A quantum finite-lattice study*. *Phys. Rev. B* **81**, 064412 (2010)
- [172] C. DOMB, M. GREEN, editors. *Phase transitions and critical phenomena Vol.3*. New York: Academic Press (1974)
- [173] M. P. GELFAND, R. R. P. SINGH. *High-order convergent expansions for quantum many particle systems*. *Adv. Phys.* **49**, 93 (2000)
- [174] H. PADÉ. *Sur la représentation approchée d'une fonction par des fractions rationnelles*. *Ann. Ecole Norm.* **9**, 3 (1892)
- [175] G. A. BAKER, P. R. GRAVES-MORRIS. *Padé approximants*. Encyclopaedia of mathematics and its applications. Addison-Wesley, Reading, MA (1981)
- [176] A. J. GUTTMANN. *Asymptotic Analysis of Power-Series Expansions*. In *Phase transitions and critical phenomena*, edited by C. DOMB, J. L. LEBOWITZ, volume 13. New York: Academic Press (1989)
- [177] A. J. GUTTMANN, G. S. JOYCE. *On a new method of series analysis in lattice statistics*. *J. Phys. A* **5**, L81 (1972)
- [178] J. S. R. CHISHOLM. *Rational approximants defined from double power series*. *Math. Comp.* **27**, 841 (1973)
- [179] M. E. FISHER, R. M. KERR. *Partial Differential Approximants for Multicritical Singularities*. *Phys. Rev. Lett.* **39**, 667 (1977)
- [180] V. I. YUKALOV, E. P. YUKALOVA. *Self-Similar Perturbation Theory*. *Ann. Phys.* **277**, 219 (1999)
- [181] E. P. YUKALOVA, V. I. YUKALOV, S. GLUZMAN. *Self-similar factor approximants for evolution equations and boundary-value problems*. *Ann. Phys.* **323**, 3074 (2008)
- [182] S. GLUZMAN, V. YUKALOV. *Self-similar extrapolation from weak to strong coupling*. *J. Math. Chem.* **48**, 883 (2010)
- [183] N. LAFLORENCIE, D. POILBLANC. *Simulations of pure and doped low-dimensional spin-1/2 gapped systems*. *Lect. Notes Phys.* **645**, 227 (2004)
- [184] A. LÄUCHLI. *Numerical Simulations of Frustrated Systems*. In *Introduction to Frustrated Magnetism: Materials, Experiments, Theory*, edited by C. LACROIX, P. MENDELS, F. MILA. Springer Berlin Heidelberg (2011)
- [185] J. STOER, R. BULIRSCH. *Numerische Mathematik II*. Springer Berlin / Heidelberg (2005)

-
- [186] S. WOLFRAM. *The Mathematica Book, 5th ed.* Wolfram Media (2003)
- [187] A. WEISSE. *Divide and conquer the Hilbert space of translation-symmetric spin systems.* *Phys. Rev. E* **87**, 043305 (2013)
- [188] C. J. MORNINGSTAR, M. WEINSTEIN. *Contractor renormalization group technology and exact Hamiltonian real-space renormalization group transformations.* *Phys. Rev. D* **54**, 4131 (1996)
- [189] E. ALTMAN, A. AUERBACH. *Plaquette boson-fermion model of cuprates.* *Phys. Rev. B* **65**, 104508 (2002)
- [190] T. DE NEEF, I. G. ENTING. *Series expansions from the finite lattice method.* *J. Phys. A* **10**, 801 (1977)
- [191] I. G. ENTING. *Finite lattice series expansions for the triangular lattice.* *J. Phys. A* **13**, L279 (1980)
- [192] D. POILBLANC, M. MAMBRINI, D. SCHWANDT. *Effective quantum dimer model for the kagome Heisenberg antiferromagnet: Nearby quantum critical point and hidden degeneracy.* *Phys. Rev. B* **81**, 180402 (2010)
- [193] W. ZHU, S. S. GONG, F. D. M. HALDANE, D. N. SHENG. *Identifying Non-Abelian Topological Order through Minimal Entangled States.* [arxiv:1308.3878](https://arxiv.org/abs/1308.3878) (2013)
- [194] M. KAMFOR, S. DUSUEL, J. VIDAL, K. P. SCHMIDT. *Spectroscopy of a topological phase.* [arxiv:1308.6150](https://arxiv.org/abs/1308.6150) (2013)
- [195] J. KNOLLE, D. L. KOVRIZHIN, J. T. CHALKER, R. MOESSNER. *Dynamics of a two-dimensional quantum spin liquid: signatures of emergent Majorana fermions and fluxes.* [arXiv:1308.4336](https://arxiv.org/abs/1308.4336) (2013)

Declaration of Authorship

I, Marc Daniel Schulz, declare that this thesis titled, “Topological phase transitions driven by non-Abelian anyons” and the work presented in it are my own. I confirm that:

- This work was done wholly or mainly while in candidature for a research degree at the TU Dortmund and the UPMC Paris.
- Where any part of this thesis has previously been submitted for a degree or any other qualification at this University or any other institution, this has been clearly stated.
- Where I have consulted the published work of others, this is always clearly attributed.
- Where I have quoted from the work of others, the source is always given. With the exception of such quotations, this thesis is entirely my own work.
- I have acknowledged all main sources of help.
- Where the thesis is based on work done by myself jointly with others, I have made clear exactly what was done by others and what I have contributed myself.

Signed:

Date:

Acknowledgements

*As you set out for Ithaca
hope that your journey is a long one, ...
- Konstantin P. Kavafis -*

I would first of all like to thank my family, who has continuously supported me during all the years of my studies.

Not less, I want to thank both of my thesis advisors, Dr. Kai P. Schmidt and Dr. Julien Vidal. Their enthusiasm and assistance guided me through the preparation of this thesis. I think that the close collaboration we have established during the last few years has been very rewarding.

I'm very grateful to Dr. Sébastien Dusuel, who provided not only most of the exact diagonalization results in collaboration with Dr. Julien Vidal, but also many valuable insights on the physics of topologically-ordered states as well as the life in Paris.

I enjoyed very much the collaboration with Jprof. Dr. Román Orús on the \mathbb{Z}_N -toric code.

I thank Prof. Philippe Lecheminant, Prof. Joachim Stolze, and Prof. Simon Trebst for being the referees of this work.

I have enjoyed a lot my time in Dortmund and Paris. I want to thank the members of the Lehrstuhl für theoretische Physik I/II and the LPTMC for sharing their insights and many good discussions, especially Michael Kamfor (who also proof-read the manuscript), Kris Coester, Gregor Foltin, Hong-Yu Yang, Björn Zelinski, Daniel Klagges, Thiago Milanetto-Schlittler, Karim Essafi, Fabian Closa, Frederik Keim, Sebastian Fey, Dominic Ixert, Henning Kalis, Michael Powalski, Mike Nemeč, Johannes Splinter, Saeed S. Jahromi, Frederik Herbst, Sebastian Clever, Marcel Bornemann, Wiebke Malitz, Maik Malki, and Paul Westphälinger.

Financial support by the Université franco-allemande - Deutsch-Französische Hochschule is gratefully acknowledged.